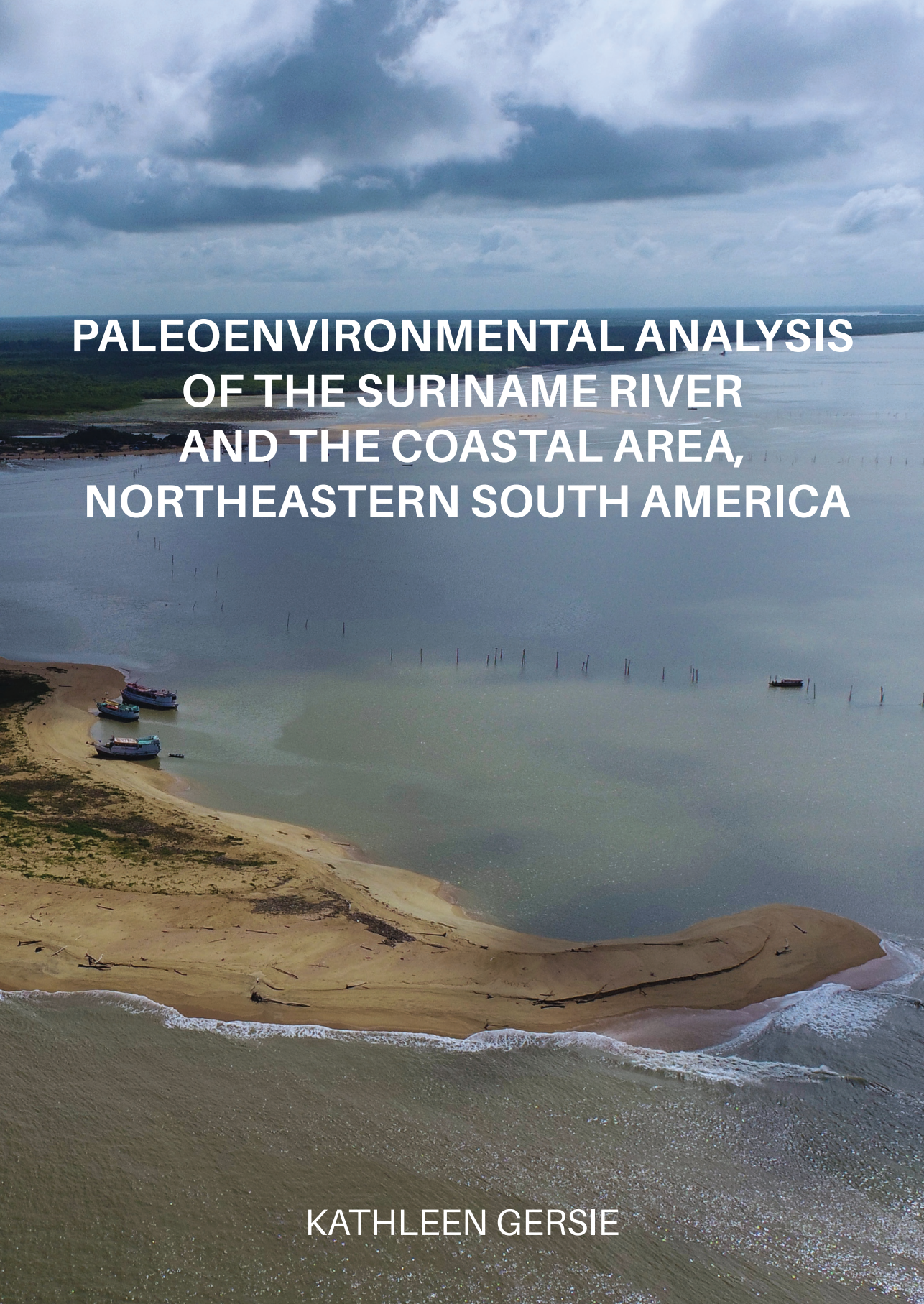


PALEOENVIRONMENTAL ANALYSIS OF THE SURINAME RIVER AND THE COASTAL AREA, NORTHEASTERN SOUTH AMERICA

KATHLEEN GERSIE

Paleoenvironmental analysis of the Suriname River and the coastal area, Northeastern South America.

Kathleen Gersie

Cover photo: The sandspit Braamspunt located at the right corner of the Suriname river mouth and the Atlantic Ocean (photocredits: Green Heritage Fund Suriname)
Illustrations and photography: Kathleen Gersie
Funding: Suriname Conservation Foundation

© copyright Kathleen Gersie, Maastricht 2026

Printing & layout: ProefschriftMaken || www.proefschriftmaken.nl

ISBN 978-94-6534-375-4

All rights reserved. No part of this publication may be reproduced, stored in a retrieval system or transmitted, in any form or by any means, electronic, mechanical, photocopying, recording or otherwise, without prior permission of the author or the copyright-owning journals for previous published chapters.

VRIJE UNIVERSITEIT

Paleoenvironmental analysis of the Suriname River and the coastal area, Northeastern South America.

Reconstructing the environmental change and coastal dynamics from the Paleogene to the present of the Suriname coastal area, northeastern South America

ACADEMISCH PROEFSCHRIFT

ter verkrijging van de graad Doctor aan
de Vrije Universiteit Amsterdam,
op gezag van de rector magnificus
prof.dr. J.J.G. Geurts,
volgens besluit van de decaan
van de Faculteit der Bètawetenschappen
in het openbaar te verdedigen
op donderdag 2 juli 2026 om 11.45 uur
in de universiteit

door

Kathleen Simone Gersie
geboren te Paramaribo, Suriname

promotor:	prof.dr. R.T. van Balen
copromotor:	dr. M.C. Hoorn
promotiecommissie:	dr.ir. Y. van der Velde prof.dr. W.D. Gossling dr. J. Storms prof.dr. E. Stouthamer prof.dr. S.M. de Jong

“Forever in my heart, forever my guiding light”

This thesis is dedicated to my late mother
Junita Beatrice Woerdings

CONTENTS

Contents		6
Summary		7
Samenvatting		8
Chapter 1	General introduction	11
Chapter 2	Evolution of the suriname coastal environment based on a cenozoic sedimentary record (powisi-01)	25
Chapter 3	Tracing amazon influence on the suriname coastline: results from a study on a neogene coastal sedimentary record	105
Chapter 4	The interplay between tectonics, climate and sea-level change in the holocene floodplain and pleistocene terraces of the suriname river, tropical south america	167
Chapter 5	Understanding westward deflection due to river-coast interactions in the holocene coastal plain of suriname	199
Chapter 6	Marine and anthropogenic controls on the estuary of the suriname river over the past 50 years	231
Chapter 7	General discussion	253
Co-authorship statement		272
Acknowledgements		274
Biography		278

https://doi.org/10.5463/thesis.1718

SUMMARY

The low-lying coastal zone of Suriname, which is vital for the country's population and economy, is increasingly vulnerable to sea-level rise driven by climate change. This coastline is naturally protected by a dynamic system of mangroves, hydrodynamic processes, and sediment deposition, strongly influenced by variable mud discharge from the Amazon River through longshore mudbank cycles.

This thesis studies the role of sediments from the Amazon River, the Suriname River, and smaller rivers in shaping the geological and morphological evolution of the Suriname Coastal Plain from the Paleogene to the present. An integrated approach was used to answer the research questions by combining palynological analysis, sediment geochemistry, light microscopy, satellite imagery, and historical geomorphological and topographic maps.

The Paleocene–Eocene Thermal Maximum in Paleogene sediments and a major shift in mangrove composition between the Paleogene and Neogene were recorded, independent from influence of the Amazon River. During the Neogene, vegetation evolution coincided with a transition in sediment supply from local Guiana Shield rivers to the inclusion of Andean-derived material, which occurred during the Pliocene–Pleistocene. River terraces along the Suriname River reflect different controlling processes: upstream and middle terraces formed through combined tectonic uplift and climate-driven changes in discharge and sediment supply, while downstream terraces are primarily controlled by sea-level fluctuations. Suriname's south-north running rivers have largely kept pace with coastal progradation, though anthropogenic activities, especially the Afobaka hydroelectric dam, have significantly altered river hydrodynamics and channel morphology.

SAMENVATTING

De laaggelegen kustvlakte van Suriname, die van belang is voor de bevolking en economie van het land, wordt steeds kwetsbaarder voor stijging van de zeespiegel welke veroorzaakt wordt door klimaatverandering. De kustlijn van Suriname wordt natuurlijk beschermd door een dynamisch systeem van mangrovebossen, hydrodynamische processen en sedimentafzetting. Het wordt sterk beïnvloed door de variatie in afvoer modder en slib van de Amazone Rivier via de cyclus van langs-migrerende modderbanken.

Deze studie onderzoekt de rol van sedimenten afkomstig van de Amazone-, de Surinamerivier en andere kleine rivieren in de geomorfologische ontwikkeling van de Surinaamse kustvlakte vanaf het Paleogeen tot heden. Voor het beantwoorden van de onderzoeksvragen werd gebruik gemaakt van een combinatie van palynologische en geochemische analyses, lichtmicroscopie, satellietbeelden, en historische geomorfologische en topografische kaarten.

Het Paleoceen-Eoceen Thermisch Maximum, ookwel bekend als het PETM, werd in Paleogene sedimenten geregistreerd. Hetzelfde geldt voor een grote verschuiving in de samenstelling van mangrovebossen tussen het Paleogeen en het Neogeen, welke onafhankelijk is van de invloed van de Amazone. Tijdens het Plioceen-Pleistoceen viel de ontwikkeling van de kustvegetatie samen met een overgang in de sedimentaanvoer van lokale rivieren afkomstig van het Guiana-schild naar de aanvoer van materiaal afkomstig uit de Andes. Rivierterrassen langs de Surinamerivier weerspiegelen verschillende sturende processen: terrasen in het boven- en middenstrooms rividerdeel zijn gevormd door een combinatie van tektonische opheffing en klimaatgedreven veranderingen in het rivierdebiet en sedimentaanvoer, terwijl terrassen langs het benedenstrooms deel van de rivier voornamelijk zijn bepaald door zeespiegel fluctuaties. De zuid-noord stromende rivieren van Suriname hebben grotendeels gelijke tred gehouden met de kust progradatie, terwijl antropogene factoren, met name de Afobaka stuwdam, de hydrodynamica en morfologie van de riviergeul aanzienlijk hebben veranderd.



Chapter 1

General Introduction



I. INTRODUCTION

In this study I address the interrelation between rivers and the coastal evolution of Suriname on different time-scales, ranging from the Paleogene to the Neogene.

I reconstruct paleoenvironments and paleoecosystems of the Suriname coast before and after the onset of sediment input from the Amazon River, I address how the Suriname river evolved, and I study how local rivers have adapted to the development of the coastal plain.

A major contributing factor to the development of the present-day Suriname coastal area is the sediment input by the Amazon River, in the form of alongshore migrating mudbanks. The interaction of these moving banks with waves results in fluctuating shorelines which are associated with depositional 'bank' phases and erosional 'inter-bank' phases (Anthony et al., 2010). Ever since the uplift of the Andes started supplying large amounts of fine-grained sediments to the Amazon River, the attachment of mud and cheniers along the Suriname coast has led to shoreline progradation (Eisma and Van der Marel, 1971; Augustinus, 1980).

1.1 STUDY AREA

The Suriname coastal plain forms the onshore part of the Suriname-Guyana Basin, together with those of French Guiana and Guyana. In the offshore area, two distinct morphological units can be identified: the Continental Plateau and the Demerara Rise (Wong, 1994) (Fig. 1). This basin originated in the Late Jurassic to Early Cretaceous during the opening of the Atlantic Ocean, and was accompanied by steep faulting in the coastal area which continued into the Early Tertiary (Wijmstra; 1971, Krook; 1979). Hereafter the Suriname-Guyana Basin has been governed by the gradual subsidence of a passive continental margin that resulted in deposition characterized by slight tectonic activity and many periods of erosion (Hanou, 1981). Sedimentary units on the Suriname coastal plain have been grouped in the Corantijn Group of Late Cretaceous to Holocene age. Various transgressions and regressions, as well as periods of non-deposition have occurred. The continuous south to north- and east to west thickening of the Corantijn Group (Fig. 2A,B) suggests a relatively constant rate of subsidence of the Suriname-Guyana Basin during deposition where the rate of deposition continually outpaced basement subsidence (Wong, 1986).

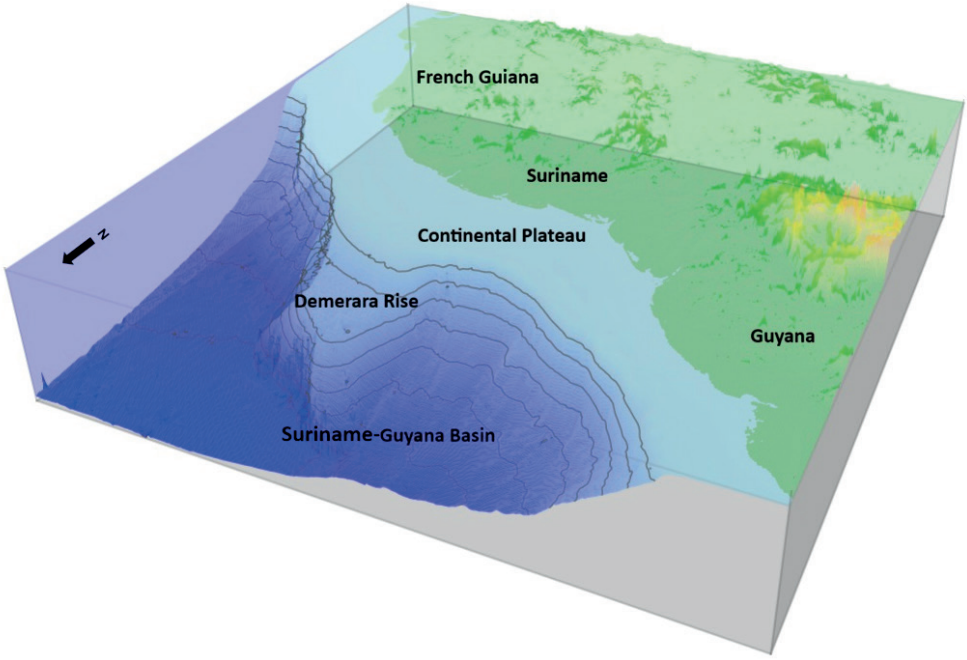


Figure 1: Sketch view of the bathymetry of the Suriname-Guyana Basin in front of the three Guianas: French-Guiana, Suriname and Guyana (map created with Gebco, 2024 model; source: https://www.bodc.ac.uk/data/published_data_library/)

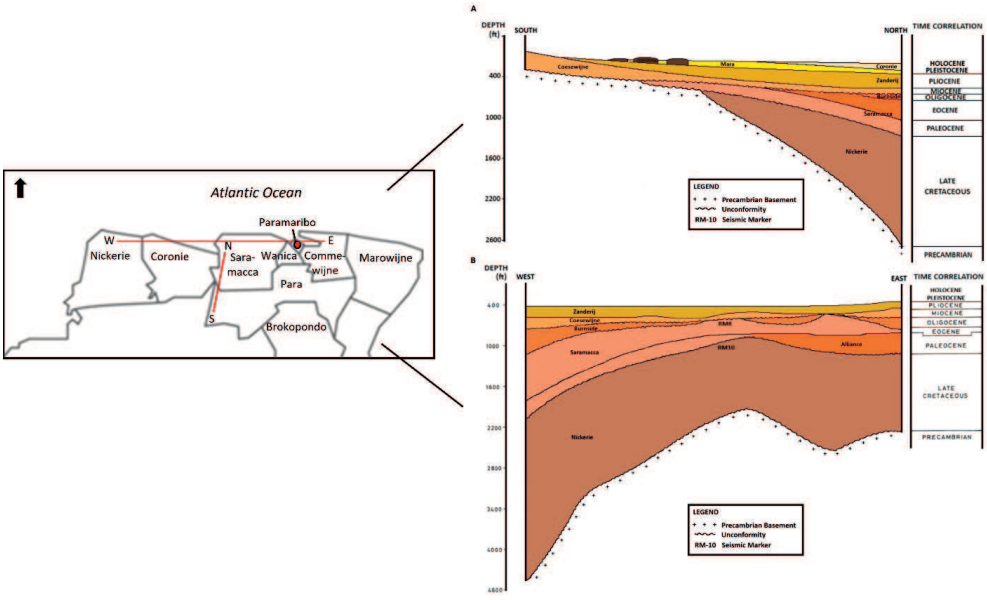


Figure 2: (A) S-N and (B) E-W stratigraphic profile of the Suriname coastal plain (modified after Wong, 1986); (RM8=Regional Marker 8; RM10 = Regional Marker 10).

The present-day coast of Suriname is part of the 1500 km mud-dominated Guianas coastline in the northeastern part of South America (Eisma et al., 1991), situated between Amapá and the Orinoco River delta (Fig. 3) (Augustinus, 1978; Wong et al., 2009; Anthony et al., 2014), has often been the subject of research. Several studies have evidenced that the development of this wave-dominated coast (Gratiot et al., 2007) is controlled by sediment from the Amazon River (Anthony et al., 2019), resulting in a series of alongshore migrating mudbanks, moving in westward direction towards the Orinoco River in Venezuela (Augustinus, 1994). The migration mechanism is by wave action: winnowing at the upstream side, transport by currents (coastal drift), and resettling at the downstream side (Augustinus, 1983; Eisma et al., 1991). This mechanism is the cause behind mudflat migration along the shore (Wong et al., 2009).

It is likely that sediment delivered by the Amazon River was also an important contributor to the coastal development in the past. However, the question remains when this has started. The only precise age constraint for the Amazon River and its submarine fan is derived from the deep-sea Ceará Rise (Dobson et al., 2001; Figueiredo et al., 2009; Van Soelen et al., 2017). It is estimated that the development of the Amazon River to a transcontinental system occurred sometime between the Late Miocene to the Late Pliocene (e.g. Damuth and Kumar, 1975; Figueiredo et al., 2009; Van Soelen et al., 2017). At continental level this river has controlled the supply of muddy, fine-grained sediments and evolution (Anthony et al., 2010, 2014; Augustinus, 2004) of the Holocene coastal plain of Suriname. Apart from the mud supply by the Amazon River, sedimentation and erosion along the Suriname coast is mainly determined by waves, nearshore currents, and -on a more longer-term-, relative sea-level changes (Eisma et al., 1991; Augustinus, 2004).

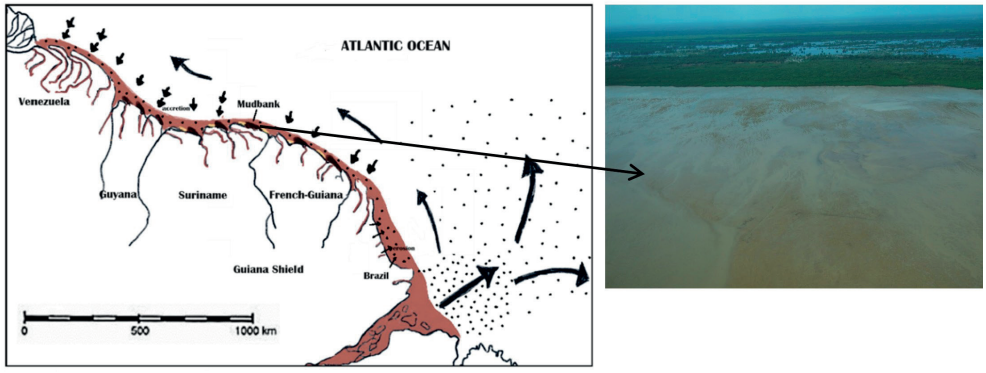


Figure 3: Mud dispersal and transport from the Amazon along the Guianas (modified after Parizanganeh et al., 2008; Photo credits: World Wildlife Fund, 2023)

1.2 THE DEVELOPMENT OF THE SURINAME COASTAL AREA

Suriname's coastal evolution and its controlling factors have been studied on multiple time-scales. On the long term (tens of million years (My)), the impact of the mud supply from the Amazon River plays an important role. On shorter time-scales (My's) fluvial incision by local rivers, such as the Suriname River, has resulted in sediment supply and a terraced landscape. On the Holocene time-scale (1-10 thousand years (Ky)), coastal processes including mud-bank migration and erosion, affected coastal evolution and interacted with fluvial sytems. On the shortest time-scale (tens of yrs), the coast is affected by human activities, such as dam construction and dredging.

1.2.1 The Suriname coast in the Paleogene and the Neogene

During the Cretaceous, the Nickerie Formation of the Corantijn Group was deposited on a weathered Precambrian basement, influenced by sea-level fluctuations and sediment supply from the Guiana Shield (Wong et al., 2016). A major sea-level regression at the end of the Cretaceous caused erosion and formed a regional unconformity (RM10) marking the Cretaceous–Paleocene boundary (Noorthoorn van der Kruyff, 1970). The Paleocene began with a major transgression, depositing the Onverdacht, Saramacca, and Alliance formations (Wijmstra, 1971; Wong, 1986). Prolonged weathering led to bauxitization during the Late Eocene–Oligocene, continuing into the earliest Miocene (Noorthoorn van der Kruyff, 1970). Fluvial deposition during the Oligocene formed the Burnside Formation (Wong, 1986; Wong et al., 2016), followed by Miocene transgressive deposition of the Coesewijne Formation, which ended due to Andean uplift. The Amazon River delivered large volumes of mud to the Atlantic Ocean, strongly influencing sedimentation along the Suriname coast (Figueiredo et al., 2009; Wong et al., 2016). Thus, the onset of the Amazon River has had a significant impact on the development of the coastal area of Suriname (Anthony et al., 2013), in addition to local rivers like the Suriname river (see below). Despite its importance, the timing of the Amazon's onset remains debated (Figueiredo et al., 2009; Hoorn, 1995; Hoorn et al., 2017; van Soelen et al., 2017). In the Suriname coastal area, until present, research efforts were mostly focused on the complex Holocene development of the slowly moving mudflats, whereas very little information is available about the timespan ranging from Late Miocene (c. 11.5 million years ago (Ma)) to Holocene (0.01 Ma).

1.2.2 Terrace formation along the Suriname River

The Suriname River has been an important local source of sediment to the coast. Its evolution is recorded in a series of fluvial terraces, which likely formed through the interplay of climate and tectonic processes (Gersie et al., 2021). Although the distribution, number, and ages of these terraces have been studied in previous studies, a synthesis is still lacking.

The Pliocene may have been the most recent period when global temperatures exceeded those of today (Crowley, 1996). Global glacial conditions accompanied by a dry climate resulted in braided rivers that transported and deposited gravel deposits. Incising rivers flowing through stable craton areas are typified by low sediment discharge (Latrubesse et al, 2005) and are more or less dominated by the transport of suspended sediment load (Garner, 1967). The development of river terraces along the Suriname River, considered as levelled abandoned floodplains, closely follow the present drainage pattern (Kroonenberg, 1983). Even though absolute ages from the terraces are yet unknown, Kroonenberg and Noordam (2018) concluded that they might have developed in periods with dry arid climates and reduced vegetation cover.

1.2.3 The Pleistocene and Holocene development of the Suriname coastal area

The mud delivered by the Amazon River forms a series of banks that move along the coastline, driven by waves and currents. The mudbanks promote sediment accumulation, in contrast to the interbank areas that experience higher wave energy and are prone to erosion. This creates alternating phases of coastal accretion and erosion (Augustinus, 1979; Anthony et al., 2014; Anthony et al., 2019). Augustinus (1979) and Augustinus et al., (1989) suggested that the interaction between these marine processes and fluvial forces (e.g. the forming of cheniers) have played an important role in the morphology of the Suriname coastal plain over the past 5-6000 years.

1.2.4 Morphodynamics of the Present-day Suriname River

Coastal changes and related processes to the development of the Suriname Coastal Plain can be described on different levels. The coastal development and morphology is largely determined by the 30-year cycle of westward migrating mudbank and interbank areas. The presence of these mudbanks control the degree of erosion and deposition at certain locations along the coast, such as river mouths (Wong et al., 2016). The sandspit at Braamspunt and the Weg naar Zee area, respectively at the eastern and western side of the Suriname River mouth is an example of the result of the combined effect of marine and anthropogenic factors in and along the Suriname River. Over more than a century the Suriname River has been the most important river due to intensive land use activities in its catchment, the location of the capital and its harbour, and the Afobaka hydro-electric dam (Gersie et al., 2016).

1.3 OBJECTIVE AND THESIS OUTLINE

Historical, present, and future development of the Suriname coast has been and still is highly dependent on the discharge and transport of sediments from the Amazon River and Suriname River. Migrating mudbanks play an important role in protecting the coast against high-energy waves and erosion processes. Estuaries, including the Suriname River estuary,

also depend on the import of silt transported during high and low tides which is important for mangrove forests. These processes still play a role today, but it is not yet known to what extent they do so. The impact this will have now and in the future on the Suriname coastline must also be taken into account, for example, in case of reduced water or sediment discharge of the Amazon River and/or its tributaries.

To study the evolution of the paleoenvironments and paleoecosystems from the Paleogene up to Present-day, five research questions have been formulated:

1) What characterizes the depositional conditions and the vegetation in the nearshore coastal area of Suriname during the Paleogene and Neogene? What can sporomorphs and geochemistry in the sediments in the Powisi-01 well tell us on coastal development and the onset and evolution of Amazonian influence on the Suriname coast?
2) What can sporomorph assemblages and geochemistry in the sediments in the Hepp-3 well reveal about past vegetation and ecological conditions along the Suriname coastline in the Neogene?
3) What was the long-term evolution of the Suriname River? What are the key controls for terrace development along the Upper and Lower River valleys of the Suriname rivers during the Pleistocene?
4) What are the driving processes behind the westward deflection of the small main rivers in the Holocene Young Coastal Plain of Suriname? What was the interaction between fluvial and coastal processes?
5) How was the behaviour of the Suriname River controlled by natural and anthropogenic activities, like land use and building of the Afobaka dam?

Chapter 2 delves into the Cenozoic evolution of the Suriname coastal area. Sediment samples from the Powisi-1 well, located in the nearshore area of Suriname, are used to identify the provenance of the sediment deposits by means of sediment chemical analyses while palynological and dinoflagellate analyses, are used to provide a biostratigraphic framework and study the paleoecosystems through time.

Chapter 3 studies the provenance and sporomorph composition in the Hepp-3 well located in the district of Nickerie, West-Suriname, to determine the past vegetation and ecology of Suriname in the Neogene.

Chapter 4 studies the development of river terraces along the Suriname River. The upper and middle part of the Suriname River dissect the Precambrian basement and are characterized by river terraces and many knickpoints, also known as sulas. Climate variations, uplift and sea-level changes seem to have been the primary drivers behind these morphological features along the Suriname river.

Chapter 5 focuses on the westward deflecting rivers in the Suriname Coastal plain, and the role of mudbanks and cheniers influencing this river behaviour. These rivers have kept pace with the progradation of the coastline in seaward direction.

Chapter 6 covers the development of the Suriname River over the last 50 years. Human intervention in the Suriname River has caused many changes in the downstream part of the river. The construction of the Afobaka Dam has not only regulated the river discharge but also impacted the coastline westward of the Suriname river mouth.

REFERENCES:

Anthony, E.J., Gardel., A., Gratiot, N., Proisy, C. Allison, M. A., Dolique, F., Fromard, F. (2010). The Amazon-influenced muddy coast of South America: A review of mud-bank–shoreline interactions

Earth-Science Reviews, 103 (3-4), 99-121. https://doi.org/10.1016/j.earscirev.2010.09.008.

Anthony, E.J., Gratiot, N. (2012). Coastal engineering and large-scale mangrove destruction in Guyana, South America: Averting an environmental catastrophe in the making. Ecological Engineering, 47, 268-273. https://doi.org/10.1016/j.ecoleng.2012.07.005.

Anthony, E.J. (2013). Storms, shoreface morphodynamics, sand supply, and the accretion and erosion of coastal dune barriers in the southern North Sea. Geomorphology, 199, 8-21. https://doi.org/10.1016/j.geomorph.2012.06.007.

Anthony, E. J., Gardel, A., Gratiot, N. (2014). Fluvial sediment supply, mud banks, cheniers and the morphodynamics of the coast of South America between the Amazon and Orinoco river mouths. In: Sedimentary Coastal Zones from High to Low Latitudes: Similarities and Differences. Eds. Martini, I. P., Wanless, H. R. Geological Society of London, 388: 1-29 https://doi.org/10.1144/SP388.8.

Anthony, E. J., Brunier, G., Gardel, A., Hiwat, M. (2019). Chenier Morphodynamics on the Amazon-Influenced Coast of Suriname, South America: Implications for Beach Ecosystem Services. Frontiers in Earth Science, 7: 1-20. https://doi.org/10.3389/feart.2019.00035.

Augustinus, P. G. E. F. (1978). The changing shoreline of Surinam (South America). PhD Thesis Utrecht University, 232 pp. Uitgaven "Natuurwetenschappelijke studiekring voor Suriname en de Nederlandse Antillen, Utrecht, 95, 232 pp.

Augustinus, P. G. E. F. (1980). Actual development of the chenier coast of Suriname (South America). Sedimentary Geology, 26(1-3), 91-113. https://doi.org/10.1016/0037-0738(80)90007-X.

Augustinus, P. G. E. F., Hazelhoff, L., & Kroon, A. (1989). The chenier coast of Suriname: modern and geological development. Marine Geology, 90(4), 269-281. https://doi.org/10.1016/0025-3227(89)90129-1.

Augustinus, P.G.E.F., (1993). Coastal development in Suriname at different temporal and spatial scales. In: List, J.H. (ed.): Large scale coastal behavior '93. US Geological Survey Open File Report 93, 1–4.

Augustinus, P. G. E. F. (1994). Ontwikkelingen in de kust-en kustvlaktegenese van Suriname. *Recente geologische en mijnbouwkundige ontwikkelingen in Suriname. Publ. Found. Sci. Res. Caribbean Region, Amsterdam*, 3-22.

Augustinus, P. G. E. F. (2004). The influence of the trade winds on the coastal development of the Guianas at various scale levels: a synthesis. Marine Geology, 208 (2-4), 145-151. https://doi.org/10.1016/j.margeo.2004.04.007.

Bridgland, D. River terrace systems in north-west Europe: An archive of environmental change, uplift and early human occupation. *Quaternary Scienc*e Review 2000, 19, 1293–1303. https://doi.org/10.1016/S0277-3791(99)00095-5.

Crowley, T. J. (1996). Pliocene climates: the nature of the problem. Marine Micropaleontology, 27(1-4), 3-12. https://doi.org/10.1016/0377-8398(95)00049-6.

Damuth, J. E., Kumar, N. (1975). Amazon cone: morphology, sediments, age, and growth pattern. Geological Society of America Bulletin, 86 (6), 863–878. DOI: 10.1130/0016-7606(1975)86<863:ACMSAA>2.0.CO;2.

De Boer, M.W.H. *Landform and Soils in Eastern Surinam (South America)*; Pudoc: Wageningen, The Netherlands, 1972; p. 169.

De Jong, S., Shen, Y., de Vries, J., Bijnaar, G., Van Maanen, B., Augustinus, P. G. E. F., Verweij, P. (2021). Mapping mangrove dynamics and colonization patterns at the Suriname coast using historic satellite data and the LandTrendr algorithm. International Journal of Applied Earth Observation and Geoinformation, 97, 102293. https://doi.org/10.1016/j.jag.2020.102293.

Dobson, D. M., Dickens, G. R., & Rea, D. K. (2001). Terrigenous sediment on Ceara Rise: a Cenozoic record of South American orogeny and erosion. Palaeogeography, Palaeoclimatology, Palaeoecology, 165(3-4), 215-229. https://doi.org/10.1016/S0031-0182(00)00161-9.

Eisma, D., Augustinus, P. G. E. F., Alexander, C. (1991). Recent and subrecent changes in the dispersal of Amazon mud. Netherlands Journal of Sea Research 28: 181-192.

Eisma, D., & Van der Marel, H. W. (1971). Marine muds along the Guyana coast and their origin from the Amazon Basin. *Contributions to Mineralogy and Petrology*, *31*(4), 321-334.

Figueiredo, J.; Hoorn, C.; Van der Ven, P.; Soares, E. (2009). Late Miocene onset of the Amazon River and the Amazon deep-sea fan: Evidence from the Foz do Amazonas Basin. Geology, 37 (7): 619–622. https://doi.org/10.1130/G25567A.1.

Garner, H.F. Rivers in the making. Scientific American 1967, 216, 84–94.

Gersie, K. S., Augustinus, P. G. E. F., Van Balen, R. T. (2016). Marine and anthropogenic controls on the estuary of the Suriname River over the past 50 years. Netherlands Journal of Geosciences – Geologie en Mijnbouw, 95: 419-428. https://doi.org/10.1017/njg.2016.18.

Gratiot, N., Gardel, A., Anthony, E. J., (2007). Trade-wind waves and mud dynamics on the French Guiana coast, South America: Input from ERA-40 wave data and field investigations. Marine Geology, 236 (1-2), 15-26. https://doi.org/10.1016/j.margeo.2006.09.013.

Hanou, M. J. (1981). Geologic and petroleum analysis of the Surinam coastal region. Int. Rep. HTC, Gulf Oil Co., 57 pp.

Hoorn, C. (1993). Marine incursions and the influence of Andean tectonics on the Miocene depositional history of northwestern Amazonia: results of a palynostratigraphic study. Palaeogeography, Palaeoclimatology, Palaeoecology, 105 (3-4), 267-309. https://doi.org/10.1016/0031-0182(93)90087-Y.

Hoorn, C, Javier Guerrero, J., Sarmiento - Pérez, G. A., Lorente, M. A. (1995). Andean tectonics as a cause for changing drainage patterns in Miocene northern South America. Geology, 23: 237-240.

Hoorn, C., Bogotá-A, G. R., Romero-Baez, M., Lammertsma, E. I., Flantua, S. G. A., Dantas. E. L., Dino, R., Do Carmo, D. A., Chemale Jr, F. (2017). The Amazon at sea: Onset and stages of the Amazon River from a marine record, with special reference to Neogene plant turnover in the drainage basin. Global and Planetary Change, 153, 51-65. https://doi.org/10.1016/j.gloplacha.2017.02.005.

https://www.bodc.ac.uk/data/published_data_library/

Inter American Development Bank, (2022). Inter-American Development Bank Annual Report 2022: Financial Statements, 132 pp.

Krook, L. (1979). Sediment petrographical studies in Northern Suriname. PhD Thesis, VU University Amsterdam. 154 pp.

Kroonenberg, S. B., Melitz, P. J. (1983). Summit levels, bedrock control and the etchplain concept in the basement of Suriname. Geologie en Mijnbouw, 95: 389-399.

Kroonenberg, S., Noordam, D. (2018). Geology, Landforms, and Soils. In: Natural history and ecology Suriname: 22-39.

Latrubesse, E.; Stevaux, J.; Sinha, R. Tropical rivers. Geomorphology 2005, 70, 187–206.

Noorthoorn van der Kruyff, J. F. (1970). *Suriname onshore exploration 1968/1970. Summary, petroleum engineering and geology - Shell Suriname Exploratie en Productie Maatschappij*.

Parizanganeh, A., Lakhan, V. C., Ahmad, S. R. (2008). Dynamics of mudbanks along a coast experiencing recurring episodes of erosion and accretion. Journal of Marine Engineering, 4 (7), 70-79.

Sinha, R., Jain, V., Tandon, S. K. (2012). River Systems and River Science in India: Major Drivers and Challenges. In: Earth System Processes and Disaster Management. Eds. Sinha, R., Ravindra, R. Berlin, 67-90. https://doi.org/10.1007/978-3-642-28845-6_6.

Vandenberghe, J. River terraces as a response to climatic forcing: Formation processes, sedimentary characteristics and sites for human occupation. Quaternar International 2015, 370, 3–11. https://doi.org/10.1016/j.quaint.2014.05.046.

Van Soelen, E. E., Kima, J-H., Santos, R. V., Dantas, E. L., Vasconcelos de Almeida, F., Pires, J. P., Roddaz, M., Sinninghe Damsté, S. S. (2017). A 30 Ma history of the Amazon River inferred from terrigenous sediments and organic matter on the Ceará Rise. Earth and Planetary Science Letters 474, 40–48. http://dx.doi.org/10.1016/j.epsl.2017.06.025.

Wijmstra, T. A. (1971). The palynology of the Guiana Coastal Basin. PhD Thesis, Vrije Universiteit Amsterdam, 71 pp.

Winterwerp, J. C., De Graaff, R.F., Groeneweg, J., Luijendijk, A. P. (2007) Coastal engineering, 54 (3), 249-261. https://doi.org/10.1016/j.coastaleng.2006.08.012.

Wong, Th. E. (1986). Outline of the stratigraphy and the geological history of the Suriname coastal plain. Geologie en Mijnbouw, 65, 223-241.

Wong, Th. E. (1989). Revision of the stratigraphy of the coastal plain of Suriname. Uitgaven "Natuurwetenschappelijke studiekring voor Suriname en de Nederlandse Antillen, 25: 64pp.

Wong, Th. E. (1994). The Paleocene-Eocene succession in the Guiana Basin. Bulletin van de Belgische Vereniging voor Geologie, 103 (3-4), 281-291.

Wong, Th. E., de Kramer, R., de Boer, P. L., Langereis, C., & Sew-A-Tjon, J. (2009). The influence of sea-level changes on tropical coastal lowlands; the Pleistocene Coropina Formation, Suriname. *Sedimentary Geology*, *216*(3–4), 125–137. https://doi.org/10.1016/j.sedgeo.2009.02.003

Wong, Th. E. Kroonenberg, S.B., Augustinus, P. G. E. F. (2016). Geologie en landschap van Suriname. LM Publishers, Edam, 182 pp.

Zhao, M., Cheng, C., Zhou, Y., Li, X., Shen, S., Song, C. (2021). Aglobal dataset of annual urban extents (1992–2020) from harmonized nighttime lights. Earth System Science Data, 14, 517–534. https://doi.org/10.5194/essd-14-517-2022.



Chapter 2

Evolution of the Suriname coastal environment based on a Cenozoic sedimentary record (Powisi-01)

Kathleen Gersie[a,b,h*], Roel Verreussel[c], Elton Luiz Dantas[d], Roberto Ventura Santos[d], Martin Roddaz[e], Raul Giovanni Bogota-Angel[f], Henry Hooghiemstra[b], Angelo Plata Torres[g], Hanna van den Hil[b], Ronald van Balen[h], Carina Hoorn[b]

* Corresponding author
Affiliations:
[a.] *Department of Geosciences, Anton de Kom University of Suriname, Leysweg 86, Paramaribo, Suriname, kathleen.gersie@uvs.edu*
[b.] *Institute for Biodiversity and Ecosystem Dynamics, University of Amsterdam, Science Park 904, 1098XH, Amsterdam, The Netherlands, k.gersie@uva.nl; h.hooghiemstra@uva.nl; hanna.vandenhil@justformail.nl; m.c.hoorn@uva.nl*
[c.] *TNO Reseacrh Institute, Princetonlaan 6, 3584CB, Utrecht, The Netherlands, roel.verreusel@tno.nl*
[d.] *Labaratório de Geocronologia, Instituto de Geociências, Universidade de Brasilia, Brasilia, DF 70910-900, Brazil, elton@unb.br;* rventura@unb.br
[e.] *Géosciences-Environnement Toulouse, Université de Toulouse; UPS (SVT-OMP); CNRS; IRD; 14 Avenue Édouard Belin, F-31400 Toulouse, France, martin.roddaz@get.omp.eu*
[f.] *Facultad del Medio Ambiente y Recursos Naturales, Universidad Distrital Francisco Joséde Caldas, Bogotá D.C. Colombia, angeloplata@gmail.com*
[g.] *Instituto de Investigaciones en Estratigrafía (IIES), Grupo de Investigaciones en Estratigrafía y Vulcanología (GIEV-Cumanday) y Departamento de Ciencias Geológicas, Universidad de Caldas, Calle 65 # 26-10, Manizales, Colombia, ragiob@yahoo.com*
[h.] *. Department of Earth Sciences, VU University of Amsterdam, De Boelelaan 1100, 1081HZ, Amsterdam, The Netherlands, r.t.van.balen@vu.nl*

ABSTRACT

The coastline of the Guianas is characterized by mudflats formed by Amazon River sediments. In this study we investigate the history of the Suriname coastal environment and vegetation. We analysed samples from the nearshore Powisi-01 well and determined the palynological and geochemical composition of these sediments. We identified two main palynological zones and six subzones, which represent biome changes throughout the Cenozoic. In the well-section, between 700 to 600 metres below sea level (mbsl), diagnostic palynomorphs of Late Paleocene to earliest Eocene age occur, including abundant palms and other angiosperms. A peak of Apectodinium spp. dinoflagellate cysts at 610 mbsl signals the Paleocene-Eocene Thermal Maximum (PETM), the first formal documentation of this hyperthermal along the Equatorial Atlantic Margin. A barren section follows, that is overlain by Early Miocene (500 to 275 mbsl), and Middle/Late Miocene to Pleistocene sediments (200 to 175 mbsl). The Neogene record is dominated by Rhizophoraceae mangrove pollen, but their appearance is not concomitant to Amazon muds. Throughout the section palynological diversity is high and pointing at a tropical lowland flora in the hinterland. The Sm-Nd isotopic composition further indicate that sediments are mainly of cratonic provenance, with the top c. 200 m of the section presenting a mixed sediment signal of Andean/Amazon, Orinoco, and Amazon craton-derived sediments. Regional literature suggests a Late Miocene arrival of (Andean) sediments at the Guiana coastline. However, further study is needed to pinpoint the precise onset of Amazon River influence along the Guianas coastline and its transformative effect on coastal vegetation.

Keywords: Guianas, PETM, geochemistry, biostratigraphy, Rhizophoraceae, mangroves

1. INTRODUCTION

The 350-km long coastline of Suriname forms part of the c. 1500 km long Guianas coastal system (Fig. 1) that stretches between the Amazon River delta (Brazil), on the southeastern side, and the Orinoco River delta (Venezuela), on the northwestern side. The shore-attached mud banks of 10 to 40 km long (Baltzer et al., 2004) are fed through cyclic sediment input from the Amazon River and form the stand-out feature of this coastline (Lyell, 1832 - cited by Krook, 1984; Eisma et al., 1991; Eisma & van der Marel, 1971). The Amazon mud distribution along the Guianas' coastline dates back at least as far as the Pleistocene period (Wong et al., 2009; see also Anthony et al., 2013), but it is still uncertain when this system first developed in Suriname. However, geological exploration in the Guyana Basin suggests a Late Miocene age for Amazon River influence along the coastline (Mapes and Torres, 2017 & 2022).

The Guianan coastal mud banks host a highly diverse mangrove ecosystem, a unique feature when compared to similar settings in West Africa and Southeast Asia (Baltzer et al., 2004). Recently, Antoine et al. (2024) showed that during the last interglacial (c. 120 ka; prior to human disturbance), the mangrove ecosystem of French Guiana harboured a rich species assemblage consisting of foraminifers, molluscs, bony fish, bryozoans, decapods, and sharks among others. This ecosystem likely evolved alongside the mud banks, which raises the question "W*hen did this biodiverse mud bank ecosystem originate*?".

The development of the Suriname-Guyana Basin is linked to significant plate tectonic activity and global sea level changes. The stratigraphic record in this basin (Fig. 2) reveals that production of carbonates in the Suriname-Guyana Basin was halted in the Late Miocene by the delivery of siliciclastic sediments from the crystalline Guiana Shield (Wong & Van Geuns, 2020). The Demerara Rise, an offshore marine mount (similar to the Ceara Rise) situated in the proximity of the Guianan coastline, displays a transitional zone of Late Miocene to Pliocene sediments derived from the Amazon River (Patier et al., 2015; Fanget et al., 2020). These findings suggest a different type of coastal setting prevailed in Suriname since the Late Neogene.

The Suriname coastal evolution resembles in many ways the evolution of the Foz do Amazonas Basin. In the Early Miocene the eastern Amazon was dissected by a proto-Amazon River, which transported modest volumes of craton-derived clastic sediments to the continental margin (Figueiredo et al., 2009, 2010; Hoorn et al., 2017a). In the Middle Miocene, this fluvial system extended westward. In the Late Miocene, after Andean sediments reached the Equatorial Atlantic Margin, marine carbonate production was halted in the Foz do Amazonas (Figueiredo et al., 2009, 2010; Hoorn et al., 2017a; Moizinho et al., 2025), aswell as at the Ceara Rise (Dobson et al., 1997; van Soelen et al., 2017).

In this study we hypothesize that: a) the Paleogene section is dominated by cratonic sediments and a mangrove system with no modern analogue; b) the Guianan mangrove ecosystem developed its modern character after the arrival of Amazon River mud, and c) the Neogene section shows the influence of the Amazon River along the Suriname coastline. To investigate this, we pursue the following objectives: a) correlate the Cenozoic biostratigraphic record of the Suriname section with pre-existing biostratigraphic zonations for the Amazon Fan, Guiana coastline and Caribbean (i.e., Colombia, Venezuela, and Trinidad), b) determine the geochemical composition of the Cenozoic sedimentary record in the Powisi-01 section and differentiate between Andean and cratonic provenance, and c) to reconstruct the paleoenvironments and paleoecosystems recorded in this section by means of palynological, lithological and geochemical analyses.

To reach our objectives, we selected the Powisi-01 well, which reaches about 900 (mbsl) and is located approximately 30 km offshore with water depths around 10–20 m. The results of this study will enable us to discriminate the different sediment source areas (Andean or cratonic), to reevaluate the pre-existing age model and, potentially, determine the effect of Andean muds on the coastal landscape and vegetation of Suriname coast.

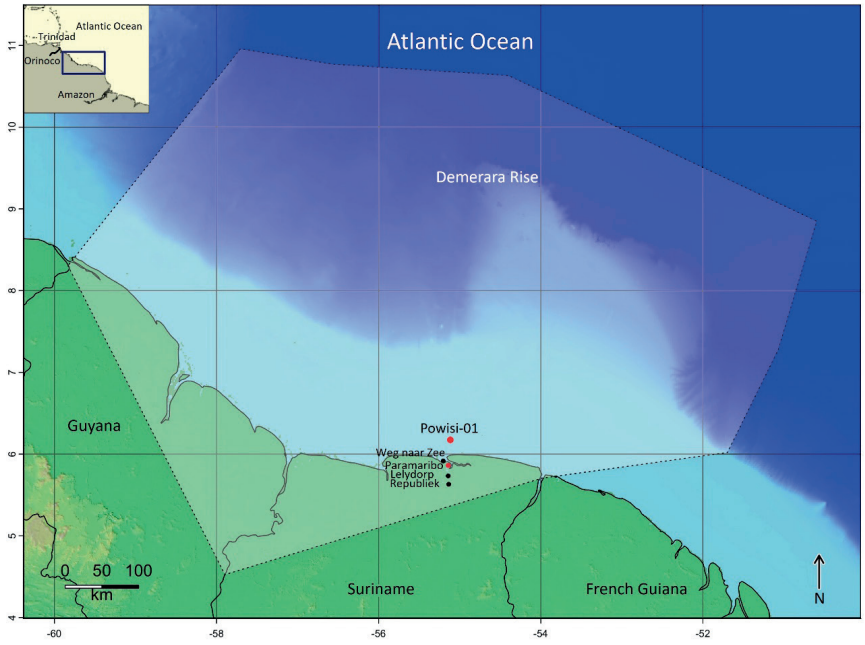


Figure 1: Map with the outline of the Suriname-Guyana Basin and location of the Powisi-01 well.

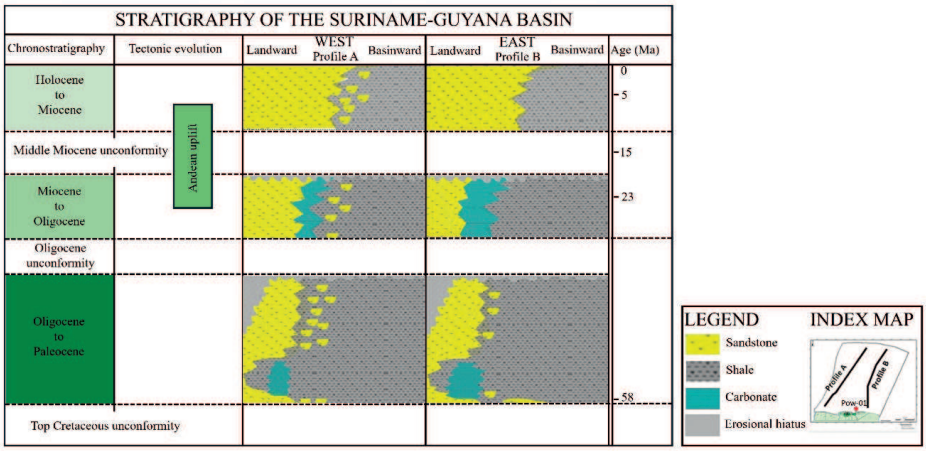


Figure 2: General stratigraphy of the Suriname-Guyana Basin (modified after www.staatsolie.com; source: online, May 2025). Two south-north profiles A and B situated in the Guyana Basin display the lithology from the Paleocene to Holocene. Remarkable are the carbonates present in the basin from the Paleocene, and disappear during the Miocene.

2. GEOGRAPHICAL AND GEOLOGICAL SETTING

2.1 STRATIGRAPHY OF THE SURINAME-GUYANA BASIN

Situated on the northern part of South America (Fig. 1), the Suriname-Guyana Basin includes offshore areas and coastal plains of French Guiana, Suriname, Guyana and eastern Venezuela (Wong, 1986). The basin is characterized by its passive-margin setting, which dates back to the Cretaceous period (Delhaye-Prat et al., 2024). In the south, it is bordered by a craton of Proterozoic age, also known as the Precambrian crystalline Guiana Shield. The main clastic sediments in the basin are the result of weathering, erosion and transport of this shield (Wong & Van Geuns, 2020). At the northern end of the basin, Oligocene-Miocene reef carbonates (www.staatsolie.com, 2023) occur at the paleo-shelf edges, while in the deeper parts of the basin turbidites occur, with submarine fans originating from vast shelf-edge canyons (Kelly & Doust, 2016). Major plate tectonic movements and global sea level movements have played an important role in the development of the Suriname-Guyana Basin (Wong & Van Geuns, 2020), which is also related to the evolution of the North Atlantic (Pindell & Kennan, 2001).

2.2 THE CORANTIJN GROUP

The Alliance, Burnside, Coesewijne and Zanderij Formations are part of the Cenozoic Corantijn Group that predominantly consists of clastic sediments mainly formed by an alterna-

tion of sands and clays. These sediments were deposited under fluvial and marine conditions on the coastal plain of Suriname (Fig. 3) (Wong, 1986). The ages of these formations were established by means of palynological studies by Van der Hammen & Wijmstra (1964), Wijmstra (1971), and Amstelveen (1969, 1971).

The Paleocene Alliance Formation occurs in a narrow strip along the northern part of the coastal plain. It extends from the northwestern part of French Guiana to Weg naar Zee (Suriname), and the near coastal offshore areas. The base of the Alliance Formation corresponds to the seismic marker RM 10, an unconformity between the Upper Cretaceous and the Lower Paleocene (Wong, 1986). Microfossils in this formation indicate that deposition took place in a protected coastal lagoon during the last part of the Paleocene (58 to 55 Ma) (Drooger, 1960). The thickness of the formation in the coastal plain reaches 40 to 60 m, gradually increasing northwards (Wong et al., 2016). The time-equivalents of the Alliance Formation are the Onverdacht and Saramacca formations, with the development of the Onverdacht Formation extending into the Eocene (Wong et al., 2009). During the Late Eocene to Oligocene, pronounced weathering processes transformed alluvial sediments into bauxite, marking the so-called Bauxite Hiatus — a period characterized by non-deposition (Monsels & Van Bergen, 2019) and uplift in the Guiana Shield (Japsen et al., 2025).

The Burnside Formation consists of a thick package of coarse-grained sand and several thin clay layers. Like the Saramacca and Alliance formations, this formation has a patchy geographical distribution and may reach up to 80 m thickness in the western part of the coastal plain. This formation was deposited in the Oligocene (34 to 23 Ma), when rivers deposited large amounts of erosive material from the hinterland in incised depressions of the coastal plain (Wong et al., 2016).

The Miocene Coesewijne Formation consists of sandy clays and clays with interbedded sands (Dixon, 1972). According to Wijmstra (1971), this unit corresponds to pollen zones E and F, Early and Middle Miocene respectively (Fig. 4). In the coastal area the thickness of the formation varies from 90 m in the east to 150 m in the west. Locally, this formation is in unconformable contact with the underlying Alliance Formation (Paleocene-Lower Eocene), the Burnside Formation (Oligocene), and the Precambrian basement. During a major Early Miocene transgression, beach sands and swampy clays were deposited as far south as Lelydorp (Wong, 1986). Krook (1979) attributed this to beach drifting and associated the considerable clay deposits with sediment contributions from the developing Amazon River. Wijmstra (1971) further noted that this transgression significantly transformed coastal vegetation, marked by the initial emergence of mangrove species such as *Rhizophora*.

Following this brief depositional cycle, which continued until the mid-Early Miocene, a gentle uplift led to a regression and erosion of a significant part of Lower Miocene and underlying sedimentary sequence (Wong, 1986). The resulting unconformity is associated to seismic

reflector RM 8 (mid Lower Miocene) that can be traced throughout the entire coastal plain (Noorthoorn van der Kruyff, 1970; Wong, 1986). Subsequently, during the Middle Miocene an extensive transgression occurred, that extended Suriname coastline southward to Republiek (Krook, 1979). Deposition of the Coesewijne Formation ceased during this period, as the Late Miocene marks a return to regressive conditions and a shift of the coastline far north by the end of the Miocene (Wong, 1989). Palynological studies conducted by Noorthoorn van der Kruyff (1970) and Wijmstra (1971) indicated that much, if not all, of the Middle and Upper Miocene sequences are absent along the entire coastline.

The overlying Zanderij Formation was deposited in the Pliocene (5.33-2.58 Ma) (cf. Dixon, 1972; Wong, 1989) by rivers that, during a relatively dryer climate, flowed from the hinterland of Suriname to the north (Wong et al., 2016). This unit, which overlies unconformably the Coesewijne Formation, consists of white and brown kaolinitic quartz sands interbedded clays, and is unconformable overlying the Coesewijne Formation (Fig.3).

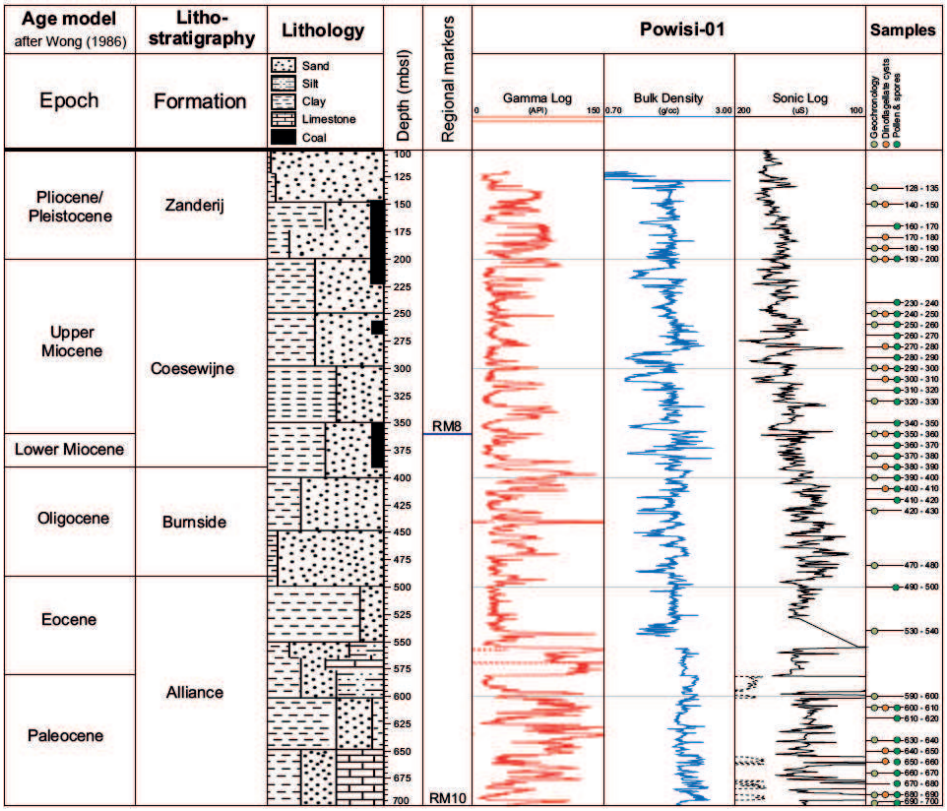


Figure 3: Powisi-01 well log data and geological formations (source: Staatsolie). With age model based on Wong (1986). The gamma ray log is the result of natural radioactivity of the subsurfae formations; the resistivity log is the result of the electrical resistivity of the formations that surround the borehole; the density log is the result of the bulk density of formations. RM8 = Regional Marker 8; RM10 = Regional Marker 10)

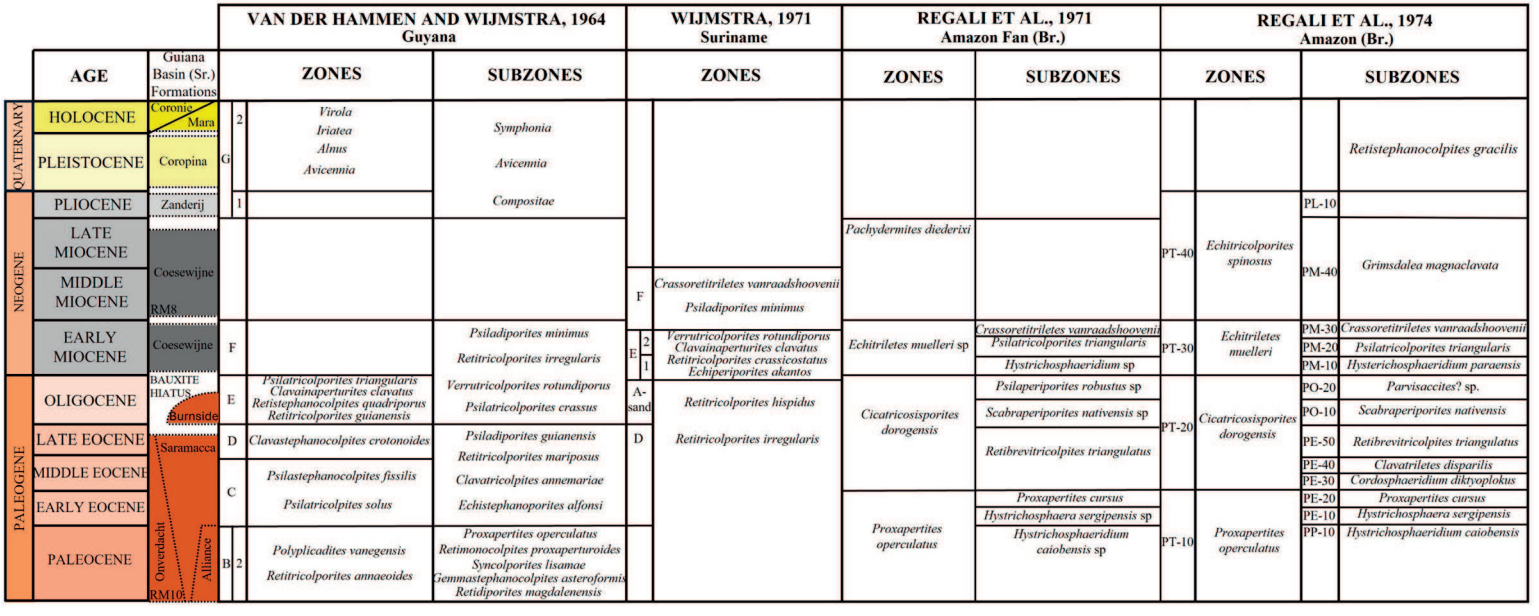


Figure 4: Stratigraphic correlation diagram of sedimentary basin along the Guianas coastline and the Brazilian Equatorial Margin.

3. MATERIALS AND METHODS

3.1 POWISI-01 WELLSITE AND LITHOSTRATIGRAPHY

3.1.1 Well information

The Powisi-01 exploration well, operated by Staatsolie Maatschappij Suriname N.V., was drilled by Halliburton N.V. in October 2019. The well is located 30 km offshore at lat. 6.1738° N, long. 55.1161° W (Fig. 1). The drilled section covers a total depth of 900 m below mean sea level (mbsl) and was part of a hydrocarbon exploration campaign in the nearshore area of Suriname. Geophysical measurements of the subsurface lithology were conducted by Schlumberger, and lithostratigraphic interpretations—including geological formations and their estimated ages—were derived from downhole well log data (Fig. 3). Water-based drilling mud, sourced from the Baroid facility in the United States, was used throughout the operation. Cutting samples acquired at 10-meter intervals were made available for geochemical and palynological study by Staatsolie N.V. (Table 1).

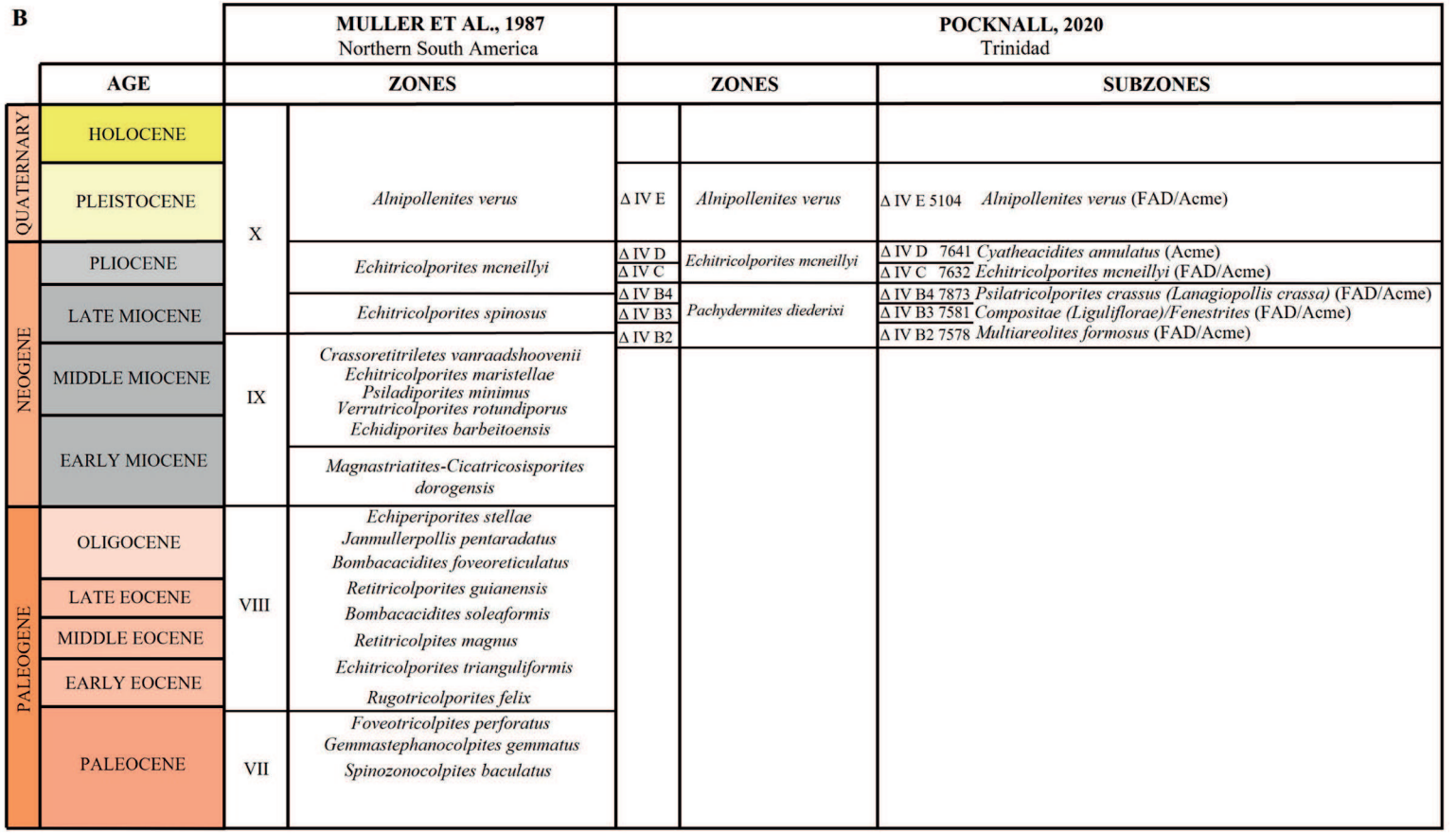
3.1.2 Biostratigraphic reference models

Wong (1986) presented an age model for the Suriname coastal lithostratigraphy based on palynological data by Van der Hammen & Wijmstra (1964), Wijmstra (1969), Noorthoorn van der Kruyff (1970), Wijmstra (1971) and Regali (1971) (Fig. 4). These palynostratigraphic schemes were tied to the foraminifer stratigraphy by Bolli (1966) and Hopping (1967) (see Wijmstra, 1969). According to Wong (1986; and pers. comment, 2024), the studied section ranges in age from Late Paleocene to Pleistocene. In our study, we reassess this age model using palynostratigraphic markers from the aforementioned studies together with those posterior ones from northeast South America and the Caribbean (Jaramillo et al., 2011; Lorente, 1986; Muller et al., 1987; Plata-Torres et al., 2024; Pocknall, 2020) (Fig. 5a,b).

A

	AGE	JARAMILLO ET AL., 2011 Colombia Llanos and Llanos foothills ZONES		PLATA-TORRES, 2024 Colombian Caribbean ZONES		LORENTE, 1986 Venezuela ZONES	
QUATERNARY	HOLOCENE	T-18	*Bombacacidites baculatus*	Car-12	*Cyatheadites annulatus* *Multiareolites formosus*	IX	*Alnipollenites*
	PLEISTOCENE						
NEOGENE	PLIOCENE	T-17	*Cytheacidites annulatus*			VIII	*Fenestrites longispinosus*
	LATE MIOCENE	T-16	*Fenestrites spinosus*	Car-11	*Fenestrites spinosus*	VII	*Asteraceae*
	MIDDLE MIOCENE	T-15	*Crassoretitriletes vanraadshoovenii*	Car-10	*Crassoretitriletes vanraadshoovenii*	VI	*Grimsdalea*
		T-14	*Grimsdalea magnaclavata*			V	*Crassoretitriletes*
						IV	*Psiladiporites*
	EARLY MIOCENE	T-13	*Echitricolporites maristellae*	Car-09	*Malvacipolloides maristellae*	III	*Verrutricolporites*
		T-12	*Horniella lunarensis*	Car-08	*Bombacacidites muinaneorum/* *Cibroperidinium enuitabulatum/* *Achomosphaera alcicornu/D.galea*	II	Interzone *Cicatricosisporites* *Verrutricolporites*
PALEOGENE	OLIGOCENE	T-11	*Cicatricosisporites dorogensis*	Car-07	*Proteacidites triangulatus*	I	*Magnastriatites-Cicatricosisporites dorogensis*
		T-10	Combined acme	Car-06	*Mauritiidites* Acme		
		T-09	*Foveotricolporites etayoi*	Car-05	*Psilatricolporites pachydermites* *Crassiectoapertites columbianus* *Magnastriatites grandiosus*		
		T-08	*Nothofagidites huertasii*				
	LATE EOCENE	T-07	*Echitricolporites trianguliformis orbicularis*	Car-04	*Polypodiisporites usmensis*		
	MIDDLE EOCENE	T-06	*Spinozonocolpites grandis*	Car-03	*Cicatricosisporites dorogensis* *Perisyncolporites pokornyi*		
	EARLY EOCENE	T-05	*Striatopollis catatumbus*	Car-02	*Cyclusphaera scabrata* *Spirosyncolpites spiralis* *Striatopollis catatumbus*		
		T-04b					
		T-04a					
	PALEOCENE	T-03b	*Foveotricolpites perforatus*	Car-01	*Foveotricolpites perforatus/* *Psilaperiporites suarezi-boliviensis*		
		T-03a	*Bombacacidites annae*				
		T-02	*Monocolporopollenites ovatus*				
		T-01	*Spinozonocolpites baculatus*				

Figure 4A: Stratigraphic correlation chart of some selected areas (Llanos and Llanos foothills, Colombian Caribbean, Venezuela) in Northern South America.



B		MULLER ET AL., 1987 Northern South America		POCKNALL, 2020 Trinidad		
	AGE	ZONES		ZONES		SUBZONES
QUATERNARY	HOLOCENE	X	*Alnipollenites verus*			
	PLEISTOCENE			Δ IV E	*Alnipollenites verus*	Δ IV E 5104 *Alnipollenites verus* (FAD/Acme)
NEOGENE	PLIOCENE		*Echitricolporites mcneillyi*	Δ IV D Δ IV C	*Echitricolporites mcneillyi*	Δ IV D 7641 *Cyatheacidites annulatus* (Acme) Δ IV C 7632 *Echitricolporites mcneillyi* (FAD/Acme)
	LATE MIOCENE		*Echitricolporites spinosus*	Δ IV B4 Δ IV B3 Δ IV B2	*Pachydermites diederixi*	Δ IV B4 7873 *Psilatricolporites crassus (Lanagiopollis crassa)* (FAD/Acme) Δ IV B3 7581 *Compositae (Liguliflorae)/Fenestrites* (FAD/Acme) Δ IV B2 7578 *Multiareolites formosus* (FAD/Acme)
	MIDDLE MIOCENE	IX	*Crassoretitriletes vanraadshoovenii* *Echitricolporites maristellae* *Psiladiporites minimus* *Verrutricolporites rotundiporus* *Echidiporites barbeitoensis*			
	EARLY MIOCENE		*Magnastriatites-Cicatricosisporites dorogensis*			
PALEOGENE	OLIGOCENE	VIII	*Echiperiporites stellae* *Janmullerpollis pentaradatus* *Bombacacidites foveoreticulatus*			
	LATE EOCENE		*Retitricolporites guianensis* *Bombacacidites soleaformis*			
	MIDDLE EOCENE		*Retitricolpites magnus*			
	EARLY EOCENE		*Echitricolporites trianguliformis* *Rugotricolporites felix*			
	PALEOCENE	VII	*Foveotricolpites perforatus* *Gemmastephanocolpites gemmatus* *Spinozonocolpites baculatus*			

Figure 5B: Stratigraphic correlation chart of some selected areas (Llanos and Llanos foothills, Colombian Caribbean, Venezuela) in Northern South America.

3.1.3 Lithology

At the base of the studied section (700 mbsl) sediments of the Alliance Formation occur, which consist of a mix of limestones, sands, and clays (from 700 to 620 mbsl), silt (from 620 to 590 mbsl), limestones (590 to 580 mbsl) and a mix of sands, clays and silts up to the top of the unit at 490 mbsl. The overlying interval, from 490 to 390 mbsl, is represented by sediments of the Burnside Formation. There is a notable dominance of clays over sands between 480 and 440 mbsl and between 420 and 390 mbsl. The interval from 390 to about 200 mbsl is represented by the Coesewijne Formation and starts off with dominance of clays over sands up to 330 mbsl. The remaining interval of the Coesewijne Formation, between 330 and 200 mbsl is dominated by sands. The upper part of the studied section, i.e. from 200 to 100 mbsl, is represented by the Zanderij Formation and consists predominantly of clays. Stratigraphic unconformities, known as Regional Marker 8 (RM 8) and Regional Marker 10 (RM 10) occur at respectively 700 and 360 mbsl (Fig. 3).

3.2. GEOCHEMISTRY

3.2.1 Sample collection

To determine the provenance of the Powisi-01 sediments, we collected 27 samples between 700 to 128 mbsl. Twenty samples were analysed for their major and trace element concentrations, and 27 samples were analysed for their Sm-Nd isotopic composition. The major and trace element concentrations were measured at the Service d'Analyse des Roches et Minéraux (SARM, INSU facility, Vandoeuvre-Les-Nancy, France) by ICP-OES (Na, Mg, K, Ca, Sc, Ti, Mn, Fe, Al, Si and P) and ICP-MS (Rb, Cs, Ba, Sr, Th, U, Y, Zr, Nb, Hf, Cr, V, Co, Cu, Ni, Zn, La, Ce, Pr, Nd, Sm, Eu, Gd, Tb, Dy, Ho, Er, Tm, Yb, Lu and Ta) after alkali fusion. Analytical details are available on http://Helium.Crpg.Cnrs-Nancy.Fr/SARM/ and in Carignan et al. (2001). Uncertainty is lower than 5% for elements measured by ICP-OES, and lower than 10% for elements measured by ICP-MS.

To facilitate comparisons with sediments derived from basic or felsic sources (Cullers & Podkovyrov, 2000) and the Post Archean Australian Shales (PAAS) (McLennan, 2001; Pourmand et al., 2012; Taylor & McLennan, 1985), the Eu anomaly is calculated with respect to chondrites: $Eu/Eu^{*} = EuN/(SmN \times GdN)1/2$, where N refers to the chondrite-normalised concentration value (Condie, 1993). The Cerium anomaly (ΩCe) normalised to PAAS is calculated following (De Baar et al., 1985): $\Omega Ce = 2 \times (Cesample/CePAAS) / [(Lasample/LaPAAS) + (Prsample/PrPAAS)]$, where Xsample is the concentration of samples and XPAAS refers to the concentrations of the PAAS standard.

The Nd-Sm isotopic analysis was carried out at the Laboratório de Estudos Geodinâmicos, Geocronológicos e Ambientais (LEGGA) of the Universidade de Brasília (UnB). The $^{147}Sm/^{144}Nd$ and $^{143}Nd/^{144}Nd$ isotopic ratios were measured using the Neptune High Resolu-

tion Multicollector ICP-MS. Sample preparation comprised crushing sample aliquots with a ball mill followed by sample digestion. Rare Earth Element (REEs), Sm, and Nd elements were separated by chromatography columns, as described by Gioia & Pimentel (2000). To achieve the accuracy and quality of the measurements, repeated analyses were done on the BHVO-2 reference material (standard). The $^{143}Nd/^{144}Nd$ ratio was normalized using $^{146}Nd/^{144}Nd = 0.7219$ to correct the signal for mass fractionation. The measured $^{143}Nd/^{144}Nd$ sample ratios are expressed in epsilon notation as the fractional deviation in parts per 10^4 (units) from $^{143}Nd/^{144}Nd$ value of the Chondritic Uniform Reservoir (CHUR). This notation is defined as:

$$\varepsilon Nd(t) = [(^{143}Nd/^{144}Nd)sample(t) / (^{143}Nd/^{144}Nd)CHUR(t) - 1] \times 10^4$$

where t indicates the time at which εNd is calculated. Here, no time correction was applied

(t = 0) and the $^{143}Nd/^{144}NdCHUR(0) = 0.512638$ (Jacobsen & Wasserburg, 1981).

The Nd model age (T_{DM}) is calculated by the following formula:

$$T_{DM} = \frac{1}{\lambda} \ln \left(\frac{(^{143}Nd/^{144}Nd)_0 - (^{143}Nd/^{144}Nd)_{DM}}{(^{147}Sm/^{144}Nd)_0 - (^{147}Sm/^{144}Nd)_{DM}} + 1 \right)$$

The measured isotope values (sample, now) are $^{143}Nd/^{144}Nd_0$ and $^{147}Sm/^{144}Nd_0$. Calculated Sm-Nd isotope ratios for Depleted Mantle (DM) are presented as DM ratios in the formula (Hoorn et al., 2017b).

3.2.2 Provenance using elemental geochemistry and Nd isotopes

Providing that they are not modified by sedimentary sorting and clay authigenesis, (McLennan et al., 1993; Mourlot et al., 2018; Roddaz et al., 2021, 2014), selected trace element ratios (e.g. Eu/Eu*, Cr/Th and Th/Sc ratios), REE concentrations, and Nd isotopes can be used for determining the provenance of ancient marine sediments. The effects of sedimentary sorting can be evaluated using correlation of provenance proxies listed above with the Al/Si ratio which is considered as a proxy for grain size (Bouchez et al., 2011). The influence of authigenesis can be checked by inspecting REE patterns because authigenic smectites are characterized by Light Rare-Earth Elements (LREE) depletion, Heavy Rare-Earth Elements (HREE) enrichment, and negative Ce anomalies ($\Omega Ce < 0.50$, (De Baar et al., 1985), typical of seawater (Piper, 1974).

The provenance ratios and the Nd isotopes have been proven useful tools for ancient marine sediments to reconstruct a) past oceanic circulations (Mourlot et al., 2018; Roddaz et al., 2020), b) erosional history of the adjacent cratons (Liu et al., 2017; Mourlot et al., 2018;

Roddaz et al., 2020) and c) continent wide paleodrainage histories (Clift & Blusztajn, 2005; Figueiredo et al., 2009; Hoorn et al., 2017a; Liu et al., 2017; van Soelen et al., 2017) because Nd as REE is not easily fractioned by sedimentary or post-depositional processes ((McLennan et al., 1993) and references therein). In the case of the northern part of South America, the Nd isotopes are particularly useful because the sediment transported by rivers draining the northern part of South America are characterized by distinct Nd isotopic composition.

The Suspended Particular Material (SPM) of the Orinoco River have εNd(0) values of -14.1 ±0.3 (Rousseau et al., 2019), whereas SPM transported by modern cratonic rivers have less radiogenic Nd isotopic composition with εNd(0) values < -15 (Allegre et al., 1996; Bayon et al., 2015; Rousseau et al., 2019) and SPM transported by Andean Amazonian rivers are more radiogenic in Nd isotopic composition with εNd(0) values > -12.1 (Viers et al., 2008). The Nd isotopic composition of the SPM of Madeira River, which drains the southern part of the Amazonian Andes, are less radiogenic than those of the Solimões River, which drains the northern part of the Amazonian Andes (Viers et al., 2008). The Nd isotopic composition of the SPM of the Amazon River is a mix of those of the Madeira and Solimões with εNd(0) values of-10.6 ±0.6 (Rousseau et al., 2019) and are similar to the εNd(0) values of the Amazon Delta sediments (-10.5 and -10.7, (Bayon et al., 2015)). These differences in the Nd isotopic compositions of modern sediments can be used for determining the provenance of ancient Amazonian sediments. The cratonic sedimentary rocks are characterized by εNd(0) values lower than -14.5, whereas sedimentary rocks sourced by the Andes have εNd(0) values > -13.8 (Figueiredo et al., 2009; Horbe et al., 2013; Roddaz et al., 2005).

3.3 PALYNOLOGY

The palynological analysis of the marine palynomorphs (dinoflagellate cysts) was carried out separately from the terrestrial palynological analysis (pollen and spores). The processing of samples to dinoflagellate cyst analysis differs slightly from the processing to pollen and spore. The methodology and the results of the dinoflagellate cyst analysis are therefore presented separately from the pollen and spore analysis.

3.3.1 Dinoflagellate cyst analysis

Fifteen samples were selected and processed for dinoflagellate cysts (Table 1). The samples range from 690 to 150 mbsl, comprising the Alliance, Burnside, Coesewijne and Zanderij formations.

Table 1: Sample list displaying the selected cutting samples from the Pow-01 for the geochronological, dinoflagellate cyst and pollen and spore analyses.

Samples (mbsl)	Geochemistry REE/LREE/HREE	Geochemistry Sm/Nd	Dinoflagellate cysts	Pollen and spore	Lithostratigraphy
128-135	X	X			
135-140		X			Zanderij Fm
140-150	X	X	X		
150-160		X			
160-170		X		X	
170-180		X	X		
180-190	X	X	X		
190-200	X	X	X	X	
200-210		X			
220-230		X			
230-240		X		X	
240-250	X	X	X	X	Coesewijne Fm
250-260	X	X		X	
260-270				X	
270-280			X	X	
280-290				X	
290-300	X	X	X	X	
300-310			X	X	
310-320				X	
320-330	X	X		X	
340-350			X	X	
350-360	X	X		X	
360-370				X	
370-380	X	X		X	
380-390			X	X	
390-400	X	X		X	
400-410			X	X	Burnside Fm
410-420				X	
420-430	X	X			
470-480	X	X			

Table 1: Sample list displaying the selected cutting samples from the Pow-01 for the geochronological, dinoflagellate cyst and pollen and spore analyses. (*continued*)

Samples (mbsl)	Geochemistry REE/LREE/HREE	Geochemistry Sm/Nd	Dinoflagellate cysts	Pollen and spore	Lithostratigraphy
490-500				X	
530-540	X	X			Alliance Fm
590-600	X	X			
600-610	X	X	X	X	
610-620				X	
630-640	X	X		X	
640-650			X	X	
650-660			X	X	
660-670	X	X		X	
670-680				X	
680-690	X	X	X	X	
690-700	X	X		X	
Total samples	20	27	15	30	

3.3.1.1 Processing and analysis

All samples were processed at the Institute of Biodiversity and Ecosystem Dynamics (IBED), University of Amsterdam, following the standard palynological method. About 2.0 g of each sediment was processed to isolate the organic fraction. Thereafter samples were decalcified with HCl, dispersed of clays with sodium pyrophosphate (Na4P2O7), acetolysed to remove cellulose, and underwent bromoform separation to isolate concentrate organic material. Subsequently, residues were sieved with a 15µ sieve mesh to concentrate dinoflagellate cysts. It is worth mentioning that no *Lycopodium* tablets have been added. The resulting organic matter was mounted on microscope slides, embedded in glycerin jelly and sealed with paraffin. The microscope slides were then analyzed for dinoflagellate cysts only at the Netherlands Organisation for Applied Scientific Research (TNO). The dinoflagellate cysts were counted to 100 specimens if possible. The aim for the dinoflagellate cyst analysis was to provide additional information on age and paleoenvironment of the studied interval. Residues are stored at the IBED laboratory.

3.3.2 Sporomorph analysis

3.3.2.1 Sample collection

Out of the 100 cutting samples available for the Powisi-01 well 30 were selected for sporomorph (pollen and spores) analysis. The sample depths ranged between 700 and 100 mbsl and each cuttings sample represents an interval of 10 meters.

3.3.2.2 Processing method

As the sediment samples in this well were mainly composed of sandstone and limestone, they needed to be decalcified using hydrochloric acid. This was followed by deflocculation, which means separation of the inorganic clay fraction from the organic one, using sodium pyrophosphate, and acetolysis. Finally, bromoform (s.g. 2.9 g/cm^3) was used for density separation. The resulting organic matter residue was kept in glycerin. For estimation the pollen concentration within each sample-sediment, a tablet of *Lycopodium clavatum* spores (18.407 spores; batch number 42.206–42.427) was added at the beginning of the process (Hoorn et al., 2017).

3.3.2.3 Analysis

In this study we applied classic palynostratigraphy combined with palaeoecological approaches to reconstruct composition and changes in coastal vegetation. These data also formed the basis for a palynological diversity assessment. The sediment samples that were used in this study were cuttings; therefore, we primarily use last occurrence datum (LOD) events before the first occurrence datum (FOD) as support for the age model. In this case, the LOD is most informative. This is because during the drilling process downhole contamination of sporomorphs and sedimentary material occurs (also known as caving), and consequently some sporomorphs can appear deeper than their original stratigraphic position.

A Leica light microscope type DM-DB was used for morphological description and identification of the pollen grains and fern spores, which were also photographed for later verification of the identification using concise metadata. The analysis was performed at 400x and 1000x magnification. Of the 30 samples, the pollen concentration of one sample was too low, three samples had a pollen sum of < 100, while 26 samples reached a pollen sum of > 100 grains. The pollen sum included all pollen grains and spores, and based on these counts we calculated the proportions of each pollen taxon enabling us to detect changes in pollen spectra between samples across the well. Together, the data reflect changes in terrestrial vegetation associated to the lowland areas of eastern Amazonia and on of Suriname's Guiana Shield. Andes Mountain taxa were rare to absent. The sporomorphs were tentatively grouped according to the ecological preferences of the nearest living relatives in the Amazon drainage basin and the Guiana Shield (Hoorn et al., 2017) (Table 1). After calculating the percentages, pollen diagrams were created using Tilia (Grimm, 2022) to show the variation of taxa with depth.

For the sporomorph identification we used reference works from the following countries and areas: Guyana (Van der Hammen & Wijmstra, 1964), Suriname (Wijmstra, 1971), Amazon Fan (Regali et al., 1974; Regali, 1971) (Fig. 4), Colombian Llanos (Jaramillo et al., 2011), Colombian Caribbean (Plata-Torres et al., 2024), Venezuela (Lorente, 1986), Northern South America (Muller et al., 1987), and Trinidad (Pocknall, 2020) (Fig. 5a,b). We used the biostratigraphic schemes in these works as a basis for our biostratigraphic interpretation. All identified taxa are listed in Table 2, including the botanical affinity, reference paper, England Finder location in the palynological slide, photo plate in this paper, laboratory number and sample depth.

3.3.4 Paleoecological grouping

The sporomorphs are grouped following ecological categories and the environments that they characterize (Table 2). The ecological significance and botanical affinities of these sporomorphs are based on Marchant et al. (2002) and Mabberley (1987). The composition by plant family of each category is listed in Table 3. The groups are: I) Mangroves, II) Palms, III) Herbs (Poaceae), IV) Ferns, V) Andean, VI) Taxa of known ecology subdivided in VI.a–VI.g, and VII) Taxa with unknown ecology.

Table 2: List with species names, authorities, botanical affinities, location in well and samples, and laboratory code

Taxon name	Family	Genus/Species	Reference	EF	Plate	Lab number	Depth (m)
#Caperonia	Euphorbiaceae			V15-4		T42.548	300-310
#Combretaceae-Melastomataceae	Combretaceae-Melastomataceae			K18-3		T42.552	290-300
#Odontadenia				V21		T42.543	610-620
#Sapotaceae-Burseraceae	Sapotaceae-Burseraceae		Hoorn 1993	Y22-4		T42.552	290-300
Aglaoreidia? *Foveolata*			Jaramillo and Dilcher 2001	U23-1		T42.550	690-700
Alnipollenites verus	Betulaceae	*Alnus*	Potonie 1934 [ex Potonie 1931]	Q31-2	III.4	T42.543	610-620
Annutriporites iversenii			Van der Hammen 1954	U17-4		T42.548	300-310
Arecipites cf. *perfectus*	Arecaceae			L30		T42.553	280-290
Arecipites spp.				U25-1	IV.2	T42.548	670-680
Baculamonocolpites sp. 1				U33-1		T42.553	280-290
Bombacacidites annae	Malvaceae (Bombac.)	*Bombax*	Van der Hammen 1954	U-23	II.1	T42.550	690-700
Bombacacidites baculatus	Malvaceae (Bombac.)	*Pachira*	Muller et al. 1987	X27-2		T42.417	270-280
Bombacacidites brevis	Malvaceae (Bombac.)		Dueñas 1980	M9-2		T42.423	350-360
Bombacacidites cf. *araracuarensis*	Malvaceae (Bombac.)	*Ceiba sp.*	Hoorn 1994	M23-1	III.1	T42.547	660-670
Bombacacidites fossulatus	Malvaceae (Bombac.)			Z22-4	III.2	T42.545	640-650
Bombacacidites protofoveoreticulates	Malvaceae (Bombac.)		Jaramillo and Dilcher 2001	Q8		T42.546	650-660
Bombacacidites psilatus	Malvaceae (Bombac.)		Jaramillo and Dilcher 2001	L26		T42.543	610-620
Brevitricolporites molinae	Apocynaceae		Schuler and Doubinger 1970	H26-4		T42.423	350-360
Brevitricolporites spp.				N36-3		T42.553	280-290

Table 2: List with species names, authorities, botanical affinities, location in well and samples, and laboratory code *(continued)*

Taxon name	Family	Genus/Species	Reference	EF	Plate	Lab number	Depth (m)
Catostemma altonii			Germeraad et al. 1968	F14		T42.425	390-400
Clavatricolpites densiclavatus	Euphorbiaceae		Jaramillo and Dilcher 2001	N22		T42.549	680-690
Crassiectoapertites columbianus	Fabaceae		(Dueñas) emend. Lorente 1986	V14		T42.552	290-300
Cricotriporites guianensis	Apocynaceae	*Forsteronia*	Leidelmeyer 1966	L16-4		T42.544	630-640
Cricotriporites operculatus			van Hoeken-Klinkenberg 1966	G19-4		T42.546	650-660
Crototricolpites cf. *annemariae*	Euphorbiaceae		Leidelmeyer 1966	S32-4		T42.540	410-420
Crototricolpites cf. *manihot*	Euphorbiaceae			R33-4		T42.542	600-610
Crototricolpites cf. *protoannemariae*	Euphorbiaceae		Jaramillo and Dilcher 2001	F12-4		T42.546	650-660
Cyperaceapollis sp.	Cyperaceae		Krutzsch 1970	R33		T42.542	600-610
Echidiporites barbeitoensis	Arecaceae (Mauritiinae)	*Korthalsia ferox*	Muller et al. 1987	T32-3		T42.417	270-280
Echimonocolpites spp.				L28-4		T42.542	600-610
Echiperiporites akanthos	Alismataceae	*Sagittaria*	Van der Hammen and Wijmstra 1964	K31	IV.15	T42.540	410-420
Echiperiporites germeraadii			Leite et al 2020	R20-3		T42.540	410-420
Echistephanoporites sp.				M12-2		T42.546	650-660
Echitricolpites spinosus	Asteraceae		Van der Hammen 1956	J35-1	IV.22	T42.553	280-290
Echitriporites suescae	Proteaceae		Van der Hammen 1954	N22		T42.546	650-660
Echitriporites trianguliformis	Proteaceae		Van Hoeken-Klinkenberg 1964	X12-4		T42.549	680-690
Foveotricolpites simplex	Euphorbiaceae	*Sapium*	D'Apolito et al. 2021 [Gonzalez 1967]	T10-1	II.9	T42.542	600-610
Gemmastephanocolpites gemmatus			Van der Hammen and Garcia 1966	P7-1	II.2	T42.548	670-680
Grimsdalea magnaclavata	Arecaceae (Mauritiinae)		Germeraad et al. 1968	E14-4	III.3	T42.546	650-660
Illexpollenites tropicales	Aquifoliaceae	*Illex*	Silva-Caminha et al. 2010	N19-3	IV.1	T42.552	290-300

Table 2: List with species names, authorities, botanical affinities, location in well and samples, and laboratory code *(continued)*

Taxon name	Family	Genus/Species	Reference	EF	Plate	Lab number	Depth (m)
Jandufouria saemrogiformis	Malvaceae	*Catostemma*	Germeraad et al. 1968	K25	III.12	T42.545	360-370
Ladakhipollenites? *garzonii*	Marcgraviaceae	*Norantea*	D'Apolito et al. 2021 [Hoorn 1993]	S35		T42.419	310-320
Lanagiopollis crassa	Tetrameristaceae		Frederiksen 1988 [Van der Hammen and Wijmstra 1964]	M17-2	III.11	T42.547	340-350
Longapertites cf. *vaneendenburgi*	Arecaceae		Germeraad et al. 1968	P33-2	II.6	T42.542	600-610
Longapertites proxapertites reticuloides	Arecaceae		Van der Hammen and Garcia 1966	U15-2	II.8	T42.544	630-640
Longapertites proxapertitoides proxapertitoides	Arecaceae		Van der Hammen and Garcia 1967	P21-2	II.7	T42.544	630-640
Longapertites spp.				K28-4		T42.548	670-680
Malvacipolloides maristellae	Malvaceae		Silva-Caminha et al. 2010 [Muller et al. 1987]	O9-2	III.5	T42.542	600-610
Mauritiidites crassibaculatus	Arecaceae	*Mauritia*	Van Hoeken-Klinkenberg 1964	V30		T42.545	640-650
Mauritiidites franciscoi franciscoi	Arecaceae	*Mauritia*	Van der Hammen 1956	M15	II.11	T42.548	300-310
Mauritiidites franciscoi minutus	Arecaceae	*Mauritia*	Van der Hammen and Garcia 1966	H22/3	II.12	T42.548	300-310
Microfoveotriporites cretaceous			Van Hoeken-Klinkenberg 1966	W25-4		T42.547	660-670
Momipites africanus	Betulaceae	*Corylus*	Van Hoeken-Klinkenberg 1966	Q20-2		T42.550	690-700
Monoporopollenites annulatus	Poaceae		Van der Hammen 1954	N21-4	II.13	T42.545	360-370
Paleosantalaceaepites cingulatus	Euphorbiaceae		Jaramillo et al. 2010	F14-3	IV.17	T42.423	350-360
Perfotricolpites digitatus	Convolvulaceae	*Merremia*	Gonzalez 1967	W20-3		T42.549	680-690
Perisyncolporites pokornyi	Malpighiaceae		Germeraad et al. 1968	L12-3	IV.20	T42.552	290-300
Podocarpidites spp.	Podocarpaceae	*Podocarpus*	Graham 1993	W24-3		T42.548	670-680
Proxapertites cursus	Araceae		van Hoeken-Klinkenberg 1964	L25	II.4	T42.544	630-640
Proxapertites humbertoides	Annonaceae		Van der Hammen 1954	J20-4	IV.3	T42.547v	660-670
Proxapertites minuthumbertoides			Jaramillo et al. 2010	O30		T42.545	640-650

Table 2: List with species names, authorities, botanical affinities, location in well and samples, and laboratory code *(continued)*

Taxon name	Family	Genus/Species	Reference	EF	Plate	Lab number	Depth (m)
Proxapertites minutus	Nymphaeaceae		Duenas 1980	Q27	IV.4	T42.549	680-690
Proxapertites operculatus	Araceae		Van der Hammen 1954	S31	II.3	T42.545	640-650
Proxapertites psilatus	Nymphaeceae		Sarmiento 1992	P30-3	IV.5	T42.548	670-680
Proxapertites tertiara	Annonaceae	*Crematosperma*	Van der Hammen and Garcia 1965	L25-3		T42.546	650-660
Psilabrevitricolporites cf. *triangularis*				L22		T42.548	300-310
Psilabrevitricolporites devriesii	Humiriaceae	*Humiria*	Lorente 1986	L14-2	IV.19	T42.552	290-300
Psiladiporites minimus	Moraceae		Van der Hammen and Wijmstra 1964	K30	III.6	T42.548	300-310
Psilamonocolpites amazonicus	Arecaceae	*Euterpe*	Hoorn 1994	T28-1	IV.10	T42.545	360-370
Psilamonocolpites grandis	Arecaceae		Van der Hammen 1954	S13-3		T42.540	410-420
Psilamonocolpites medius	Arecaceae		Van der Hammen 1956	K18	IV.12	T42.541	380-290
Psilamonocolpites nanus	Arecaceae	*Euterpe*	Hoorn 1993	P13-2	IV.9	T42.547	660-670
Psilamonocolpites rinconii	Arecaceae		Dueñas 1986	L30-1	IV.11	T42.552	290-300
Psilamonocolpites sp.				W28-4		T42.552	290-300
Psilaperiporites aff.	Apocynaceae			X23-1		T42.544	630-640
Psilaperiporites sp.				N22-2	IV.6	T42.549v	680-690
Psilastephanocolporites schneideri	Rhizophoraceae		Hoorn 1993	N31	IV.13	T42.552	290-300
Psilastephanoporites aff. *Apocynaceae*				V18-1		T42.552	290-300
Psilatricolpites papilioniformis			Regali et al. 1974	R17		T42.543	370-380
Psilatricolpites protoclarensis			Jaramillo and Dilcher 2001	O19-3		T42.550	690-700
Psilatricolporites costatus			Dueñas 1980	R27-1		T42.550	690-700
Psilatricolporites crassoexinatus			Hoorn 1993	S20		T42.552	290-300
Psilatricolporites exiguus				J23-3		T42.545	360-370

Table 2: List with species names, authorities, botanical affinities, location in well and samples, and laboratory code *(continued)*

Taxon name	Family	Genus/Species	Reference	EF	Plate	Lab number	Depth (m)
Psilatricolporites venezuelanus			Lorente 1986	S28-2		T42.552	290-300
Psilatriporites aff. *Moraceae*				S17-1		T42.548	670-680
Psilatriporites cf. *minimus*	Cannabaceae	*Celtis*	D'Apolito 2020	L25-1		T42.552	290-300
Psilatriporites corstanjei	Rubiaceae	*Faramea*	Hoorn 1993	Q23-3	IV.8	T42.542	600-610
Psilatriporites desilvae	Fabaceae (Caesalpin.)		Hoorn 1993	M17	IV.7	T42.547	340-350
Psilatriporites samientoi			Hoorn 1993	N29-3		T42.548	300-310
Racemonocolpites facilis	Arecaceae		Gonzalez 1967	M10		T42.544	630-640
Racemonocolpites racematus	Arecaceae	*Iriartea*	Van der Hammen 1954	K21-3		T42.550	690-700
Ranunculacidites operculatus	Euphorbiaceae	*Alchornea*	Jaramillo and Dilcher 2001 [Van der Hammen and Wijmstra 1964]	W25-2	II.14	T42.543	370-380
Retibrevitricolpites indet.							
Retibrevitricolpites retibolus	Rubiaceae	*Psychotria*	Leidelmeyer 1966	E24-2		T42.552	290-300
Retibrevitricolpites sp.1			Jaramillo and Dilcher 2001	U17		T42.550	690-700
Retibrevitricolporites catatumbus			Gonzalez Guzman 1967	T28-4		T42.552	290-300
Retibrevitricolporites pseudoretibolus			D'Apolito et al. 2021	N31-2		T42.542	600-610
Retibrevitricolporites solimoensis			Hoorn 1993	E19-4		T42.548	670-680
Retidiporites magdalenensis			Van der Hammen and Garcia 1966	N10		T42.546	650-660
Retimonocolpites bernardii			Gonzalez 1967	G24-4		T42.549	680-690
Retimonocolpites maximus	Arecaceae		Hoorn 1993	J15		T42.543	370-380
Retimonocolpites spp.				N27		T42.545	360-370
Retistephanocolpites williamsi	Ctenolophonaceae	*Ctenolophon*	Germeraad et al. 1968	T21-1		T42.545	360-370
Retitrescolpites? irregularis	Phyllantaceae	*Amanoa*	Jaramillo and Diclher 2001 [Van der Hammen and Wijmstra 1964]	N34-4	III.9	T42.547	340-350

Table 2: List with species names, authorities, botanical affinities, location in well and samples, and laboratory code *(continued)*

Taxon name	Family	Genus/Species	Reference	EF	Plate	Lab number	Depth (m)
Retitricolporites (Rhoipitus) guianensis	Malvaceae		Van der Hammen and Wijmstra 1964	Q24-1	II.10	T42.425	390-400
Retitricolporites brevis			Duenas 1980	V30		T42.553	280-290
Rhoipites crassicostatus			Van der Hammen and Wijmstra 1964	Q25-2		T42.548	670-680
Rhoipites hispidus			Jaramillo and Dilcher 2001 [Van der Hammen and Wijmstra 1964]	M31-2	III.10	T42.548	300-310
Rhoipites indet.							
Rhoipites oblatus			D'Apolito et al. 2021 [Hoorn 1994]	Y26		T42.539	400-410
Scabratriporites simpliformis			Van Hoeken-Klinkenberg 1966	M28		T42.548	670-680
Siltaria dilcheri			Silva-Caminha et al. 2010	G28-4		T42.423	350-360
Stephanocolpites cf. *nertera*				R18/3		T42.548	300-310
Striatopollis catatumbus	Fabaceae (Ceasalpin.)		Takahashi and Jux 1989 [Gonzalez 1967]	W20	IV.21	T42.548	300-310
Striatopollis sp.				V26-1		T42.549	680-690
Syncolpites loranthaceae				X23-1		T42.548	300-310
Syncolporites incomptus	Myrtaceae		Van Hoeken-Klinkenberg 1964	Q28-2		T42.552	290-300
Syncolporites poricostatus	Myrtaceae		Van Hoeken-Klinkenberg 1966	U29-3		T42.552	290-300
Tetracolporites quadratus			Sah 1967	Q29-4		T42.544	630-640
Trichotomonosulcites sp.				Q31-3		T42.552	290-300
Verrutricolporites aff. Haplites				M31-3		T42.552	290-300
Verrutricolporites desmodiensis	Fabaceae	*Desmodium*	Jaramillo et al. 2014	K11		T42.542	600-610
Verrutricolporites rotundiporus	Lythraceae	*Ammania maritima*	Van der Hammen and Wijmstra 1964	F21	III.7	T42.545	360-370
Verrutricolporites simplex	Simaroubaceae		D'Apolito et al. 2021	U31-2		T42.414	240-250
Zonocostites duquensis	Rhizophoraceae		Dueñas 1980	S14-1	IV.16	T42.423	350-360

Table 2: List with species names, authorities, botanical affinities, location in well and samples, and laboratory code *(continued)*

Taxon name	Family	Genus/Species	Reference	EF	Plate	Lab number	Depth (m)
Zonocostites ramonae	Rhizophoraceae	*Rhizophora*	Germeraad et al. 1968	Q31-1	II.15	T42.553	280-290
Zonocostites spp.				N22-3	II.5	T42.553	280-290
			Ferns and Spores				
Deltoidospora adriennis	Pteridaceae	*Acrostichum*	Potonie and Gelletich 1933	M26-1	IV.14	T42.425	390-400
Foveotriletes ornatus	Lycopodiaceae	*Huperzia*	Regali et al. 1974	O33-1		T42.542	600-610
Hamulatisporis caperatus			Van Hoeken-Klinkenberg 1964	V17		T42.552	290-300
Hydrosporis minor	Salviniaceae	*Salvinia*	Silva-Caminha et al. 2010	Q33		T42.539	400-410
Crassoretitriletes vanraadshoovenii	Schizaeaceae	*Lygodium microphyllum*	Germeraad et al. 1968	E20-3	III.13	T42.553	280-290
Polypodiisporites aff. *specious*	Polypodiaceae	*Polypodium*		Q28-3		T42.550	690-700
Polypodiisporites planus	Polypodiaceae	*Polypodium*	D'Apolito 2021 [Silva-Caminha et al. 2010]	M20		T42.413	230-240
Polypodiisporites usmensis	Polypodiaceae	*Polypodium*	Van der Hammen 1956a [Khan & Martin 1972]	F25	IV.18	T42.553	280-290
Psilatriletes aff. *Cyathea*	Cyatheaceae	*Cyathea*		W12-4		T42.544	630-640
Psilatriletes marginatus	Cyatheaceae	*Cyathea*	D'Apolito et al. 2021	S33-4		T42.545	640-650
Magnastriatites grandiosus	Pteridaceae	*Ceratopteris*	D'Apolito et al. 2021 [Dueñas 1980; Kedves and Solé de Porta 1963]	T24-3	III.8	T42.425	390-400
Verrucatotriletes pseudoviruleoides			D'Apolito et al. 2021 [van Hoeken-Klinkenberg 1964]	J27-2		T42.544	630-640

Table 3: Ecological category division of ecological markers of the Powisi-01 well (based on Marchant et al. (2015); Mabberley, 1987). All pollen and spores that were identified, but also many that were not identified are displayed (see Table 2) (#: extant family name)

		Ecological category	Taxonomic affinity
I		Mangroves	Lythraceae (*Ammannia*); Rhizophoraceae; Tetrameristicaceae; *Acrostichum*
II		Palms	Arecaceae
III		Herbs	Asteraceae; Cyperaceae; Poaceae
IV		Ferns	Polypodiaceae; Cyathaeceae; Anemiaceae; Pteridaceae; Salviniaceae; Schizaeaceae
V		Andean	Betulaceae; Podocarpaceae; Lycopodiaceae
VI		Taxa of known ecology	
	VI.a	Marsh forest	Aquifoliaceae; Malvaceae (Bombacoideae)
	VI.b	Lowland and montane forest	Araliaceae; Bromeliaceae; Euphorbiaceae; Humiriaceae; Marcgraviaceae; Proteaceae
	VI.c	Lowland rainforest	Apocynaceae; Celastraceae; Fabaceae
	VI.d	Dry forest	Cannabaceae; Fabaceae
	VI.e	Floodplain	Alismataceae; Araceae; Phyllantaceae; Rubiaceae
	VI.f	Tropical rainforest	Annonaceae; Combretaceae-Melastomataceae; Convolvulaceae; Malpighiaceae; Moraceae-Urticaceae; Myrtaceae; Sapotaceae- Burseraceae
	VI.g	Aquatic environment	Arecaceae; Nymphaeaceae
VII		Taxa of unknown ecology	Simaroubaceae

3.3.5 Statistical analysis

All statistical analysis (Species Richness and Shannon Index) were done with and without the taxon *Zonocostites*, because of its dominant presence in the samples. Of the 30 samples, the sample that corresponds to the interval 167–160 m was excluded because of its low count. The raw count data was used to calculate and create rarefaction curves for species richness and the Shannon index in R Studio Posit Team, 2024 and Past 5.01 software programs. The rarefaction curve of species richness was created using functions 'rarecurve' and 'ordiplot' from R package 'vegan' software (v2.6-8; Oksanen et al., 2024). The counts of the samples (Appendix A.1) were then transformed into percentages which were used for all subsequent statistical analysis. Constrained incremental sums of squares cluster analysis (CONISS) was done using Tilia 3.0.3 software (Grimm, 2022) and R Studio software version 2024.04.1+748 (Posit team, 2024), to identify distinct palynological zones. The CONISS analysis was done in R software using the functions 'dist' and 'chclust' from the R packages 'stats' (v4.3.1;R Core Team, 2023) and 'rioja' (v1.0-7; Juggins, 2024) with Euclidian distances. To determine the diversity of the samples, the Shannon index, species richness (Appendix A.2–A.5) were calculated using the 'diversity' and 'specnumber' functions from the 'vegan' R package software, respectively. Pielou's evenness was calculated by dividing the Shannon Index values with the log of the species richness. The diversity indices were then plotted against the depth of the

samples, to show the diversity of the vegetation over time. Additionally, a non-metric multidimensional scaling (nMDS) analysis was conducted using the 'Bray Curtis' dissimilarity to identify any clusters in the taxa and the samples. The nMDS was conducted using the function 'metaMDS' from the 'vegan' R package software.

The presence of some characteristic pollen in the Paleocene/PETM interval were considered to be the result of caving (downhole contamination) from the Miocene upper interval. Therefore, a diversity curve was conducted eliminating the Paleocene caving (Appendix A.6).

4. RESULTS AND INTERPRETATION

Due to the difference in temporal resolution, geochemical and palynological data are presented separately. The geochemical data and interpretation are presented in relation to the source area. On the other hand, palynological zones are based on the palynological assemblages and their respective occurrence throughout the well.

4.1 SEDIMENT GEOCHEMISTRY

4.1.1 Results

The elemental concentrations of major elements, Large-Ion Lithophile Elements (LILE), High Field Strength Elements (HFSE) and Trace Transition Elements (TTE) of analyzed samples normalized to the PAAS concentrations (Pourmand et al., 2012; Taylor & McLennan, 1985) are reported in Fig. 6. Individual analysis is available in the supplementary dataset (Appendix B.1). Overall, the analyzed samples have similar patterns and there is no trend with depth. Most of the analyzed samples are enriched in CaO, Ba, Y and Co relative to PAAS and depleted in other elements (Fig. 6). The Al/Si ratios of the analyzed samples range from 0.01 to 0.36 (mean=0.13). The Cr/Th ratios are variable and range from 3.7 to 11.5 (Appendix B.1). The Th/Sc ratios are also variable (0.86-2.02, mean=1.32) except for the deepest sample, where the Th/Sc ratios are higher than those of the PAAS (0.92). Finally, all the analyzed samples have higher Zr/Sc ratios (13.25-37.54, mean 26.10) than those of the PAAS (13.22). There is no correlation of the Al/Si ratios with the Th/Sc, Cr/Th and Zr/Sc ratios.

The samples from the Powisi-01 well have different REE concentrations but overall flat REE patterns with slight positive Eu anomalies (Eu/Eu^*~0.59-0.77) and Ce anomalies close to or above to those of the PAAS (ΩCe between 0.92 and 1.21). The REE concentrations are correlated with the Al/Si ratios. There is no correlation between the Al/Si ratios and the Eu/Eu^* and ΩCe ratios (Appendix B.2).

The $^{143}Nd/^{144}Nd$ isotopic compositions of the Powisi-01 samples range from 0.511385 to 0.511956 with ƐNd(0) values between -24.4 to -10.3 (See Appendix B.3). Only three samples located between 200 and 140 mbsl depths have ƐNd(0) values >-13.5. The concentration of ƐNd(0) in the Powisi-01 well reflects the sources: crustal rocks (> 10–20 ppm) and basalt and mafic rocks (< 10 ppm). The calculated TDM ages range between 1.40 and 2.28 Ga with fSm/Nd values between 0.0959 and 0.1156. There is no correlation between the T_{DM} and ƐNd(0) values and the Al/Si, Cr/Th,Zr/Sc, Eu/Eu* and ΩCe ratios (Appendix B.2). The T_{DM} and ƐNd(0) values are strongly negatively correlated.

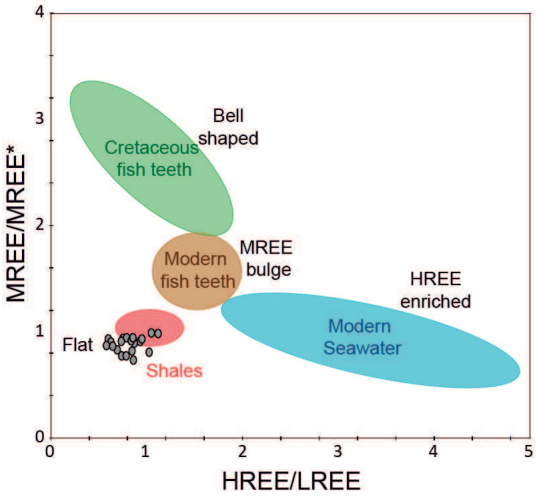


Figure 6: Elemental concentrations of major elements (grey dots represent Pow-01 samples).

4.1.2 Interpretation

The absence of any correlation between Al/Si ratios and provenance proxies (Eu/Eu*, Cr/Th, Th/Sc, ƐNd(0) values and T_{DM} ages) suggest that sedimentary sorting did not influence these provenance ratios. Flat REE patters, ΩCe ratios close or superior to 1, and the fact that all the Powisi-01 samples plot close or within the Shales field in figure 6 indicate that authigenesis did not control the REE concentrations and the Sm-Nd isotopic compositions. Hence, the Eu/Eu*, Cr/Th, Th/Sc, ƐNd(0) values and T_{DM} ages can be used as provenance proxies. All the Eu/Eu* ratios are superior to those of the PAAS, suggesting less differentiated sources than those of the Continental Crust. However, the Cr/Th ratios as well as the Th/Sc ratios rather suggest a differentiated source because the Cr/Th and Th/Sc ratios are lower and higher, respectively, than those of the PAAS. More information can be gained from the Nd isotopic compositions. All samples at stratigraphic depths below 200 mbsl have ƐNd(0) values <-20.1, which we interpret to reflect the sedimentary input of a cratonic drainage quite similar to that of the Marowijne River (Fig. 7). At 200 mbsl, there is a strong shift in the ƐNd(0) values with two samples having similar ƐNd(0) value as those of the Orinoco (Rousseau et al., 2019). This could reflect either input of the Orinoco River or input of the Amazon River with some dilu-

tion of the cratonic detritus. We favor the second hypothesis because at stratigraphic depth 150–140 mbsl, the εNd(0) value is similar to those of the Amazon River and delta (Rousseau et al., 2019 and Bayon et al., 2015), which we interpret to reflect contribution of the Amazon River to the Powisi-01 well. Another shift in εNd(0) value is found for the shallowest sample which has εNd(0) values within the range of those of the Marowijne River (Rousseau et al., 2019). In short, we interpret a cratonic provenance for sediments below stratigraphic depths of 200 mbsl, followed by a progressive input of the Amazon River, until stratigraphic depths of 140 mbsl, and then a return to contributions from cratonic rivers in the Powisi-01 well for the shallowest samples.

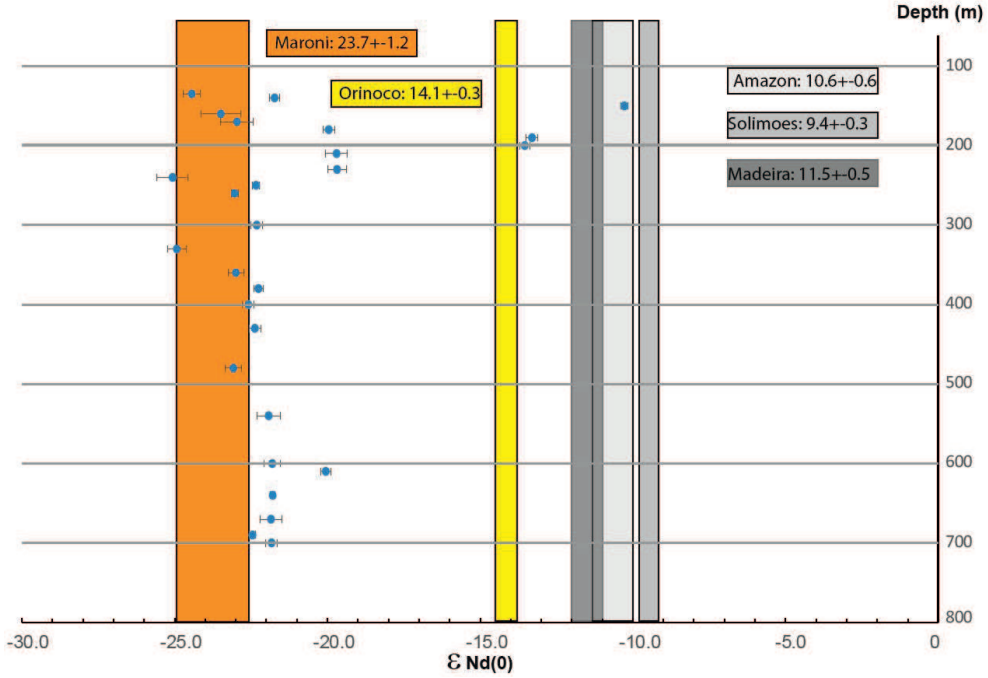


Figure 7: Stratigraphic variation of the Nd isotopic composition expressed as εNd(0) of analysed sample as a function of the depth where the samples were collected. Given that the samples were collected in interval depths (e.g. X-Y in m), we ascribed the deepest value (the Y value) of the interval to the εNd(0) (see Table S2 in the supplementary dataset). The lengths of the horizontal bar for theNd isotopic compositions correspond to 2σ analytical errors (see Table S2). The εNd(0) mean values for the Maroni, Orinoco, Amazon, Madeira and Solimoes rivers are taken from Rousseau et al. (2019) and Viers et al. (2008).

4.2 PALYNOLOGY

4.2.1 Dinoflagellate cysts

All samples were relatively poor in dinoflagellate cysts (< 100 specimens) and two samples (150–140 mbsl and 180–170 mbsl) were completely barren (Fig. 8; Appendix C.1). Two main associations can be distinguished: a) from sample 690–680 to 610–600 to mbsl, the assemblages were diverse and characterized by Paleogene types; b) from sample 410–400 to 180–170 mbsl, the dinoflagellate cyst assemblages were characterized by low species diversity and the dominance of common, long-ranging extant taxa.

Age assessment based on dinoflagellate cysts

Sample 610–600 mbsl displays the most diverse dinoflagellate cyst assemblage of the entire studied section. This sample is dominated by the dinoflagellate cyst *Apectodinium* spp. and also contains *Eocladopyxis peniculata, Homotrybilium* spp., *Kallosphaeridium yorubaense, Muratodinium fimbriatum* and *Operculodinium israelianum,* and microforaminifer linings (Fig. 8; Plate I.1–4, 12). A global *Apectodinium* acme (peak of high abundance) was consistently associated with the PETM (see e.g. Bujak & Brinkhuis, 1998 and Sluijs & Brinkhuis, 2009) and it is therefore suggested that the PETM is represented within the sample interval 610–600 mbsl.

The age assessment can be narrowed down to the earliest Ypresian (PETM), on account of the co-occurrence of the *Apectodinium* acme with *Kallosphaeridium yorubaense* and with common *Eocladopyxis peniculata* and *Homotryblium* spp. *Kallosphaeridium yorubaense* is known to occur in combination with abundant *Apectodinium* spp. in Nigeria (Jan du Chêne & Adediran, 1984). The common occurrences of *Eocladopyxis* and *Homotryblium,* both epicystal *Goniodomidae* which are indicative of seasonal changes in salinity levels and warm stratified waters (Frieling & Sluijs, 2018), are associated with the PETM on the New Jersey Shelf (Sluijs & Brinkhuis, 2009). The occurrence of *Adnatosphaeridium multispinosum* in sample 660–650 mbsl is interesting (Plate I.5). An *Adnatosphaeridium* acme is known from the Early Eocene Ypresian of the Caribbean (Plata-Torres et al., 2022), possibly suggesting that this taxon is also related to high sea surface temperatures.

The upper interval, 410–400 to 180–170 mbsl, contained dinoflagellate cysts such as *Hystrichokolpoma rigaudiae, Lingulodinium machaerophorum, Operculodinium centrocarpum, Polysphaeridium zoharyi, Selenopemphix* spp., *Spiniferites mirabilis, Spiniferites* spp., *Spiniferites* spp., and *Tuberculodinium vancampoae* (Fig. 8; Plate I.6–11). These are all long ranging and extant taxa that make it impossible to provide a detailed age assessment. The oldest record of the coastal-estuarine extant taxon *Tuberculodinium vancampoae* was in the Eocene (Bijl, 2022), but common and consistent records were from the Miocene and younger.

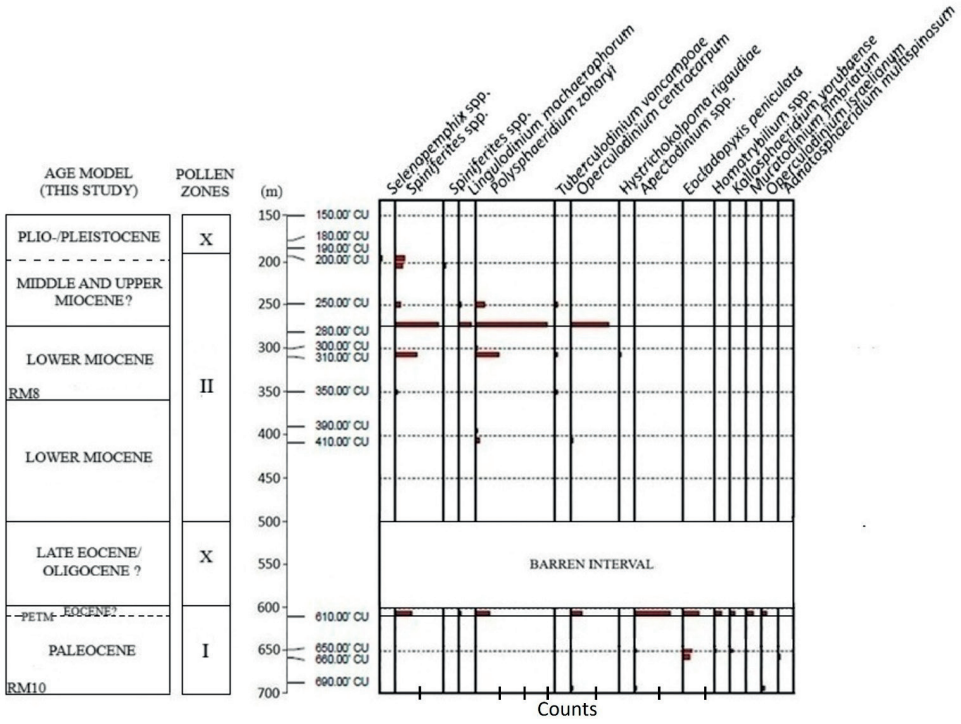


Figure 8: Biostratigraphy based on dinoflagellate cyst composition and based on specimen count (note: absolute counts, one mark is 10 specimens)

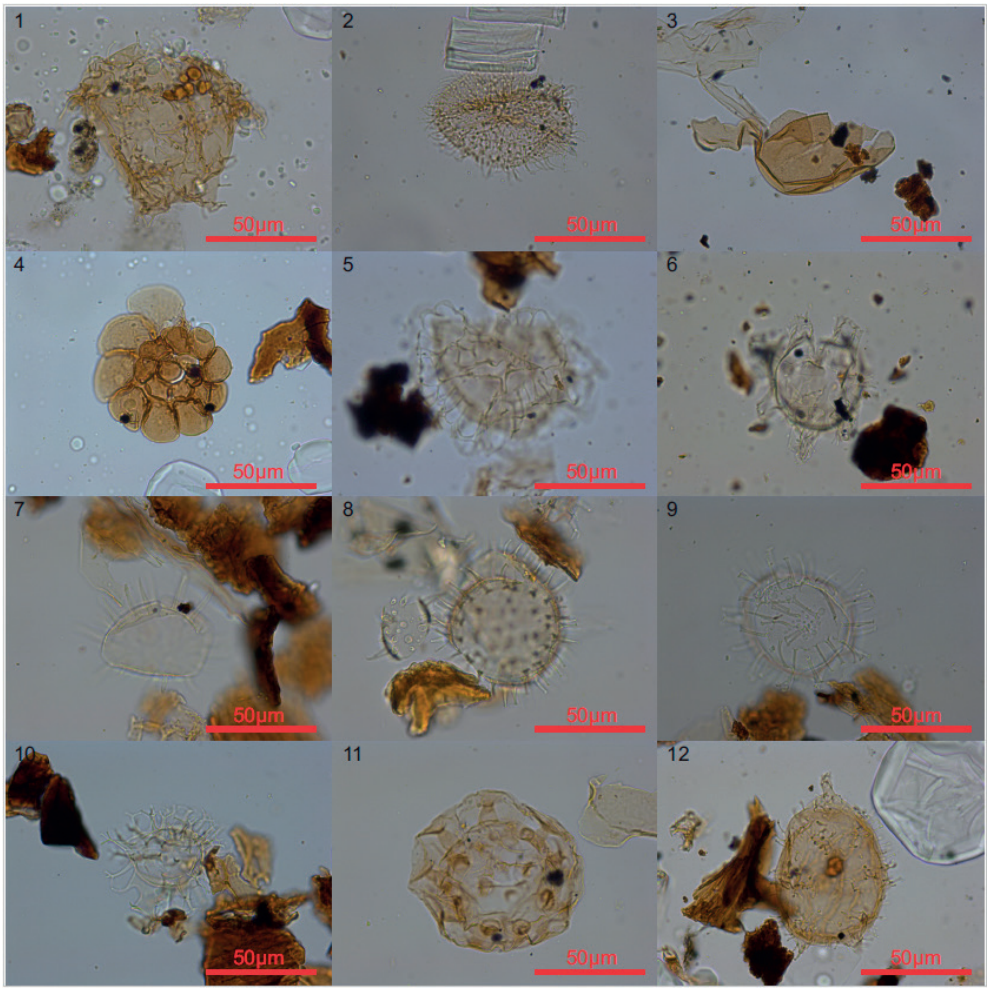


Plate I: (1) Apectodinium sp.; (2) Eocladopyxis peniculata; (3) Kallosphaeridium yorubaense; (4) Foraminifer lining; (5) Adnatosphaeridium multispinosum; (6) Hystrichokolpoma rigaudiae; (7) Lingulodinium machaerophorum; (8) Operculodinium centrocarpum; (9) Polysphaeridium zoharyi; (10) Spiniferites mirabilis; (11) Tuberculodinium vancampoae, (12) Apectodinium spp.

4.2.2 Palynology - sporomorphs

A total of 9952 sporomorphs were counted in the Powisi-01 well samples (Appendix C.2). The abundance of palynomorphs in the samples ranged from low to very abundant. The preservation of terrestrial sporomorphs was generally good, but marine palynomorphs (such as dinoflagellates) ranged from poorly to well preserved. Dinoflagellate cysts and selected sporomorphs were shown with respect to two biostratigraphic schemes (Figs. 8 and 9). All counted sporomorphs of the Powisi-01 well with percentages are presented in a detailed sporomorph diagram (Fig. 10a-d). CONISS analysis differentiated two main ecological zones representing changes in coastal and regional plant biomes. Pollen zones I and II were sepa-

rated by a barren interval (Fig. 9). Zone I was divided into subzones I1 and I2, while zone II is divided into four subzones (II1 to 4).

SPOROMORPH BIOSTRATIGRAPHY

700–600 mbsl - This interval comprises the Alliance Formation and includes biostratigraphic species such as *Bombacacidites annae* (Plate II.1)*, Gemmastephanocolpites gemmatus, Proxapertites operculatus,* and *Proxapertites cursus and Longapertites vaneendenburgi* (Plate II.2–5). An age of Middle to Late Paleocene to Paleocene-Eocene boundary (including PETM) was assigned to this interval based on the common occurrence of *Proxapertites* group, indicative of the Pantropical *Proxapertites* Zone and *Ctenolophonidites lisamae* and *Foveotricolpites perforatus* zones from the Caribbean (Germeraad et al., 1968) and the zones T03a (*B. annae* zone) to T04b (PETM interval zone) from the Llanos and Llanos Foothills zones (Jaramillo et al., 2011). The occurrence of *Gemmastephanocolpites gemmatus* is very common for the Paleocene (Van der Hammen & Garcia De Mutis, 1965 and zone VII (Muller et al., 1987). Germeraad et al. (1968) used this taxon as a common marker to indicate the Paleocene in Caribbean zones. *Proxapertites operculatus* and other *Proxapertites* species are emblematic for the pantropical *Proxapertites operculatus* zone, with an age of Cretaceous to Early Eocene (Germeraad et al., 1968). In the Powisi-01 well the LODs of these taxa were situated at 640 to 630 mbsl. Notably, in the Amazon Fan the FODs of these taxa were during the Paleocene, while their LODs occurred at the top of the Lower Eocene (Regali et al., 1974, 1971). In the same way, Jaramillo et al. (2011) reported a *P. operculatus* Acme from 62.78 to 55.70 Ma (Paleocene) and the last occurrence of *P. cursus* in the Middle Eocene (41.15 Ma). In this interval we found low percentages (up to 5%) of *Zonocostites* spp., a mangrove genus with affinity to Rhizophoraceae (Plate II.6). The appearance of this genus in this interval is considered a result of caving contamination as its FOD has been assigned to the Middle Eocene.

The top meters of this interval (<630 to 600 mbsl) were characterized by the occurrence of *Longapertites* aff. *vaneendenburgi,* with a common occurrence of this taxon between 610 and 600 mbsl. Germeraad et al. (1968) put the top of *L. vaneendenburgi* in the Paleocene, but in the Llanos and Llanos foothills the LOD of this taxon was at 44.83 Ma (Middle Eocene) (Jaramillo et al., 2011). Leidelmeyer (1966) described various *Longapertites* taxa in Guyana, which he dates as Paleocene to Lower Eocene. In our section, these (i.e. *L. proxapertoides proxapertoides* and *Longapertites proxapertoides reticuloides*) (Plate II.7–8), together with other morphotypes, emerge at the LOD of *Proxapertites operculatus* and *P. cursus.* Further inspection of the Suriname morphotypes may yield new species, however it suggests they may represent an additional PETM to Lower Eocene biostratigraphic zone. *Foveotricolporites (Retitricolpites) simplex,* known from the Eocene sediments of the Catatumbo Basin (Colombia; Gonzalez-Guzman (1967) is common throughout this zone and the lower one.

We consider that the occurrence of *Rhoipites (Retitricolporites) guianensis, Mauritiidites franciscoi franciscoi, Mauritiidites franciscoi minutus, Monoporopollenites annulatus, Ranunculacidites operculatus* and *Zonocostites ramonae* (Plate II.9–15) observed in the lower part of the section could be the result of caving contamination due the high abundance of these species at the upper part of the well. This is also in agreement with our proposed age-depth model. A high diversity of *Bombacacidites* taxa was reported in Eocene sediments of the Colombian Caribbean (Plata-Torres et al. 2022). Here, however, the observed *Bombacacidites* species (e.g. *Bombacacidites araracuarensis* and *Bombacacidites fossulatus*) correspond with species that were reported youngest during the Miocene, except for *Bombacacidites annae* (which was restricted from the Paleocene to the PETM) (Plate III.1–2).

Grimsdalea magnaclavata (Plate III.3) also occurred in this interval, which could be congruent with Plata-Torres et al. (2022), who studied cores in the Sinú-San Jacinto area and reported non-regular first occurrences for this taxon in the Caribbean during the Eocene. However, we consider that the early appearance of *G. magnaclavata* in our study is due to caving, as this pollen grain is considered a marker from the Middle-Late Miocene (Zone PM-40 for the Amazon Fan (Regali et al., 1974); Zone T-14 for the Colombia Llanos and Llanos hills (Jaramillo et al., 2011). This is in agreement with the nature of the cutting samples studied, as well as the occurrence of younger species in this interval.

Podocarpidites sp. and other typical Andean taxa such as *Alnipollenites verus*, together with *Malvacipolloides maristellae, Psiladiporites minimus* and *Rhoipites (Retitricolporites) guianensis* (Plate III.4–6) make a much earlier appearance here than observed in the Llanos and Llanos foothills, Venezuela, Guyana and Amazon Fan. We interpret this as caving and/or drilling mud contamination and therefore exclude it from our interpretation.

600– >500 mbsl - This interval lacked palynomorph recovery and may correspond to the Burnside Formation, a palynologically barren interval that Wong (1986) considered of Oligocene age. The precise age cannot be confirmed or refuted due to the absence of palynological data.

<500– >275 mbsl - This interval represents the Coesewijne Formation and includes Regional Marker (RM) 8 at 360 mbsl. According to Wong (1986 and pers. comm. 2024) this marker represents the top of the Lower Miocene. However, here we follow Noorthoorn van der Kruyff (1970), who placed this marker bed in the middle of the Lower Miocene. This view is supported by the composition of the palynological assemblage. First, the absence of *Cicatricosisporites dorogensis,* a spore typical observed in the Caribbean and used as marker for the Middle Eocene to Oligocene, suggests that an Oligocene age can be discarded here. Second, we observed the following assemblage: *Verrutricolporites rotundiporus* (FOD 500–490 and LOD 250–240 mbsl), with an acme between 290 and 270 mbsl; *Magnastriatites grandiosus* (FOD 410–400 and LOD 400–390) (Plate III.7–8); *Psiladiporites minimus* (FOD 320–310

and LOD 290–280 mbsl), and one grain recorded in a sample from the depth-interval of the Paleogene (likely due to caving); *Retitrescolpites irregularis* (FOD 410–400 and LOD 290–280 mbsl); *Retitricolporites hispidus* (FOD 370–360 and LOD 290–280 mbsl); and the mangrove *Lanagiopollis crassa* (formerly *Psilatricolporites crassus*) (FOD 370–360 and LOD 350–340 mbsl) coincided with one appearance of *Jandufouria saemrogiformis* (370–360 mbsl) (Plate III.9–12).

Van der Hammen & Wijmstra (1964) and Wijmstra (1971) first reported these taxa in Guyana and Suriname and considered this assemblage indicative of Oligocene to Lower Miocene age (zones E and F). Moreover, they mention *Jandufouria saemrogiformis* occurred at the base of the *Verrutricolporites rotundiporus* zone and *Psiladiporites minimus* in the top half, the latter extending into the Middle Miocene. This agrees with Dueñas (1980) who suggests that in the Caribbean *Jandufouria saemrogiformis* is no older than the Early Miocene. *Magnastriatites grandiosus* is placed in the Oligocene in the zonation of Venezuela zone I (Lorente, 1986) and Colombian Caribbean zone Car-05 (Plata-Torres et al., 2024), but is reported as Early Miocene in Northern South America zone IX (Muller et al., 1987). Furthermore, Germeraad et al. (1968) place the FOD of *Psiladiporites minimus* in the Lower Miocene and in the biostratigraphic zonation of Venezuela (Lorente, 1986), and Northern South America (Muller et al., 1987) the taxon is considered as a Lower to Middle Miocene marker.

In the Powisi-01 section we also found *Crassoretitriletes vanraadshoovenii* (290–280 mbsl) (Plate III.13), which Regali et al. (1974; 1971) reported as Lower Miocene in the Amazon Fan, but Wijmstra (1971) placed it in the Middle Miocene and assigned it as pollen zone F in his work. *Ilexpollenites tropicalis* (FOD 320–310 and LOD 240–230 mbsl) was first described by Silva-Caminha et al. (2010), who reported this species for the Upper Miocene to Pliocene in the Solimões Basin (Brazil) (Plate IV.1). Based on these studies, we tentatively interpret the section between <500 up to >275 mbsl as Early Miocene (zone E in Wijmstra (1971), and the interval from <275 to >200 mbsl, i.e. the top 80 m of the Coesewijne Formation, as Middle to Late Miocene age (zone F in Wijmstra, 1971). Based on the lithostratigraphy, the top 200 mbsl is likely of Pliocene to Pleistocene age (zone G in van der Hammen and Wijmstra (1964).

Paleoecological zones or biomes

All sporomorphs that were counted in the Powisi-01 well samples are grouped according to their ecology or biome (Tables 1 and 3). The CONISS application in Tilia detected two principal palynological zones (zones I and II). These zones will be discussed in consecutive order from deepest to shallowest. The lower part of the well (<700 to 600 mbsl) is zone I, which is subdivided into two zones (I1 and I2). After the barren interzone (600– >500 mbsl) we assigned zone II, which includes the interval from <500 up to 200 mbsl and is composed of four subzones (II1 to 4). From 200 to 100 mbsl there is another a barren palynological interval (Fig. 11).

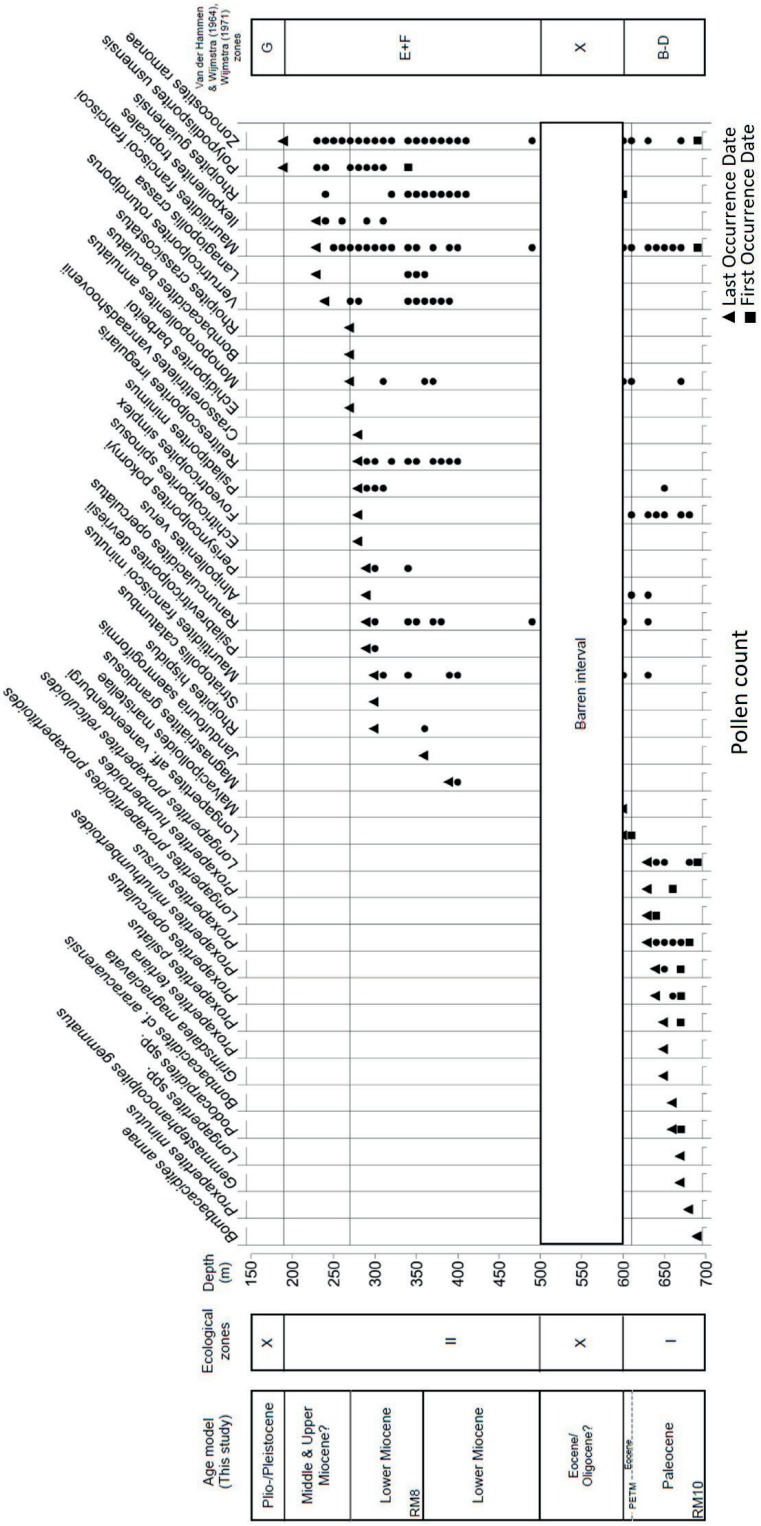


Figure 9: Biostratigraphy based on pollen and spores first and last occurrences.

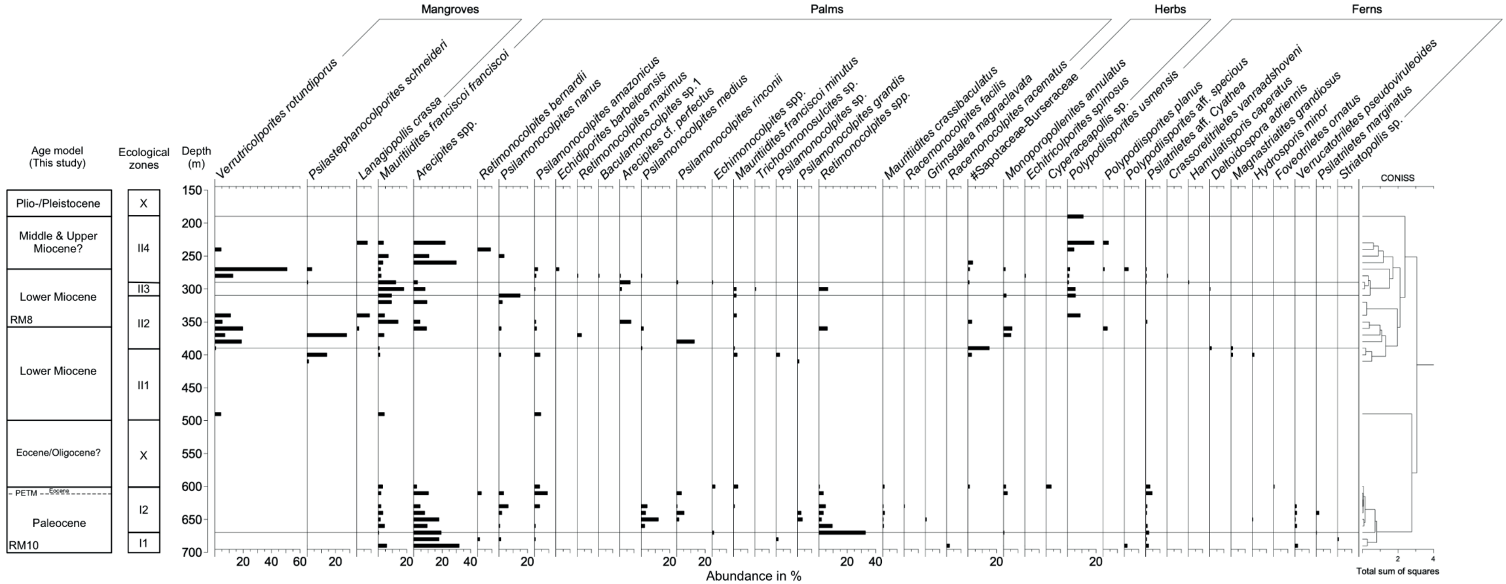


Figure 10A: Detailed sporomorph diagram of the Powisi-01 well with percentages based on pollen sum (without the Zonocostites group).

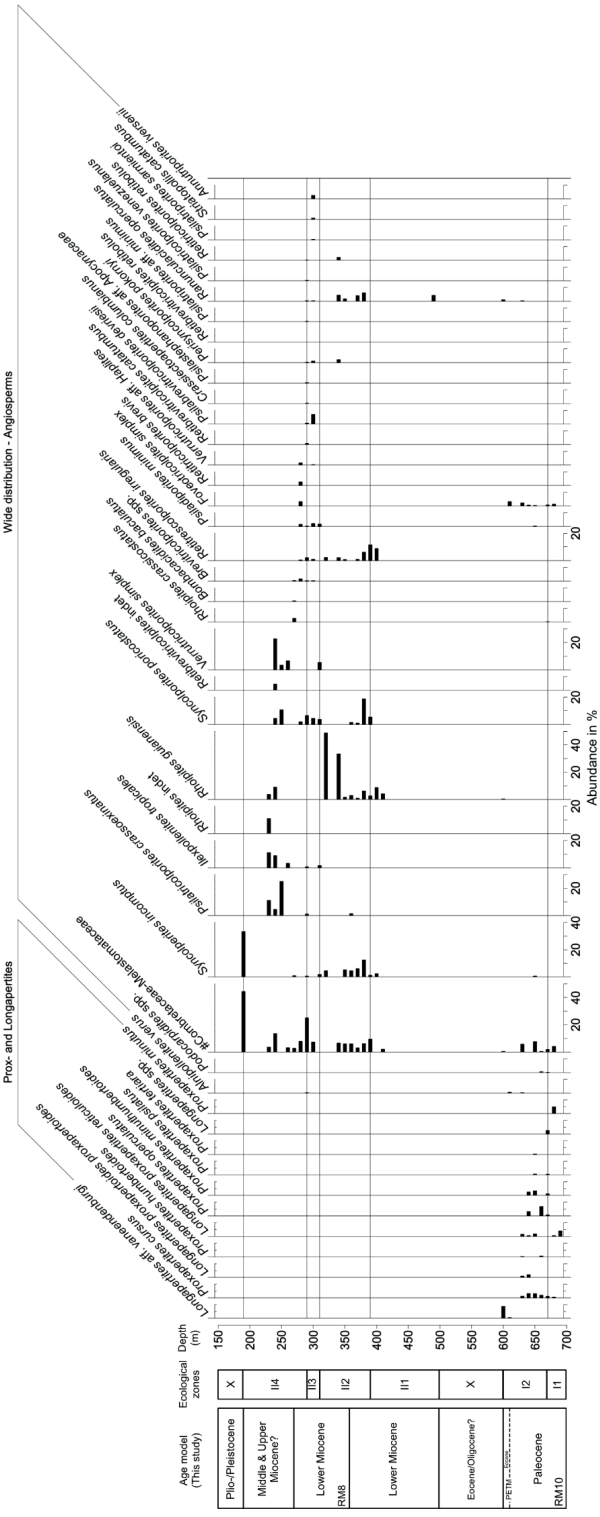


Figure 10B: Detailed sporomorph diagram of the Powisi-01 well with percentages based on pollen sum (without Zonocostites group).

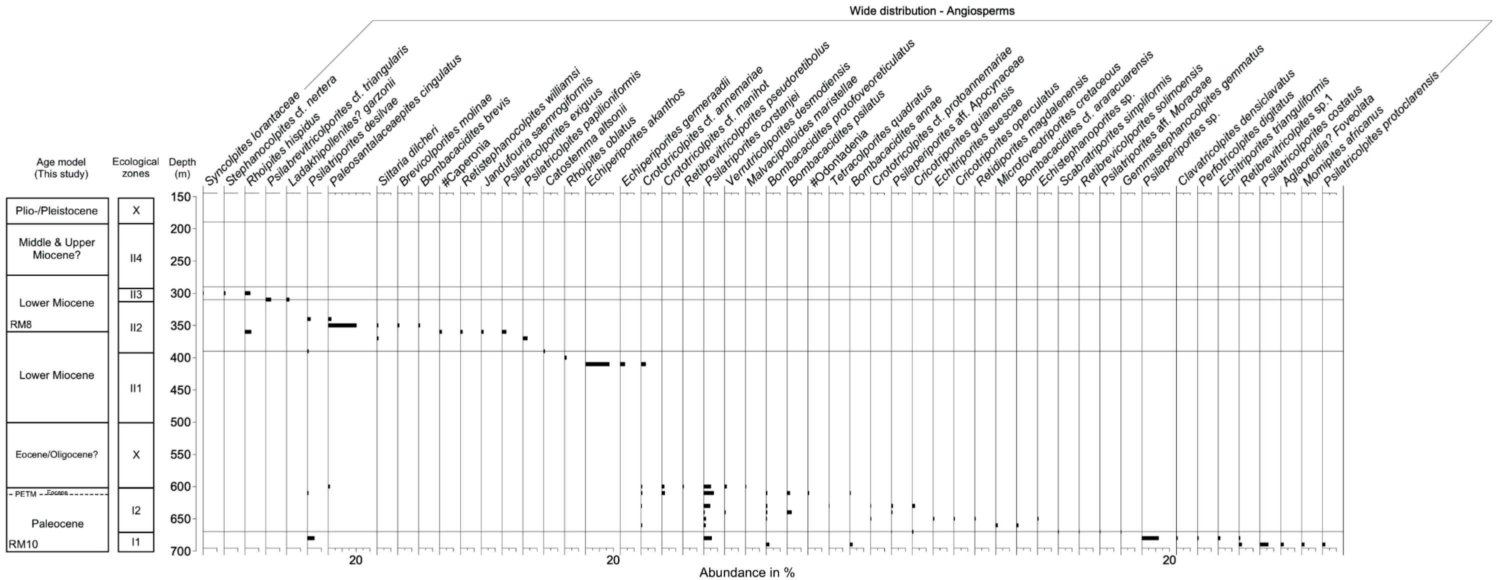


Figure 10C: Detailed sporomorph diagram of the Powisi-01 well with percentages based on pollen sum (without Zonocostites group).

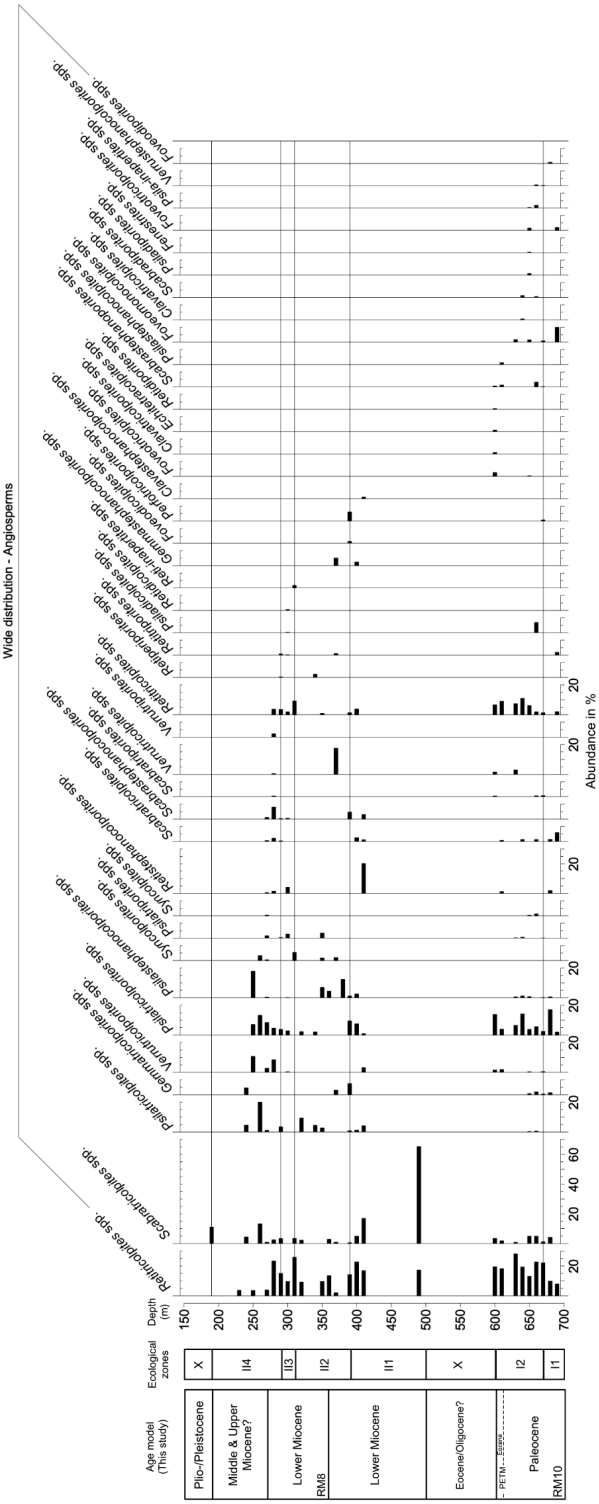


Figure 10D: Detailed sporomorph diagram of the Powisi-01 well with percentages based on pollen sum (without Zonocostites group).

Paleocological zone I (<700 to 600 mbsl; Paleocene to Lower Eocene)

- Subzone I1 (700–670 mbsl; Paleocene)

In total, 637 sporomorphs were counted in this zone, including taxa of unknown affinity. This zone is dominated by palms such as *Arecipites* spp., *Retimonocolpites* spp. and *Longapertites* types. Associated taxa are taxa with proxaperturate pollen types belonging to the Araceae (*Proxapertites operculatus* of *P. cursus),* Annonaceae (*P. humbertoides),* and Nymphaceae (*P. minutus* and *P. psilatus*). Other common taxa are *Psilaperiporites* sp., *Psilatricolporites* spp., Combretaceae-Melastomataceae, *Psilatriporites desilvae*, and *Psilatriporites corstanjei* (Fig. 10; Plate IV.2–8) and psilatrilete spores. Such an assemblage can be expected in a coastal wetland system. Sporomorph diversity was high and mostly composed of palms and tropical lowland taxa of wide distribution; many morphotypes remained unclassified.

- Subzone I2 (<670–600 mbsl; Paleocene to Early Eocene)

In this zone, the sporomorphs added up to 1263. Like in zone I1, palm taxa prevail, but here the assemblage is more diverse than in the previous zone. The following pollen species were observed: *Arecipites* spp., *Psilamonocolpites nanus, P. amazonicus, P. rinconii*, *P. medius, P. grandis, Longapertites vaneendenburghi* and *Retimonocolpites* spp (Fig. 9; Plate IV.9–12). The Mauritiinae palm *Mauritiidites crassibaculatus* and proxaperturate pollen types also are common in this zone. Furthermore, there are a high number of taxa with unknown affinity, thought to be part of the tropical lowland vegetation of wide distribution. The former include *Retitricolporites* spp., *Psilatricolporites* spp., *Retritricolpites* spp., *Scabratricolporites* spp. and *Verrucatotriletes pseudoviruleoides.* Also abundant in this zone were: *Foveotricolpites simplex* (aff. Euphorbiaceae*, Sapium*), *Psilatriporites corstanjei* (aff. Rubiaceae*, Faramea)* and Combretaceae-Melastomataceae. Sporomorph diversity is high and mostly composed of palms and tropical lowland taxa of wide distribution; many morphotypes remained unclassified. This zone represents a continuation of the coastal wetland system and contrasts with the previous subzone in the higher diversity of palms.

<600–500 m Eocene to Oligocene?: no palynological record.

Pollen zone II (<500–200 m; Lower Miocene to Plio-Pleistocene)

The entire zone is characterized by the presence of mangroves such as *Zonocostites ramonae* and *Psilastephanocolporites schneideri* (both aff. Rhizophoraceae) and *Verrutricolporites rotundiporus* (Lythraceae, *Ammania maritima*) (Plate IV.13). In comparison to zone A, there is a very marked turnover in the composition of the coastal vegetation. Four subzones were distinguished, which mainly reflect landward shifts in the mangrove belt and can be described as following.

- Subzone II1 (<500–390 mbsl; Lower Miocene)

In this zone 736 sporomorph grains were counted. *Zonocostites* (Rhizophoraceae) mangroves, accompanied by the mangrove fern *Deltoidospora adriennis,* are relatively modest (Fig. 10; Plate IV.14). Instead, percentages of tropical lowland taxa such as *Retitrescolpites irregularis* (Phyllantaceae, *Amanoa*), and species with affinity to Sapotaceae/Burseraceae and Combretaceae-Melastomataceae are high. Other characteristic taxa for this zone are *Rhoipites guianensis* (Malvaceae), *Retistephanocolporites* spp., *Psilatricolporites* spp. and *Scabratricolporites* spp.. The freshwater taxon *Echiperiporites akanthos* (Alismataceae, *Sagittaria*; Plate IV.15) presents a peak and there are also occurrences of the freshwater fern *Magnastriatites grandiosus*. Pollen diversity is high, but many morphotypes remain unclassified. The assemblage suggests the presence of highly diverse tropical lowland forest and freshwater swamps and in the proximity a mangrove forest.

- Subzone II2 (<390–310 mbsl; Lower Miocene)

In this zone, 4241 sporomorph grains were counted. This zone was dominated by *Zonocostites ramonae,* but also additional mangroves such as *Zonocostites duquensis* (Rhizophoraceae) (Plate IV.16), high amounts of *Verrutricolporites rotundiporus* (Lythraceae, *Ammania maritima*) and *Lanagiopollis crassa* (Tetrameristaceae, *Pelliciera*). *Rhoipites guianensis* (Malvaceae) peak in this zone. Other common taxa with known affinity occurred such as *Paleosantalaceaepites cingulatus* and the palms (e.g. *Mauritiidites franciscoi franciscoi, Arecipites* spp., *A. perfectus*) and minor amounts of ferns spores (freshwater aquatic species such as *Polypodiisporites usmensis* (Plate IV.17–18). Surprisingly, the RM 8 marker bed, which is situated in the middle of the zone, does not coincide with any ecological changes. The presence of palms suggests this assemblage suggest a back mangrove setting. The sporomorph diversity is relatively low in this zone.

- Subzone II3 (<310–290 mbsl; Lower Miocene)

This zone is based on only two samples in which 950 sporomorphs were counted. These samples are characterized by a drop in *Zonocostites* (Rhizophoraceae) percentages. The zone is dominated by almost equal amounts of mangroves and tropical lowland taxa. Combretaceae-Melastomataceae are abundant. Other common taxa are suggestive of dryer climatic conditions or preference for nutrient poor soils, such as *Syncolporites poricostatus* (Myrtaceae), *Psilabrevitricolporites devriesii (Humiriaceae,* Humiria*), Perisyncolporties pokornyi* (Malpighiaceae), *Rhoipites hispidus*, *Striatopollis catatumbus* (Fabaceae) (Fig. 10; Plate IV.19–21). Taxa of unknown affinity such as *Retitricolporites* spp. and *Retistephanocolporites* spp. are also common. Fern spores such as *Polypodiisporites usmensis*, followed by palms, especially *Mauritiidites franciscoi franciscoi, Psilamonocolpites medius, Arecipites perfectus* sp. also occur. Like zone II1, the assemblage suggests the presence of highly diverse tropical lowland forest and freshwater swamps, with a mangrove forest in the further distance.

- Subzone II4 (<290–190 mbsl; top Lower Miocene to Upper Miocene)

In this pollen zone 2120 sporomorphs were counted. The zone is dominated by Rhizophoraceae mangroves; *Verrutricolporites rotundiporus* is high at the base, but drops after 270 mbsl. Combretaceae-Melastomataceae are common; other taxa are mainly from the 'unknown affinity group', followed by the palms, herbs such as *Echitricolporites spinosus* (Asteraceae), and fern spores (Fig. 10; Plate IV.22). The palynological composition suggests a resemblance to zone II2, but marks the disappearance of the important mangrove component *V. rotundiporus*. There are palms in a back mangrove setting and a tropical lowland forest in the wider region. The sporomorph diversity dropped in this zone, but it should be noted that counts are very low.

<190 m Plio-Pleistocene: no palynological record (Fig. 10)

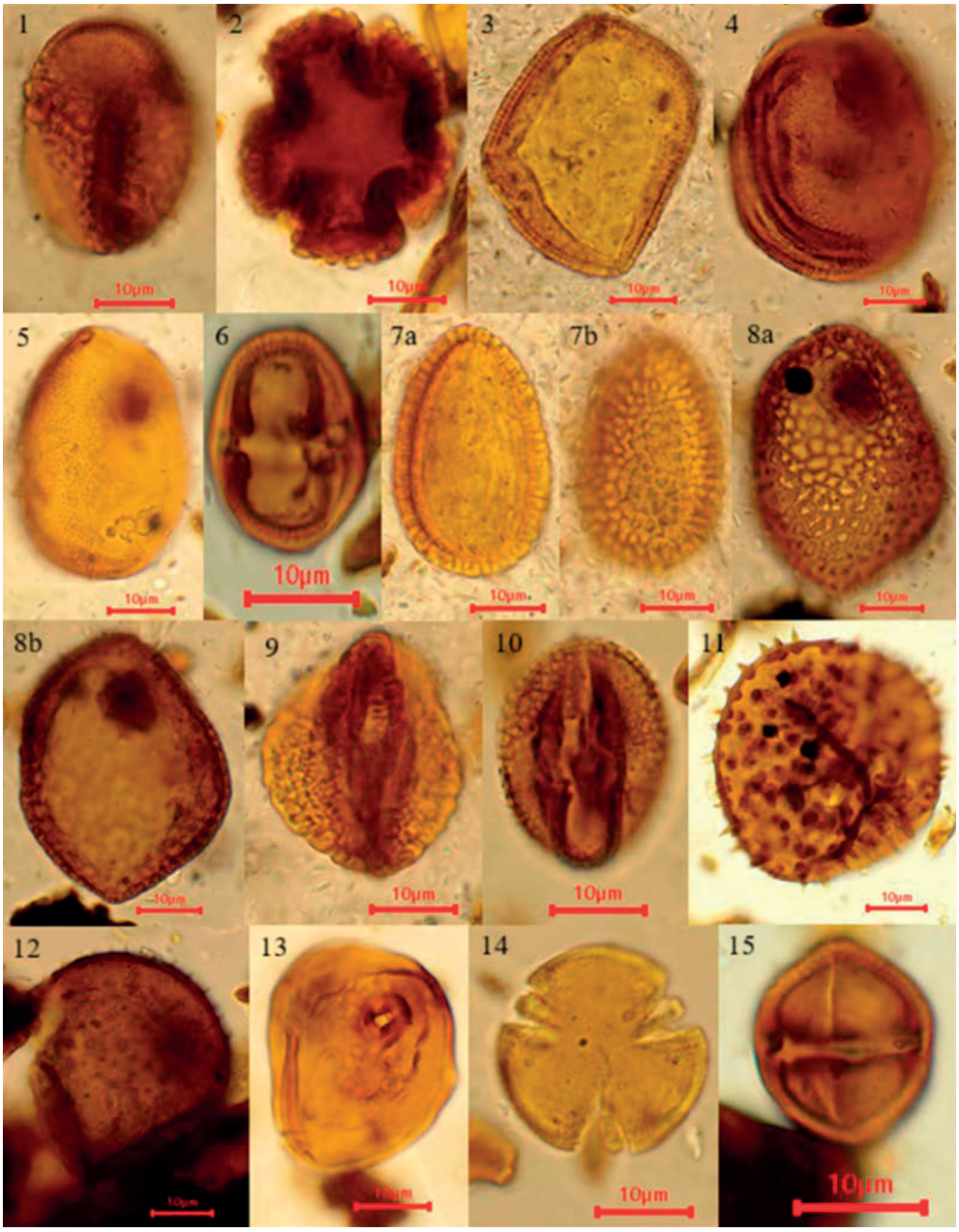


Plate II: (1) *Bombacacidites annae*; (2) *Gemmastephanocolpites gemmatus*; (3) *Proxapertites operculatus*; (4) *Proxapetites cursus*; (5) *Longapertites vaneendenburghi*; (6) *Zonocostites* spp; (7a,b) *Longapertites proxapertitoides proxapertitoides*; (8a,b) *Longapertites proxapertites reticuloides*; (9) *Foveotricolpites simplex*; (10) *Rhoipites guianensis*; (11) *Mauritiidites franciscoi franciscoi*; (12) *Mauritiidites franciscoi minutus*; (13) *Monoporopollenites annulatus*; (14) *Ranunculacidites operculatus*; (15) *Zonocostites ramonae*.

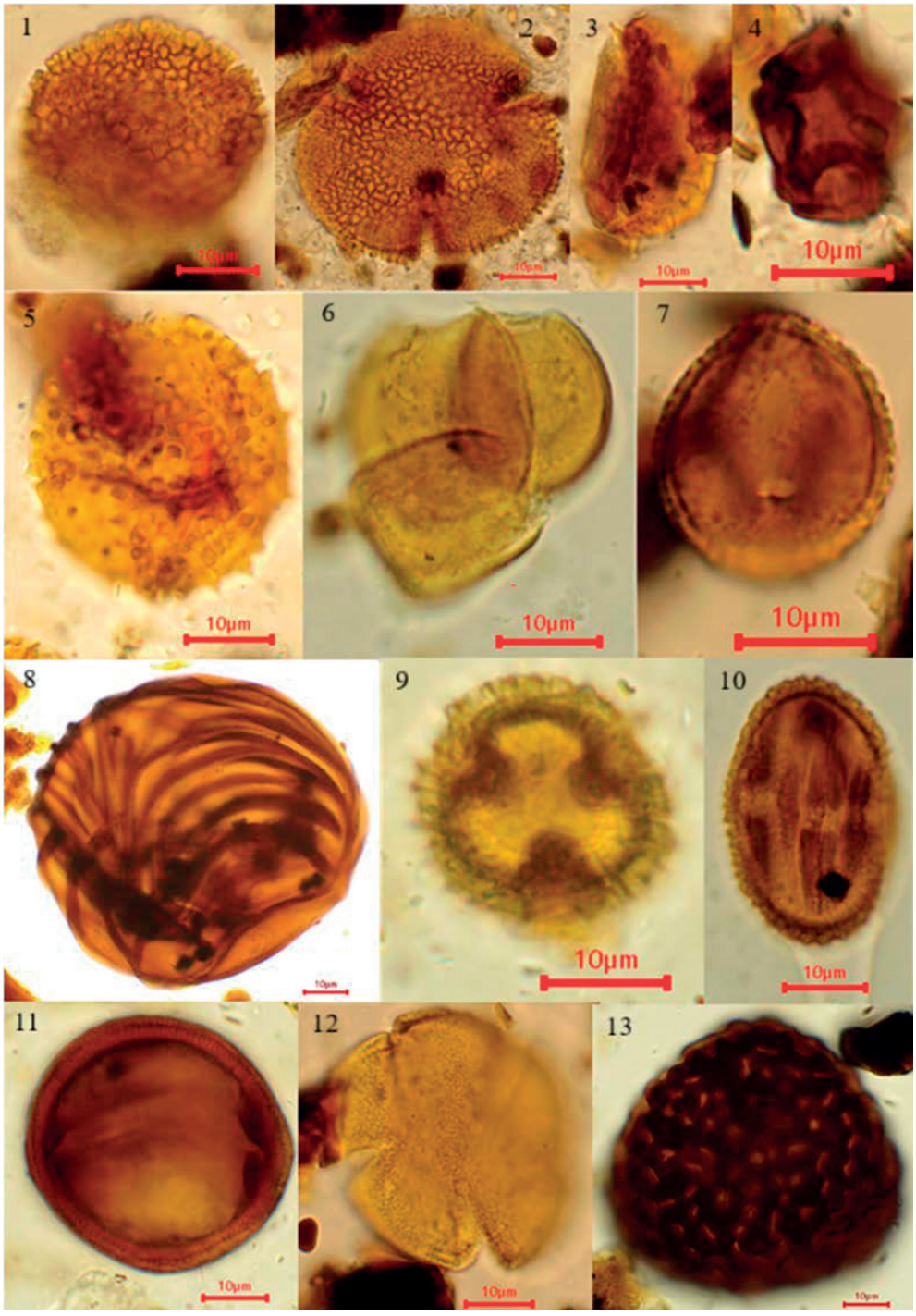


Plate III: (1) *Bombacacidites* cf. *araracuarensis*; (2) *Bombacacidites fossulatus*; (3) *Grimsdalea magnaclavata*; (4) *Alnipollenites verus*; (5) *Malvacipolloides maristellae*; (6) *Psiladiporites minimus*; (7) *Verrutricolporites rotundiporus*; (8) *Magnastriatites grandiosus*; (9) *Retitrescolpites irregularis*; (10) *Rhoipites hispidus*; (11) *Lanagiopollis crassa*; (12) *Jandufouria saemrogiformis*; (13) *Crassoretitriletes vanraadshoovenii*.

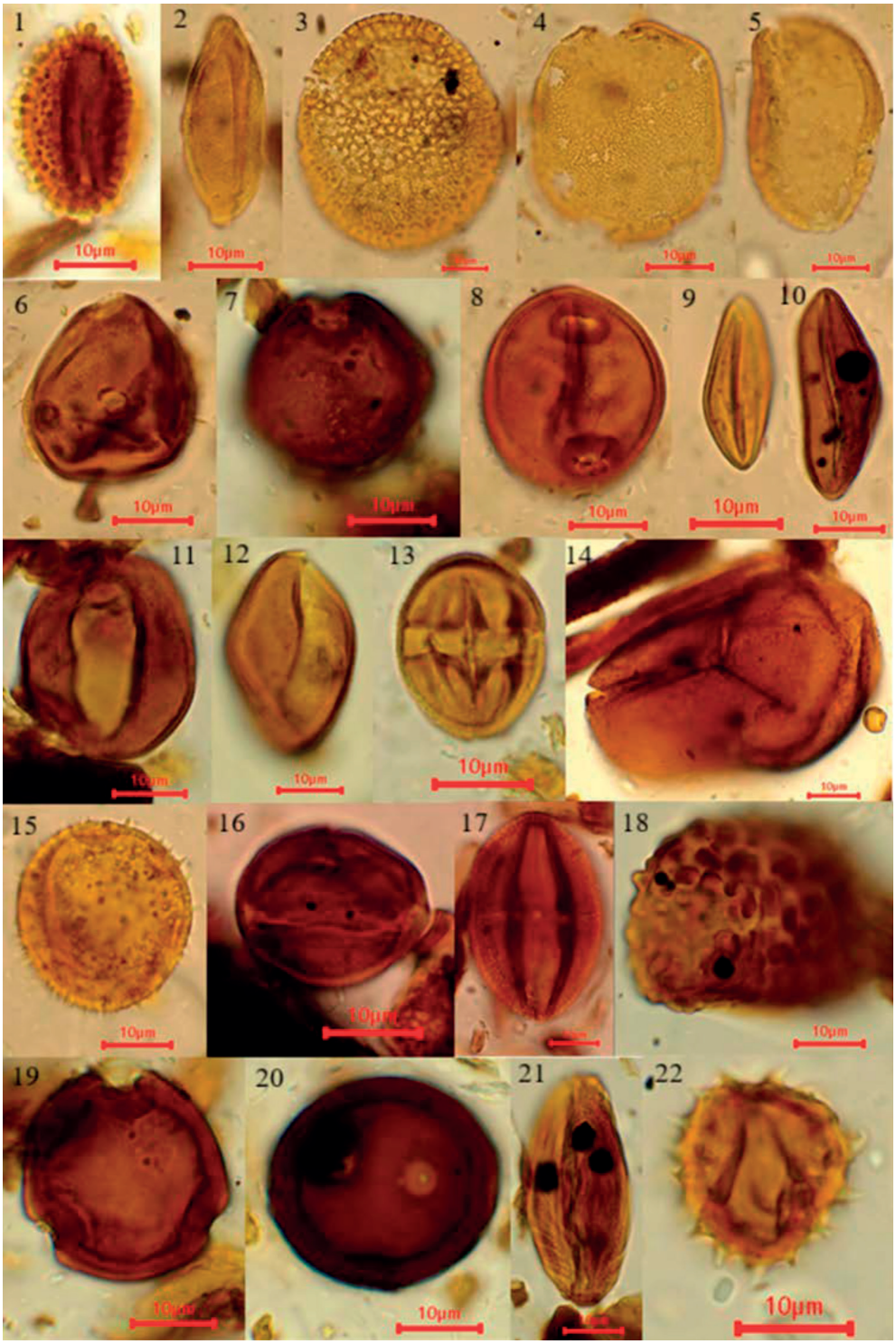


Plate IV: (1) *Ilexpollenites tropicales*; (2) *Arecipites* spp.; (3) *Proxapertites humbertoides*; (4) *Proxapertites*

minutus; (5) *Proxapertites psilatus*; (6) *Psilaperiporites* sp.; (7) *Psilatricolporites desilvae*; (8) *Psilatriporites corstanjei*; (9) *Psilamonocolpites nanus*; (10) *Psilamonocolpites amazonicus*; (11) *Psilamonocolpites rinconii*; (12) *Psilamonocolpites medius*; (13) *Psilatricolporites schneideri*; (14) *Deltoidospora adriennis*; (15) *Echiperiporites akanthos*; (16) *Zonocostites duquensis*; (17) *Paleosantalaceaepites cingulatus*; (18) *Polypodiisporites usmensis*; (19) *Psilabrevitricolporites devriesii*; (20) *Perisyncolporites pokornyi*; (21) *Striatopollis catatumbus*; (22): *Echitricolpites spinosus*.

SPOROMORPH PALEODIVERSITY

The relative palynological diversity in the samples was assessed by means of the Shannon Index. From the results we conclude that the lower part (Paleocene to Eocene) was more diverse than the upper part of the section (Oligocene to Neogene). However, we should take into account that the diversity index is likely altered by caving (downhole contamination) from Miocene and Pleistocene overlying strata (e.g. *Grimsdalea magnaclavata*, *Alnipollenites verus,* other taxa, and unidentified sporomorphs). The diversity is displayed better when the mangroves, which are very dominant, and other caving species were left out of the calculations (Appendix A.6). The results of the palms and other angiosperms were better expressed when the mangroves do not dominate. The pollen count, and in particular the mangrove component, was also higher in the upper part of the well during the Early to Middle Miocene which can be attributed to local variations due to coastal dynamics (Fig. 11).

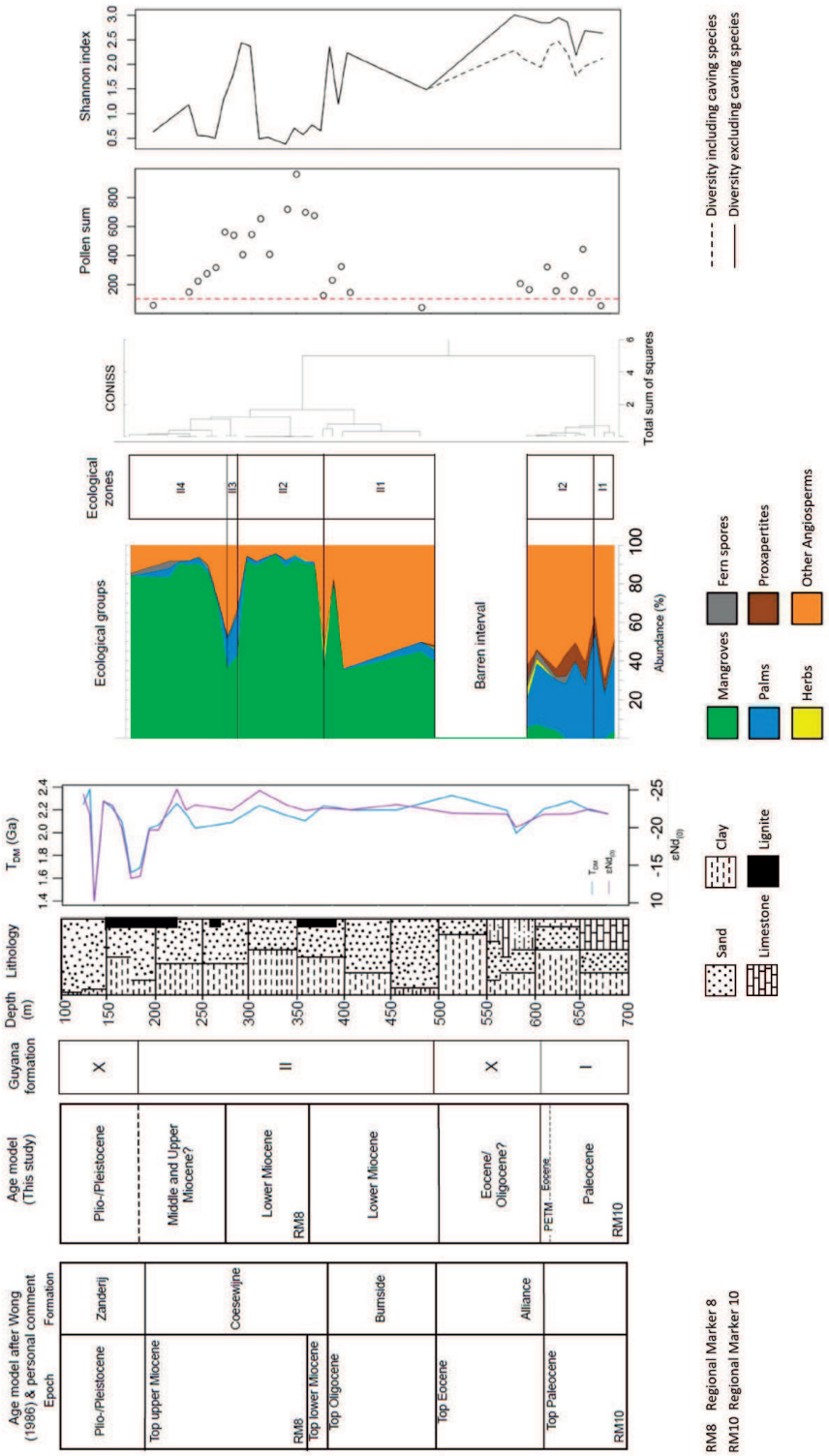


Figure 11: Summary of the main results. Age model, geological formations and lithology from Staatsolie; results of the paleocological analysis, pollen zones, CONISS clustering, pollen sum and Shannon Index.

5. DISCUSSION

In this paper we have questioned, the age of arrival and the effect of the Amazon River sediments along the Guiana coastline and the development of the coastal vegetation. Below we discuss our findings.

5.1 AN ADJUSTED AGE MODEL FOR POWISI-01 (SURINAME–GUYANA BASIN)

Through demands of the hydrocarbon industry, biostratigraphic research has focused on northern South America (e.g. Colombia, Colombian Caribbean, Venezuela, and Trinidad) and the Amazon and Guiana coastlines. The resulting biostratigraphic zonation schemes have played an important role in constructing an age model for the Powisi-01 section (Wong, 1986) and pers. comm. (2024). Based on our work on samples from this site we present, a tentative new age model for this coastal record in Suriname. When compared to other palynological schemes, we highlight the following differences:

5.1.1 The Paleocene Eocene Thermal Maximum (PETM) in the Suriname coastal record

When comparing the Powisi-01 age model with that of Wong (1986)—who integrates seismic data, wireline logs (e.g., gamma-ray, resistivity, and density logs), and biostratigraphic information—the present study identifies several differences between the two models. Most notable is that the boundary between the Late Paleocene and Early Eocene is at greater depth in the earlier model, as according to our palynological results the Eocene starts at approximately 610–600 mbsl.

In the Powisi-01 well, the occurrence of *Bombacacidites annae* (zone T03a from Jaramillo et al., 2011) indicates an age no older than the Late Paleocene. The presence of *Proxapertites operculatus* and *P. cursus*, respectively, correspond to the 'guide species' B2-zone for Guyana (Van der Hammen & Wijmstra, 1964) and zone PT-10 for the Amazon Fan (Regali et al., 1974; 1971), indicating an age no older than Early Eocene. Above this level, we find the *Apectodinium* spp. acme, commonly linked to the PETM (Bujak & Brinkhuis, 1998) (Figs. 8 & 9). The PETM is a relative short period of global warming and one of the most severe climatic events of the Cenozoic Era (Srivastava & Prasad, 2019). During this event, which lasted ~180 kyr, huge amounts of carbon were injected into the oceans and atmosphere, resulting in a sudden global warming of at least 5° C (Kopp et al., 2007; Sluijs et al., 2007), and tropical sea surface temperatures reached extremes of 36°C (Frieling et al., 2017). The base of the PETM correlates with the Paleocene-Eocene boundary (Bijl et al., 2013; Sluijs & Brinkhuis, 2009). However, the *Apectodinium* acmes are not necessarily limited to the PETM, as acmes have been described from the Early Eocene of the Paris Basin (Heilmann-Clausen, 2020).

The actual range top of *Apectodinium* is in the Ypresian, within Chron C22N, indicating that sample 610–600 mbsl is at least Ypresian or older in age.

As yet, there are virtually no published records on how the coastal and shallow marine biota of the western tropical Atlantic responded to the global thermal maximum of the PETM. This means that the sedimentary records in the subsurface of the Guiana coastline provide us with a unique first opportunity to research how the coastal tropical vegetation responded to this event.

5.1.2 The Neogene

In the Powisi-01 well we follow Noorthoorn van der Kruyff (1970), who positioned the RM8 in the mid Lower Miocene. We base this on the presence of characteristic biostratigraphic markers above the RM8 level. Specifically, we highlight the LODs of the *Verrutricolporites rotundiporus*, *Rhoipites guianensis,* and *Crassoretitriletes vanraadshoovenii*, which we position at the top of the Lower Miocene at 275 mbsl, making the Lower Miocene at the Powisi-01 site about 200 metres thick (Fig. 9 & 10a-d). This agrees with Van der Hammen & Wijmstra (1964), who documented the palynological records from Guyana and assigned the palynological zones E and F for the Oligocene and Lower Miocene. This interpretation contrasts with Wong (1986), who considers the RM8 as the top of the Lower Miocene. We also note that the RM8 differs from R1 in the Demerara Rise, where the R1 represents a major unconformity above which the Late Miocene to Pliocene sedimentary sequence is positioned (Patier et al., 2015). The age difference between these two markers can be attributed to the dominance of oceanographic processes in the Demerara Rise, while coastal and fluvial processes influence the near-shore area, and the amount of Mg-rich clays in which a basalt source is required.

5.2 A MAJOR TURNOVER IN MANGROVE COMPOSITION ALONG THE SURINAME COASTLINE BUT NO CORRELATION WITH AMAZON RIVER INFLUENCE

The palynological data from our Powisi-01 study show that the well section can be divided into two parts. The lower section was formed by taxa from a diverse Late Paleocene to Early Eocene coastal and hinterland vegetation. Here, proxaperturate pollen types with affinity to Araceae, Annonaceae, Nymphaceae, and longaperturate pollen types with affinity to palm taxa dominated (paleoecological zone I). The upper part of the well section was also formed by a diverse coastal and hinterland vegetation of mostly Early Miocene age (paleoecological zone II). In this part of the section, Rhizophoraceae, a true mangrove, dominated the coastal vegetation (Fig. 11).

5.2.1 The Paleogene

The interval between 700 to 600 mbsl (zone I) consisted of high percentages of palms (32%), *Proxapertites* types (6%), and other Angiosperms (56%). Mangrove percentages were very low and in some depth intervals almost absent. The appearance of mangroves and other caved species (e.g. *Alnipollenites verus*, *M. maristellae* due to downhole contamination) from the Miocene interval gave a distorted picture of the diversity (Appendix A.3). Eliminating these caved species resulted in a more realistic diversity of the lower interval (Fig. 11). According to Van der Hammen (1957), a palm maximum appeared just before the onset of a transgression, whereas Wijmstra (1971) suggested that the high number of palms represents a temporarily period of a lower sea level. The resulting diagram of the Powisi-01 well shows similar findings to the study of Gonzalez-Guzman (1967) on the Eocene of Colombia, where the higher percentages of palm pollen correspond to lower sea level. The above described palynological association resembles that of the global Paleogene pantropics (Bogota-Angel et al., 2021; Lim et al., 2022), but has no modern analogue.

5.2.2 The Neogene

After the barren interval between 600 to 500 mbsl, organic-rich sediments reappeared from 410–400 mbsl (paleoecological zone II1). Here, the true mangrove *Zonocostites* (Rhizophoraceae) emerges and subsequently increases up to 90%, after which coastal dynamics lead to a decrease again shortly after at 400–390 mbsl (paleoecological zone II2).

The subsequent decline in the number of mangroves (40%) and a rise in palms at c. 275 mbsl, represented a local decrease in mangrove vegetation (paleoecological zone II3), which marked the transition to Middle to Upper Miocene. A final phase of high mangroves increase followed, with the termination of the deposition of the Coesewijne Formation occurring at 200 mbsl. Due to intensive denudation a large part of the Late Miocene is missing over the entire coastal plain. This erosion phase was noticed by Noorthoorn van der Kruyff (1970) and Wijmstra (1971) by means of palynological research, and by Kumar (1978) for several coastal basins in Brazil.

Krook (1984) proposed that the intermediate clays of the Lower Miocene Coesewijne Formation were of Amazon River origin. However, our study of the sediment geochemistry in suggests no such thing, and points at cratonic source for these sediments. We thus conclude that the emergence of the modern mangrove belt is unrelated to the Amazon River mud deposition along the Suriname shoreline.

5.3 THE AMAZON RIVER AND SEDIMENT PROVENANCE IN THE SURINAME CENOZOIC COASTAL RECORD

The marine extension of the Amazon River, or Amazon submarine fan, has been an area of interest to the hydrocarbon industry at least since the seventies. This vast sediment pile also is an archive of the history of the Amazon drainage and carries evidence on the timing of the onset of the Amazon transcontinental river system (Figueiredo et al., 2009, 2010; Hoorn et al., 2017a; van Soelen et al., 2017).

Research by Pasley et al. (2005) and Figueiredo et al. (2009) indicated that the combined effect of the ongoing uplift in the Andes and the global low sea level during the Late Miocene resulted in the birth of the transcontinental Amazon River (Figueiredo et al., 2009; 2010; Hoorn et al., 2017). At present, about 15-20% of the muddy discharge is transported along the French Guiana-Suriname-Guyana coastline through the formation and migration of mud banks of the Amazon River (Anthony et al., 2010) by the NBCC. Various studies have suggested that the flow patterns of the NBCC was flowing through the SW in the Miocene and its modern configuration with a direction toward the NE took place somewhere in the Late Miocene-Pliocene due to the closure of the Isthmus of Panama (Heinrich & Zonneveld, 2013; Kameo & Sato, 2000; Nisancioglu et al., 2003). But to date, the timing of the arrival of Andean Amazonian sediments on the Suriname coastal area remain unknown.

Based on the results from geochemical analyses we conclude that most of the Powisi-01 sedimentary record is characterized by craton-derived sediments (Fig. 7). The first Andean sediments of the Amazon River origin occur in the top of the section, between 200 and 175 mbsl depth, an interval that in terms of biostratigraphy is poorly constrained and most likely of Plio-Pleistocene age (based on the lithostratigraphy). Moreover, Orinoco and Amazon River sediments are intercalated between cratonic sediments.

When compared to the Amazon submarine fan record (Figueiredo et al., 2009; Hoorn et al., 2017b) the arrival of Andean sediments was delayed by at least 5 Ma, and this is much later than previously proposed by Krook (1979), Wijmstra (1971), and Wong (1986). Moreover, coastal sedimentary records from Guyana point at a Late Miocene arrival of Amazon sediments (Mapes & Torres, 2017, 2022). This is in agreement with data from the Demerara Rise where a Late Miocene/Pliocene section is described that is thought to be formed by sediments derived by the Amazon River (Patier et al., 2015). This suggest that at Powisi-01 we do have an uncomplete sedimentary record, and that additional studies from the subsurface of the Suriname coastline (e.g. from onshore and offshore wells) will be needed to determine the timing of the arrival sediments with an Andean provenance.

6. CONCLUSIONS

Based on this study we draw the following conclusions:

The Powisi-01 well presents the first insight into the PETM coastal vegetation in the Atlantic Equatorial zone and a coastal vegetation with no modern analogue, although resembling the coastal paleoflorar of other tropical regions around the globe. It also shows us the rise of a modern-like mangrove vegetation belt in the Early Miocene, that was formed by Rhizophoraceae. In the course of the Miocene, and under influence of local coastal processes mangrove percentages fluctuated.

The combined biostratigraphic and geochemical data reveal the sedimentary and paleoenvironmental history of the Suriname coastline, Geochemical data identified two distinct sediment sources —a cratonic source from the Paleocene to upper Miocene and an Amazon and Orinoco river sources emerge. In the context of regional literature, the arrival of Andean-derived sediments is estimated to be from Late Miocene onwards, comparable to what is known for the Foz do Amazonas (Brazil).

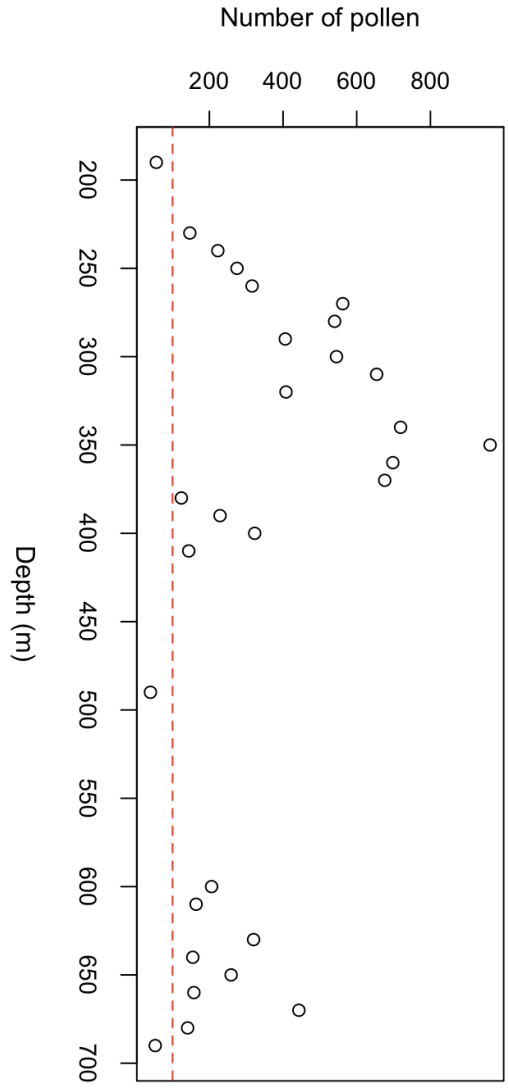
Overall, the Powisi-01 well provides valuable archive for understanding climate–vegetation–sediment interactions along the Amazon–Guyana margin, with further offshore studies (deep-sea wells) needed to confirm and refine the timing of these findings.

7. ACKNOWLEDGEMENTS

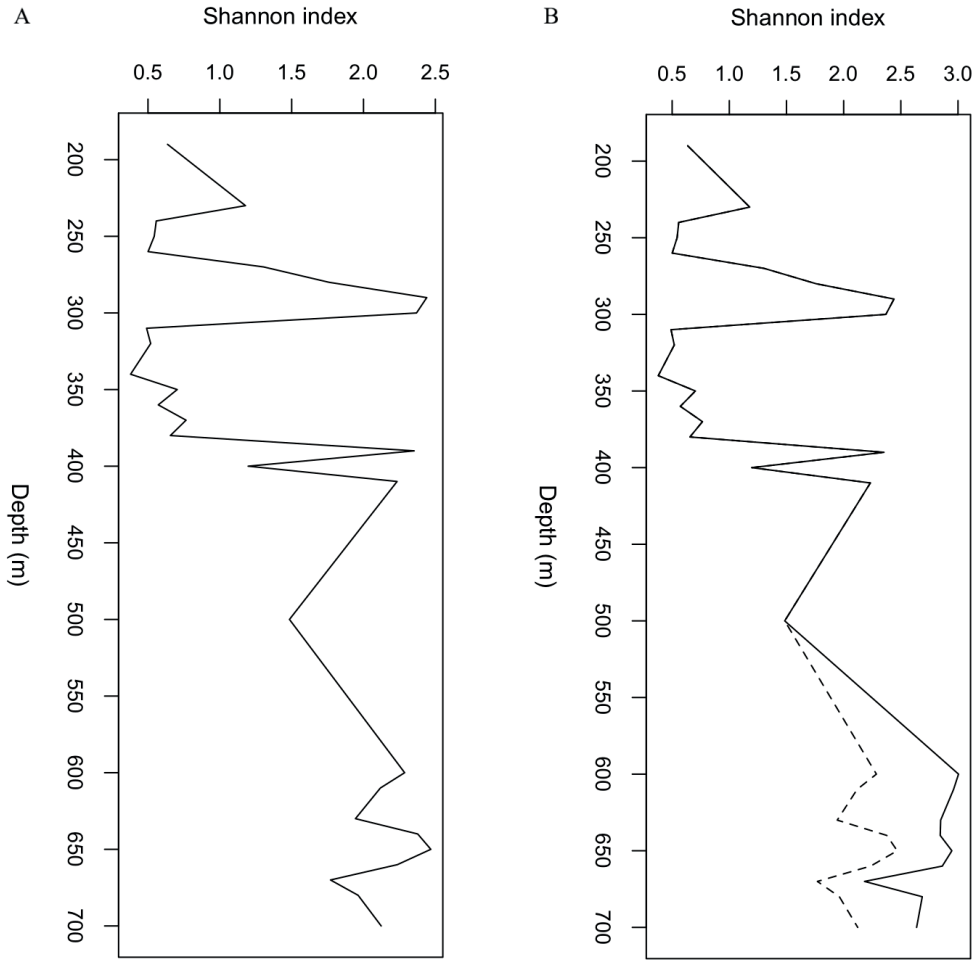
KG would like to thank the Suriname Conservation Foundation (SCF) for funding this part of my PhD-research, Staatsolie Maatschappij Suriname N.V. and Suriname Hydrocarbon Institute (SHI) for providing samples and important data from the Powisi-01 well; Soraya Tirbenie and Faisel Idoe of Staatsolie Maatschappij Suriname for help with all the paperwork to get the samples. Patrick Wandi form Halliburton for additional information regarding the drilling process. Annemarie Philip of the UvA Lab; Johannes de Groeve and Stacy Shinneman for helping with the maps in ArcGis, and the late prof. dr. Theo Wong† who helped with crucial geological information until his sickbed.

APPENDIX

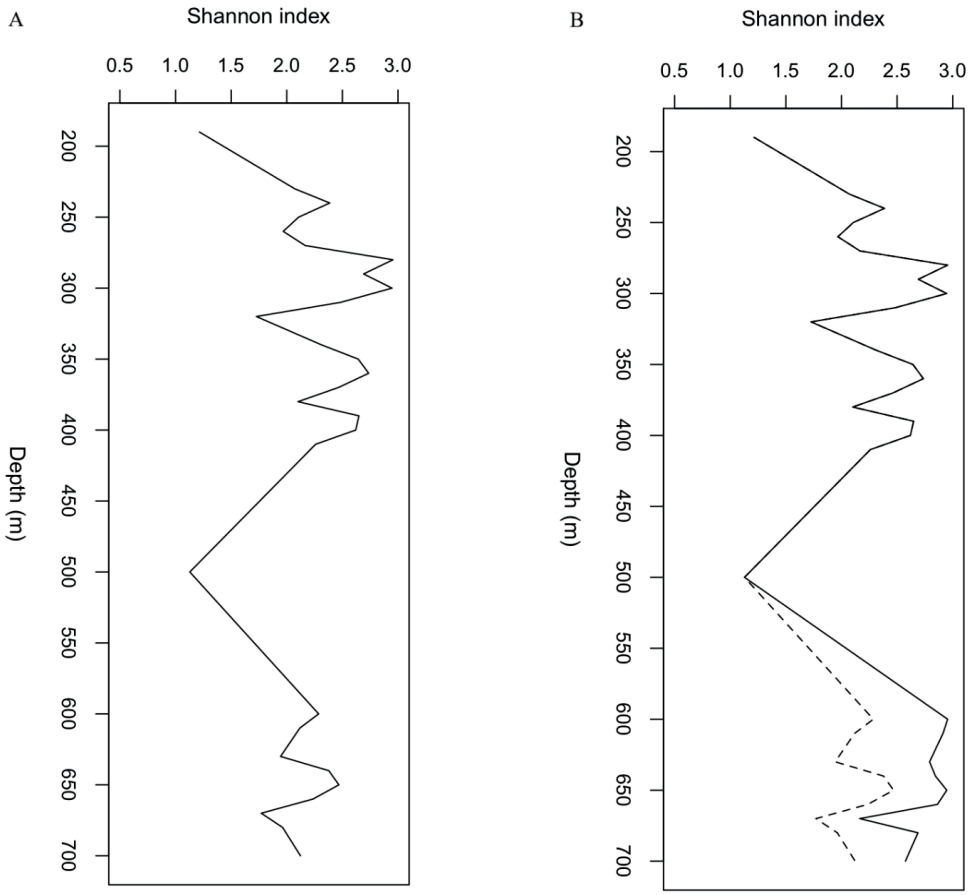
A.1 Pollen count diagram of the Powisi-01 well



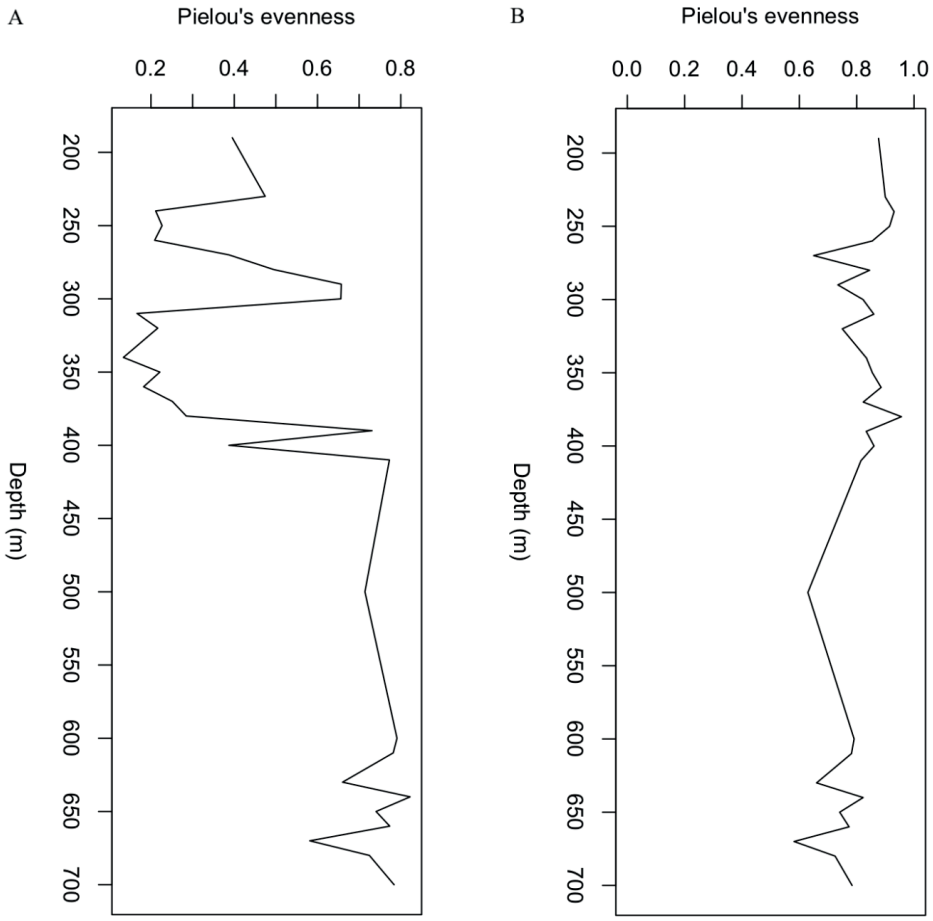
A.2 Shannon Index curves with the *Zonocostites* group included. Curve (A) is not filtered and curve (B) filtered with caving species in the 700–500 mbsl interval



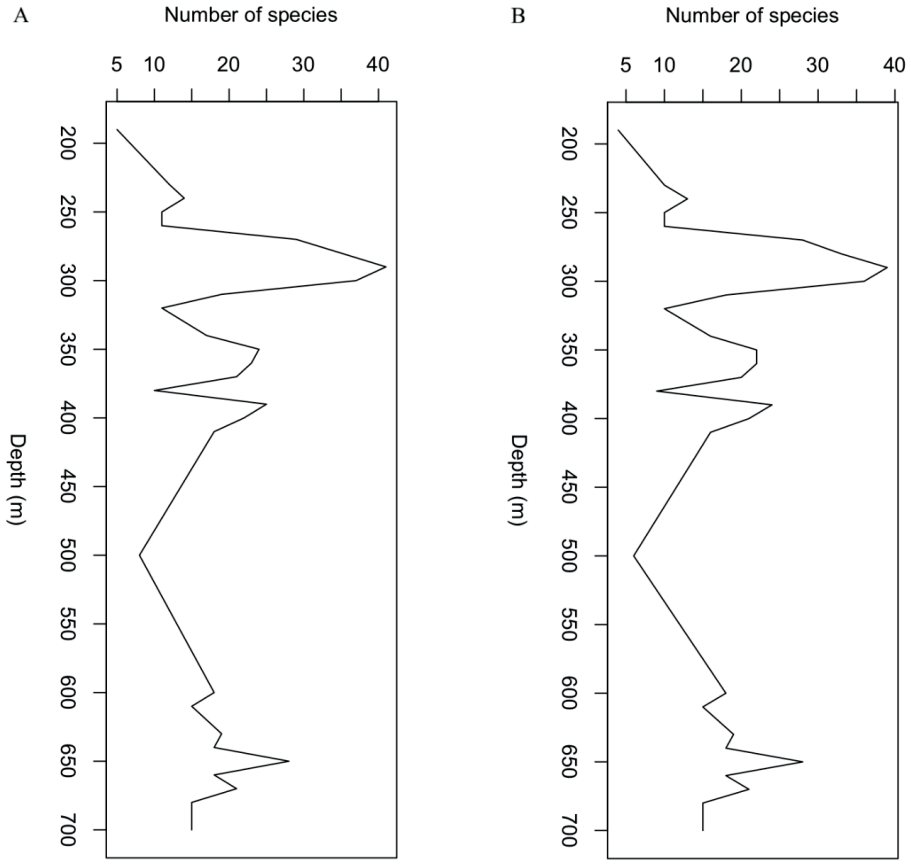
A.3 Shannon Index curves without the *Zonocostites* group. Curve (A) is not filtered and curve (B) filtered with caving species in the 700–500 mbsl interval



A.4 Pielou's eveness curves with (A) and without (B) the *Zonocostites* group (both curves filtered with caving species)



A.5 Species richness curves with (A) and without (B) the Zonocostites group (both curves filtered with caving species)



B.1 major and trace lement concentration and Sm-N isotopic composition of the 20 analysed samples

Sample depth		530-540	630-640	240-250	290-300	690-700	140-150	420-430	390-400	370-380	190-200	320-330	470-480	250-260	350-360	600-610	660-670	590-600	180-190	680-690	120-135	
wt%																						
SiO2	%	74,96	44,29	85,89	78,61	34,79	78,78	36,06	80,94	48,55	78,09	91,84	81,01	38,55	80,67	94,83	85,89	11,41	77,92	87,92	95,39	
SiMol		94,98	20,67	40,08	86,68	16,21	86,77	40,16	87,77	22,66	86,91	42,86	87,80	17,99	87,63	16,25	16,86	5,32	86,36	17,70	44,51	
Al2O3	%	1,27	11,97	3,54	8,24	9,84	8,31	1,11	1,00	4,68	2,65	1,17	1,12	4,84	8,79	10,85	10,22	2,82	5,22	12,05	1,06	
AlMol		0,67	6,33	1,88	1,71	5,26	4,40	0,59	0,53	2,47	1,40	0,62	0,59	2,50	2,01	5,74	5,41	1,49	2,76	6,38	0,56	
Al2O3 mol		0,01	0,12	0,03	0,08	0,10	0,08	0,01	0,01	0,05	0,03	0,01	0,01	0,04	0,04	0,11	0,10	0,03	0,05	0,12	0,01	
Fe2O3	%	8,70	6,47	2,57	1,34	8,89	9,19	1,11	1,62	2,02	4,17	0,52	0,51	2,76	1,50	3,21	3,25	1,26	8,53	4,24	0,48	
MnO	%	0,01	0,04	0,02	0,01	0,02	0,03	0,01	0,01	0,03	0,02	0,00	0,01	0,02	0,01	0,02	0,02	0,01	0,10	0,02	0,04	
MgO	%	0,04	2,06	0,35	1,12	2,24	0,79	0,54	0,44	2,46	0,30	0,23	1,21	0,71	0,72	3,82	1,41	10,60	0,59	1,83	0,03	
CaO	%	0,22	11,00	0,46	1,31	19,71	0,66	4,56	6,95	17,68	0,40	1,38	6,86	25,44	2,77	18,19	19,84	31,63	1,29	16,12	0,20	
CaO mol		0,00	0,20	0,01	0,02	0,35	0,01	0,08	0,12	0,32	0,01	0,02	0,12	0,45	0,05	0,34	0,35	0,56	0,02	0,29	0,00	
Na2O	%	0,05	0,47	0,28	0,27	0,68	0,55	0,07	0,10	0,51	0,33	0,10	0,07	0,54	0,38	0,27	0,66	0,18	0,45	0,83	0,04	
Na2O mol		0,00	0,01	0,00	0,00	0,01	0,01	0,00	0,00	0,01	0,01	0,00	0,00	0,01	0,01	0,00	0,01	0,00	0,01	0,01	0,00	
K2O	%	0,04	1,79	0,31	0,19	1,47	1,52	0,06	0,07	0,82	0,40	0,11	0,05	0,21	0,31	1,64	2,09	0,37	1,14	1,97	0,36	
K2O mol		0,00	0,02	0,00	0,00	0,02	0,02	0,00	0,00	0,00	0,00	0,00	0,00	0,00	0,00	0,02	0,02	0,00	0,01	0,02	0,00	
TiO2	%	0,07	0,57	0,19	0,19	0,93	0,37	0,06	0,07	0,20	0,18	0,06	0,05	0,21	0,18	0,47	0,47	0,11	0,27	0,50	0,03	
P2O5	%	< LD.	0,03	0,06	0,03	0,06	0,06	0,02	0,03	0,06	0,02	0,01	0,02	0,06	0,03	0,04	0,04	0,01	0,06	0,04	0,01	
LOI	%	14,45	20,89	7,03	10,16	27,07	5,92	7,24	9,72	22,46	11,57	5,66	8,02	22,63	8,15	25,83	25,89	40,38	8,04	24,51	1,10	
Total	%	99,81	99,51	100,72	100,41	99,70	100,22	100,85	100,95	98,97	99,13	99,08	96,92	95,46	98,51	99,85	99,39	98,78	99,84	99,85	98,76	
Al/Si		0,02	0,91	0,05	0,05	0,92	0,12	0,01	0,01	0,11	0,04	0,01	0,02	0,13	0,05	0,35	0,32	0,28	0,08	0,96	0,01	0,13
CIA		70	88	68	24	20	69	12	7	12	61	29	8	8	39	23	21	5	55	27	56	
CIA*		10	11	6	6	7	7	7	5	4	4	5	7	4	5	16	7	7	5	8	10	
ppm																						
Sc	ug/g	2,694	9,036	3,706	3,284	7,458	7,848	2,66	1,819	4,979	3,479	2,327	1,838	3,475	3,43	7,972	8,119	2,017	5,181	9,665	2,998	
Rb	ug/g	1,7612	40,1941	11,1593	5,905	28,6062	61,3303	2,3585	3,081	12,9012	18,3008	3,1211	2,272	9,7782	10,2784	44,948	46,5516	9,4071	30,1808	44,3635	8,7859	
Cs	ug/g	0,1052	1,8368	0,7123	0,4851	1,3211	3,9916	0,1583	0,3028	0,9571	1,2769	0,171	0,2421	0,7986	0,6803	1,8746	1,0323	0,8714	2,4828	2,0699	0,1509	
Ba	ug/g	761,9291	5696,1179	844,5905	786,5883	6948,8745	677,4483	59,8898	56,3272	849,9057	427,5903	306,1499	182,856	1084,5603	951,5797	9035,4602	8011,7065	488,3621	721,5889	5900,1773	172,3443	
Sr	ug/g	29,4551	291,0978	60,2652	299,9127	720,4591	92,21	56,5092	93,2572	992,558	51,0248	46,7391	94,8454	2016,9419	139,162	297,4974	473,2702	478,019	104,0935	473,1172	21,7575	
Th	ug/g	2,9243	15,5762	5,1048	3,8944	9,8894	7,7055	3,8857	2,9783	4,9149	3,4128	2,4087	3,0898	7,0146	6,0879	12,2962	12,1665	2,8986	5,0022	13,7592	1,1273	
U	ug/g	0,9486	4,3449	1,1397	1,2873	2,9451	1,442	1,4408	1,2115	1,9945	0,991	0,8571	0,9794	1,8837	1,242	5,0821	3,6918	3,1216	1,1207	3,5977	0,4727	
Y	ug/g	1,9022	21,1472	6,7055	4,4894	12,1928	12,8728	2,8761	4,1133	7,2468	5,7787	2,8929	2,9257	6,4252	5,6916	17,1872	16,7975	4,1076	8,9056	16,7388	1,5751	
Zr	ug/g	56,7784	329,7781	124,5382	123,2854	126,3928	105,2874	75,7665	54,8788	80,0152	116,0124	65,0122	52,289	99,3548	106,6612	325,1688	222,2001	43,8297	105,9728	181,7019	46,3161	
Nb	ug/g	1,2818	11,3475	2,7564	2,0497	6,64	6,5568	1,1627	1,0281	3,1025	3,6572	1,0548	1,0961	3,5664	2,6605	9,6248	8,6991	2,1657	4,5281	9,5108	1,1476	
Hf	ug/g	1,0839	8,6296	2,781	2,6457	3,1987	2,5939	1,6755	1,0559	1,8641	2,0503	1,1394	0,8047	2,4417	2,3637	7,7361	5,6275	1,0332	2,2458	4,7522	0,6827	
Cr	ug/g	20,429	58,0716	34,7608	37,0699	59,5193	43,6971	20,9656	28,0245	42,6749	33,6552	18,2092	18,1357	44,2942	36,1254	48,186	60,9563	24,7505	33,9679	69,8477	13,0008	
V	ug/g	14,5984	50,8369	19,2096	15,0888	49,3918	56,0316	13,1513	11,5871	21,7248	51,0512	6,4469	4,1904	20,9123	15,4814	49,4082	49,362	26,9647	51,2406	62,4383	2,7094	
Co	ug/g	258,5012	54,7563	157,2004	164,4492	66,8201	115,47	247,0239	184,596	122,8303	215,3288	232,5948	226,5707	51,5135	158,0516	45,3102	39,1835	148,3567	159,0725	42,6855	462,4177	
Cu	ug/g	6,7182	24,6826	9,6794	7,5462	11,753	13,567	4,7787	4,3681	5,0275	6,0503	7,6887	3,5235	9,0084	5,182	11,6157	14,0761	5,7181	7,791	13,6523	3,7663	
Ni	ug/g	36,1701	19,0381	8,8393	22,4279	19,2527	16,9713	11,5291	9,8867	18,918	16,8923	5,5269	4,8954	8,7129	11,0755	15,7938	17,5968	7,2633	15,5879	22,3596	5,8482	
Zn	ug/g	43,3731	41,6456	24,8866	25,1587	45,2515	65,6894	16,7489	31,858	29,3876	42,6175	13,9151	12,2797	24,3721	28,8372	82,1189	612,5189	12,875	42,806	50,7546	12,8807	
La	ug/g	5,0654	42,675	16,7099	11,5162	26,5269	23,6702	7,8225	7,9699	17,7636	8,8974	6,1029	6,1812	15,1802	14,8034	34,1809	31,9633	7,5486	14,1655	32,1893	4,4123	
Ce	ug/g	9,2333	84,7389	32,5748	21,7491	52,5295	44,8228	14,4888	15,6612	35,5205	17,9024	10,5114	11,6781	29,0462	27,7611	67,4028	63,3879	16,0049	28,1443	64,2944	6,7655	
Pr	ug/g	0,8938	8,9502	3,2846	2,1458	5,4921	4,842	1,4058	1,6212	3,4498	1,8337	1,0594	1,1661	3,4026	2,8311	7,325	6,8878	1,612	2,9822	6,163	0,6951	
Nd	ug/g	3,1355	33,0493	11,6035	7,4543	19,7048	17,794	4,8606	5,8671	12,6587	6,974	3,6098	4,0548	12,7124	10,1074	26,7769	25,313	5,847	11,2718	23,6943	2,3208	
Sm	ug/g	0,6287	6,1895	2,0418	1,2888	3,9564	3,3461	0,8579	1,1124	2,1675	1,1831	0,621	0,7443	2,1113	1,7177	4,824	4,6247	1,1159	2,1612	5,4471	0,403	
Eu	ug/g	0,1083	1,2267	0,4547	0,2668	0,8488	0,7072	0,1394	0,2028	0,4647	0,2781	0,1341	0,1258	0,4888	0,3627	0,9564	1,0096	0,2286	0,501	1,151	0,0849	
Gd	ug/g	0,4537	4,8265	1,6106	0,9776	3,8058	2,6762	0,693	0,8548	1,6493	1,1367	0,4813	0,5668	1,5067	1,3318	3,6932	3,5575	0,8768	1,8211	3,9883	0,3151	
Tb	ug/g	0,0703	0,7213	0,2219	0,1389	0,5672	0,4008	0,0971	0,134	0,2345	0,1804	0,0683	0,08	0,2013	0,1818	0,55	0,5192	0,1251	0,2747	0,5512	0,0454	
Dy	ug/g	0,4179	4,2665	1,2435	0,8061	2,9259	2,4095	0,5065	0,726	1,3446	1,074	0,405	0,474	1,1678	1,0559	3,2217	3,0229	0,7393	1,6604	3,2936	0,2817	
Ho	ug/g	0,083	0,8788	0,2521	0,1655	0,6745	0,5059	0,1022	0,145	0,2608	0,2264	0,0849	0,0989	0,2304	0,2083	0,6495	0,6069	0,1498	0,3418	0,6535	0,0609	
Er	ug/g	0,2527	2,4474	0,6486	0,4592	1,2607	1,378	0,2856	0,39	0,7046	0,6253	0,2357	0,2747	0,6105	0,5784	1,8184	1,6718	0,4059	0,9587	1,7481	0,1697	
Tm	ug/g	0,0402	0,3727	0,0929	0,0676	0,1878	0,2135	0,0463	0,0597	0,1019	0,0964	0,0371	0,0438	0,0875	0,0879	0,2838	0,2602	0,062	0,1462	0,2661	0,027	
Yb	ug/g	0,2859	1,4774	0,5376	0,4511	1,2185	1,381	0,3238	0,3859	0,6645	0,6254	0,2548	0,3057	0,5834	0,5626	1,881	1,6957	0,4028	0,9859	1,7801	0,1816	
Lu	ug/g	0,0462	0,3894	0,0892	0,0717	0,1882	0,2105	0,0515	0,0581	0,1007	0,0956	0,0433	0,0473	0,088	0,0892	0,293	0,263	0,0636	0,1421	0,2745	0,0324	
Ta	ug/g	1,5751	1,2828	1,1965	1,8102	0,7622	1,9607	1,4898	1,0124	0,7156	1,6922	1,4871	1,5022	0,5061	1,2169	1,1089	1,0117	0,4565	1,4275	1,0293	2,7514	
ΣREE		20,8149	192,81	71,4165	48,3948	117,5618	104,3523	31,7115	35,2216	78,0867	41,3791	24,0489	25,8416	74,3687	61,762	153,9366	143,7915	35,1872	65,5044	149,5455	15,6033	
LREE		0,2857566669	2,7250110087	1,0095212745	0,6706781166	1,6643833294	1,4853038003	0,4465376606	0,4868910068	1,0777465555	0,5721123837	0,3380059157	0,3622532555	1,0165932457	0,8819695508	2,2062425871	2,0751664476	0,4848822812	0,9137411108	2,1457159042	0,2196751156	
HREE		0,2926338981	2,5962787001	0,6043212119	0,4630438677	1,2498778882	1,4116575522	0,3290044111	0,3929185101	0,6760722	0,6392689036	0,2655046698	0,3063847951	0,5883650342	0,5651075211	1,8746	1,6923	0,4076053	0,9587783667	1,8065923419	0,1972908549	
MREE		0,2323877341	2,3769449671	0,7492885396	0,4691599944	1,3584600577	1,3435553366	0,29806987	0,4170059159	0,7883162239	0,5923932932	0,3323954438	0,2726753838	0,6957381386	0,6228714417	1,8388881011	1,739509067	0,4244932802	0,92111621	1,9331010568	0,1557007467	
MREE*		0,2891853325	2,6380446894	0,8069219982	0,5666585221	1,4571380588	1,4483947763	0,3877705859	0,4466426852	0,8576809878	0,6056989253	0,3017619927	0,3343235675	0,8023988857	0,7125088515	2,0638669086	1,8972947227	0,4650594892	0,9952573887	2,131857866	0,2134636002	
Sm/Nd		0,2005510285	0,1873080812	0,1759661498	0,1728706986	0,1820139905	0,1877605398	0,1765000844	0,1895996832	0,1712125808	0,1903012234	0,1720816962	0,1835960225	0,1660819986	0,1699447999	0,1801552881	0,1827005589	0,1814813503	0,1917951127	0,1834892446	0,1736844817	
Eu/Eu*		0,4169447209	0,7016577496	0,7662529699	0,7818547995	0,6117389357	0,7227453576	0,5553679	0,6338979341	0,7518078107	0,6777875559	0,7496857663	0,5618538294	0,7513419573	0,7832276493	0,6924986933	0,7606457946	0,7051610272	0,7717389225	0,7536125326	0,7804005737	
CIA		1,04737829	1,0442561457	1,0567351211	1,0007944473	1,0475915	1,0075095546	1,0381389525	1,0479500158	1,0286314466	1,0591122991	1,0346529469	1,0435974479	1,1088265752	1,0891744418	1,0272724217	1,0211338554	1,1051860159	1,0427018228	1,0133815913	1,0153965536	
Cr/Th		6,7859322911	3,7282713387	6,8084934258	9,5187770542	6,0115308786	5,6706974111	5,2411669328	7,7437527393	8,6827605265	9,8611737821	7,5581101881	5,8695384461	6,3055583186	5,9691067094	4,0001079502	5,0101754821	8,5387777941	6,7634930369	5,0859218222	11,5326887	
Th/Sc		0,8627669117	1,7234112259	1,3774419886	1,1856708889	1,3279359178	0,9694896181	1,4607989474	1,6340758499	1,1223878938	0,9826895076	1,0351095583	1,6810663876	2,0214676526	1,7603207	1,5424234821	1,4985219585	1,4370847778	0,9698485046	1,4229590171	0,4170100088	
Zr/Sc		21,0822631	36,4879750617	33,6044782	37,5412302	16,9392330	13,2470307	28,4836466	30,1696366	16,2724823	33,4040088	27,9382037	28,4488574	28,5913095	31,1548688	28,2468946	27,3679477	21,7304378	20,4512083	18,7998965	19,3144709	
$^{143}Nd/^{144}Nd$		0,1133967802	0,1090556992	0,1050784	0,1014582001	0,1071065611	0,1133084124	0,1066662219	0,1077118404	0,1032920045	0,1155866651	0,0996497754	0,1041875923	0,0955834078	0,1020217716	0,1049421188	0,1121095519	0,1038464177	0,1141219432	0,1022990171	0,1018775595	
$^{147}Nd/^{144}Nd$ x																						
2SE		0,5115144/-10	0,5115214/-4	0,5114838/-6	0,5114844/-10	0,5115194/-9	0,5121114/-6	0,5114814/-10	0,5114804/-11	0,5114974/-8	0,5115444/-11	0,5113604/-16	0,5114554/-14	0,5114574/-8	0,5114594/-18	0,5114614/-8	0,5115184/-18	0,5115204/-14	0,5113564/-10	0,5114874/-5	0,5113854/-15	
$\varepsilon_{Nd(0)}$		-21,9	-21,8	-22,3	-23,3	-21,8	-10,3	-22,4	-22,6	-23,8	-13,5	-24,9	-23,1	-23,0	-23,0	-20,1	-21,8	-23,8	-19,0	-22,5	-24,4	
$T_{DM\ (Ga)}$		1,9272039883	1,2049806884	1,1632899299	1,0905559527	1,2476801179	1,4010827702	1,1980088113	1,2365670019	1,2080488979	1,6928899889	1,2976793212	1,2988554431	1,2388615801	1,2501112742	1,1894962899	1,2786852382	1,1945735894	1,6511612245	1,2559809866	1,2485150442	

LREE = La_{PAAS} + Pr_{PAAS} + Nd_{PAAS} (in ppm); MREE = Gd_{PAAS} + Tb_{PAAS} + Dy_{PAAS} (in ppm); HREE = Tm_{PAAS} + Yb_{PAAS} + Lu_{PAAS} (in ppm); MREE* = (MREE+LREE) / 2;
CIA=[Al_2O_3/(Al_2O_3+CaO^*+Na_2O+K_2O)] ·100 (in molar proportion). Eu/Eu^* = Eu_{PAAS}/(Sm_{PAAS} · Gd_{PAAS})$^{1/2}$ where X_{PAAS} refers to the chondrite-normalized concentration value (Condie, 1993);
$\varepsilon Nd_{(0)}$ = 2 x [(Ce_{sample}/Ce_{PAAS}) / [(La_{sample}/La_{PAAS}) + (Pr_{sample}/Pr_{PAAS})]

B.2 Correlations based on correlation coefficient (R^2) for geochemical proxies used in this study based on a data matrix without outlier data. Significant correlations are presented in blue

	$^{147}Sm/^{144}Nd$	εNd(0)	Eu/Eu*	ΩCe	Cr/Th	Th/Sc	Zr/Sc	LREE	HREE	MREE	MREE*	Al/Si	CIA	T_{DM} (Ga)
$^{147}Sm/^{144}Nd$	1	0,69	-0,18	-0,16	-0,06	-0,32	-0,20	0,15	0,29	0,25	0,22	0,14	0,47	-0,40
εNd(0)		1	0,07	-0,02	-0,06	-0,31	-0,27	0,13	0,25	0,22	0,19	0,00	0,51	**-0,94**
Eu/Eu*			1	-0,01	0,01	-0,12	-0,25	0,40	0,31	0,38	0,36	0,40	0,15	-0,17
ΩCe				1	-0,23	0,63	0,18	-0,03	-0,08	-0,05	-0,05	0,10	-0,34	-0,04
Cr/Th					1	-0,66	-0,08	-0,72	-0,71	-0,71	-0,72	-0,57	0,25	0,03
Th/Sc						1	0,45	0,35	0,27	0,30	0,32	0,33	-0,62	0,25
Zr/Sc							1	-0,04	-0,03	-0,05	-0,04	-0,20	-0,12	0,25
LREE								1	**0,97**	**0,99**	**0,99**	**0,85**	-0,06	-0,08
HREE									1	**0,99**	**0,99**	**0,82**	0,02	-0,18
MREE										1	**1,00**	**0,84**	-0,01	-0,15
MREE*											1	**0,84**	-0,03	-0,13
Al/Si												1	-0,29	0,07
CIA													1	-0,43
T_{DM} (Ga)														1

B.3 Sm-Nd isotopic compositon of analysed samples; See text for details

Sample	Depth (m)	Chosen depth in Fig7	$^{143}Nd/^{144}Nd$	± 2σ	$e_{Nd(0)}$	± 1σ	$T_{DM\ (Ga)}$	$^{147}Sm/\ ^{144}Nd$
pow01 128-135	128-135	135	0,511385	0,000015	-24,4	0,3	2,24851504	0,1018756
pow01 135-140	135-140	140	0,511524	0,000008	-21,7	0,2	2,37877581	0,11672309
pow01 140-150	140-150	150	0,512111	0,000006	-10,3	0,1	1,4010827	0,11308412
pow01 150-160	150-160	160	0,511434	0,000033	-23,5	0,6	2,27801385	0,10658527
pow01 160-170	160-170	170	0,511461	0,000027	-23,0	0,5	2,21076929	0,10519617
pow01 170-180	170-180	180	0,511615	0,00001	-20,0	0,2	2,0987574	0,11060294
pow01 180-190	180-190	190	0,511956	0,00001	-13,3	0,2	1,65116125	0,11421943
pow01 190-200	190-200	200	0,511944	0,000008	-13,5	0,2	1,6929897	0,11556665
pow01 200-210	200-210	210	0,511628	0,000018	-19,7	0,4	2,03666818	0,10846146
pow01 220-230	220-230	230	0,511629	0,000016	-19,7	0,3	2,06828855	0,11012206
pow01 230-240	230-240	240	0,511353	0,000026	-25,1	0,5	2,25443177	0,09997445
pow01 240-250	240-250	250	0,511493	0,000006	-22,3	0,1	2,1632993	0,1050794
pow01 250-260	250-260	260	0,511457	0,000006	-23,0	0,1	2,0386158	0,09585408
pow01 290-300	290-300	300	0,511494	0,00001	-22,3	0,2	2,09055353	0,1014532
pow01 320-330	320-330	330	0,51136	0,000016	-24,9	0,3	2,23767321	0,09964975
pow01 350-360	350-360	360	0,511459	0,000013	-23,0	0,3	2,15011274	0,10202772
pow01 370-380	370-380	380	0,511497	0,000008	-22,3	0,2	2,10304898	0,10232005
pow01 390-400	390-400	400	0,51148	0,00001	-22,6	0,2	2,23656701	0,1077118
pow01 420-430	420-430	430	0,511491	0,00001	-22,4	0,2	2,19808813	0,10666623
pow01 470-480	470-480	480	0,511455	0,000014	-23,1	0,3	2,19885543	0,10418793
pow01 530-540	530-540	540	0,511514	0,00002	-21,9	0,4	2,32720398	0,1139678
pow01 590-600	590-600	600	0,51152	0,000014	-21,8	0,3	2,19497359	0,10848418
pow01 600-610	600-610	610	0,51161	0,000009	-20,1	0,2	1,9949629	0,10494219
pow01 630-640	630-640	640	0,511521	0,000004	-21,8	0,1	2,20490868	0,10905699
pow01 660-670	660-670	670	0,511518	0,000018	-21,8	0,4	2,27668528	0,11210951
pow01 680-690	680-690	690	0,511487	0,000005	-22,5	0,1	2,19599099	0,10628488
pow01 690-700	690-700	700	0,511519	0,00001	-21,8	0,2	2,16768018	0,10710651

C.1 Dinoflagellate cyst counts

Depth (m)	*Adnatosphaeridium multispinosum*	*Apectodinium* spp.	*Eocladopyxis peniculata*	*Homotryblium* spp.	*Hystrichokolpoma rigaudiae*	*Kallosphaeridium yorubaense*	*Lingulodinium machaerophorum*	*Muratodinium fimbriatum*
190								
200								
250							1	
280							5	
300								
310					1			
350								
390								
410								
610		15	7	3		2	1	3
650		1	4	1		1		
660	1		3					
690								

C.1 Dinoflagellate cyst counts

Depth (m)	*Operculodinium centrocarpum*	*Operculodinium israelianum*	*Polysphaeridium zoharyi*	*Selenopemphix* spp.	*Spiniferites mirabilis*	*Spiniferites* spp.	*Tuberculodinium vancampoae*
190				1		4	
200					1	3	
250			4			2	1
280	16		30			18	
300			1				
310			10			9	1
350						1	1
390			1				
410	1		2				
610	5	2	6			7	
650							
660							
690	1	1					

C.2 Pollen count sheet of the Powisi-01 well

Depth	*160-170*	*190-200*	*230-240*	*240-250*	*250-260*	*260-270*	*270-280*	*280-290*	*290-300*	*300-310*	*310-320*	*320-330*	*340-350*	*350-360*	*360-370*	*370-380*	*380-390*	*390-400*	*400-410*	*410-420*	*490-500*	*600-610*	*610-620*	*630-640*	*640-650*	*650-660*	*660-670*	*670-680*	*680-690*	*690-700*
Taxa																														
Mangroves																														
Zonocostites ramonae	0	47	102	201	247	286	385	342	140	233	600	365	674	844	632	579	108	82	244	45	15	12	12	13	0	0	0	2	0	2
Zonocostites duquensis	0	0	20	0	0	0	0	0	0	0	0	0	0	4	0	0	0	0	0	0	0	0	0	0	0	0	0	0	0	0
Verrutricolporites rotundiporus	0	0	0	1	0	0	90	24	0	0	0	0	5	6	13	7	3	1	0	0	1	0	0	0	0	0	0	0	0	0
Psilastephanocolporites schneideri	0	0	0	0	0	0	6	0	1	0	0	0	0	0	0	27	0	0	11	1	0	0	0	0	0	0	0	0	0	0
Zonocostites spp.	0	0	0	0	0	0	0	9	7	0	0	0	0	0	0	0	0	0	0	5	2	0	0	0	0	0	0	0	0	0
Lanagiopollis crassa	0	0	2	0	0	0	0	0	0	0	0	0	4	0	1	0	0	0	0	0	0	0	0	0	0	0	0	0	0	0
Palms																														
Mauritiidites franciscoi franciscoi	0	0	1	0	2	1	3	4	32	56	5	4	2	16	0	4	0	1	1	0	1	6	3	6	5	4	7	2	0	3
Arecipites spp.	0	0	6	0	3	9	0	0	7	25	0	4	0	5	6	0	0	0	0	0	0	4	16	14	12	46	15	85	25	16
Retimonocolpites bernardii	0	0	0	2	0	0	0	0	0	0	0	0	0	0	0	0	0	0	0	0	0	0	4	0	0	0	0	0	2	0
Psilamonocolpites nanus	0	0	0	0	1	0	0	0	0	0	8	1	0	0	1	0	0	0	1	0	0	0	5	20	3	0	1	0	2	0
Psilamonocolpites amazonicus	0	0	0	0	0	0	4	2	0	1	0	0	0	1	1	0	0	0	3	0	1	7	14	11	0	0	1	0	1	0
Echidiporites barbeitoensis	0	0	0	0	0	0	4	0	0	0	0	0	0	0	0	0	0	0	0	0	0	0	0	0	0	0	0	0	0	0
Retimonocolpites maximus	0	0	0	0	0	0	0	1	0	0	0	0	0	0	0	3	0	0	0	0	0	0	0	0	0	0	0	0	0	0
Baculamonocolpites sp.1	0	0	0	0	0	0	0	1	0	0	0	0	0	0	0	0	0	0	0	0	0	0	0	0	0	0	0	0	0	0
Arecipites cf. *perfectus*	0	0	0	0	0	0	0	1	19	4	0	0	0	9	0	0	0	0	0	0	0	0	0	0	0	0	0	0	0	0
Psilamonocolpites medius	0	0	0	0	0	0	0	1	0	0	0	0	0	0	1	0	0	1	0	0	0	0	0	13	5	31	4	0	0	0

C.2 Pollen count sheet of the Powisi-01 well

Depth	*160-170*	*190-200*	*230-240*	*240-250*	*250-260*	*260-270*	*270-280*	*280-290*	*290-300*	*300-310*	*310-320*	*320-330*	*340-350*	*350-360*	*360-370*	*370-380*	*380-390*	*390-400*	*400-410*	*410-420*	*490-500*	*600-610*	*610-620*	*630-640*	*640-650*	*650-660*	*660-670*	*670-680*	*680-690*	*690-700*
Psilamonocolpites rinconii	0	0	0	0	0	0	0	0	2	0	0	0	0	0	0	0	2	0	0	0	0	0	5	1	8	4	0	0	0	0
Echimonocolpites spp.	0	0	0	0	0	0	0	0	1	0	0	0	0	0	0	0	0	0	0	0	0	4	0	0	0	0	0	5	0	0
Mauritiidites franciscoi minutus	0	0	0	0	0	0	0	0	0	6	1	0	1	0	0	0	0	1	2	0	0	6	0	2	0	0	0	0	0	0
Trichotomonosulcites sp.	0	0	0	0	0	0	0	0	0	2	0	0	0	0	0	0	0	0	0	0	0	0	0	0	0	0	0	0	0	0
Psilamonocolpites sp.	0	0	0	0	0	0	0	0	0	0	0	0	0	0	0	0	0	0	2	0	0	0	0	0	0	0	0	0	2	0
Psilamonocolpites grandis	0	0	0	0	0	0	0	0	0	0	0	0	0	0	0	0	0	0	0	1	0	0	0	0	4	9	0	0	0	0
Retimonocolpites spp.	0	0	0	0	0	0	0	0	0	20	0	0	0	0	4	0	0	0	0	0	0	1	5	15	5	5	15	145	0	0
Mauritiidites crassibaculatus	0	0	0	0	0	0	0	0	0	0	0	0	0	0	0	0	0	0	0	0	0	2	0	1	2	1	1	0	0	0
Racemonocolpites facilis	0	0	0	0	0	0	0	0	0	0	0	0	0	0	0	0	0	0	0	0	0	0	0	1	0	0	0	0	0	0
Grimsdalea magnaclavata	0	0	0	0	0	0	0	0	0	0	0	0	0	0	0	0	0	0	0	0	0	0	0	0	0	2	0	0	0	0
Racemonocolpites racematus	0	0	0	0	0	0	0	0	0	0	0	0	0	0	0	0	0	0	0	0	0	0	0	0	0	0	0	0	0	1
Herbs																														
#Sapotaceae-Burseraceae	0	0	0	0	0	1	2	0	2	0	0	0	0	3	0	0	0	22	2	0	0	2	0	0	0	0	0	0	0	0
Monoporopollenites annulatus	0	0	0	0	0	0	2	0	0	0	1	0	0	0	4	5	0	0	0	0	0	3	4	0	0	0	0	2	0	0
Echitricolporites spinosus	0	0	0	0	0	0	0	1	0	0	0	0	0	0	0	0	0	0	0	0	0	0	0	0	0	0	0	0	0	0
Cyperaceapollis sp.	0	0	0	0	0	0	0	0	0	0	0	0	0	0	0	0	0	0	0	0	0	7	0	0	0	0	0	0	0	0
Ferns/ Spores																														
Polypodiisporites usmensis	0	1	5	1	0	0	3	2	2	17	3	0	4	0	0	0	0	0	0	0	0	0	0	0	0	0	0	0	0	0
Polypodiisporites planus	0	0	1	0	0	0	2	0	0	0	0	0	0	0	2	0	0	0	0	0	0	0	0	0	0	0	0	0	0	0
Polypodiisporites aff. *specious*	0	0	0	0	0	0	5	0	0	0	0	0	0	0	0	0	0	0	0	0	0	0	0	0	0	0	0	0	0	1

C.2 Pollen count sheet of the Powisi-01 well

Depth	*160-170*	*190-200*	*230-240*	*240-250*	*250-260*	*260-270*	*270-280*	*280-290*	*290-300*	*300-310*	*310-320*	*320-330*	*340-350*	*350-360*	*360-370*	*370-380*	*380-390*	*390-400*	*400-410*	*410-420*	*490-500*	*600-610*	*610-620*	*630-640*	*640-650*	*650-660*	*660-670*	*670-680*	*680-690*	*690-700*
Crassoretitriletes vanraadshoovenii	0	0	0	0	0	0	0	1	0	0	0	0	0	0	0	0	0	0	0	0	0	0	0	0	0	0	0	0	0	0
Hamulatisporis caperatus	0	0	0	0	0	0	0	0	1	0	0	0	0	0	0	0	0	0	0	0	0	0	0	0	0	0	0	0	0	0
Deltoidospora adriennis	0	0	0	0	0	0	0	0	0	1	0	0	0	0	0	0	0	2	0	0	0	0	0	0	0	0	0	0	0	0
Magnastriatites grandiosus	0	0	0	0	0	0	0	0	0	0	0	0	0	0	0	0	0	2	1	0	0	0	0	0	0	0	0	0	0	0
Hydrosporis minor	0	0	0	0	0	0	0	0	0	0	0	0	0	0	0	0	0	0	1	0	0	0	0	0	0	1	0	0	0	0
Foveotriletes ornatus	0	0	0	0	0	0	0	0	0	0	0	0	0	0	0	0	0	0	0	0	0	1	0	0	0	0	0	0	0	0
Verrucatotriletes pseudoviruleoides	0	0	0	0	0	0	0	0	0	0	0	0	0	0	0	0	0	0	0	0	0	0	0	3	2	1	2	0	0	1
Psilatriletes marginatus	0	0	0	0	0	0	0	0	0	0	0	0	0	0	0	0	0	0	0	0	0	0	0	0	3	0	0	1	0	0
Striatopollis sp.	0	0	0	0	0	0	0	0	0	0	0	0	0	0	0	0	0	0	0	0	0	0	0	0	0	0	0	0	1	0
Andean																														
Alnipollenites verus	0	0	0	0	0	0	0	0	1	0	0	0	0	0	0	0	0	0	0	0	0	0	1	1	0	0	0	0	0	0
Podocarpidites spp.	0	0	0	0	0	0	0	0	0	0	0	0	0	0	0	0	0	0	0	0	0	0	0	0	0	0	1	1	0	0
Other Angiosperms																														
#Combretaceae-Melastomataceae	1	4	1	3	0	1	5	15	65	23	0	0	3	7	4	3	1	14	0	2	0	1	0	18	0	20	1	9	6	0
Syncolperites incomptus	0	3	0	0	0	0	2	0	2	0	1	2	0	6	3	6	2	2	2	0	0	0	0	0	0	2	0	0	0	0
Psilatricolporites crassoexinatus	0	0	3	1	7	0	0	0	3	0	0	0	0	0	1	0	0	0	0	0	0	0	0	0	0	0	0	0	0	0
Ilexpollenites tropicales	0	0	3	2	0	1	0	0	2	0	1	0	0	0	0	0	0	0	0	0	0	0	0	0	0	0	0	0	0	0
Rhoipites indet	0	0	3	0	0	0	0	0	0	0	0	0	0	0	0	0	0	0	0	0	0	0	0	0	0	0	0	0	0	0
Rhoipites guianensis	0	0	1	2	0	0	0	0	0	0	0	21	15	2	2	1	1	4	7	4	0	1	0	0	0	0	0	0	0	0
Syncolporites poricostatus	0	0	0	1	3	0	0	4	17	14	2	0	0	0	1	1	3	8	0	0	0	0	0	0	0	0	0	0	0	0
Retibrevitricolpites indet	0	0	0	1	0	0	0	0	0	0	0	0	0	0	0	0	0	0	0	0	0	0	0	0	0	0	0	0	0	0

C.2 Pollen count sheet of the Powisi-01 well

Depth	*160-170*	*190-200*	*230-240*	*240-250*	*250-260*	*260-270*	*270-280*	*280-290*	*290-300*	*300-310*	*310-320*	*320-330*	*340-350*	*350-360*	*360-370*	*370-380*	*380-390*	*390-400*	*400-410*	*410-420*	*490-500*	*600-610*	*610-620*	*630-640*	*640-650*	*650-660*	*660-670*	*670-680*	*680-690*	*690-700*
Rhoipites crassicostatus	0	0	0	0	0	0	5	0	0	0	0	0	0	0	0	0	0	0	0	0	0	0	0	0	0	0	0	1	0	0
Bombacacidites baculatus	0	0	0	0	0	0	1	0	0	0	0	0	0	0	0	0	0	0	0	0	0	0	0	0	0	0	0	0	0	0
Brevitricolporites spp.	0	0	0	0	0	0	1	3	1	1	0	0	0	0	0	0	0	0	0	0	0	0	0	0	0	0	0	0	0	0
Retitricolporites irregularis	0	0	0	0	0	0	0	1	6	3	0	1	1	1	0	1	1	17	7	0	0	0	0	0	0	0	0	0	0	0
Psiladiporites minimus	0	0	0	0	0	0	0	3	1	7	1	0	0	0	0	0	0	0	0	0	0	0	0	0	0	1	0	0	0	0
Foveotricolpites simplex	0	0	0	0	0	0	0	6	0	0	0	0	0	0	0	0	0	0	0	0	0	0	5	7	1	1	0	4	2	0
Retitricolporites brevis nov. sp.	0	0	0	0	0	0	0	5	0	0	0	0	0	0	0	0	0	0	0	0	0	0	0	0	0	0	0	0	0	0
Verrutricolporites aff. *haplites*	0	0	0	0	0	0	0	3	0	1	0	0	0	0	0	0	0	0	0	0	0	0	0	0	0	0	0	0	0	0
Retibrevitricolpites catatumbus	0	0	0	0	0	0	0	0	2	0	0	0	0	0	0	0	0	0	0	0	0	0	0	0	0	0	0	0	0	0
Psilabrevitricolporites devriesii	0	0	0	0	0	0	0	0	2	22	0	0	0	0	0	0	0	0	0	0	0	0	0	0	0	0	0	0	0	0
Crassiectoapertites columbianus	0	0	0	0	0	0	0	0	1	0	0	0	0	0	0	0	0	0	0	0	0	0	0	0	0	0	0	0	0	0
Psilastephanoporites aff. Apocynaceae	0	0	0	0	0	0	0	0	1	0	0	0	0	0	0	0	0	0	0	0	0	0	0	0	0	0	0	0	0	0
Perisyncolporites pokornyi	0	0	0	0	0	0	0	0	1	4	0	0	1	0	0	0	0	0	0	0	0	0	0	0	0	0	0	0	0	0
Retibrevitricolpites retibolus	0	0	0	0	0	0	0	0	1	0	0	0	1	0	0	0	0	0	0	0	0	0	0	0	0	0	0	0	0	0
Psilatriporites aff. *minimus*	0	0	0	0	0	0	0	0	1	0	0	0	0	0	0	0	0	0	0	0	0	0	0	0	0	0	0	0	0	0
Ranunculacidites operculatus	0	0	0	0	0	0	0	0	1	1	0	0	2	2	0	4	1	0	0	0	1	2	0	1	0	0	0	0	0	0
Psilatricolporites venezuelanus	0	0	0	0	0	0	0	0	1	0	0	0	0	0	0	0	0	0	0	0	0	0	0	0	0	0	0	0	0	0
Psilatriporites sarmientoi	0	0	0	0	0	0	0	0	0	1	0	0	0	0	0	0	0	0	0	0	0	0	0	0	0	0	0	0	0	0
Striatopollis catatumbus	0	0	0	0	0	0	0	0	0	3	0	0	0	0	0	0	0	0	0	0	0	0	0	0	0	0	0	0	0	0
Annutriporites iversenii	0	0	0	0	0	0	0	0	0	8	0	0	0	0	0	0	0	0	0	0	0	0	0	0	0	0	0	0	0	0
Syncolpites lorantaceae	0	0	0	0	0	0	0	0	0	1	0	0	0	0	0	0	0	0	0	0	0	0	0	0	0	0	0	0	0	0
Stephanocolpites cf. *nertera*	0	0	0	0	0	0	0	0	0	3	0	0	0	0	0	0	0	0	0	0	0	0	0	0	0	0	0	0	0	0
Rhoipites hispidus	0	0	0	0	0	0	0	0	0	12	0	0	0	0	3	0	0	0	0	0	0	0	0	0	0	0	0	0	0	0

C.2 Pollen count sheet of the Powisi-01 well

Depth	*160-170*	*190-200*	*230-240*	*240-250*	*250-260*	*260-270*	*270-280*	*280-290*	*290-300*	*300-310*	*310-320*	*320-330*	*340-350*	*350-360*	*360-370*	*370-380*	*380-390*	*390-400*	*400-410*	*410-420*	*490-500*	*600-610*	*610-620*	*630-640*	*640-650*	*650-660*	*660-670*	*670-680*	*680-690*	*690-700*
Ladakhipollenites? garzonii	0	0	0	0	0	0	0	0	0	0	1	0	0	0	0	0	0	0	0	0	0	0	0	0	0	0	0	0	0	0
Psilatriporites desilvae	0	0	0	0	0	0	0	0	0	0	0	0	1	0	0	0	0	1	0	0	0	0	1	0	0	0	0	0	7	0
Paleosantalaceaepites cingulatus	0	0	0	0	0	0	0	0	0	0	0	0	1	23	0	0	0	0	0	0	0	2	0	0	0	0	0	0	0	0
Siltaria dilcheri	0	0	0	0	0	0	0	0	0	0	0	0	0	1	0	1	0	0	0	0	0	0	0	0	0	0	0	0	0	0
Brevicolporites molinae	0	0	0	0	0	0	0	0	0	0	0	0	0	1	0	0	0	0	0	0	0	0	0	0	0	0	0	0	0	0
Bombacacidites brevis	0	0	0	0	0	0	0	0	0	0	0	0	0	1	0	0	0	0	0	0	0	0	0	0	0	0	0	0	0	0
#Caperonia	0	0	0	0	0	0	0	0	0	0	0	0	0	0	1	0	0	0	0	0	0	0	0	0	0	0	0	0	0	0
Retistephanocolpites williamsi	0	0	0	0	0	0	0	0	0	0	0	0	0	0	1	0	0	0	0	0	0	0	0	0	0	0	0	0	0	0
Jandufouria saemrogiformis	0	0	0	0	0	0	0	0	0	0	0	0	0	0	1	0	0	0	0	0	0	0	0	0	0	0	0	0	0	0
Psilatricolporites exiguus	0	0	0	0	0	0	0	0	0	0	0	0	0	0	2	0	0	0	0	0	0	0	0	0	0	0	0	0	0	0
Psilatricolpites papilioniformis	0	0	0	0	0	0	0	0	0	0	0	0	0	0	0	3	0	0	0	0	0	0	0	0	0	0	0	0	0	0
#Catostemma alstonii	0	0	0	0	0	0	0	0	0	0	0	0	0	0	0	0	0	1	0	0	0	0	0	0	0	0	0	0	0	0
Rhoipites oblatus	0	0	0	0	0	0	0	0	0	0	0	0	0	0	0	0	0	0	1	0	0	0	0	0	0	0	0	0	0	0
Echiperiporites akanthos	0	0	0	0	0	0	0	0	0	0	0	0	0	0	0	0	0	0	0	16	0	0	0	0	0	0	0	0	0	0
Echiperiporites germeraadii	0	0	0	0	0	0	0	0	0	0	0	0	0	0	0	0	0	0	0	3	0	0	0	0	0	0	0	0	0	0
Crototricolpites cf. *annemariae*	0	0	0	0	0	0	0	0	0	0	0	0	0	0	0	0	0	0	0	3	0	1	1	1	0	0	1	0	0	0
Crototricolpites cf. *manihot*	0	0	0	0	0	0	0	0	0	0	0	0	0	0	0	0	0	0	0	0	0	3	3	0	0	0	0	0	0	0
Retibrevitricolpites pseudoretibolus	0	0	0	0	0	0	0	0	0	0	0	0	0	0	0	0	0	0	0	0	0	1	0	0	0	0	0	0	0	0
Psilatriporites corstanjei	0	0	0	0	0	0	0	0	0	0	0	0	0	0	0	0	0	0	0	0	0	10	11	14	1	4	2	0	8	0
Verrutricolporites desmodiensis	0	0	0	0	0	0	0	0	0	0	0	0	0	0	0	0	0	0	0	0	0	3	0	0	1	0	0	0	0	0
Malvacipolloides maristellae	0	0	0	0	0	0	0	0	0	0	0	0	0	0	0	0	0	0	0	0	0	1	0	0	0	0	0	0	0	0
Bombacacidites protofoveoreticulatus	0	0	0	0	0	0	0	0	0	0	0	0	0	0	0	0	0	0	0	0	0	0	1	2	1	1	0	0	0	1
Bombacacidites psilatus	0	0	0	0	0	0	0	0	0	0	0	0	0	0	0	0	0	0	0	0	0	0	3	0	5	0	0	0	0	0

C.2 Pollen count sheet of the Powisi-01 well

Depth	*160-170*	*190-200*	*230-240*	*240-250*	*250-260*	*260-270*	*270-280*	*280-290*	*290-300*	*300-310*	*310-320*	*320-330*	*340-350*	*350-360*	*360-370*	*370-380*	*380-390*	*390-400*	*400-410*	*410-420*	*490-500*	*600-610*	*610-620*	*630-640*	*640-650*	*650-660*	*660-670*	*670-680*	*680-690*	*690-700*
Tetracolporites quadratus	0	0	0	0	0	0	0	0	0	0	0	0	0	0	0	0	0	0	0	0	0	0	0	1	0	0	0	0	0	0
Bombacacidites annae	0	0	0	0	0	0	0	0	0	0	0	0	0	0	0	0	0	0	0	0	0	0	1	0	0	0	0	0	0	1
Crototricolpites cf. *protoannemariae*	0	0	0	0	0	0	0	0	0	0	0	0	0	0	0	0	0	0	0	0	0	0	0	1	0	1	0	0	0	0
Psilaperiporites aff. *Apocynaceae*?	0	0	0	0	0	0	0	0	0	0	0	0	0	0	0	0	0	0	0	0	0	0	0	3	1	0	0	1	0	0
Cricotriporites guianensis	0	0	0	0	0	0	0	0	0	0	0	0	0	0	0	0	0	0	0	0	0	0	0	6	0	0	0	3	0	0
Echitriporites suescae	0	0	0	0	0	0	0	0	0	0	0	0	0	0	0	0	0	0	0	0	0	0	0	0	0	2	0	0	0	0
Cricotriporites operculatus	0	0	0	0	0	0	0	0	0	0	0	0	0	0	0	0	0	0	0	0	0	0	0	0	0	1	0	0	0	0
Retidiporites magdalenensis	0	0	0	0	0	0	0	0	0	0	0	0	0	0	0	0	0	0	0	0	0	0	0	0	0	1	0	0	0	0
Microfoveotriporites cretaceous	0	0	0	0	0	0	0	0	0	0	0	0	0	0	0	0	0	0	0	0	0	0	0	0	0	0	2	0	0	0
Bombacacidites cf. *araracuarensis*	0	0	0	0	0	0	0	0	0	0	0	0	0	0	0	0	0	0	0	0	0	0	0	0	0	0	2	0	0	0
Echistephanoporites sp.	0	0	0	0	0	0	0	0	0	0	0	0	0	0	0	0	0	0	0	0	0	0	0	0	0	2	0	0	0	0
Scabratriporites simpliformis	0	0	0	0	0	0	0	0	0	0	0	0	0	0	0	0	0	0	0	0	0	0	0	0	0	0	0	1	0	0
Retibrevicolporites solimoensis	0	0	0	0	0	0	0	0	0	0	0	0	0	0	0	0	0	0	0	0	0	0	0	0	0	0	0	1	0	0
Psilatriporites aff. *Moraceae*	0	0	0	0	0	0	0	0	0	0	0	0	0	0	0	0	0	0	0	0	0	0	0	0	0	0	0	1	0	0
Gemmastephanocolpites gemmatus	0	0	0	0	0	0	0	0	0	0	0	0	0	0	0	0	0	0	0	0	0	0	0	0	0	0	0	1	0	0
Psilaperiporites sp.	0	0	0	0	0	0	0	0	0	0	0	0	0	0	0	0	0	0	0	0	0	0	0	0	0	0	0	0	17	0
Clavatricolpites densiclavatus	0	0	0	0	0	0	0	0	0	0	0	0	0	0	0	0	0	0	0	0	0	0	0	0	0	0	0	0	1	0
Perfotricolpites digitatus	0	0	0	0	0	0	0	0	0	0	0	0	0	0	0	0	0	0	0	0	0	0	0	0	0	0	0	0	1	0
Echitriporites trianguliformis	0	0	0	0	0	0	0	0	0	0	0	0	0	0	0	0	0	0	0	0	0	0	0	0	0	0	0	0	2	0
Retibrevitricolpites sp.1	0	0	0	0	0	0	0	0	0	0	0	0	0	0	0	0	0	0	0	0	0	0	0	0	0	0	0	0	1	1
Psilatricolporites costatus	0	0	0	0	0	0	0	0	0	0	0	0	0	0	0	0	0	0	0	0	0	0	0	0	0	0	0	0	0	3
Aglaoreidia? *Foveolata*	0	0	0	0	0	0	0	0	0	0	0	0	0	0	0	0	0	0	0	0	0	0	0	0	0	0	0	0	0	1
Momipites africanus	0	0	0	0	0	0	0	0	0	0	0	0	0	0	0	0	0	0	0	0	0	0	0	0	0	0	0	0	0	1

C.2 Pollen count sheet of the Powisi-01 well

Depth	*160-170*	*190-200*	*230-240*	*240-250*	*250-260*	*260-270*	*270-280*	*280-290*	*290-300*	*300-310*	*310-320*	*320-330*	*340-350*	*350-360*	*360-370*	*370-380*	*380-390*	*390-400*	*400-410*	*410-420*	*490-500*	*600-610*	*610-620*	*630-640*	*640-650*	*650-660*	*660-670*	*670-680*	*680-690*	*690-700*
Retitricolporites spp.	4	0	1	0	1	0	7	44	39	30	14	4	0	11	9	2	0	21	18	16	4	38	28	87	30	34	36	98	14	4
Scabratricolporites spp.	0	1	0	1	0	4	2	5	9	0	2	1	0	0	2	1	0	1	4	16	15	7	3	3	0	13	8	6	6	0
Psilatricolpites spp.	0	0	0	1	0	6	2	0	9	0	0	4	2	3	0	0	0	1	1	4	0	0	0	0	0	1	1	0	0	0
Gemmatricolporites spp.	0	0	0	1	0	0	0	0	0	0	0	0	0	0	0	3	0	11	0	0	0	0	0	0	0	2	3	2	2	0
Verrutricolporites spp.	0	0	0	0	3	0	5	16	0	1	0	0	0	0	0	0	0	0	0	3	0	3	3	0	0	1	0	2	0	0
Psilatricolporites spp.	0	0	0	0	2	4	15	9	10	9	0	1	1	0	0	0	0	14	6	1	0	27	6	20	22	10	9	11	24	1
Psilastephanocolporites spp.	0	0	0	0	5	0	1	0	0	1	0	0	0	8	3	0	2	2	2	0	0	0	0	2	2	2	0	1	1	0
Syncolporites spp.	0	0	0	0	0	1	1	0	0	0	3	0	0	2	0	2	0	0	0	0	0	0	0	0	0	0	0	0	0	0
Psilatriporites spp.	0	0	0	0	0	0	3	0	1	9	0	0	0	4	0	0	0	0	0	0	0	0	0	1	1	0	0	1	0	0
Syncolpites spp.	0	0	0	0	0	0	1	0	0	0	0	0	0	0	0	0	0	0	0	0	0	0	0	0	0	1	2	0	0	0
Retistephanocolporites spp.	0	0	0	0	0	0	1	3	0	13	0	0	0	0	0	0	0	0	0	19	0	0	2	0	0	0	0	0	3	0
Scabratricolpites spp.	0	0	0	0	0	0	1	4	1	0	0	0	0	0	0	0	0	0	2	1	0	0	1	0	2	0	2	0	2	3
Scabrastephanocolporites spp.	0	0	0	0	0	0	2	15	1	2	0	0	0	0	0	0	0	7	0	3	0	0	0	0	0	0	0	0	0	0
Scabratriporites spp.	0	0	0	0	0	0	0	1	0	0	0	0	0	0	0	0	0	0	0	0	0	1	0	0	0	0	1	3	0	0
Verrutricolpites spp.	0	0	0	0	0	0	0	1	0	0	0	0	0	0	0	17	0	0	0	0	0	3	0	9	0	0	0	0	0	0
Verrutriporites spp.	0	0	0	0	0	0	0	4	0	0	0	0	0	0	0	0	0	0	0	0	0	0	0	0	0	0	0	0	0	0
Retitricolpites spp.	0	0	0	0	0	0	0	7	9	6	5	0	0	1	0	0	0	2	3	0	0	13	14	23	17	16	3	6	0	1
Retiperiporites spp.	0	0	0	0	0	0	0	0	1	0	0	0	1	0	0	0	0	0	0	0	0	0	0	0	0	0	0	0	0	0
Retitriporites spp.	0	0	0	0	0	0	0	0	2	1	0	0	0	0	0	1	0	0	0	0	0	0	0	0	0	0	0	0	0	1
Psiladicolpites spp.	0	0	0	0	0	0	0	0	0	1	0	0	0	0	0	0	0	0	0	0	0	0	0	0	0	0	11	0	0	0
Retidicolpites spp.	0	0	0	0	0	0	0	0	0	2	0	0	0	0	0	0	0	0	0	0	0	0	0	0	0	0	0	0	0	0
Reti-inapertites spp.	0	0	0	0	0	0	0	0	0	0	1	0	0	0	0	0	0	0	0	0	0	0	0	0	0	0	0	0	0	0

C.2 Pollen count sheet of the Powisi-01 well

Depth	*160-170*	*190-200*	*230-240*	*240-250*	*250-260*	*260-270*	*270-280*	*280-290*	*290-300*	*300-310*	*310-320*	*320-330*	*340-350*	*350-360*	*360-370*	*370-380*	*380-390*	*390-400*	*400-410*	*410-420*	*490-500*	*600-610*	*610-620*	*630-640*	*640-650*	*650-660*	*660-670*	*670-680*	*680-690*	*690-700*
Foveodicolpites spp.	0	0	0	0	0	0	0	0	0	0	0	0	0	0	0	0	0	2	0	0	0	0	0	0	0	0	0	0	0	0
Perfotricolporites spp.	0	0	0	0	0	0	0	0	0	0	0	0	0	0	0	0	0	9	0	0	0	0	0	0	0	0	0	3	0	0
Clavastephanocolporites spp.	0	0	0	0	0	0	0	0	0	0	0	0	0	0	0	0	0	0	0	1	0	0	0	0	0	0	0	0	0	0
Foveotricolpites spp.	0	0	0	0	0	0	0	0	0	0	0	0	0	0	0	0	0	0	0	0	0	5	0	0	0	1	0	0	0	0
Clavatricolporites spp.	0	0	0	0	0	0	0	0	0	0	0	0	0	0	0	0	0	0	0	0	0	2	0	0	0	0	0	0	0	0
Echitetracolpites spp.	0	0	0	0	0	0	0	0	0	0	0	0	0	0	0	0	0	0	0	0	0	2	0	0	0	0	0	0	0	0
Retidiporites spp.	0	0	0	0	0	0	0	0	0	0	0	0	0	0	0	0	0	0	0	0	0	1	0	0	0	0	0	0	0	0
Scabrastephanoporites spp.	0	0	0	0	0	0	0	0	0	0	0	0	0	0	0	0	0	0	0	0	0	1	2	0	0	0	5	1	0	0
Psilastephanocolpites spp.	0	0	0	0	0	0	0	0	0	0	0	0	0	0	0	0	0	0	0	0	0	0	2	0	0	0	0	0	0	0
Foveomonocolpites spp.	0	0	0	0	0	0	0	0	0	0	0	0	0	0	0	0	0	0	0	0	0	0	0	5	0	4	0	4	0	5
Clavatricolpites spp.	0	0	0	0	0	0	0	0	0	0	0	0	0	0	0	0	0	0	0	0	0	0	0	0	1	0	0	0	0	0
Scabradiporites spp.	0	0	0	0	0	0	0	0	0	0	0	0	0	0	0	0	0	0	0	0	0	0	0	0	2	0	1	0	0	0
Psiladiporites spp.	0	0	0	0	0	0	0	0	0	0	0	0	0	0	0	0	0	0	0	0	0	0	0	0	0	3	0	0	0	0
Fenestrites spp.	0	0	0	0	0	0	0	0	0	0	0	0	0	0	0	0	0	0	0	0	0	0	0	0	0	1	0	0	0	0
Foveotricolporites spp.	0	0	0	0	0	0	0	0	0	0	0	0	0	0	0	0	0	0	0	0	0	0	0	0	0	4	0	0	0	1
Psila-inapertites spp.	0	0	0	0	0	0	0	0	0	0	0	0	0	0	0	0	0	0	0	0	0	0	0	0	0	1	3	0	0	0
Verrustephanocolporites spp.	0	0	0	0	0	0	0	0	0	0	0	0	0	0	0	0	0	0	0	0	0	0	0	0	0	0	1	1	0	0
Foveodiporites spp.	0	0	0	0	0	0	0	0	0	0	0	0	0	0	0	0	0	0	0	0	0	0	0	0	0	0	0	0	1	0
Proxapertites and Longapertites																														
Longapertites aff. *vaneendenburgi*	0	0	0	0	0	0	0	0	0	0	0	0	0	0	0	0	0	0	0	0	0	17	1	0	0	0	0	0	0	0
Proxapertites cursus	0	0	0	0	0	0	0	0	0	0	0	0	0	0	0	0	0	0	0	0	0	0	0	4	5	8	3	5	1	0
Longapertites proxapertoides proxapertoides	0	0	0	0	0	0	0	0	0	0	0	0	0	0	0	0	0	0	0	0	0	0	0	3	3	0	0	0	0	0
Proxapertites humbertoides	0	0	0	0	0	0	0	0	0	0	0	0	0	0	0	0	0	0	0	0	0	0	0	1	0	0	1	0	0	0

C.2 Pollen count sheet of the Powisi-01 well

Depth	*160-170*	*190-200*	*230-240*	*240-250*	*250-260*	*260-270*	*270-280*	*280-290*	*290-300*	*300-310*	*310-320*	*320-330*	*340-350*	*350-360*	*360-370*	*370-380*	*380-390*	*390-400*	*400-410*	*410-420*	*490-500*	*600-610*	*610-620*	*630-640*	*640-650*	*650-660*	*660-670*	*670-680*	*680-690*	*690-700*
Proxapertites operculatus	0	0	0	0	0	0	0	0	0	0	0	0	0	0	0	0	0	0	0	0	0	0	0	0	5	0	11	4	0	0
Proxapertites minuthumbertoides	0	0	0	0	0	0	0	0	0	0	0	0	0	0	0	0	0	0	0	0	0	0	0	0	4	9	0	6	0	0
Proxapertites psilatus	0	0	0	0	0	0	0	0	0	0	0	0	0	0	0	0	0	0	0	0	0	0	0	0	0	2	0	3	0	0
Proxapertites tertiara	0	0	0	0	0	0	0	0	0	0	0	0	0	0	0	0	0	0	0	0	0	0	0	0	0	1	0	0	0	0
Longapertites spp.	0	0	0	0	0	0	0	0	0	0	0	0	0	0	0	0	0	0	0	0	0	0	0	0	0	0	0	12	0	0
Proxapertites minutus	0	0	0	0	0	0	0	0	0	0	0	0	0	0	0	0	0	0	0	0	0	0	0	0	0	0	0	0	7	0

REFERENCES

Amstelveen, C. J., Dupre, B., Negrel, Ph., & Gaillardet, J. (1996). Sr Nd Pb isotope systematics in Amazon and Congo River systems: constraints about erosion processes. *Chemical Geology*, *131*(1–4), 93–112.

Amstelveen, A. L. E. (1969). A palynological on three water wells in the coastal area of Surinam (Saramacca and Suriname Districts). *Geologische Mijnbouwkundige Dienst Mededeling*, *20*, 165–172.

Amstelveen, A. L. E. (1971). A palynostratigraphical correlation of seven test wells in the coastal plain of Surinam. *Geologie En Mijnbouw, 21*, 177182.

Anthony, E. J., Gardel, A., Gratiot, N., Proisy, C., Allison, M. A., Dolique, F., & Fromard, F. (2010). The Amazon-influenced muddy coast of South America: A review of mud-bank–shoreline interactions. *Earth-Science Reviews*, *103*, 99–121.

Anthony, E. J., Gardel, A., Proisy, Ch., Fromard, F., Gensac, E., Peron, Ch., Walcker, R., & Lesourd, S. (2013). The role of fluvial sediment supply and river-mouth hydrology in the dynamics of the muddy, Amazon-dominated Amapá-Guianas coast, South America: A three-point research agenda. *Journal of South American Earth Sciences*, *44*, 18–24. https://doi.org/10.1016/j.jsames.2012.06.005.

Antoine, P., Wieringa, L. N., Adnet, S., Aguilera, O., Bodin, S. C., Cairns, S., Conejeros-Vargas, C. A., Cornée, J. J., Ežerinskis, Ž., Fietzke, J., Gribenski, N. O., Grouard, S., Hendy, A., Hoorn, C., Joannes-Boyau, R., Langer, M. R., Luque, J., Marivaux, L., Moissette, P., … Heuret, A. (2024). A Late Pleistocene coastal ecosystem in French Guiana was hyperdiverse relative to today. *Proceedings of the National Academy of Sciences of the United States of America*, *121*(14). https://doi.org/10.1073/pnas.2311597121

Baltzer, F., Allison, M., & Fromard, F. (2004). Material exchange between the continental shelf and mangrove-fringed coasts with special reference to the Amazon-Guianas coast. *Marine Geology*, *208*(2 4), 115–126. https://doi.org/10.1016/j.margeo.2004.04.024.

Bayon, G., Henderson, G. M., Etoubleau, J., Caprais, J.-C., Ruffine, L., Marsset, T., Dennielou, B., Cauquil, E., Voisset, M., & Sultan, N. (2015). U-Th isotope constraints on gas hydrate and pockmark dynamics at the Niger delta margin. *Marine Geology*, *370*, 87–98.

Bijl, P. K. (2022). DINOSTRAT: a global database of the stratigraphic and paleolatitudinal distribution of Mesozoic–Cenozoic organic-walled dinoflagellate cysts. *Earth System Science Data*, *14*(2), 579–617.

Bijl, P. K., Bendle, J. A. P., Bohaty, S. M., & Yamane, M. (2013). Eocene cooling linked to early flow across the Tasmanian Gateway. *Earth, Atmospheric, and Planetary Sciences*, *110*(24), 9645–9650.

Bogotá-Ángel, G., Huang, H., Jardine, P. J., Chazot, N., Salamanca, S., Banks, H., Pardo-Trujillo, A., Plata, A., Dueñas, H., Star, W., Langelaan, R., Eisawi, A., Umeji, O. P., Enuenwemba, L.O., Parmar, S., Rocha da Silveira, R., Lim, J. Y., Prasad, V., Morley, R. J., Bacon, C. D., Hoorn, C. (2021). Climate and geological change as drivers of Mauritiinae palm biogeography. *Journal of Biogeography*, 48(5), 1001-1022. DOI: 10.1111/jbi.14098

Bolli, H. M. (1966). Zonation of Cretaceous to Pliocene marine sediments based on planktonic foraminifera. *Boletin Informativo Associacion Venezolana Geologia, Mineria y Petroleo*, *9*, 3–31.

Bouchez, J., Gaillardet, J., France-Lanord, Ch., Maurice, L., & Dutra-Maia, P. (2011). Grain size control of river suspended sediment geochemistry: Clues from Amazon River depth profiles. *Geochemistry, Geophysics, Geosystems*, *12*(3), 1–24.

Bujak, J. P., & Brinkhuis, H. (1998). Global warming and dinocyst changes across the Paleocene/Eocene epoch boundary. In M.-P. Aubry (Ed.), *Late-Plaeocene-Early Eocene climatic and biotic events in the marine and terrestrial records* (pp. 277–295). Columbia University Press.

Carignan, J., Hild, P., Mevelle, G., Morel, J., & Yeghicheyan, D. (2001). Routine analyses of trace elements in geological samples using flow injection and low pressure on-line liquid chromatography coupled to

ICP-MS: A study of geochemical reference materials Br, Dr-N, Ub-N, An-G and Gh. *Geostandards Newsletter*, *25*(2–3), 187–198.

Clift, P. D., & Blusztajn, J. (2005). Reorganization of the western Himalayan river system after five million years ago. *Nature*, *438*, 1001–1003.

Condie, K. C. (1993). Chemical composition and evolution of the upper continental crust: Contrasting results from surface samples and shales. *Chemical Geology*, *104*(1–4), 1–37.

Cullers, R. L., & Podkovyrov, V. N. (2000). Geochemistry of the Mesoproterozoic Lakhanda shales in southeastern Yakutia, Russia: implications for mineralogical and provenance control, and recycling. *Precambrian Research*, *104*(1–2), 77–93.

De Baar, H. J. W., Brewer, P. G., & Bacon, M. P. (1985). Anomalies in rare earth distributions in seawater: Gd and Tb. *Geochimica et Cosmochimica Acta*, *49*(9), 1961–1969.

Delhaye-Prat, V., Bourget, J., Gaillot, G., Gaillot, J., Sapin, F., Fillon, C., Ye, J., Wright, T., Chaboureau, A., Buratti, N., Magnier, B., Belopolsky, A., Martine Bez, M., Heumann, M. J., Sullivan, M., Mathieu, J., Cole, S., Ladner, B., Bull, J., & Dal, J. (2024). Tectono-sedimentary evolution of the Suriname margin in the cretaceous: A sequence-stratigraphic framework. *Earth-Science Reviews*, *253*(104770).

Dixon, V. R. (1972). *Public water supplies and sewerage, Sur. draft III: Hydrogeological and hydrological investigation UNDP/SF, PAHO/WHO/UN proj., Paramaribo*.

Dobson, D. M., Dickens, G. R., & Rea, D. K. (1997). Terrigenous sedimentation at Ceara Rise 1. In N. Shackleton, W. B. Curry, C. Richter, & T. J. Bralower (Eds.), *Proceedings of the Ocean Drilling Program, Scientific Results* (Vol. 154, pp. 465–473).

Drooger, C. W. (1960). Some early rotaliid Foraminifera. *Proceedings Koninklijke Nederlandse Akademie van Wetenschappen, Serie B.*, *63*(3), 287–334.

Dueñas, H. (1980). Palynology of Oligocene-Miocene strata of borehole Q-E-22. Planeta Rica, Northern Colombia. *Review of Palaeobotany and Palyrtology*, *30*, 313–328.

Eisma, D., Augustinus, P. G. E. F., & Alexander, C. (1991). Recent and subrecent changes in the dispersal of Amazon mud. *Netherlands Journal of Sea Research*, *28*(3), 181–192. https://doi.org/https://doi.org/10.1016/0077-7579(91)90016-T.

Eisma, D., & van der Marel, H. W. (1971). Marine muds along the Guyana Coast and their origin from the Amazon Basin. *Contributions to Mineralogy and Petrology*, *31*, 321–334.

Fanget, A. S., Loncke, L., Pattier, F., Marsset, T., Roest, W. R., Tallobre, C., Durrieu de Madron, X., Hernandez-Molina, F. J. (2020). A synthesis of the sedimentary evolution of the Demerara Plateau (Central Atlantic Ocean) from the late Albian to the Holocene. *Marine and Petroleum Geology*, *114*, 104195. https://doi.org/10.1016/j.marpetgeo.2019.104195Get rights and content.

Figueiredo, J., Hoorn, C., van der Ven, P., & Soares, E. (2009). Late Miocene onset of the Amazon River and the Amazon deep-sea fan: Evidence from the Foz do Amazonas Basin. *Geology*, *37*(7), 619–622. https://doi.org/10.1130/G25567A.1.

Figueiredo, J., Hoorn, C., van der Ven, P., & Soares, E. (2010). Late Miocene onset of the Amazon River and the Amazon deep-sea fan: Evidence from the Foz do Amazonas Basin: Reply. *Geology*, *38*(7), e213. https://doi.org/10.1130/G31057Y.1.

Frederiksen, N. O. (1988). Sporomorph biostratigraphy, floral changes, and paleoclimatology, Eocene and Earliest Oligocene of the Eastern Gulf Coast. *U.S. Geological Survey Professional Paper*, *1448*, 59.

Frieling, J., Gebhardt, H., Huber, M., Adekeye, O. A., Akande, S. O., Reichart, G.-J., Middelburg, J. J., Schouten, S., & Sluijs, A. (2017). Extreme warmth and heat-stressed plankton in the tropics during the Paleocene-Eocene Thermal Maximum. *Science Advances*, *3*(3), 1–9.

Frieling, J., & Sluijs, A. (2018). Towards quantitative environmental reconstructions from ancient non-analogue microfossil assemblages: Ecological preferences of Paleocene – Eocene dinoflagellates. *Earth-Science Reviews*, *185*, 956–973.

Germeraad, J. H., Hopping, C. A., & Muller, A. J. (1968). Palynology of Tertiary sediments from tropical areas. *Review of Palaeobotany and Palynology*, *6*, 189–348.

Gioia, S. M. C. L., & Pimentel, M. M. (2000). Open-access The Sm-Nd isotopic method in the geochronology laboratory of the University of Brasília. *Earth Sciences*, *72*(2), 1–17.

Gonzalez-Guzman, A. E. (1967). *A palynologic study on the Upper Los Cuervos and Mirador Formations (Lower and Middle Eocene), Tibu Area, Colombia*.

Graham, A. (1993). Contribution toward a Tertiary palynostratigraphy for Jamaica: The status of Tertiary paleobotanical studies in northern Latin America and preliminary analysis of the Guys Hill Member (Chapelton Formation, middle Eocene) of Jamaica. In R. E. Wright (Ed.), *Biostratigraphy of Jamaica* (p. 443).

Grimm, E. (2022). *Tilia* (3.0.3). https://www.neotomadb.org/apps/tilia

Heilmann-Clausen, C. (2020). Observations of the dinoflagellate Wetzeliella in Sparnacian facies (Eocene) near Epernay, France, and a note on tricky acmes of Apectodinium. *Proceedings of the Geologists' Association*, *131*(5), 450–457.

Heinrich, S., & Zonneveld, K. A. F. (2013). Influence of the Amazon River development and constriction of the Central American Seaway on Middle/Late Miocene oceanic conditions at the Ceara Rise. . *Palaeogeography, Palaeoclimatology, Palaeoecology*, *386*, 599–606.

Hoorn, C., Bogotá-A, G. R., Romero-Baez, M., Lammertsma, E. I., Flantua, S. G. A., Dantas, E. L., Dino, R., do Carmo, D. A., & Chemale, F. (2017a). The Amazon at sea: Onset and stages of the Amazon River from a marine record, with special reference to Neogene plant turnover in the drainage basin. *Global and Planetary Change*, *153*, 51–65. https://doi.org/10.1016/j.gloplacha.2017.02.005.

Hoorn, C., Bogotá-A, G. R., Romero-Baez, M., Lammertsma, E. I., Flantua, S. G. A., Dantas, E. L., Dino, R., do Carmo, D. A., & Chemale, F. (2017b). The Amazon at sea: Onset and stages of the Amazon River from a marine record, with special reference to Neogene plant turnover in the drainage basin. *Global and Planetary Change*, *153*, 51–65. https://doi.org/10.1016/j.gloplacha.2017.02.005.

Hopping, C. A. (1967). Palynology and the oil industry. *Review of Palaeobotany and Palynology*, *2*, 23–48.

Horbe, A., Andrade Queiroz, M. M., Moura, C., & Galarza, M. A. (2013). Chemistry of waters of the middle and lower Madeira River and its main tributaries - Amazonas - Brazil. *Acta Amazonica*, *43*(4), 489–504. *http://helium.crpg.cnrs-nancy.fr/SARM/*. (n.d.).

Jacobsen, S. B., & Wasserburg, G. J. (1981). Transport models for crust and mantle evolution. *Tectonophysics*, *75*(1–2), 163–179.

Jan du Chêne, R. E., & Adediran, S. A. (1984). Late Paleocene to early Eocene dinoflagellates from Nigeriav. In *Cahiers de Micropaléontologie* (Vol. 3, pp. 1–88).

Japsen, P., Green, P. F., & Bonow, J. M. (2025). Ups and downs of the Guiana Shield and Amazon Basin over the last 500 Myr. *Gondwana Research*, *148*, 415–444.

Jaramillo, C. A., & Dilcher, D. L. (2001). *Middle Paleogene palynology of Central Colombia, South America: a study of pollen and spores study from tropical latitudes*.

Jaramillo, C. A., Rueda, M., & Torres, V. (2011). A palynological zonation for the Cenozoic of the Llanos and Llanos Foothills of Colombia. *Palynology*, *35*(1), 46–84. https://doi.org/10.1080/01916122.2010.515069.

Jaramillo, C., Hoorn, C., Silva, S. A. F., Leite, F., Herrera, F., Quiroz, L., Dino, R., & Antonioli, L. (2010). *The origin of the modern Amazon rainforest: implications of the palynological and palaeobotanical record* (M. C. Hoorn & F. P. Wesselingh, Eds.). Wiley-Blackwell. https://doi.org/DOI:10.1002/9781444306408.ch19.

Juggins, S. (2024). *Rioja: Analysis of Quaternary science data, R package version* (1.0-7). https://cran.r-project.org/package=rioja.

Kameo, K., & Sato, T. (2000). Biogeography of Neogene calcareous nannofossils in the Caribbean and the eastern equatorial Pacific—floral response to the emergence of the Isthmus of Panama. *Marine Micropaleontology*, *39*, 201–218.

Kelly, J., & Doust, H. (2016). Exploration for Late Cretaceous turbidites in the Equatorial African and northeast South American margins. *Geologie En Mijnbouw/Netherlands Journal of Geosciences*, *95*(4), 393–403. https://doi.org/10.1017/njg.2016.36.

Khan, A. M., & Martin, A. R. H. (1971). A note on genus Polypodiisporites R.Potonie. *Pollen et Spores*, *13*, 475–480.

Kopp, R. E., Raub, T. D., Schumann, D., Vali, H., Smirnov, A. V., & Kirschvink, J. L. (2007). Magnetofossil spike during the Paleocene-Eocene thermal maximum: Ferromagnetic resonance, rock magnetic, and electron microscopy evidence from Ancora, New Jersey, United States. *Paleoceanography*, *22*(4), 1–7. https://doi.org/10.1029/2007PA001473.

Krook, L. (1979). *Sediment petrographical studies in Suriname*. Free University Amsterdam.

Krook, L. (1984). Sediment petrographical studies in Northern Suriname. In *Contributions to the geology of Suriname 9* (pp. 1–143).

Krutzsch, W. (1970). *Atlas der mittel- und jungtertiaeren dispersen Sporen- und Pollen- sowie der Microplanktonformen des noerdlichen Mitteleuropas, VII. VEB Gustav Fischer Verlag, Jena*.

Kumar, N. (1978). Sediment distribution in Western Atlantic Off Northern Brazil - Structural Controls and Evolution. *AAPG Bulletin*, *62*((2)), 273–294. https://doi.org/https://doi.org/10.1306/C1EA4829-16C-11D7-8645000102C1865D.

Leidelmeyer, P. (1966). *The Paleocene and lower Eocene pollen flora of Guyana* (Vol. 38).

Leite, F. P. R., Silva-Caminha, S. A. F., & D'Apolito, C. (2021). New Neogene index pollen and spore taxa from the Solimões Basin (Western Amazonia), Brazil. *Palynology* , *45*(1), 115–141.

Lim, J. Y., Huang, H., Farnsworth, A., Lunt, D. J., Baker, W. J., Morley, R. J., Kissling, W. D., Hoorn, C. (2021). The Cenozoic history of palms: Global diversification, biogeography and the decline of megathermal forests. *Global Ecology and Biogeography, 31*, 425–439. DOI: 10.1111/geb.13436.

Liu, C. , Clift, P. D., Carter, A., Böning, P., Hu, Z., Sun, Z., & Pahnke, K. (2017). Controls on modern erosion and the development of the Pearl River drainage in the late Paleogene. *Marine Geology, Evolution of the Deep South China Sea: Integrated IODP Expedition 349 Results*, *394*, 52–68.

Lorente, M. A. (1986). *Palynology and palynofacies of the Upper Tertiary in Venezuela: Vol. Diss. Bol, 99*.

Mabberley, D. J. (1987). *The Plant-Book: A portable dictionary of the higher plants* (First). Cambridge University Press.

Mapes, R., Torres, V. (2017). Paleodrainage evolution of northern South America and its impact on exploration success in the Guyana Basin: AAPG Latin American Region GTW. *Deepwater Exploration of the Columbus & Guiana Basins, November*, 6-8.

Marchant, R., Almeida, L., Behling, H., Carlos Berrio, J., Bush, M., Cleef, A., Duivenvoorden, J., Kappelle, M., De Oliveira, P., Teixeira De Oliveira-Filho, A., Lozano-Garc ¤ia, S., Hooghiemstra, H., Ledru, M.-P., Ludlow-Wiechers, B., Markgraf, V., Mancini, V., Paez, M., Prieto, A., Rangel, O., & Salgado-Labouriau, M. L. (2002). Distribution and ecology of parent taxa of pollen lodged

within the Latin American Pollen Database. In *Review of Palaeobotany and Palynology* (Vol. 121). https://doi.org/https://doi.org/1016/S0034-6667(02)00082-9.

Martin Roddaz, M., Dera, G., Mourlot, Y., Calvès, G., Kim, J.-H., Chaboureau, A.-C., Mounic, S., & Raisson, F. (2021). Provenance constraints on the Cretaceous-Paleocene erosional history of the Guiana Shield as determined from the geochemistry of clay-size fraction of sediments from the Arapaima-1 well (Guyana-Suriname basin). *Marine Geology*, *434*, 1–19.

McLennan, S. M. (2001). Relationships between the trace element composition of sedimentary rocks and upper continental crust. *Geochemistry, Geophysics, Geosystems*, *2*(4), 1–24.

McLennan, S. M., Hemming, S., McDaniel, D. K., & Hanson, G. N. (1993). Geochemical approaches to sedimentation, provenance, and tectonics. In M. J. Johnsson & A. Basu (Eds.), *Processes Controlling the Composition of Clastic Sediments* (pp. 21–40). Geological Society of America. https://doi.org/https://doi.org/10.1130/SPE284-p21.

Moizinho, G. R., Santos, T. P., Bayon, G., Roddaz, M., Riveiros, N. V., Rabineau, M., Aslanian, D., Carreira, V., Dantas, E. L., & Santos, R. V. ,. (2025). Orbital and sea-level controls on long-term sediment deposition in the Amazon Fan. . *Global and Planetary Change*, *255*(105068), 1–13.

Monsels, D. A., & Van Bergen, M. J. (2019). Bauxite formation on Tertiary sediments in the coastal plain of Suriname. *Journal of South American Earth Sciences*, *89*, 275–298.

Mourlot, Y., Roddaz, M., Dera, G., Calvès, G., Kim, J.-H., Chaboureau, A.-C., Mounic, S., & Raisson, F. (2018). Geochemical evidence for large-scale drainage reorganization in Northwest Africa during the Cretaceous. *Geochemistry, Geophysics, Geosystems*, *19*(5), 1690–1712.

Muller, J., Di Giacomo, E., & Van Erve, A. (1987). A palynologic zonation for the Cretaceous, Tertiary and Quaternary of northern South America. In *American Association of Stratigraphic Palynologists Contribution Series 19* (pp. 7–76).

Nisancioglu, K. H., Raymo, M. E., & Stone, P. H. (2003). Reorganization of Miocene deep water circulation in response to the shoaling of the Central American Seaway. *Paleoceanography*, *18*, 1–12.

Noorthoorn van der Kruyff, J. F. (1970). *Suriname onshore exploration 1968/1970. Summary, petroleum engineering and geology - Shell Suriname Exploratie en Productie Maatschappij*.

Oksanen, J., Simpson, G., Blanchet, F., Kindt, R., Legendre, P., Minchin, P., O'Hara, R., Solymos, P., Stevens, M., Szoecs, E., Wagner, H., Barbour, M., Bedward, M., Bolker, B., Borcard, D., Carvalho, G., Chirico, M., De Caceres, M., Durand, S., Weedon, J. (2024). *vegan: Community ecology package_.R package version 2.6-8*. https://CRAN.R-project.org/package=vegan.

Pasley, M. A., Shepherd, D. B., Pocknall, D. T., Boyd, K. P., Andrade, V., Picanço, J., & Figueiredo, D. (2005). *Sequence Stratigraphy and Basin Evolution of the Foz do Amazonas Basin, Brazil* *. https://www.searchanddiscovery.com/documents/2005/pasley/index.htm.

Patier, F., Loncke, L., Imbert, P., Gaullier, V., Basile, C., Maillard, A., Roest, W. R., Patriat, M., & Vendeville, B. C. (2015). Origin of an enigmatic regional Mio-Pliocene unconformity on the Demerara Plateau. *Marine Geology*, *365*, 21–35.

Pindell, J., & Kennan, L. (2001). Processes and events in the Terrane Assembly of Trinidad and Eastern Venezuela. In *Petroleum Systems of Deep-water basins: Global and Gulf of Mexico experience* (Vol. 21). https://doi.org/https://doi.org/10.5742/gcs.01.21.0159.

Piper, D. Z. (1974). Rare earth elements in the sedimentary cycle: A summary. *Chemical Geology*, *14*(4), 285–304.

Plata-Torres, A., Pardo-Trujillo, A., & Flores, J. A. (2024). A contribution to the knowledge of Cretaceous to Neogene Palynology in the Colombian Caribbean. *Review of Palaeobotany and Palynology*, *325*, 1–25. https://doi.org/https://doi.org/10.1016/j.revpalbo.2024.105098.

Plata-Torres, A., Pardo-Trujillo, A., Vallejo-Hincapié, F., Abel Flores, J., & Trejos Tamayo, R. (2022). Early Eocene (Ypresian) palynology of marine sediments from the colombian Caribbean. *Journal of South American Earth Sciences*, *121*(58: 104146).

Pocknall, D. T. (2020). *Biostratigraphic evaluation of Miocene to Pleistocene strata in Trinidad using palynology and micropaleontology*.

Posit team. (2024). *RStudio: Integrated development environment for R. Posit software, PBC, Boston, MA*. https://www.posit.co/

Potonie, R. (n.d.). Zur Morphologie der fossilen Pollen und Sporen. *Arb.-Inst. Paläobot. Und Petr. Brennsteine, Preuß. Geol. LA.4, S. 1–24, 44 Abb. Berlin 1934.*

Potonie, R., & Gelletich. (1933). *Sitzungsber. Ges.Naturf. Freunde Berlin 1933: 521. nom. rej. prop.*

Pourmand, A., Dauphas, N., & Ireland, Th. J. (2012). A novel extraction chromatography and MC-ICP-MS technique for rapid analysis of REE, Sc and Y: Revising CI-chondrite and Post-Archean Australian Shale (PAAS) abundances. *Chemical Geology*, *291*, 38–54.

R Core Team. (2023). *_R: A language and environment for statistical computing_.R Foundation for statistical computing, Vienna, Austria*. https://www.R-project.org/

Regali, M. D. S. P. (1971). *Palinologia dos sedimentos Cenozoicos da foz do Rio Amazonas*. Universidade de Sao Paolo.

Regali, M., Uesugui, N., & Santos, A. (1974). Palinologia dos sedimentos Meso-Cenozoico do Brasil. *Boletin Tecnico Da Petrobras 17*, 177–191.

Roddaz, M., Nauton-Fourteu, M., Ventura Santos, R., Dantas, E. L., & Gérôme Calves, G. (2020). Controls on the provenance of late Eocene to Quaternary Mozambique Channel shales (DSDP 25 Site 242). *Marine Geology*, *421*(106090), 1–17.

Roddaz, M., Viers, J., Brusset, S., Baby, P., & Hérail, G. (2005). Sediment provenances and drainage evolution of the Neogene Amazonian foreland basin. *Earth and Planetary Science Letters*, *239*(1–2), 57–78.

Roddaz, M., Viers, J., Moreira-Turcq, P., Blondel, C., Sondag, F., Guyot, J.-L., & Moreira, L. (2014). Evidence for the control of the geochemistry of Amazonian floodplain sediments by stratification of suspended sediments in the Amazon. *Chemical Geology*, *387*, 101–110.

Rouby, D., Loparev, A., Chardon, D., Bajolet, F., Dall'Asta, M., Paquet, F., Fillon, C., Roig, J.-Y., & Ye, J. (2025). Sediment routing systems to the Atlantic rifted margin of the Guiana Shield. *Geosphere*, *19*, 957–974.

Rousseau T. C. C., Roddaz M., Moquet J. S., Handt Delgado H., Calves G., & Bayon G. (2019). Controls on the Geochemistry of Suspended Sediments From Large Tropical South American Rivers (Amazon, Orinoco, and Maroni). *Chemical Geology*, *522*, 38–54. https://doi.org/10.1016/j.chemgeo.2019.05.

Sah, S. C. D. (1967). Palynology of a Upper Neogene Neogene profile from Rusizi Valley, Burundi. *Annales. Musee Royal l'Afrique Centrale. Sciences Geologiques Serie IN-80 (No. 57)*, 173.

Sarmiento, G. (1992). Estratigrafía y medios de depósito de la Formación Guaduas . *Boletín Geológico*, *32*(1–3).

Silva-Caminha, S. A. F., Jaramillo, C. A., Absy, M. L., & Jaramillo, A. (2010). Neogene palynology of the Solimões Basin, Brazilian Amazonia. *Palaeontographica*, *283*(1–3), 1–67.

Sluijs, A., & Brinkhuis, H. (2009). A dynamic climate and ecosystem state during the Paleocene-Eocene Thermal Maximum: inferences from dinoflagellate cyst assemblages on the New Jersey Shelf. *Biogeosciences*, *6*(8), 1755–1781.

Sluijs, A., Brinkhuis, H., Schouten, S., Bohaty, S. M., John, C. M., Zachos, J. C., Reichart, G. J., Sinninghe Damsté, J. S., Crouch, E. M., & Dickens, G. R. (2007). Environmental precursors to rapid light carbon injection at the Palaeocene/Eocene boundary. Nature, 450(7173), 1218–1221. https://doi.org/10.1038/nature06400.

Srivastava, J., & Prasad, V. (2019). Evolution and paleobiogeography of mangroves. In *Marine Ecology* (Vol. 40, Issue 6, pp. 1–12). Blackwell Publishing Ltd. https://doi.org/10.1111/maec.12571.

Staatsolie, 2023a. Stratigraphy of the Suriname-Guyana Basin, Staatsolie Hydrocarbon Institute. https://www.staatsolie.com/media/fqjpxkyl/stratigraphy-of-the-surinam e-guyana-basin.jpg.

Takahashi, K., & Jux, U. (1989). Palynology of Middle Tertiary lacustrine deposits from the Jos Plateau, Nigeria. Bulletin of the Faculty of Free Arts, University of Nagasaki. Natural Sciences, 29(2), 181–367.

Taylor, S. R., & McLennan, S. M. (1985). *The continental crust: its composition and evolution* (A. Hallam, Ed.). Blackwell Scientific Publications.

Van der Hammen, T. (1954). Principios para la nomenclatura palinológica sistemática. *Boletín Geológico*, *2*(2), 1–24.

Van der Hammen, T. (1957). A palynological systematic nomenclature. *Boletín Geológico*, *4*(2–3), 63–101.

Van der Hammen, T., & Garcia De Mutis, C. (1965). The Paleocene pollen flora of Colombia. *Leidse Geologische Mededelingen* , *Deel 35*, 105–116.

Van der Hammen, T., & Garcia de Mutis, C. (1966). The Paleogene pollen flora of Colombia. *Leidse Geologische Mededelingen*, *35*, 105–116.

Van der Hammen, Th. (1957). Climatic periodicity of South American Maestrichtian and Tertiary floras: a study based on pollen analysis in Colombia. *Boletin Geologico*, *5*, 49–91.

Van der Hammen, Th., & Wijmstra, T. A. (1964). *A palynological study on the Tertiary and Upper Cretaceous of British Guyana. Leidse Geologische Mededelingen, 30*. 183–241.

Van Soelen, E. E., Kim, J. H., Santos, R. V., Dantas, E. L., Vasconcelos de Almeida, F., Pires, J. P., Roddaz, M., & Sinninghe Damsté, J. S. (2017). A 30 Ma history of the Amazon River inferred from terrigenous sediments and organic matter on the Ceará Rise. *Earth and Planetary Science Letters*, *474*, 40–48. https://doi.org/10.1016/j.epsl.2017.06.025.

Viers, J., Roddaz, M., Filizola, N., Guyot, J.-L., Sondag, F., Brunet, P., Zouiten, C., Boucayrand, C., Martin, F., & Resende Boaventura, G. (2008). Seasonal and provenance controls on Nd–Sr isotopic compositions of Amazon rivers suspended sediments and implications for Nd and Sr fluxes exported to the Atlantic Ocean. *Earth and Planetary Science Letters*, *274*(3–4), 511–523. https://doi.org/10.1016/j.epsl.2008.08.011

Wijmstra, T. A. (1969). Palynology of the first 30 metres of a 120 m deep section in northern Greece. *Acta Botanica Neerlandica*, *18*(4), 511–527.

Wijmstra, T. A. (1971). *The palynology of the Guiana Coastal Basin*.

Wong, Th. (1986). Outline of the stratigraphy and the geological history of the Suriname coastal plain. *Geologie En Mijnbouw/Netherlands Journal of Geosciences*, *65*(3), 223–241.

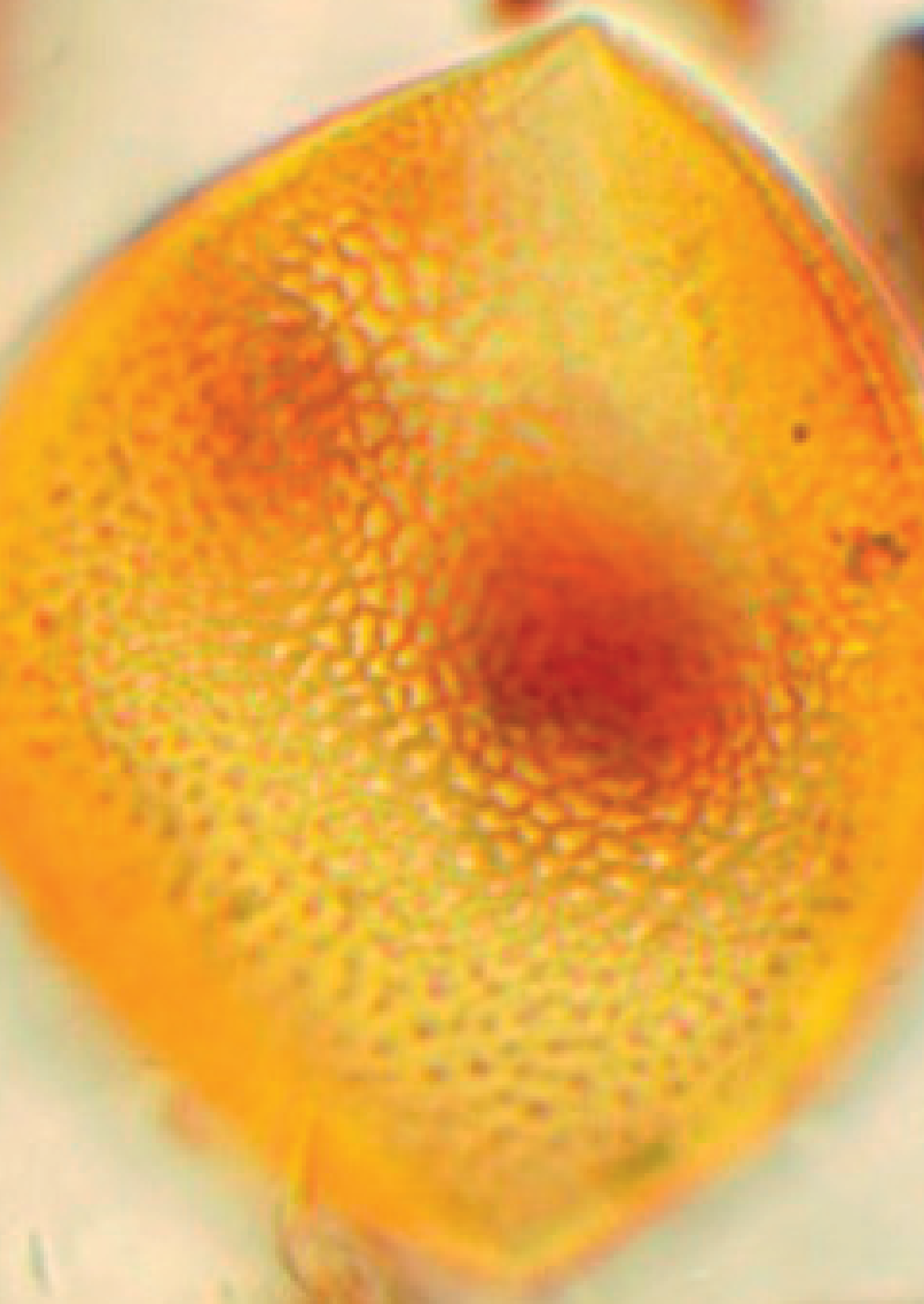
Wong, Th. E. (1986). Outline of the stratigraphy and the geological history of the Suriname coastal plain. *Geologie En Mijnbouw*, *65*, 223–241.

Wong, Th. E. (1989). Revision of the stratigraphy of the coastal plain of Suriname. *Natuurwetenschappelijke Studiekring Voor Suriname En de Nederlandse Antillen (Publications of the Foundation for Scientific Research in Surinam and the Netherlands Antilles*, *125*, 1–64.

Wong, Th. E., de Kramer, R., de Boer, P. L., Langereis, C., & Sew-A-Tjon, J. (2009). The influence of sea-level changes on tropical coastal lowlands; the Pleistocene Coropina Formation, Suriname. *Sedimentary Geology*, *216*(3–4), 125–137. https://doi.org/10.1016/j.sedgeo.2009.02.003

Wong, Th., Kroonenberg, S. B., & Augustinus, P. G. E. F. (2016). *Geologie en Landschap van Suriname* (Th. Berghuis & T. Markus, Eds.; 1st ed.). LM Publishers.

Wong, Th., & Van Geuns, L. (2020). The discovery of a major hydrocarbon occurrence in the Guiana Basin, offshore Suriname: a blessing or a curse? *Academic Journal of Suriname*, *11*, 1–6. https://oilnow.gy/featured/suriname-discovery- *www.staatsolie.com*. (2023).



Chapter 3

Tracing Amazon influence on the Suriname coastline: Results from a study on a Neogene coastal sedimentary record

Eva Visser[a*], Kathleen Gersie[a,b,c*], Roel Verreussel[d], Elton Luiz Dantas[e], Roberto Ventura Santos[e], Martin Roddaz[f], Raul Giovanni Bogota-Angel[g], Henry Hooghiemstra[a], Carina Hoorn[a+]

* first co-author
\+ corresponding author
Affiliations
[a.] *Institute for Biodiversity and Ecosystem Dynamics, University of Amsterdam, Science Park 904, 1098XH, Amsterdam, The Netherlands, k.gersie@uva.nl; h.hooghiemstra@uva.nl; m.c.hoorn@uva.nl*
[b.] *Department of Geosciences, Anton de Kom University of Suriname, Leysweg 86, Paramaribo, Suriname, kathleen.gersie@uvs.edu*
[c.]. *Department of Earth Sciences, VU University of Amsterdam, De Boelelaan 1100, 1081HZ, Amsterdam, The Netherlands*
[d.] *TNO Reseacrh Institute, Princetonlaan 6, 3584CB, Utrecht, The Netherlands, roel.verreusel@tno.nl*
[e.] *Labaratório de Geocronologia, Instituto de Geociências, Universidade de Brasilia, Brasilia, DF 70910-900, Brazil, elton@unb.br;* rventura@unb.br
[f.] *Géosciences-Environnement Toulouse, Université de Toulouse; UPS (SVT-OMP); CNRS; IRD; 14 Avenue Édouard Belin, F-31400 Toulouse, France, martin.roddaz@get.omp.eu*
[g.] *Instituto de Investigaciones en Estratigrafía (IIES), Grupo de Investigaciones en Estratigrafía y Vulcanología (GIEV-Cumanday) y Departamento de Ciencias Geológicas, Universidad de Caldas, Calle 65 # 26-10, Manizales, Colombia, ragiob@yahoo.com*

ABSTRACT

Suriname's coastal evolution has been shaped by sediment transported from the Andes via the Amazon River. While offshore records confirm early Amazon influence, the timing of its impact on Suriname's coastal plain remained uncertain. This study reconstructs the Neogene development of Suriname's coastline using palynological and geochemical data from the Hepp-3 borehole (Nickerie district). Pollen and spore assemblages reveal a shift in vegetation from mangroves and freshwater swamps to rainforest and brief savanna phases reflecting dynamic coastal environments. The Andean pollen signal first appear in the Pliocene indicating microfossil transport preceding sediment delivery. Provenance analyses show that a transition from eastern Guiana Shield sources to Andean-derived detritus occurs in the Pliocene, towards the top of the Zanderij Formation. These results tentatively suggest that Amazon connectivity to the Guianas' coastal margin began later, and was driven by a change in sediment routing. The integrated approach refines the timing of Amazon influence on the coast and links coastal plain records to the growth of the Amazon Submarine Fan.

Keywords: Neogene, biostratigraphy, palynology, provenance, Andean, Amazon

1 INTRODUCTION

Suriname's muddy coastline traces its origin to the distant Andes, where snowmelt and rainfall feed a web of tributaries that merge into the Amazon River. As the Amazon River discharges into the Atlantic, it becomes a massive plume of fresh water and suspended sediment that fans out across the ocean for thousands of kilometers (Molleri et al., 2010). Driven northwestward by trade winds and currents (Dengler et al., 2004), this plume builds mudbanks migrating along the Guianan coasts, alternately nourishing mangroves or exposing them to erosion (Anthony et al., 2010; Augustinus, 2004). Yet this modern dynamic is only the most recent phase of a process set in motion during the late Miocene (~10 Ma), when Andean uplift reorganized drainage patterns and set the Amazon River on its transcontinental course to the Atlantic (Figueiredo et al., 2009; Hoorn et al., 2010, 2017).

The Guiana Shield occupies the central Guiana sector of the Atlantic Equatorial Margin, along the coast between the Amazon and Orinoco deltas. For much of the Neogene, this stable cratonic basement supplied only modest terrigenous input to the margin, sustaining a predominantly carbonate shelf (Wong et al., 2016). By the Late Miocene (~10 – 9 Ma), the transcontinental Amazon River transported Andean-derived siliciclastic sediments to the Atlantic, initiating the growth of the Amazon submarine fan (Figueiredo et al., 2009; Hoorn et al., 2017). From this point onward, Andean erosion, transcontinental routing, and Atlantic deposition became tightly coupled – setting the stage for the Guianas, including Suriname, to evolve under the downstream influence of the Amazon discharge.

The regional geomorphology and coastal dynamics of Suriname were synthesized by Krook (1984), who highlighted alternating phases of shoreline accretion and erosion linked to longshore transport of fine Amazon muds. Eisma and van der Marel (1971) demonstrated that, based on mineralogy, muds on the Suriname coast closely match Amazon sediments and differ markedly from local Guiana Shield sources, implying a predominantly Amazonian provenance for coastal mud belts. Eisma et al. (1991) linked seasonal hydrodynamic forcing – North Brazil Current/Countercurrent variability, wind regime, and tidal interaction – to the westward migration of shore-parallel mudbanks that alternately protect and erode the coast on decadal scales. Subsequent syntheses and coastal stratigraphic works adopted this mudbank paradigm for the Guianas as the canonical explanation for observed cyclical shoreline behaviour (Augustinus, 2004; Anthony et al., 2010). This historical lineage underpins the modern understanding of how Andean sediment reaches and reorganizes the Guiana margin, including Suriname.

The Amazon River does not only transport mud, it also carries sporomorphs (pollen and spores) and dinoflagellate cysts transported from Andean and lowland source areas (Hoorn et al., 2017). These microfossils are preserved together with the terrigenous mud along the Guianas margin, providing a direct proxy for the timing and evolution of Amazon influ-

ence on the Suriname coastal plain. Offshore records register the Late Miocene growth of the Amazon Fan (Figueiredo et al., 2009; Hoorn et al., 2017), but the onshore timing of Amazon influence along the Guianas – and Suriname specifically – remains poorly constrained. Palynological proxies bridge this gap by linking sediment source and coastal ecology to stratigraphic time. Sporomorphs track terrestrial vegetation and sediment provenance (e.g., Andean vs. cratonic sources), while dinoflagellate cysts respond to salinity, nutrients, and marine incursions, offering ecological and biostratigraphic control (Vernal et al., 2001; Lammertsma et al., 2018). Together, they enable us to reconstruct the timing of when Amazon-derived sediments and associated ecological signals first reached Suriname as well as how this transport process changed over time.

Although Suriname's modern coastline depends heavily on Amazon-derived sediment for shoreline stability and mangrove development, its history is unknown. In this study we hypothesize that the onset of the Amazon River and fan is recorded in the coastal plain of Suriname. To address this we pursue the following objectives: 1) to reconstruct past vegetation and ecological conditions along the Suriname coastline; 2) to examine the pollen and dinocyst assemblages in the Hepp-3 well; 3) to determine if the onset and evolution of Amazon influence on the Suriname coastline is recorded in the geochemistry and mineralogy (?), and if so, determine when this influence started. The results of this study will provide a window into the sedimentary succession which archives terrigenous, marine influence, and coastal ecological change.

2 GEOGRAPHICAL AND GEOLOGICAL SETTING

2.1 GEOLOGICAL SETTING OF SURINAME

Suriname is situated on the northern edge of the Precambrian Guiana Shield (Kroonenberg, 2025) (Fig. 1), and displays a hilly interior of crystalline rocks that dips gently northward beneath a belt of young coastal deposits (Wong, 1986). Over time this low-lying coastal area accumulated a thin layer of sediments that record repeated shifts between marine and continental conditions. To interpret that record, Suriname must be viewed within the broader tectonic and sedimentary context of northern South America, where Andean uplift and changing drainage patterns determined timing, transport mechanism and provenance of where sediments reaching the Atlantic margin (Hoorn et al., 2010; Val et al., 2021).

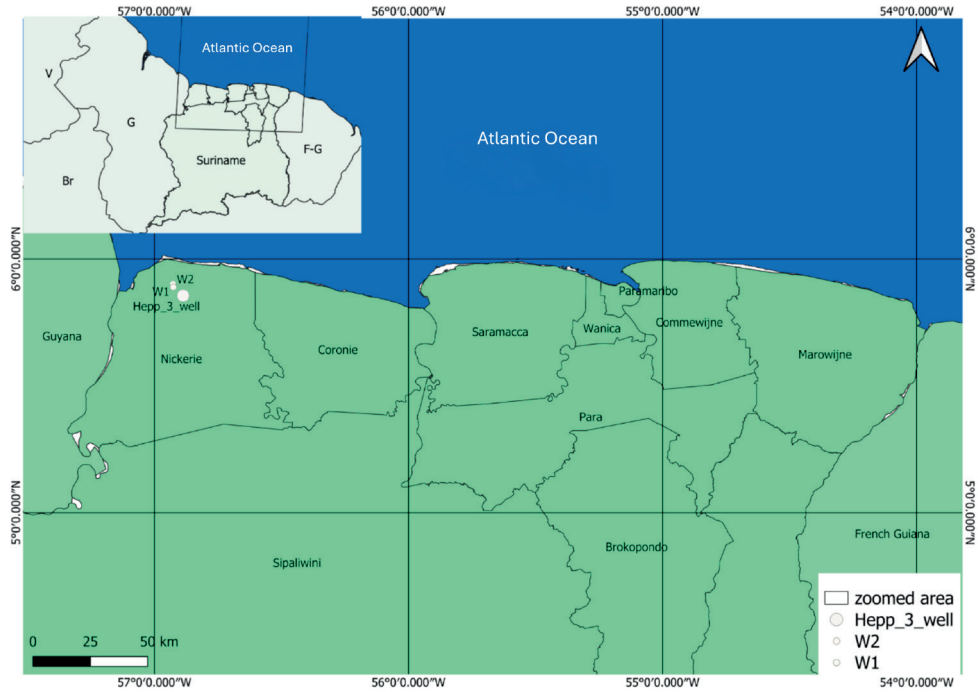


Figure 1: Map of the study area with the Hepp-3 well and nearby wells WA-1 and WA-2 in the district of Nickerie, western Suriname.

2.1.2 Suriname on the Guiana Shield

Suriname's interior consists of high-grade metamorphic and granitoid complexes of Precambrian age (Fraga et al., 2024; Wong, 1986). Towards the coast these basement rocks dip beneath unconsolidated sediments that fill the Guiana Basin, and a savannah belt marks the transition from the upland shield to the coastal plain (Wong, 1986). For much of the Neogene, rivers draining the low-relief shield supplied only modest terrigenous input, and carbonate production dominated parts of the shelf (Figueiredo et al., 2009). Provenance reconstructions indicate that during the Early Miocene sediment supply to the eastern Amazon margin of the Amazon Fan was sourced mainly from the Maroni-Itacaiúnas province, shifting by the Middle Miocene toward the Rio Negro–Juruena province as drainage reorganized (Figueiredo et al., 2009). The Late Miocene arrival of Amazon-sourced fine sediment shifted this balance toward siliciclastic accumulation along the margin (Anthony et al., 2010; Wong, 1986; Wong et al., 2009).

2.2 STRATIGRAPHY

The sedimentary succession that overlies the Guiana Shield in northern Suriname is known as the Corantijn Group. This group includes Late Cretaceous to Holocene sediments that

record the interplay of sea level, climate, and sediment supply from both the Guiana Shield and the Amazon River (Wong, 1986; Wong et al., 2009). Several unconformities interrupt the record, most notably the Bauxite Hiatus (Late Eocene to Oligocene), when deep weathering formed lateritic bauxites on an exposed land surface (Wong, 1986; Wong et al., 2009). Units within the Corantijn Group increase in thickness northward and westward, consistent with basin subsidence and coastal progradation (Wong, 1986). The group is subdivided into ten formations, i.e. from oldest to youngest: the Nickerie, Alliance, Saramacca, Onverdacht, Burnside, Coesewijne, Zanderij, Coropina, Mara, and Coronie formations (Wong, 1986) .

The Hepp-3 well (Nickerie district) intersects several of these formations. Based on regional hydrogeologic mapping, strata belonging to the Coesewijne Formation transition into the Zanderij Formation and continue through coastal deposits assigned to the Coropina/Mara Formation (Mente, 1989; Wong, 1986). The stratigraphic summaries below emphasize depositional environments relevant to provenance and palynology.

The Miocene Coesewijne Formation consists of mixed clays, sandy clays, and interbedded sands that reflect swamp, deltaic, and coastal plain deposition during major transgressions. This interval was thought to include evidence of Amazon River sedimentation (Krook, 1979), with mud-rich deposition driven by marine currents and the appearance of abundant mangrove vegetation (e.g. *Rhizophora*) (Wijmstra, 1971; Wong, 1986, 2009).

The Zanderij Formation of Pliocene age (Wong, 1989) consists of coarse white and brown quartz sands with kaolinitic clays which record a shift to fluvial deposition under semi-arid conditions. Initially formed in coastal swamps during a Pliocene transgression, followed by progradation and erosion during regression. Sands were deposited by braided rivers in valleys and on terraces (Wong, 1986, 2009; Wong et al., 2016)

The Coropina Formation of Pleistocene age is subdivided into two members that have captured interglacial highstands. The Para Member consists of laminated stiff clays with basal sand lenses and formed in tidal mudflats and chenier systems. The Lelydorp Member comprises silts, sands, and mottled clays deposited in brackish lagoons, mudflats, and offshore sandbars under strong influence of longshore transport of Amazon mud. Subsequent regression led to weathering, erosion, and reactivation of fluvial systems (Wong, 1986; 2009) (Fig. 2).

The Mara Formation of Early Holocene age (Brinkman & Pons, 1968; Roeleveld, 1969; Wong et al., 2016) consist of soft, pyrite-rich peaty clays accumulated in brackish swamps and mangrove settings during the Early Holocene transgression. Reducing conditions favoured preservation of organic matter and sulphides (Wong, 1986; Wong et al., 2009).

The Coronie Formation of ~6 ka to present age consists of clay-rich tidal-flat deposits alternate with beach-ridge (chenier) sands and estuarine units, reflecting cyclic coastal dynamics under ongoing Amazon mud supply. The Wanica, Moleson, and Comowine deposits are subdivisions that are frequently identified in Suriname; they reflect consecutive stages of incursion, beach-ridge development, and backswamp infill (Wong, 1986; Wong et al., 2009).

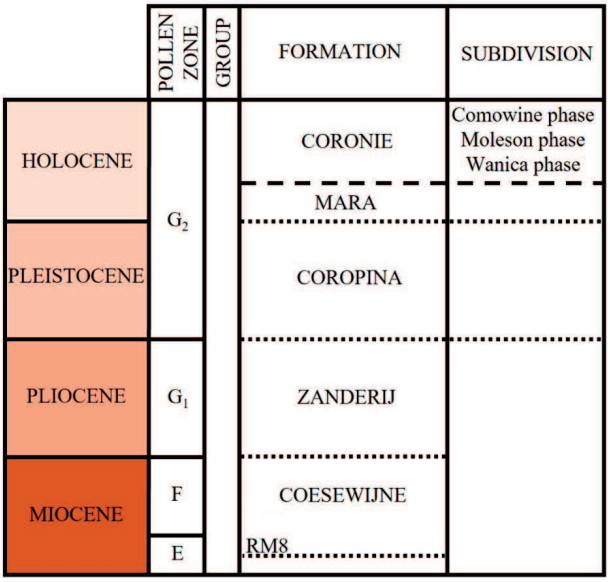


Figure 2: Relevant stratigraphic formations of the Corantijn Group (modified after Wong, 1986). Pollen zones are derived from van der Hammen & Wijmstra (1964) and Wijmstra (1971).

3. MATERIALS AND METHODS

3.1 WELL SITE AND LITHOSTRATIGRAPHY

3.1.1 Well information

The Hepp-3 borehole was drilled in 2021 by the Surinaamsche Waterleiding Maatschappij (SWM) in the Nickerie District, western Suriname (latitude 5°51.308′ N, longitude 56°3.202′ W; Fig. 1). Drilling produced ditch cuttings from 262 to 15 mbsl depth, collected at intervals of approximately 3 m. In total 68 ditch cutting samples were recovered and made available to the University of Amsterdam for scientific analysis. Thirty samples were selected for palynological processing and twenty for geochemical analysis (Table 1), to provide complementary constrains for vegetation history, age, and provenance. Unlike core material, ditch cuttings do not preserve an undisturbed stratigraphy because material may be mixed during drilling.

When collected systematically, however, they provide continuous coverage and sufficient organic residue for analysis.

The lithology alternates between clay-rich and sand-rich intervals with local occurrence of lignite or kaolinite (Fig. 3; App. A). The ~3 m spacing yields a coarse temporal resolution suited for detecting long-term depositional and ecological trends rather than short-lived events. The absolute ages were not known and form a central question addressed here.

Table 1: Sample list with selected cutting samples from the Hepp-3 for geochronological, dinoflagellate cyst and pollen and spores analyses MLA = Maximum likelihood ages

Samples (ft)	(mbsl)	Geochemistry	Dinoflagellate cysts	Pollen and spores	Maximum Likelihood Ages	Lithostratigraphy
50	15	x		x	x	
80	24	x				Coropina/
110	34			x	x	Mara/Coronie
140	47			x	x	Formation
170	52	x		x	x	
200	61	x		x	x	
330	101	x		x	x	
360	110	x		x	x	
420	128	x		x	x	
460	140	x		x	x	Zanderij
500	152	x				Formation
540	165	x				
610	186	x				
650	198	x				
680	207			x	x	
700	213	x				
710	216			x	x	
720	219			x	x	
730	223	x				
740	226			x	x	
760	232	x	x	x	x	Coesewijne
780	238			x	x	Formation
790	241	x				
800	244			x	x	
820	250			x	x	
830	253	x				
840	256			x	x	
860	262	x		x	x	

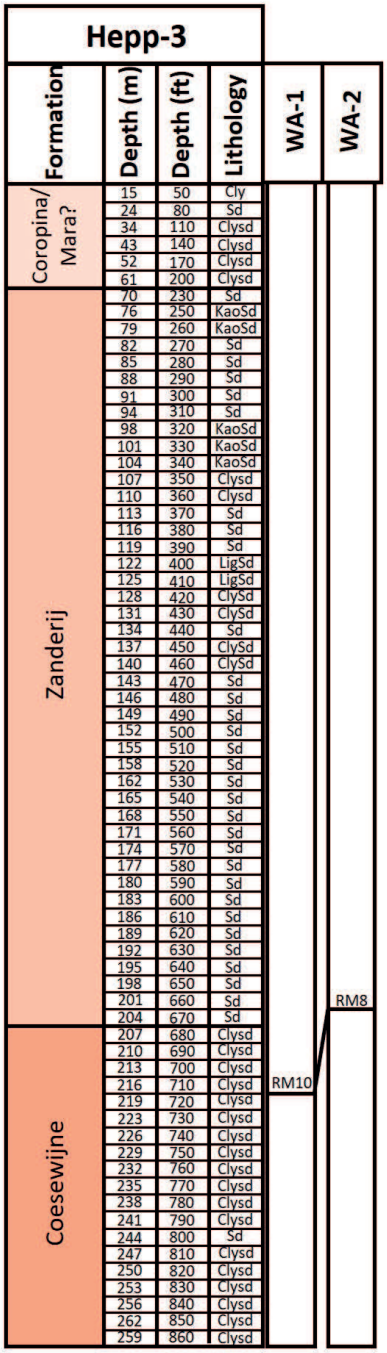


Figure 3: Lithology of the Hepp-3 well (source: Suriname Water Company N.V., 2023). Nearby located wells WA-1 and WA-2 show the indicated depth occurrence of the RM8 (Noorthoorn van der Kruyff, 1970). Detailed data is presented in Appendix A.

3.2 GEOCHEMISTRY

3.2.1 Provenance of Sediments

Neodymium (Nd) and Samarium (Sm) isotope analysis was conducted to establish the provenance and source areas of the sediments. Sample preparation followed the procedures described in Hoorn et al. (2017). Twenty sediment samples (~100 mg each; Table 1) were spiked with a mixed Nd-Sm tracer to allow for isotope dilution analysis and dissolved in a hydrofluoric (HF) and nitric acid (HNO_3) solution on a hot plate. After cooling, solutions were evaporated to dryness, the residues redissolved in hydrochloric acid (HCl), evaporated again, and finally redissolved in HCl to ensure complete dissolution. Neodymium and samarium were chemically separated from the matrix by standard chromatographic extraction.

Isotopic ratios were measured by thermal ionization mass spectrometry (TIMS). Multiple replicate runs were performed to ensure analytical precision and accuracy. Data were normalized against known standards, and depleted-mantle model ages (T_{DM}) were calculated. These model ages provide insight into the long-term evolution of source terrains, allowing for distinction between sediments derived from Precambrian cratonic areas and those from younger orogenic belts. The Nd-Sm dataset is presented alongside the palynological summary to enable direct comparison between sediment provenance and vegetation history.

3.3 PALYNOLOGY

3.3.1 Sample collection

The palynological analyses were designed to reconstruct vegetation composition and establish a biostratigraphic framework for the sedimentary succession at Nickerie. Thirty ditch cutting samples were processed at the pollen preparation laboratory of the University of Amsterdam following a standard palynological method.

3.3.2 Processing method

For each sample, approximately 2.0 g of sediment was processed to isolate the organic fraction. Treatment comprised of decalcification with HCl, dispersion of clays with sodium pyrophosphate ($Na_4P_2O_7$), acetolysis to remove cellulose, and bromoform separation to isolate concentrate organic material. Residues were stored in glycerine for microscopy. *Lycopodium clavatum* spores (18,407 spores; Batch number T42.412–T42.554) were added to each sample prior to processing to allow pollen concentration calculations.

3.3.3 Analysis

From the processed material twenty samples were counted, and morphologically described and identified using a Leica light microscope type DM-DB. In counted samples the target was a minimum pollen sum of 100 grains, and up to 300 well-preserved grains counted

where possible. Poorly preserved or reworked sporomorphs, foraminifer linings, and dinoflagellate cysts were excluded from the pollen sum. Taxonomic identification was based on morphological criteria under light microscopy at 400x and 1000x magnification, with photos captured using Amscope 4.7 software (Table 4).

Sporomorph identification in this study was based on palynological catalogues, reference databases, expert consulting the reference zonations of Suriname (Wijmstra, 1971), Guyana (Van der Hammen & Wijmstra, 1964), Brazilian Amazon and Amazon Fan (D'Apolito et al., 2021; Hoorn et al., 2017; Regali et al., 1974), Northern South America (Germeraad et al., 1968; Muller et al., 1987; Jaramillo & Rueda, 2024), and Llanos and Llanos Foothills (Jaramillo et al., 2011) (see previous chapter). The biostratigraphic schemes presented in these studies formed the basis for our biostratigraphic interpretation. The sediment samples used in this study were derived from drill cuttings. As a result, we primarily rely on last occurrence datum (LOD) events - rather than first occurrence datum (FOD) events- to support the age model. The LODs are particularly informative due to complications from casing installations during drilling and the caving of material, which can lead to downhole contamination of sporomorphs. This explains why some pollen grains appear at depths lower than their true stratigraphic position.

In accordance with Hoorn et al. (2017), species were categorized ecologically to assess vegetation change over time (Table 4). Data handling and plotting used Tilia 3.0.3 software, and stratigraphically constrained cluster analysis (CONISS) was applied to delineate pollen zones, which capture intervals of similar palynological composition. These data also formed the basis palynological diversity assessment.

3.3.1 Dinoflagellate cyst processing and analysis

An additional set of sixteen residues were analyzed for dinoflagellate cysts in collaboration with Dr. Roel Verreussel (TNO). The residues, originally processed at University of Amsterdam, were sieved over a 15-micron mesh by Nico Janssen (TNO) to concentrate dinocysts. The dinocyst data provide independent biostratigraphic and ecological markers to complement the pollen data.

Because the material consisted of ditch cuttings rather than a continuous core, the LOD was prioritized over FOD when constructing the age model. This approach reduces the influence of downhole contamination, where younger sporomorphs can be re-deposited at greater depths than their original stratigraphic position.

3.4 MAXIMUM LIKELIHOOD AGE MODEL (MLM)

Sample ages were estimated using a maximum likelihood biostratigraphic model, following the approach developed by Punyasena et al. (2012) (App. B). This model identifies, for each sample, the point in geologic time at which the observed taxa have the highest joint probability of co-occurrence, given their known temporal ranges. The reference framework was the Cenozoic palynostratigraphic zonation for the Llanos and Llanos Foothills of Colombia (Jaramillo et al., 2011), which provides first and last appearances for a wide range of Neotropical palynomorph taxa, calibrated against carbon isotopes, radiometric dating, foraminifera, and magnetostratigraphy. The model uses only taxa that are present in the sample, which limits bias from non-detections caused by preservation or sampling. This age is used as approximation, but it should be noted that there are differences between the Guiananan biostratigraphy and the Llanos Basin. Therefore the results will be used as a first age indication but then considered in the litho- and biostratigraphic framework of the Suriname-Guyana Basin.

For each analyzed sample from the Hepp-3 well, likelihood functions were evaluated across a continuous timescale, and the maximum of the likelihood was taken as sample age. Analyses were performed in R (R Development Core Team, 2009), using standard statistical libraries, while palynostratigraphic range charts were produced with the Stratigraph package (Green et al., 2010).

4. RESULTS AND INTERPRETATION

The results are organized along two complementary lines of evidence. First, samarium-neodymium (Sm–Nd) isotopes track temporal changes in sediment provenance from cratonic to Andean sources. Second, the palynological record documents ecological change through time, with lithology as supporting context. The provenance summarizes depth trends in εNd and T_{DM} and assigns samples to source provinces, highlighting levels of mixed or reworked input. The palynology begins with maximum likelihood age estimates, then applies a stratigraphically constrained cluster analysis (CONISS) to define two pollen zones that structure the interval-by-interval reconstructions.

4.1 SEDIMENT GEOCHEMISTRY

4.1.1 Results

Samarium–neodymium (Sm–Nd) isotopes provide a provenance fingerprint that distinguishes ancient cratonic sources of the Guiana Shield from younger, more juvenile sources tied to Andean orogenic belts (Fig. 4). Depth trends in εNd and T_{DM} downcore were evalu-

ated and used to classify samples into Maroni-Itacaiúnas Province (MIP), Rio Negro-Juruena Province (RNJP), and Andean input (Table 2).

Sm–Nd isotope concentrations vary throughout the Hepp-3 well (Table 2), showing an upward shift from ancient cratonic sources toward younger, more juvenile material. This trend is reflected in progressively less negative εNd values (rising from ~ -22 to ~ -11) and younger depleted mantle model ages (T_{DM}) (decreasing from ~2.1 to ~1.5 Ga). The magnitude of this isotopic change represents a fundamental shift in sediment supply, from locally derived Guiana Shield rivers to the addition of Andean-derived contributions, consistent with regional models of late Neogene Amazon drainage reorganization (McDaniel et al., 1997; Tassinari & Macambira, 1999). Two progressive changes are noticed, with two clear inflection points in εNd and T_{DM} corresponding in shifts in provenance at ~131 mbsl and ~61 mbsl depth.

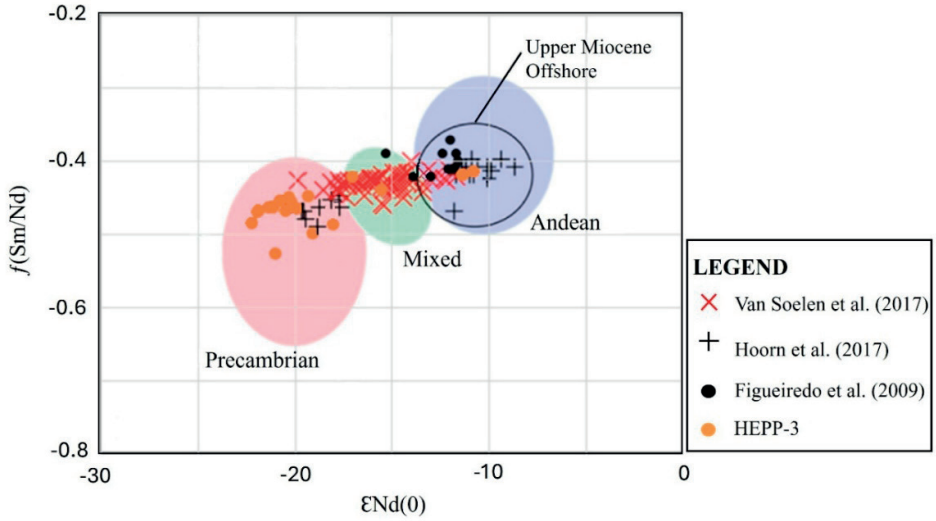


Figure 4: Diagram with Samarium-Neodymium (SM-Nd) isotope data showing the samples and related sources (i.e. Precambrian, Andean, and Mixed) compared to earlier studies (Van Soelen et al. (2017); Hoorn et al. (2017), and Figueiredo et al. (2009)

262–131 mbsl: Maroni-Itacaiúnas Province (MIP; cratonic sources)

The lower to middle part of the succession is dominated by isotopic signatures typical of the eastern Guiana Shield. Samples in this interval yield Sm = 0.6–2.8 ppm, Nd = 3.7–16.2 ppm, $^{143}Nd/^{144}Nd$ = 0.511498–0.511648, with εNd ≈ -22.24 to -19.30 and T_{DM} = 2.12–2.00 Ga. These values indicate derivation from ancient continental crust typical of the MIP, consistent with delivery from local shield rivers and the absence of external input.

131–61 mbsl: Rio Negro-Juruena Province (RNJP; younger cratonic sources)

At intermediate depths, samples yield Sm = 0.6–4.7 ppm, Nd = 3.9–28.9 ppm, $^{143}Nd/^{144}Nd$ = 0. 511561–0. 511843, εNd ≈ -21.01 to -15.50, and T_{DM} = 1.86–1.75 Ga. Relative to MIP, εNd becomes less negative and T_{DM} younger, indicating an influx from RNJP in the western/central Guiana Shield. This interval represents the first step toward more juvenile inputs. Most samples are consistent with RNJP signatures, though the sample at 110 mbsl (εNd = −19.91; T_{DM} = 1.99 Ga) is noticeably older, MIP-like value, suggests mixing or reworking of shield-derived material within otherwise RNJP-dominated deposits.

61–15 mbsl: Andean (A; juvenile sources)

In the upper section, isotopic values shift markedly toward juvenile signatures, requiring addition of Andean arc-derived material. Samples yield Sm =4.0–7.0 ppm, Nd = 21.4–36.7 ppm, $^{143}Nd/^{144}Nd$ = 0.5112055 – 0.512085, εNd ≈ -11.38 – -10.79, and T_{DM} = 1.50–1.47 Ga. This is the first geochemical evidence that the Andean sediments reached the Suriname coastal plain. A single excursion at 24 mbsl (εNd = −17.02; T_{DM} = 1.93 Ga) resembles an MIP-like signature, but does not alter the overall Andean dominance of this interval.

Collectively, the Sm–Nd record documents a stepwise provenance evolution: (i) exclusive supply from the MIP (262–131 mbsl), (ii) addition of younger RNJP sources (131–61 mbsl), and (iii) arrival of Andean-derived sediments (61–15 mbsl). The joint increase in εNd and decrease in T_{DM} define a coherent trajectory from local cratonic to mixed Andean input. This pattern provides independent geochemical evidence that Amazon-delivered Andean sediments reached the Suriname coastal plain only in the uppermost part of the Hepp-3 well.

Table 2: Sm-Nd isotope data and provenance classes for the Hepp-3. For each depth the table reports Sm and Nd concentrations (ppm), 143Nd/144Nd, ƐNd(0), and TDM (Ga). Samples are classified into provenance fields: MIP = Maroni–Itacaiúnas Provenance (eastern Guiana Shield), RNJP = Rio Negero–Juruena Province (central–western shield), and A = Andean input. Classification is based on joint ƐNd–TDM ranges; in this core the dominant fields shift stepwise from MIP (262–131 mbsl) to RNJP (131–61 mbsl) to Andean (61–15 mbsl).

Depth (m)	Depth (ft)	Sm (ppm)	Nd (ppm)	$^{147}Sm/^{144}Nd$	$^{143}Nd/^{144}Nd$	± 2SE	εNd	T_{DM} (Ga)	Source
15	50	6.6	34.7	0.114	0.512059	4	-11.30	1.50	A
24*	80	0.8	4.3	0.114	0.511766	19	-17.02	1.93	
52	170	7.0	36.7	0.115	0.512085	5	-10.79	1.47	
61	200	4.0	21.4	0.114	0.512055	8	-11.38	1.50	
70	230	0.6	3.9	0.101	0.511715	10	-18.01	1.79	RNJP
82	270	0.8	5.1	0.093	0.511561	10	-21.01	1.86	
101	330	4.7	28.9	0.099	0.511659	9	-19.09	1.82	
110*	360	1.4	8.2	0.105	0.511617	12	-19.91	1.99	
128	420	2.2	12.0	0.110	0.511843	8	-15.50	1.75	
140	460	1.1	6.1	0.107	0.511603	7	-20.19	2.05	MIP
152	500	1.0	5.7	0.105	0.51159	13	-20.44	2.02	
165	540	0.8	4.3	0.105	0.511543	7	-21.36	2.10	
186	610	0.6	3.7	0.101	0.511498	21	-22.24	2.08	
198	650	0.9	5.1	0.105	0.511515	14	-21.90	2.12	
213	700	1.4	8.1	0.106	0.511614	8	-19.98	2.00	
223	730	2.1	12.1	0.107	0.511573	10	-20.77	2.09	
232	760	2.8	16.2	0.104	0.511514	5	-21.92	2.12	
241	790	1.0	5.7	0.106	0.511556	14	-21.10	2.08	
253	830	2.6	14.6	0.109	0.511648	6	-19.30	2.01	
262	860	1.5	8.4	0.108	0.511598	12	-20.29	2.08	

4.2 PALYNOLOGY

Sporomorphs were grouped into the following ecological categories: coastal (mangrove), floodplain and swamp (including palms, freshwater aquatics, and other pteridophytes), open vegetation (including savanna), hinterland forest (including rainforest, montane forest, and other angiosperms), and Andean-affiliated types (Table 3) which helps to reconstruct vegetation and coastal settings in time.

Table 3: Ecological category division of ecological markers of the Hepp-3 well (based on Marchant et al. (2015); Mabberley, 1987). All pollen and spores that were identified, but also many that were not identified are displayed (see also Table 4).

	Ecological category	**Taxonomic affinity**
I	Mangroves	Rhizophoraceae; Lythraceae; Tetrameristaceae; *Acrostichum*
II	Tropical lowland palm swamp and forest	Arecaceae
III	Open vegetation	Poaceae; Asteraceae; Chenopodioideae
IV	Fresh water aquatic	Cyperaceae; Alismataceae; Onagraceae; Typhaceae; Pteridaceae
V	Tropical lowland rainforest to montane forest	Melastomataceae-Combretaceae; Myrtaceae; Polypodiaceae; Aquifoliaceae; Apocynaceae; Sapotaceae-Burseraceae; Moraceae & Urticaceae; Malpighiaceae; Euphorbiaceae; Araliaceae; Picrodendraceae; Bignoniaceae; Malvaceae (Bombacoideae); Phyllanthaceae; Fabaceae; Rubiaceae; Myristicaceae; Annonaceae; Proteaceae-Sapindaceae; Hypericaceae; Convolvulaceae; Meliaceae
VI	Andean vegetation	Chloranthaceae; Podocarpaceae; Rosaceae; Hypericaceae
VII	Unknown ecology	Verbenaceae or Solanaceae; Elaeocarpaceae; Slonaea. All the indeterminate pollen types.

Table 4: List with species names, authorities, botanical affinities, reference, location in well and samples, laboratory code, and depth

Taxon name	Family	Genus/Species	Reference	EF	Lab number	Depth (ft)	Depth (mbsl)
Aff. Adiantaceae, *Acrostichum*		*Acrostichum*			T42.412	50	15
Aff. *Alchornea*				R32/3	T42.550	110	34
Aff. Apocynaceae					T42.412	50	15
Aff. Araliaceae					T42.415	170	52
Aff. Arecaceae (*Mauritiinea*)	Arecaceae				T42.412	50	15
Aff. Asteraceae	Asteraceae				T42.412	50	15
Aff. *Borreria*					T42.414	170	52
Aff. Brassicaceae					T42.412	50	15
Aff. Canabaceae		*Trema*			T42.419	710	216
Aff. Cucurbitaceae		*Cucurbita*			T42.548	680	207
Aff. Cunoniaceae		*Weinmannia*?			T42.552	460	140
Aff. Cyatheaceae		*Cyathea, Trichipteris*			T42.412	50	15
Aff. Euphorbiaceae					T42.412	50	15
Aff. Euphorbiaceae		*Sapium*			T42.412	50	15
Aff. *Fabaceae*					T42.415	200	61
Aff. Fabaceae, Ceasalpinoideae		*Chamaecrista*			T42.552	460	216
Aff. Fabaceae, Fatoideae					T42.412	50	15
Aff. Humiriaceae					T42.412	50	15
Aff. *Hypericum*?	Hypericaceae	*Hypericum*			T42.552	460	216
Aff. Malpighiaceae	Malpighiaceae				T42.550	110	34
Aff. Malvaceae		*Hibiscus*			T42.553	420	128
Aff. Moraceae & Urticaceae	Aff. Moraceae & Urticaceae				T42.412	50	15
Aff. *Mycrophyllum*					T42.550	110	34

Table 4: List with species names, authorities, botanical affinities, reference, location in well and samples, laboratory code, and depth *(continued)*

Taxon name	Family	Genus/Species	Reference	EF	Lab number	Depth (ft)	Depth (mbsl)
Aff. Myristicaceae	Myristicaceae	*Virola*			T42.412	50	15
Aff. Myrtaceae	Myrtaceae			M28/0	T42.412	50	15
Aff. Nyctiganaceae					T42.541	820	250
Aff. *Phyllanthus acuminatus*	Phyllanthaceae				T42.554	330	101
Aff. Poaceae	Poaceae			Q30/0	T42.412	50	15
Aff. *Quercus*					T42.553	420	128
Aff. Rubiaceae					T42.415	200	61
Aff. Rubiaceae		*Arcythophyllum*			T42.417	360	110
Aff. Sapotaceae-Burseraceae	Sapotaceae-Burseraceae				T42.550	110	34
Aff. Saxifragaceae					T42.548	680	216
Aff. Scrophulariaceae		*Castilleja*			T42.554	330	101
Aff. Solanaceae					T42.419	710	216
Aff. Solanaceae		*Cestrum*			T42.415	200	61
Aff. Tiliaceae					T42.417	360	
Aff. Vochysiaceae					T42.414	170	52
Arecipites	Arecaceae		Graham 1993		T42.412	50	15
Bombacacidites aff. Bombacoideae	Malvaceae, Bombacoideae		Graham 1993		T42.414	170	52
Bombacacidites baculatus	Malvaceae, Bombacoideae		Muller et al., 1987	T27/4	T42.413	140	43
Byttneripollis rugulatus	Roscaceae	*Polyepsis-Acaena*	D'Apolito et al. 2021		T42.554	330	101
Clavainaperturites clavatus	Euphorbiaceae	*Croton*?	Van der Hammen and Wymstra 1964		T42.415	200	61
Clavainaperturites microclavatus	Chloranthaceae	*Hedyosmum*	Hoorn 1994b	M21/4	T42.412	50	15

Table 4: List with species names, authorities, botanical affinities, reference, location in well and samples, laboratory code, and depth *(continued)*

Taxon name	Family	Genus/Species	Reference	EF	Lab number	Depth (ft)	Depth (mbsl)
Clavatricolpites densiclavatus					T42.412	50	15
Corsinipollenites oculusnoctis	Onagraceae	*Ludwigia*	Nakoman 1965 [Thiergart 1940]		T42.425	840	256
Crocotricolpites sp.					T42.413	140	43
Cyperacidites spp.	Cyperaceae			P33/2	T42.412	50	15
Echimonocolpites spp.	Arecaceae				T42.414	170	52
Echiperiporites akanthos	Alismataceae	*Sagittaria*	Van der Hammen and Wijmstra 1964		T42.550	110	34
Echidiporites barbeitoi	Arecaceae	*Korthalsia ferox*	Muller et al., 1987	J27/2	T42.554	330	101
Echitricolporites spinosus	Asteraceae		Van der Hammen 1956	O18/2	T42.412	50	15
Fenestrites spinosus	Asteraceae		Van der Hammen 1956		T42.412	50	15
Gemmamonocolpites sp. aff. *Iriartea*?	Arecaceae	*Iriartea*			T42.550	110	34
Gemmatricolpites sp.					T42.541	820	250
Grimsdalea magnaclavata			Germeraad et al. 1968				
Heterocolpites spp.	Melastomataceae-Combreatceae				T42.412	50	15
Ilexpollenites spp.	Aff. Aquifoliaceae	*Illex*	Silva-Caminha et al. 2010	F27/3	T42.412	50	15
Jandufouria seamrogiformis	Malvaceae	*Catostemma*	Germeraad et al. 1968		T42.548	680	216
Ladakhipollenites? *garzonii*			D'Apolito et al. 2021 [Hoorn 1993]	N32/0	T42.554	330	101
Lanagiopollis crassa	Tetrameristaceae	*Pelliciera rhizophora*	Frederiksen 1988 [Van der Hammen and Wijmstra 1964]		T42.550	110	34

Table 4: List with species names, authorities, botanical affinities, reference, location in well and samples, laboratory code, and depth *(continued)*

Taxon name	Family	Genus/Species	Reference	EF	Lab number	Depth (ft)	Depth (mbsl)
Magnastriatites grandiosus	Pteridaceae	*Ceratopteris*	D'Apolito et al. 2021 [Dueñas 1980; Kedves and Solé de Porta 1963]		T42.413	140	43
Malvacipollis spinulosa	Picrodendraceae	*Piranhea cf. trifoliata*	Frederiksen 1983		T42.543	800	244
Mauritiidites franciscoi franciscoi	Arecaceae	*Mauritia*	Van Hoeken-Klinkenberg 1964 [Van der Hammen 1956]	D17/3	T42.415	50	15
Monoporopollenites 'microreticulatus'	Typhaceae	*Typha*			T42.412	50	15
Perfotricolpites digitatus	Convulvaceae	*Merremia*	Gonzalez 1967		T42.548	680	216
Podocarpidites	Podocarpaceae	*Podocarpus*	Graham 1993	Q10/1	T42.414	170	52
Polyadopollenites mariae	Fabaceae	*Acacia*	Dueñas 1980		T42.413	140	43
Polypodiisporites usmensis	Polypodiaceae	*Polypodium*	Van der Hammen 1956a [Khan & Martin 1972]		T42.550	110	34
Proteacidites triangulatus	Proteaceae-Sapindaceae		Lorente 1986		T42.548	680	216
Proxapertites tertiara	Annonaceae	*Crematosperma*	Van der Hammen and Garcia 1965		T42.417	360	110
Psiladiporites minimus	Moraceae		Van der Hammen & Wijmstra, 1964		T42.414	170	52
Psilaperiporites spp. (aff. *Chenopodium*)	Chenopodioidae	*Chenopodium*			T42.412	50	15
Psilastephanocolpites equatorialis?					T42.423	760	232
Psilastephanocolporites schneideri	Rhizophoraceae		Hoorn 1993		T42.550	110	34
Psilastephanocolporites sp.	Meliaceae	*Cedrela*			T42.550	110	34
Psilatricolpites acerbus			Gonzalez 1967		T42.417	360	

Table 4: List with species names, authorities, botanical affinities, reference, location in well and samples, laboratory code, and depth *(continued)*

Taxon name	Family	Genus/Species	Reference	EF	Lab number	Depth (ft)	Depth (mbsl)
Psilatricolpites minutus			Gonzalez 1967		T42.550	110	34
Psilatricolporites cf. *varius*			Duenas 1983		T42.550	110	34
Psilatricolporites crassoexinatus			Hoorn 1993		T42.553	420	128
Psilatricolporites exiguus			Hoorn 1993		T42.420	720	219
Psilatricolporites heysti	Euphorbiaceae, Solanaceae or Fabaceae		Wijmstra 1971		T42.553	420	128
Psilatriporites corstanjei	Rubiaceae	*Faramea?*	Hoorn 1993		T42.548	680	216
Punctatosporites latrubressei		*Thelypteris*			T42.415	200	61
Retibrevitricolpites pseudoretibolus			D'Apolito et al. 2021	O30/0	T42.412	50	15
Retibrevitricolpites sp.					T42.423	760	
Retibrevitricolporites yavarensis			Silva-Caminha et al 2010 [Hoorn 1993]		T42.412	50	15
Retimonocolpites maximus?	Arecaceae		Hoorn 1993		T42.545	780	238
Retistephanocolporites sp.					T42.415	200	61
Retitrescolpites irregularis	Phyllanthaceae	*Amanoa*	Jaramillo and Dilcher 2001 [Van der Hammen and Wymstra 1964]		T42.550	110	34
Retitricolpites colpiconstrictus			D'Apolito et al 2021 [Hoorn 1994]		T42.541	820	250
Retitricolpites maturus			Gonzalez 1967		T42.545	780	238
Retitricolpites ovalis			Van der Hammen and Wymstra 1964		T42.420	720	219
Retitricolpites sp. aff. *Avicennia*	Avicennia			D24/2	T42.412	50	15
Retitricolpites spp. (aff. Bignoniaceae)	Bignoniaceae				T42.412	50	15

Table 4: List with species names, authorities, botanical affinities, reference, location in well and samples, laboratory code, and depth *(continued)*

Taxon name	Family	Genus/Species	Reference	EF	Lab number	Depth (ft)	Depth (mbsl)
Retitricolporites latus	Verbenaceae or Solanaceae				T42.550	110	34
Retitricolporites milnei			Hoorn 1993		T42.423	760	232
Retitricolporites sp. aff. Hypericaceae, *Vismia*	Hypericaceae	*Vismia*			T42.552	460	216
Retitricolporites ticuneorum					T42.548	680	216
Retitriporites aff. *crassireticulatus*	Rubiaceae	*Tocoyena*	Leite et al. 2020		T42.417	360	110
Rhoipites caputoi	Araliaceae	*Oreopanax*?	D'Apolito et al. 2021 [Hoorn 1993]		T42.412	50	15
Rhoipites crassicostatus			D'Apolito et al. 2021 [Van der Hammen and Wymstra 1964]		T42.412	50	15
Rhoipites guianensis	Malvaceae	*Vasivea-Trichospermum*	D'Apolito et al. 2021 [Van der Hammen and Wymstra 1964]	S29/4	T42.552	460	216
Rhoipites hispidus			Jaramillo and Dilcher 2001 [Van der Hammen and Wymstra 1964]		T42.541	820	250
Rhoipites pseudopilatus	Rosaceae	*Lachemilla*	D'Apolito et al. 2021		T42.554	330	101
Rhoipites sp.					T42.552	460	216
Rhoipites sp.					T42.550	110	34
Spirosyncolpites spiralis	Bignoniaceae?		Gonzalez 1967		T42.425	840	256
Striatopollis catatumbus	Fabaceae	*Crudia*	Takahashi and Jux 1989 [Gonzalez 1967]		T42.548	680	216
Striatricolporites spp.					T42.552	460	216

Table 4: List with species names, authorities, botanical affinities, reference, location in well and samples, laboratory code, and depth *(continued)*

Taxon name	Family	Genus/Species	Reference	EF	Lab number	Depth (ft)	Depth (mbsl)
Verrutricolporites desmodiensis	Fabaceae	*Desmodium, Mucuna or Elizabetha*	Jaramillo et al. 2014		T42.414	170	52
Verrutricolporites rotundiporus	Lythraceae	*Ammannia*	Van der Hammen and Wymstra 1964	S28/4	T42.550	110	34
Zonocostites spp.	Rhizophoraceae	*Rhizophora*		O33/0	T42.412	50	15
	Spores and ferns						
Aff. Polypodiaceae		*Adianthum*			T42.412	50	15
Echimonoletes spp.					T42.541	820	250
Echinatisporis cf. *muelleri*			Silva-Caminha et al. 2010 [Regali et al. 1974]	K17/2	T42.412	50	15
Laevigatosporites aff. *tibuensis*	Polypodiaceae		Jaramillo and Dilcher 2001 [Van der Hammen 1956a]	N30/3	T42.554	330	101
Laevigatosporites spp.					T42.412	50	15
Monolete spores					T42.412	50	15
Perinomonoletes aff. *Asplenium*					T42.412	50	15
Polypodiisporites aff. *minutiverrucatus*			Leite et al. 2020		T42.415	200	61
Polypodiisporites aff. *planus*	Polypodiaceae	Serpocaulon dasypl…	D'Apolito 2021 [Silva-Caminha et al. 2010]		T42.552	460	216
Polypodiisporites aff. verruplanatus			Jaramillo et al. 2014		T42.412	50	15
Polypodiisporites densus	Polypodiaceae	Polypodium	D'Apolito et al. 2021		T42.415	200	61
Polypodiisporites fossulatus	Nephrolepidaceae	Nephrolepsis	D'Apolito et al. 2021		T42.412	50	15

Table 4: List with species names, authorities, botanical affinities, reference, location in well and samples, laboratory code, and depth *(continued)*

Taxon name	Family	Genus/Species	Reference	EF	Lab number	Depth (ft)	Depth (mbsl)
Polypodiisporites sp.	Polypodiaceae	Polypodium			T42.415	200	61
Trilete spores					T42.412	50	15

4.2.1 Maximum Likelihood Ages

Nineteen samples were dated using a maximum likelihood biostratigraphic model based on the joint occurrence of 38 identified marker taxa in the pollen assemblages (App. B). For each sample the model returns a MLA and an uncertainty interval expressed as the interquartile range (Q25–Q75). All MLAs and associated uncertainties are reported in Table 5.

Across the section, MLAs span 16.57–17.63 Ma, placing dated material within the Early Miocene (Burdigalian). In the lower part of the record (262–131 mbsl; Zone I), MLAs are tightly grouped with relatively narrow uncertainty ranges, indicating strong constraint from the marker set. In the upper part (131–15 mbsl; Zone II), MLAs are more dispersed, and few samples show broader uncertainty. Reversals in depth-age trend occur and the age ranges overlap, so sedimentation rates (about 1 meter per thousand years) cannot be inferred from these estimates alone. Consequently, the paleoecological description is organized by CONISS zones and MLAs as broad temporal brackets.

Table 5: Maximum-likelihood stratigraphic ages by depth for the Hepp-3. Depths are listed in meters and feet. Ages were estimated with a probabilistic maximum-likelihood approach based on the joint occurrence of marker palynomorph taxa (presence only) against a regional Cenozoic reference framework. "MLA" reports the maximum-likelihood age in million years. "Q25" and "Q75" give the 25th and 75th percentile bounds of the age probability distribution. Shading in the MLA column visualizes relative support with warmer colors indicating higher likelihood. Rows are grouped by the CONISS-defined palynological zones for this core (Zone I, Zone II).

Depth (m)	Depth (ft)	MLA	Q25	Q75	
15	50	17.26	12.64	26.59	
34	110	17.47	13.27	25.45	
43	140	17.28	13.74	28.26	
52	170	17.12	12.97	31.11	Zone II
61	200	17.24	12.78	23.68	
101	330	17.38	13.41	24.37	
110	360	17.63	18.83	57.27	
128	420	16.57	11.40	29.30	
140	460	17.30	13.94	25.04	
207	680	17.53	13.43	25.49	
216	710	17.45	13.25	24.65	
219	720	17.49	13.58	23.94	
226	740	17.53	13.39	24.69	
232	760	17.43	13.45	24.19	Zone I
238	780	17.47	13.80	24.06	
244	800	17.18	13.17	29.09	
250	820	17.43	13.41	28.69	
256	840	17.47	13.78	23.88	
262	860	17.45	13.84	23.62	

4.2.2 Palynology - sporomorphs

A total of 4253 sporomorphs were counted in the Hepp-3 well (App. C). All identified sporomorphs in the Hepp-3 well samples were classified based on their ecological environments and associated biomes (Fig. 5 and 6). Using the CONISS function in Tilia, two main palynological zones were identified, designated as Zone I and Zone II. These zones are discussed sequentially from the deepest to the shallowest intervals. Zone I is located in the lower part of the well (262–204 mbsl), followed by a barren interval (204–140 mbsl). Zone II extends from 140 to 15 mbsl, and is subdivided into two subzones, II-1 (140–131 mbsl) and II-2 (131–15 mbsl).

4.2.2.1 Sporomorph biostratigraphy

Determining the age of the Hepp-03 stratigraphy is crucial for interpreting coastal evolution and the arrival of Amazon influence. Absolute dates are unavailable, so the chronology rests on MLAs and on correlation to the regional palynostratigraphic schemes. MLAs provide a broad temporal window rather than sharp boundaries. To refine placement, the record is compared first to the zonation of Suriname (Wijmstra, 1971), which builds on van der Hammen & Wijmstra (1964) and is calibrated to the global marine timescale via Bolli's (1966) planktonic foraminifera zonations. Broader context comes from the Amazon submarine fan (Hoorn et al., 2017; Regali, 1974), the Venezuelan coastal basins (Germeraad et al., 1968), Pará State (Brazil) (Gomes et al., 2023), and the Sub-Andean and Llanos basins (Jaramillo et al., 2011).

Across Amazonia, biostratigraphic patterns can conflict due to diachronous first/last occurrences and repeated dispersal events documented for the Neotropics. Consequently, the age model for Hepp-03 prioritized first and last occurrences of diagnostic taxa within the sequence and coherent turnover packages (e.g., transgressive-regressive phases), using external schemes for calibration and cross-checks. This biostratigraphic approach allows Zones I-1, II-1, and II-2 of to be positioned within the established regional framework and provides a stronger basis subsequent environmental interpretation.

In Suriname, Wijmstra's Zone E corresponds to the Oligocene to Early Miocene, which is characterized by the first occurrence of *Rhizophora*. Zone F spans the latest Early to Middle Miocene, marked at its base by *Psiladiporites minimus* and *Crassoretitriletes vanraadshoovenii* in the upper part (Plate I.1). Zone G extends from the Late Miocene into the Pliocene and Pleistocene, with G1 often linked to savanna expansion. Boundaries are less distinct within the Hepp-03 well, with several marker taxa showing wide or overlapping ranges.

Zone I (262–204 mbsl): Early to Middle Miocene

This interval includes the Coesewijne Formation and records the occurrences of biostratigraphic species such as *Bombacacidites baumfalki, Fenestrites spinosus, Grimsdalea cf. magnaclavata, Jandufouria seamrogiformis, Mauritiidites franciscoi pachyexinatus, Perfotricolpites*

digitatus, Retitricolpites maturus, Retitriporites dubiosus, Spirosyncolpites spiralis, and *Striatopollis catatumbus* (Plate I.2).

Based on the (first) occurrence of *Jandufouria seamrogiformis* (FOD 256 and LOD 207 mbsl), *Verrutricolporites rotundiporus* (FOD 262 and LOD 33 mbsl) (Plate I.3), and *Psiladiporites minimus* (FOD 850 and LOD 52 mbsl) an Early to Middle Miocene age is assigned to this interval. The assemblages also correspond with pollen Zones F of Guyana (Van der Hammen and Wijmstra, 1964) and E of Suriname (Wijmstra, 1971). The appearance of *Retitricolporites (Rhoipites) guianensis* (FOD 259 and LOD 140 mbsl) is assigned to zone E of Guyana (Van der Hammen and Wijmstra, 1971) and zone VIII of Northern South America (Muller et al, 1987) of respectively Oligocene and Early Eocene to Oligocene age. However, the Oligocene age can be discarded due to the absence of *Cicatricosisporites dorogensis*, a marker for the Middle Eocene to Oligocene (Regali, 1974; Muller et al., 1987). Additional support comes from *Grimsdalea cf. magnaclavata* and *Fenestritus spinosus*, whose ranges extend from the latest Early into the Middle Miocene (Germeraad et al., 1968; Jaramillo et al., 2011). Maximum likelihood ages refine this to the Burdigalian at about 17.53–17.18 Ma.

204 to 140 mbsl; Barren interval*: there is no palynological record for this interval*

Zone II-1 (140–131 mbsl); Miocene to Pliocene

This interval comprises the Zanderij Formation and forms a distinct break between zone I and II-1, suggesting a paleobotanical turnover. In the upper part of Zone I, the increased abundance of *Verrutricolporites rotundiporus*, a short Poaceae peak (Plate I.4), and the presence of *Retitrescolpites irregularis* anticipate an extensive regression that is recorded by overlying sands. In zone II-1 the last occurrence of *Retitricolporites (Rhoipites) guianensis* support placement within lower Zone F (Wijmstra, 1971) (Plate I.5). The presence of *Bombacacidites baculatus* (FOD and LOD 140 mbsl) (Plate I.6) which is congruent with zone T-18 the Llanos and Llanos basins (Jaramillo et al., 2011) suggests a Pliocene to Pleistocene age. Other species that occur in this interval are *Echidiporites barbeitoi* (FOD 460 and LOD 330 mbsl) (Plate I.7) whose first occurrence is assigned to the Early Miocene of Northern South America (Muller et al., 1987). The occurrence of *Echitricolporites spinosus* (FOD 140 and LOD 15 mbsl) (Plate I.8) as observed from the Middle Miocene to the Pliocene in zone PT-40 of the Amazon Fan (Regali et al., 1974). The mixed occurrence of *B. baculatus* and *E. spinosus, E. barbetoi*, and *Clavainaperturites microclavatus* (Plate I.9a,b) would suggest a Miocene to Pliocene age for zone II-1. However, earlier studies by Wong (1989) established a Pliocene age for the Zanderij Formation which should be taken into account. A maximum likelihood estimate of ~17.3 Ma conflicts with a Middle Miocene placement here, which underscores the limits of probabilistic ages for single samples when stratigraphic ranges are long and preservation may be misleading.

Zone II-2 (131–15 mbsl); Plio-/Pleistocene?

The upper part of zone II-2 also comprises the Zanderij Formation, and records last occurrences of *Psilatricolporites heysti*, *Lanagiapollis crassa*, and *Echidiporites barbeitoi*, taxa that vanish by the Middle Miocene in regional schemes (Wijmstra, 1971; Muller, 1987; Hoorn et al., 2017). The first occurrence of *Retitricolpites* aff. *Avicennia* (Plate I.10) is more typical for the Pliocene to Pleistocene and supports Zone G of Guyana (Van der Hammen & Wijmstra, 1964). *C. microclavatus* (*Hedyosmum*) (FOD 128 and LOD 15 mbsl) makes its first appearance, but is normally assigned to zone E-2 of Suriname (Wijmstra, 1971) and zone E of Guyana (Van der Hammen & Wijmstra, 1971) in respectively the Early Miocene and Oligocene. Even so with *Echinatisporis muelleri*, which is assigned to the Early Miocene in the Amazon Fan (Regali et al., 1974) (Plate I.11). Other species that make their last appearance in this interval are *Proxapertites tertiara*, *Mauritiidites franciscoi minutus*, *E. barbeitoi*, *Echiperiporites akanthos*, *Magnastriatites grandiosus*, *Polypodiisporites usmensis*, *Retitrescolpites*? *irregularis*, *V. rotundiporus*, *Perisyncolporites pokornyi*, *Rancunculacidites operculatus*, *Syncolporites poricostatus*, *Rhoipites hispidus*, *Tetracolporopollenites transversalis*, *Zonocostites ramonae*, *Monoporopollenites annulatus*, *Retitricolporites simplex*, *Mauritiidites franciscoi franciscoi*, *Psilabrevitricolporites devriesii*, *E. spinosus*, *Clavainaperturites microclavatus*, *Clavatricolpites densiclavatus*, and *Retibrevitricolporites yavarensis* (Plate I.12-14). Palynology points to a Plio-/Pleistocene age for Zone II-2, but the occurence of Miocene marker species creates a dilemma. The age also conflicts with MLAs of 17.63–16.57 Ma, which still fall in the Early Miocene, and highlighting the caution needed when applying probabilistic ages to sparse, ditch-cutting assemblages.

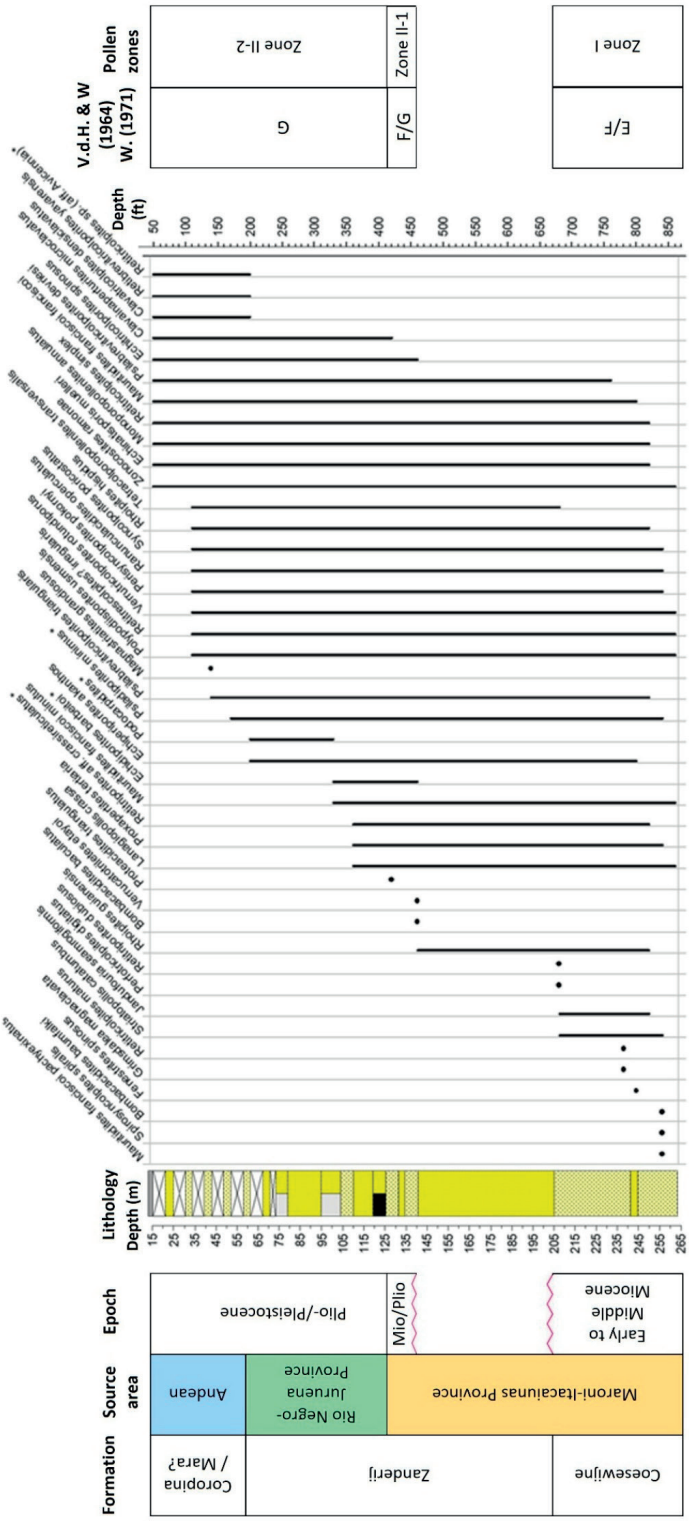


Figure 5: Palynological marker taxa in the Hepp-3 well. Stratigraphic ranges of selected marker palynomorphs plotted against the depth. *Taxa that were not used in the Maximum-Likelihood Age analysis but are informative with the regional biostratigraphic framework

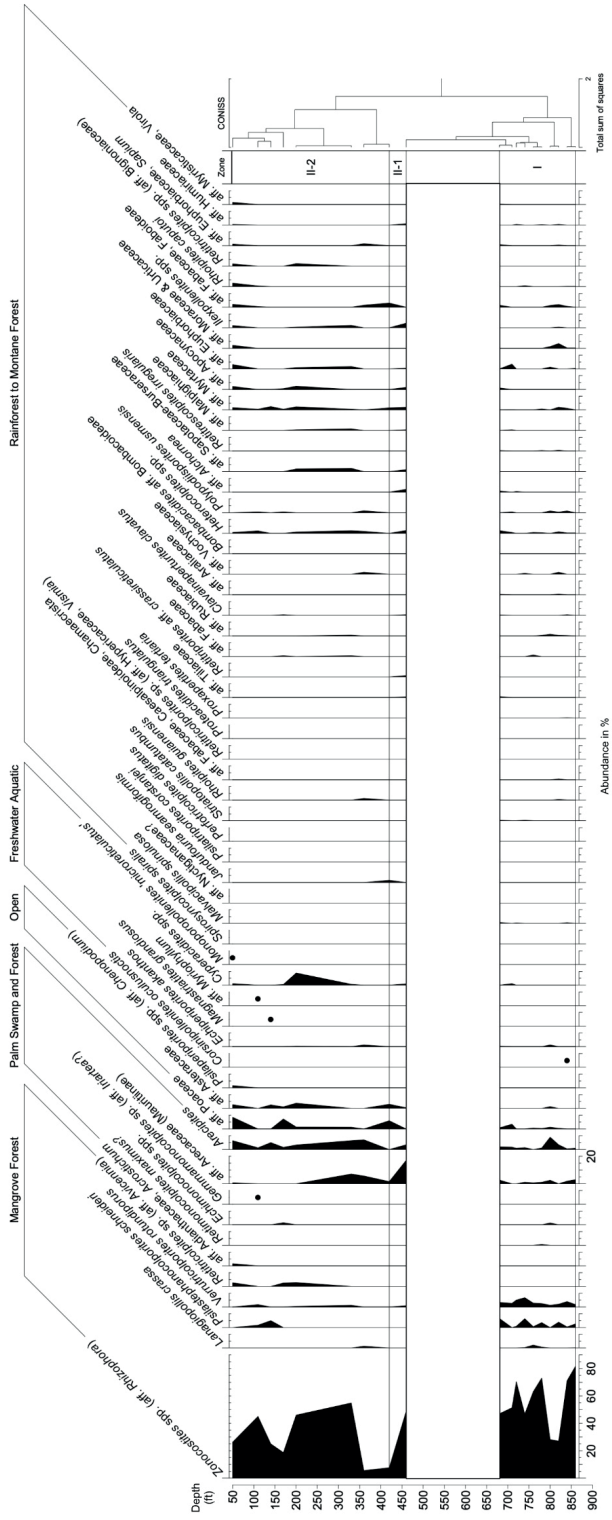


Figure 6: Detailed sporomorph diagram of the Hepp-3 well with percentages based on pollen sum.

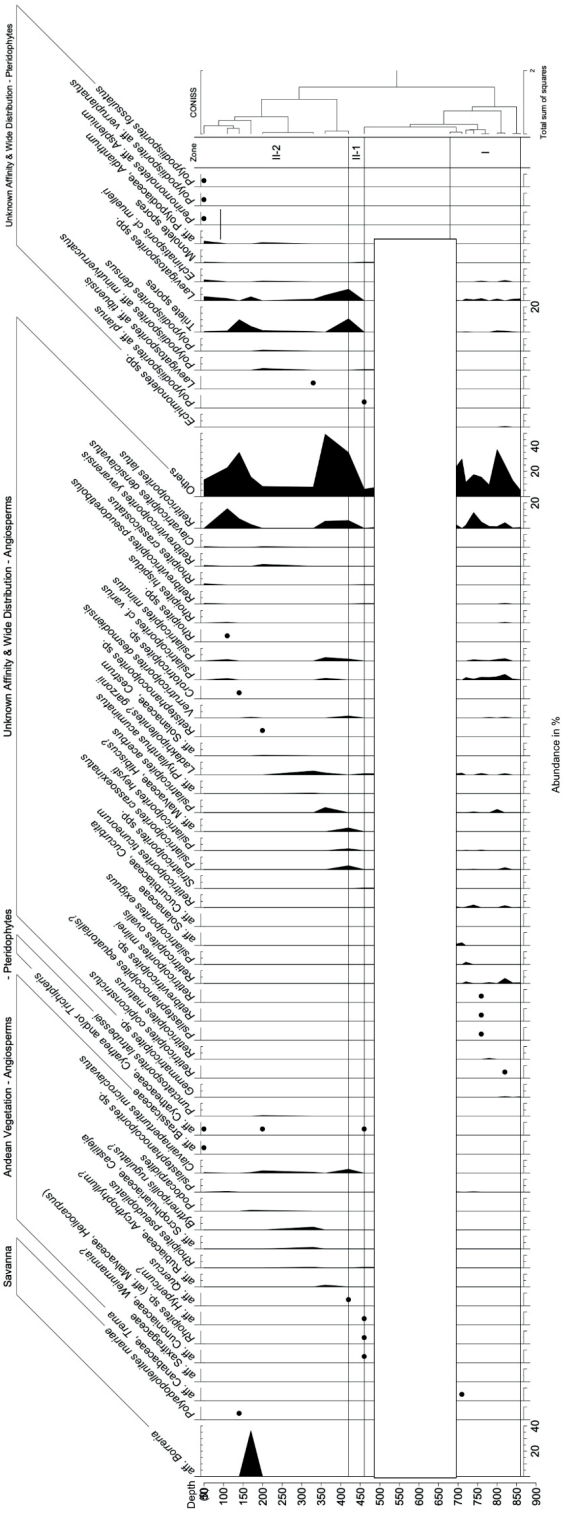


Figure 6: Detailed sporomorph diagram of the Hepp-3 well with percentages based on pollen sum (Continued).

4.2.2.2 Paleoecological zones or biomes

Pollen zone I (262–204 mbsl: Early to Middle Miocene)

The assemblage record of Zone I comprises (i) two phases of mangrove dominance separated by an interval of reduced coastal influence, (ii) repeated expansions of floodplain and hinterland forest elements, and (iii) the first occurrence of Andean-affiliated pollen (Fig. 7; Plate 1).

262–250 mbsl: *Dense mangrove thickets stretched across the intertidal wetlands, with patches of palm swamp and lowland rainforest forming a mosaic of habitats further inland.* Mangrove abundance is very high (74–85%), dominated by *Zonocostites* spp. (aff. *Rhizophora*) with sporadic *Verrutricolporites rotundiporus* (*Ammannia,* Lythraceae), *Psilastephanocolporites schneideri* (aff. *Rhizophora*), and *Lanagiopollis crassa* (aff. *Pelliciera*, Tetrameristaceae), typical of brackish, tidally influenced forests. The presence of pyrite and shell fragments within the clayey sands reinforce intermittent reducing conditions and tidal incursions. Low abundances of palm taxa (2–4%; *Mauritiidites* and other Arecaceae) indicate nearby palm swamps with *Laevigatosporites* spp. along the shaded edges (Plate I.15). The presence of lignite supports occasional waterlogging typical of swampy environments. A modest hinterland signal, comprising of lowland rainforest to montane forest elements (3–8%) such as *Heterocolpites* spp., *Ranunculacidites* (aff. *Alchornea*), and *Psiladiporites* (aff. Moraceae/Urticaceae), together with other angiosperm taxa (7–14%) indicate a diverse forested landscape beyond the immediate mangrove zone. These grains were likely transported by rivers and streams draining the inland forests.

250–238 mbsl: *A transitional landscape emerged, where once-dominant mangroves retreated seaward, while palm swamp and hinterland forests expanded across the floodplain.* Mangroves decline sharply to just ~26% but remain dominated by *Zonocostites,* with minor *V. rotundiporus* and *P. schneideri*, implying residual brackish influence. Simultaneous decreases in clay content and localized sand influx indicate higher-energy episodes that would disrupt intertidal stability. Palm swamp elements rise to ~11%, dominated by *Arecipites,* with occasional *Mauritiidites* and *Echimonocolpites* spp. And considered alongside occasional ferns, herbs, and aquatic taxa, the assemblage further indicates periodically inundated floodplains. At the same time, rainforest-montane forest pollen reaches (19–20%), and taxa such as *Heterocolpites* spp., aff. Myrtaceae (Plate I. 16), *Polypodiisporites usmensis*, and *Malvacipollis spinulosa* become more prominent. Other hinterland vegetation notably increases (39–43%), including *Retitricolporites latus*, *Psilatricolporites* cf. *varius*, and *Retitricolpites ovalis*. These assemblages indicate a stronger terrestrial input from inland catchments, likely coinciding with a flood event or temporary shift in fluvial activity that briefly introduced coarser sediments into the area. Compared to the underlying interval, this section reflects a retreat of mangroves, establishment of freshwater swamp and floodplain habitats, and a strengthened hinterland signal across a transitional coastal plain.

238–204 mbsl: *Mangrove forests once again surged inland under heightened marine influence, dominating the intertidal wetlands, before steadily withdrawing as floodplain swamps and hinterland forests reclaimed the coastal plain.* Mangroves rapidly expanded to ~75%, dominated by *Zonocostites,* with a small initial peak in *Lanagiopollis crassa*. This phase of heightened marine influence is further supported by the presence of dinoflagellate cysts at 232 mbsl, including *Polysphaeridium zoharyi*, *Systematophora placacantha*, and *Spiniferites ramosus*. And organic-rich, clayey sands with high clay content and pyrite presence are consistent with low-energy, waterlogged intertidal settings. However, this expansion is short-lived.
Mangrove representation steadily declined throughout the interval, with only a brief resurgence at 219 mbsl before continuing its retreat. The initial mangrove pulse coincides with a sharp decrease in non-mangrove taxa. Palm swamp forest falls to a minimum of ~1% at 219 mbsl, driven by the disappearance of *Mauritiidites* and *Retimonocolpites maximus*, before rising to 4% towards the top. Similarly, open vegetation and freshwater aquatic taxa disappear and only reappear above 219 mbsl. A discrete Poaceae peak at 216 mbsl signals a brief expansion of small-scale open grasslands on better-drained floodplains, in line with increasing kaolinitic clays that reflect improved drainage.

Rainforest-montane forest taxa reach their lowest representation at 226 mbsl (5%) and recover to 14% upward, while *Heterocolpites* spp., aff. Myrtaceae, aff. Euphorbiaceae remain abundant across the section. In contrast, the broader hinterland elements expand through the interval to 25-34% at the top despite a dip at 219 mbsl (18%). *Retitricolporites latus* and *Psilatricolporites* cf. *varius* are consistently present, whereas *Retitricolporites ovalis*, *Retitricolporites ticuneorum*, and *Psilatricolporites exiguus* occur more variably. Importantly, this interval also records the first occurrence of Andean pollen types (<1%), including *Psilastephanocolporites* sp., *Diporites* (aff. Cannabaceae, *Trema*), and aff. Saxifragaceae, suggesting long-distance transport of Andean-derived material together with shifting drainage dynamics. Compared to the underlying interval, which records mangrove retreat, this section begins with a short-lived marine incursion and mangrove dominance, then trends back toward increasing fluvial influence as swamp and hinterland vegetation recover after 219 mbsl.

Barren Interval (204–140 mbsl)

The barren interval separates zone I from zone II, and comprises an extensive sand-dominated unit between 204–140 mbsl, that was excluded from palynological counts. *Extensive fluvial deposition from land during a regression marks the progradation of the coastline and the replacement of once stable coastal wetlands by dynamic environments.* Nevertheless, stratigraphic context indicates a fully developed river regime, completing the coastal-to-fluvial transition below.

Pollen zone II (140–15 mbsl: Miocene to Plio-/Pleistocene)

Zone II spans the upper Zanderij and Coropina/Mara formation, characterized by (i) reduced and fluctuating mangrove cover, (ii) persistent rainforest-montane forest contributions, (iii) long-lived freshwater palm swamp elements, and (iv) a brief savanna expansion. The Andean signal remains present. Biostratigraphic markers such as *Clavainaperturites microclavatus, Clavatricolpites densiclavatus, Magnastriatites grandiosus, and Retibrevitricolporites yavarensis; Podocarpidites* and *Retitricolpites sp.* (aff. *Avicennia*) occur exclusively in this zone (Plate I.17 & I.10; Fig. 7).

Subzone II-1 (140–131 mbsl: Miocene to Pliocene)

Mangroves regained a foothold along tidal wetlands, while palm swamps spread across the floodplain, and dense rainforest flourished further inland. Mangrove forests recover to 43%, with *Zonocostites*-dominance and minor *V. rotundiporus*, indicating a more homogenous mangrove environment. Increased pyrite reinforces the interpretation of brackish, tidally influenced environments. Freshwater swamps expand rapidly, with palm taxa reaching their maximum abundance (18%), driven by an increase in *Mauritiidites*. Smaller contributions of *Arecipites* and *Cyperacidites* (Plate I.18), together with elevated lignite and interbedded clays, indicate palm-sedge mosaics in seasonally inundated wetlands. Simultaneously, rainforest-montane forest attains its highest representation (27%), including *Heterocolpites* spp., *Polypodiisporites usmensis*, aff. Fabaceae (Faboideae), and aff. Rubiaceae. Other angiosperms (7%) add to the hinterland signal, with no taxon individually abundant. Crucially, Andean-derived pollen that appeared sporadically below is more consistently represented here (e.g., *Rhoipites pseudopilatus, Hypericum,* and others), reflecting a stable long-distance connection with Andean sources. Compared to the fluvial sands beneath, this interval documents floodplain re-establishment with renewed coastal influence and freshwater wetlands. In zone B1, *Retitricolporites (Rhoipites) guianensis* has its LOD, while *Verrucatotriletes etayoi* and *Bombacacidites baculatus* are unique (Plate I; Fig. 7).

Subzone II-2 (131–15 mbsl: Plio-/Pleistocene)

131–104 mbsl (Pliocene): *The floodplain was overtaken by expansive inland forests, overshadowing the patchy grasslands and marshes that lingered in the in the waterlogged lowlands.* At the beginning of this interval, mangrove pollen collapsed to 6%, marking a decisive retreat from brackish intertidal conditions, which is reflected by the decrease in pyrite amounts. In their place, herbaceous vegetation reaches 8%, dominated by Poaceae and Asteraceae, while ferns like *Laevigatosporites* expand significantly to 17%, indicating the development of open grasslands and marshes (Plate I.16). The associated lignite-rich sands provide evidence for extensive peat-forming wetlands that sustained these open, waterlogged environments. As the interval progresses, these open habitats begin to decline, as palm swamp forests expanded within the floodplain. *Mauritiinae* palms and *Arecipites* increase from 1% to 11%. This ecological shift aligns with interbedded clayey sands bearing moderate amounts of lignite, which suggest recurrent phases of organic accumulation under waterlogged conditions. The

rainforest and montane forest components maintained a steady contribution throughout this interval (21–24%). Taxa such as *Heterocolpites* spp. and aff. Myrtaceae, reflects a stable inland influence, even as the floodplain underwent significant changes. Other hinterland elements were highly abundant, and even increased from 44% to 54%, reflecting a rise in taxa that were able to thrive in the transitional floodplain conditions. Andean elements (1–4%), including aff. *Quercus,* Rubiaceae (aff. *Arcythophyllum)*, and *Clavainaperturites microclavatus*, signal a sustained connection with Andean sources. Overall, this sequence marks the definitive retreat of coastal mangroves and the establishment of extensive wetlands of marshes and palm swamps within a highly dynamic floodplain.

104–61 mbsl (Pliocene): *Mangroves extend once more along the coast, re-establishing tidal forest, as palm swamps persisted in the floodplain and inland forest maintained their steady presence.* Mangrove pollen recovered to 51%, but the assemblage was relatively monotonous and *Zonocostites*- dominated. Pyrite preserved in the lower part of the interval provides evidence of periodic reducing conditions typical of soils under tidal influence. Freshwater swamp vegetation remains stable at 12% and is dominated by *Mauritiidites* and *Arecipites*. Their presence, together with elevated lignite content, indicate that organic-rich, waterlogged wetlands continued to play a significant role alongside the coastal mangrove environments. In contrast, open vegetation (1%) and freshwater aquatic taxa (<1%) are nearly absent, with minor hinterland ferns (2%), indicating that open marshes and aquatic habitats were limited. Rainforest and montane forest taxa, although slightly reduced compared to the preceding interval, continue to signal strong inland input (19%), particularly *Heterocolpites* spp. and *Ilexpollenites* spp (Plate I.19). However, other hinterland pollen decreased sharply to only 10%, contrasting with its strong presence earlier. Within this group, *Ladakhipollenites? garzonii* is a minor but noteworthy presence (Plate I.20). Andean pollen maintains a consistent presence (4%), with *Byttneripollis rugulatus* particularly notable, accounting for half of the Andean assemblage despite its low overall abundance. Lithological evidence depicts a coastal plain alternating between floodplain stability and weathering, and episodes of fluvial activity. Compared to the underlying interval, mangroves recover at the expense of open vegetation and inland forests, while freshwater swamps maintain their prominence.

61–15 mbsl (Pleistocene): *The landscape shifted from coastal mangroves to open savannas, and closed forests, before settling into a stable wetland system as the sequence drew to a close.* Mangrove cover fluctuated throughout the section, with moderate abundance at 61 mbsl (46%), a low at 52 mbsl (19%), and recovering around 34 mbsl (45%), then declining again to the top at 15 mbsl (31%). Interestingly, the mangrove assemblage, though still dominated by *Zonocostites* and minor contributions of *V. rotundiporus*, sees the reappearance of *Psilastephanocolporites schneideri* and the first occurrence of *Retitricolpites* sp. (aff. *Avicennia*) (Plate I-12), reflecting increased diversity. Freshwater swamp vegetation remains a consistent but minor component of the landscape (2–4%), with a slight expansion to 7% at 15 mbsl. Open aquatic vegetation peaks at 61 mbsl (9%), reflecting abundant standing water in the

floodplain. This increase is driven by the presence of *Cyperacidites* (aff. Cyperaceae) (Plate I-21). And together with other ferns (6%) in the assemblage, these taxa support the expansion of open marshes beyond the mangrove and swamps. As the interval progresses, these habitats decline to 1–2%. This is reinforced by an upward decline in lignite, which reflect a reduction in waterlogged floodplain habitats.

Open, herbaceous vegetation peaked at 52 mbsl (7%), coinciding with a surge of savanna elements (32%), more specifically in aff. *Borreria*. This shift coincides with very high amounts of oxidized yellow clays, implying a temporary phase of drier conditions and fluctuating water tables. Following this peak, savanna taxa and open vegetation sharply decline. By 15 mbsl, however, there is a partial return of open vegetation (13%), indicating the recovery of a mixed landscape, where patches of grasslands persist alongside the other more closed habitats. Rainforest and montane forest elements remained a prominent feature of the landscape (~20%), with a brief decline at 52 mbsl (13%) during the savanna expansion and a second low at 34 mbsl (12%) coincident with increased mangrove cover. Throughout this interval, there is a growing presence of hinterland taxa, increasing from 10% to 38%, before dropping to 16% at 15 mbsl, reflecting variable but persistent input from inland vegetation. The Andean signal, however, weakened (0–4%), represented by scattered occurrences of *Punctatosporites latrubessei* (aff. *Thelypteris*), *Podocarpidites*, *Psilastephanocolporites* (aff. Meliaceae, *Cedrela*), aff. Cyatheaceae, *Clavainaperturites microclavatus*, and Brassicaceae, indicating the loss of a stable long-distance connection (Plate I-21). At the same time, lithologic trends point to the development of a closed wetland system at the top of the sequence. Overall, this interval captures a transitional landscape in which mangroves fluctuate rather than dominate, freshwater swamps persist in localized patches, and savanna experienced brief expansion.

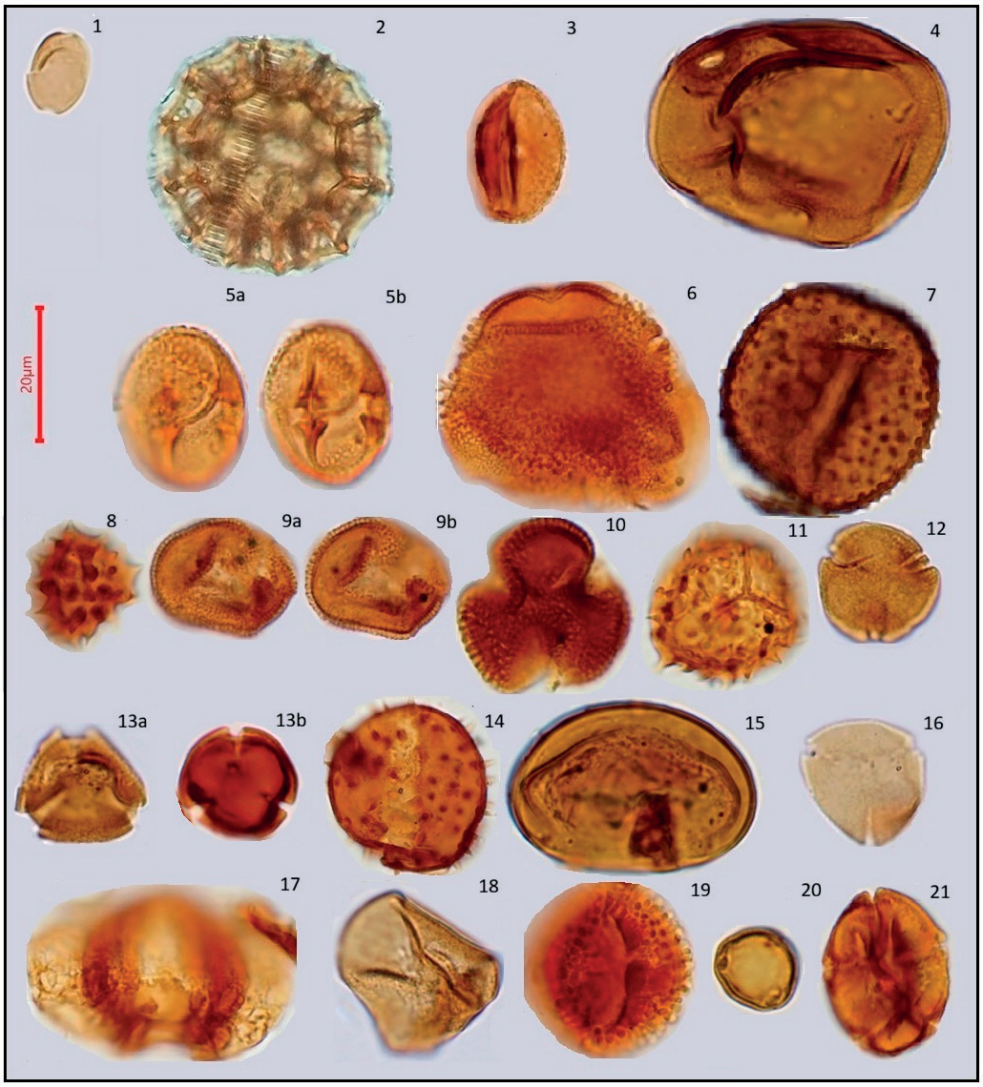


Plate 1: (1) *Psiladiporites minimus*; (2) *Fenestrites spinosus;* (3) *Verrutricolporites rotundiporus*; (4) *Monoporopollenites annulatus* (Poaceae); (5) *Rhoipites (Retitricolporites) guianensis*; (6) *Bombacacidites baculatus*; (7) *Echidiporites barbeitoi*; (8) *Echitricolporites spinosus*; (9a,b) *Clavainaperturites microclavatus*; (10) *Retitricolpites* aff. *Avicennia*; (11) *Echinatisporis muelleri*; (12) *Ranunculacidites operculatus*; (13a,b) *Zonocostites ramonae*; (14) *Mauritiidites franciscoi franciscoi*; (15) *Laevigatosporites*; (16) Myrtaceae; (17) *Podocarpidites;* (18) Cyperaceae; (19) *Ilexpollenites*; (20) *Ladhakipollenites garzonii*?; (21) *Psilastephanocolporites* aff. *Cedrela*;

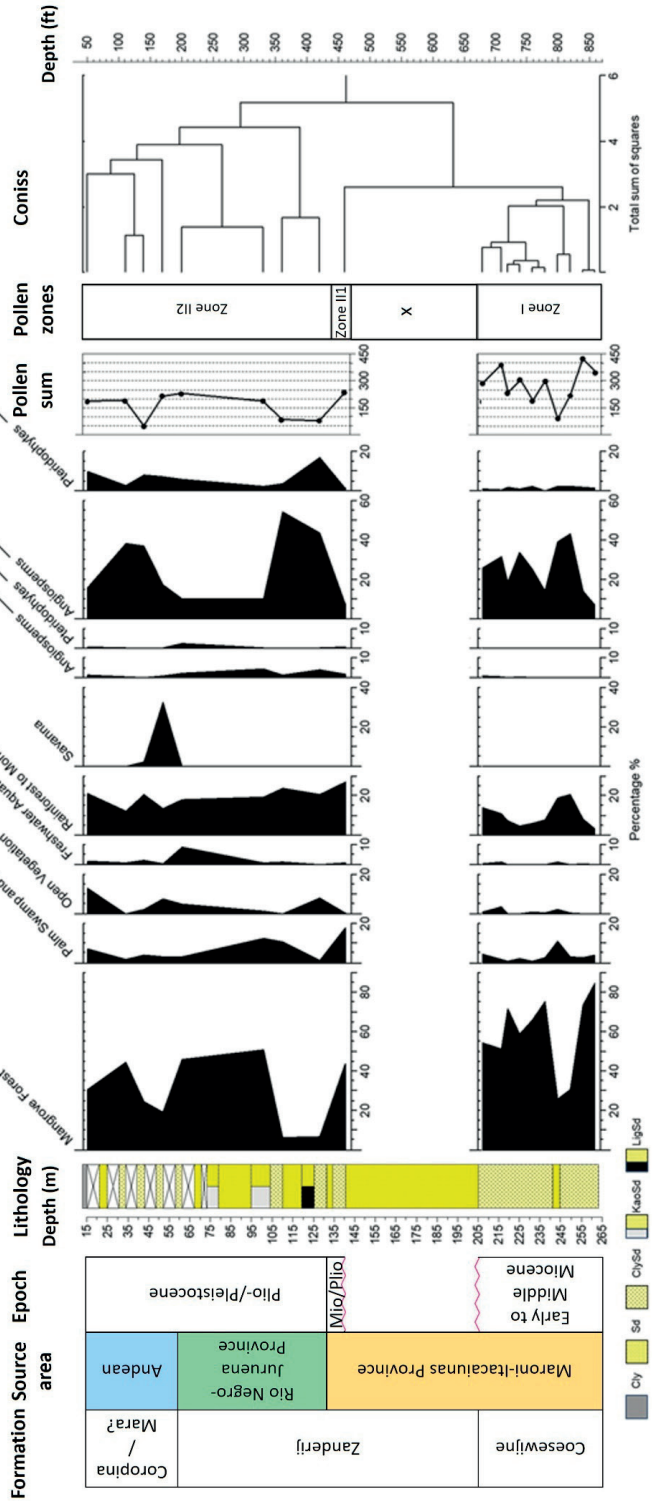


Figure 7: Summary palynological diagram for the Hepp-3 with biome representation and zonation. The cumulative diagram shows the main contrasting biomes including taxa with wide tropical distribution and unknown affinity. The CONISS dendrogram defines Zone I and Zone II (II-1. II-2).

4.2.3 Dinoflagellate Cysts: Occurrence and Implications

Sixteen samples were screened for dinoflagellate cysts. Preservation was generally poor, and nearly all residues were barren. Only one sample, at 232 mbsl, contained a small assemblage (*Polysphaeridium zoharyi*, *Systematophora placacantha*, *Spiniferites ramosus*). The widespread absence of dinocysts supports a dominantly non-marine to marginal marine depositional environment through most of the succession. Given the extremely low counts, no finer paleoenvironmental interpretation is possible.

5. DISCUSSION

Here we evaluate two research questions. First, we discuss how efficiently pollen, spores, and dinoflagellate cysts record coastal-inland ecosystem dynamics through time. We infer this by linking assemblage shifts to depositional context, using lithology as supporting evidence. Second, we exam the onset and evolution of Amazon-Andean influence along the Guiana margin by comparing the first appearances of Andean-affiliated pollen with the stepwise provenance changes. But before addressing these questions, the discussion begins by reviewing the chronological framework of the Hepp-3 succession.

5.1 AN ADJUSTED AGE MODEL FOR HEPP-3

Establishing an age model of the Hepp-3 is crucial for interpreting coastal evolution of and the arrival of Amazon influence at the Suriname coastline. The chronology is based on Maximum Likelihood ages and on correlation to the regional biostratigraphic zonations because absolute dates are unavailable. Maximum Likelihood ages provide a broad temporal window rather than sharp boundaries.

5.1.2 Limitations of the Maximum Likelihood Age Model in the Guiana Basin

The Maximum Likelihood model supplies useful temporal brackets but does not always track the Suriname zonation. Three factors explain the divergence. First, many Neotropical marker taxa are long-ranging and reappear after intervals of absence, which broadens likelihood peaks. Second, preservation and facies effects in ditch cuttings can truncate or extend apparent ranges. Oxidation and sandiness reduce counts, so the absence of a taxon may reflect taphonomy rather than time. Third, the algorithm treats each sample independently and does not use clusters of first and last occurrences that field stratigraphers rely on to fix boundaries. The maximum likelihood model is also based on the Andean Foreland (western South America), and does not apply to the Guianas. Therefore, geographical difference is significant, and should be considered in the results.

The Llanos reference set is invaluable for calibration but first and last occurrences can be diachronous between the Andean foreland and the Guiana margin (Hoorn et al., 2023; Jaramillo et al., 2011). Cross-checks with other schemes for northern South America provide context yet reveal the same problem of regional asynchrony (Germeraad et al., 1968; Regali, 1974; Muller, 1987; Hoorn et al., 2017; Gomes et al., 2023). Given these constrains, the Suriname zonation remains the primary interpretive frame, while probability ages serve as supportive context.

Uncertainty can be reduced with targeted steps. Denser sampling and higher counts across the succession would resolve clustered first and last appearances. A Suriname-specific reference set of calibrated ranges for key markers would improve model priors. One independent tie would anchor the section, for example a short magnetostratigraphic run, a detrital-zircon maximum deposit age, or a Sr-isotope age on any marine carbonate. Within the current dataset, the most robust practice is to weight ordered turnover and lithologic breaks over single-sample likelihood estimates when the two disagree.

5.1.3 Biostratigraphic zones

In the Hepp-3 well we consider the position of the RM8 marker as positioned in the mid Lower Miocene by Noorthoorn van der Kruyff (1970). The presence of the biostratigraphic marker species *Verrutricolporites rotundiporus* and *Psiladiporites minimus*, indicate an Early to Middle Miocene age is assigned to zone I, which corresponds with pollen Zones F of Guyana (Van der Hammen and Wijmstra, 1964) and E of Suriname Wijmstra (1971). The occurrence of marker species *Grimsdalea cf. magnaclavata* and *Fenestritus spinosus*, also corresponds with the Early to Middle Miocene of Venezuela and the Llanos and Llanos basin (Germeraad et al., 1968; Jaramillo et al., 2011). Furthermore, the biostratigraphical results of zone I correspond to the distinct lithological characteristics (Fig. 8) of the Coesewijne Formation (Dixon, 1972; Wong, 1989; Wong et al., 2016).

The LOD of *Retitricolporites (Rhoipites) guianensis* supports a Middle Miocene to Pliocene age for the lower part of zone II. This corresponds with the Zone F and G from Suriname (Wijmstra, 1971). The occurrence of other marker species such as *E. spinosus,* suggests a Middle Miocene to Pliocene (Zone PT-40 of the Amazon Fan from Regali et al., 1974), *E. barbetoi* suggests an Early Miocene to Pliocene (Zone IX of Northern South America from Muller et al., 1987), and *C. microclavatus* an Early Miocene age (Zone E of Suriname from Wijmstra, 1971) for the upper part of zone II-1. However, lithological characteristics (Fig. 8), sands more or less with interbedded clays (Dixon, 1979; Wong, 1989), point to the Zanderij Formation which was considered of Pliocene age by Wong (1989; 1992). Thus, results of palynology, lithostratigraphy, and the maximum likelihood model in zone II show conflicting patterns and create a dilemma, which can be solved with additional data from other nearshore (e.g. the Powisi-01) and offshore wells.

5.2 VEGETATION DEVELOPMENT ALONG THE SURINAME COAST

Within the chronological frame established above, the Hepp-3 palynological record traces how coastal and inland vegetation responded to changing shoreline position, hydrology, and climate through the Neogene. Mangrove belts expanded during transgressions and retreated during regressions, while floodplain swamps and hinterland forests repeatedly reoccupied newly exposed terrain (Fig. 8). The subsections below examine, first, the waxing and waning of mangroves and their role as indicators of shoreline dynamics, and then the structure floodplain and hinterland vegetation, including a brief savanna episode.

5.2.1 Mangrove Dynamics and Coastal Evolution

Mangroves were a dominant yet variable component of the Suriname coastal plain through the Neogene. Their abundance tracks alternating transgressive-regressive oscillations documented along the norther South American margin (Germeraad et al., 1968; Wijmstra, 1969, 1971). During highstands, mangrove belts advanced inland across low-lying terrain. During falls in sea level, they contracted and inland vegetation took their place. Pollen of *Zonocostites* (fossil Rhizophora) is abundant in these phases and is a well-known indicator of mangrove expansion, although high pollen production and dispersal can amplify its representation in nearshore settings (e.g. Muller, 1959, 1987; Noorthoorn van der Kruyff, 1970; Wymstra, 1971).

5.2.2 Floodplain vegetation, Hinterland Forests and Savanna Expansion

Beyond the intertidal belt, the Hepp-03 record documents a mosaic of freshwater marshes and palm swamps, lowland rainforest to montane forest, and a short episode of savanna. The composition of these communities reflects variations in river connectivity, hydrological standing water, and soil wetness, which tend to fluctuate with shoreline position.

Floodplain environments are most prominent when marine influence weakens. The assemblage is marked by *Mauritiidites* (aff. *Mauritia*), *Arecipites*, and *Cyperacidites*, which signal the presence of palm-dominated wetlands and open marsh habitats. Palm swamp abundance peaks near 140 mbsl at about 18% and remains present during phases with stronger fluvial connectivity. The assemblages resemble modern swamp forests just inland of the mangrove fringe, where *Mauritia* dominates the seasonally inundated zones (Muller, 1959). Elevated lignite and interbedded clays in these intervals support consistent waterlogging and accumulation of organic material.

A broad range of hinterland taxa includes *Heterocolpites*, *Polypodiisporites usmensis*, *Retitricolporites latus*, *Psilatricolporites cf. varius*, and *Ilexpollenites*, along with elements of Euphorbiaceae, Fabaceae, and Myrtaceae. This composition aligns with the descriptions of modern rainforest composition of Suriname (Lindeman, 1953). Arboreal pollen occurs throughout,

consistent with the "background rain" of inland taxa recorded in modern deltaic sediments and with repeated recolonization of floodplains following mangrove retreat (Muller, 1959).

Open environments are less dominant overall but become important during the final regressive phase. Near 51 mbsl Poaceae, Asteraceae, and *Borreria*-type pollen increase sharply to roughly 40% of the assemblage, while mangrove and rainforest elements decline. Oxidized yellow clays at these levels point to fluctuating water tables and better drainage. Classic woody-savanna indicators such as *Byrsonima* and *Curatella* are absent, which suggests a more herbaceous coastal savanna system, rather than tree-shrub-grass mosaics that are common farther inland in the Guianas and Orinoco Basin (Muller, 1959; Wymstra, 1971). The savanna signal is short-lived and gives way to renewed floodplain wetlands and mixed forest.

5.3 ONSET OF AMAZON INFLUENCE ON THE SURINAME COASTLINE

Within Zone I, rare grains assignable to Andean taxa appear at low abundance during an interval characterized by progressive mangrove retreat (238–204 mbsl). These occurrences coincide with a short pulse of marginal-marine influence (dinoflagellate cysts at 232 mbsl) and clay-rich, reducing facies, yet Sm-Nd provenance in the same stratigraphic interval remains firmly cratonic (Maroni–Itacaiúnas, MIP) (Tassinari & Macambira, 1999). The presence of *Diporites* (aff. *Trema*) and Scrophulariaceae (aff. *Castilleja*) are interpreted as the first hints of long-distance connectivity through the Amazon plume and boundary currents, not as onset in the strict sense. Because Hepp-3 material consists of ditch cuttings, limited downhole mixing may introduce younger palynomorphs into deeper samples. Isolated early grains are therefore treated as non-diagnostic and are not used to define onset.

Above the thick sand body, Zone II-1 records recurrent Andean-affiliated pollen alongside resurgent mangroves and peak palm-swamp development in waterlogged, pyrite-bearing clays. By the criterion adopted here, this is where Amazon-Andean influence begins in the Hepp-3 record. The connection strengthens from sporadic to persistent palynological evidence. The Sm-Nd signatures still reflect predominantly shield sources (transitioning toward Rio Negro–Juruena, RNJP) (Tassinari & Macambira, 1999; Wong, 1986), indicating that pollen leads provenance. In other words, long-distance sporomorphs may be able to reach the coast through plume-current system even when the detrital load is still shield-derived. This lead-lag is expected if the Amazon plume supplies episodic microfossil rain and fine organic matter widely across the Guianas, while the bulk clastic flux remains governed by local routing and shelf storage. Mudbanks migrating westward can serve as temporary reservoirs, buffering the detrital signal and delaying the local geochemical expression of Andean input (Anthony et al., 2010; Augustinus, 2004). Thus, the onset by pollen (II-1) and arrival

by mud (later) are not contradictory but reflect different transmission pathways through the source-to-sink system.

Above 131 mbsl, the coastal system reorganizes. Mangroves remain variable, freshwater wetlands persist in patches, and a brief savanna expansion marks the improved drainage near 52 mbsl. Against this ecological background, Sm-Nd values shift stepwise from older shield signatures (MIP) to younger shield inputs (RNJP) and ultimately juvenile sediment between 61 and 15 mbsl, requiring an Andean component in the detrital load. This is interpreted as the first local geochemical arrival of Andean-derived sediment at Hepp-03 (Tassinari & Macambira, 1999). In process terms, the palynological connection established in II-1 is now reinforced by provenance, i.e., the coastal plain is not only sensing Andean vegetation via microfossils but also receiving Andean mud. The richest Andean-type assemblage near 61 mbsl, which includes *Podocarpidites*, *Psilastephanocolporites* (aff. Meliaceae, *Cedrela*), *Clavainaperturites microclavatus* (*Hedyosmum*), and aff. Cyatheaceae, coincides with the interval where the geochemistry requires Andean detritus, yet the Andean pollen signal weakens toward the top of the section.

The two-stage arrival at Hepp-3, in the Pliocene and then Pleistocene, is consistent with the broader source-to-sink evolution of northern South America. Andean uplift and foreland subsidence increased erosion, reorganized drainage, and strengthened eastward export through the Neogene, while orographic barriers enhanced precipitation on the Andean flank and amplified sediment delivery to the foreland (Hoorn et al., 2010). Offshore archives record this transition: muds of the Amazon Fan show juvenile isotopic fingerprints that match an Andean provenance, and stratigraphic evidence places initiation and growth of the fan in the late Miocene (McDaniel et al., 1997; Figueiredo et al., 2009). Hoorn et al. (2017) link these offshore signals to plant-turnover evidence within the basin and emphasize that full trans-continental routing developed in stages. Their regional synthesis highlights the combined roles of mountain building, subsidence in Sub-Andean basins, and evolving topographic divides such as the Vaupés Swell and the Gurupá and Fitzcarrald arches, features that helped define pathways and barriers for eastward drainage during the Miocene and Pliocene. Within this framework, a palynological onset in the Plio-Pleistocene is a physically reasonable sequence for the Guiana margin.

5.4 COMBINING LITHO AND BIOSTRATIGRAPHY TO RESOLVE THE AGE MODEL

In the absence of absolute dating methods, the age of the consecutive sediment layers relies on the first and last occurrence unknown dates of biomarkers, the biostratigraphy, MLA, and geochemical analyses. In assessing the occurrence of Andean markers, the FOD and LOD are both relevant; however, with the use of cuttings, the LOD is more significant. The

absence of *Cicatricosisporites dorogensis*, a spore commonly found in the Caribbean and used as an indicator for the Middle Eocene–Oligocene, suggests that an Oligocene age for Zone I can be excluded. Therefore, Zone I is interpreted to postdate the Oligocene, and most likely corresponding to the Late Miocene or younger. Furthermore, the MLAs suggests an age of 17.53–17.18 Ma, pointing to a Early to Middle Miocene age of Zone I (262–204 mbsl). Earlier studies (Wong, 1986; Krook, 1979) proposed a Miocene age for the Coesewijne Formation and a Pliocene age for the Zanderij Formation.

The seismic Regional Marker 8 (RM8) of mid Lower Miocene age can be recognized over the entire coastal plain and is noticed at a depth of 216 and 201 mbsl in respectively the WA-1 and WA-2 wells (District of Nickerie), located near the Hepp-3 well (Noorthoorn vd Kruyff, 1970) (Fig.1 & 3). Given the geographical location of the wells discussed above, it can be deduced that the RM8 should appear at a comparable depth in the Hepp-3 well, placing it within Zone I. The presence of the RM8 correlates with the Early Miocene regression in our results, which is further supported by the decrease in presence of mangrove forest (Fig. 8). From this we can assume that the age of Zone I is of Early to Middle Miocene age. Since the barren interval was excluded from all analyses, its age remains uncertain.

Zone II is characterized by the occurrence of species such as *Psiladiporites minimus* corresponding to zone F and G of Suriname (Wijmstra, 1971) and Guyana (Van der Hammen & Wijmstra, 1964). Also in Zone II the absence of the typical Oligocene marker *C. dorogensis* and the rate of certainty (MLA) for the Zone I makes that we can exclude the Oligocene age. Still, the above mentioned makes it insufficient to draw conclusions based on only this. The MLA provides certainty for the lower part of the well (Zone I), but not for the upper part (Zone II), thus sedimentation rates cannot be inferred from these estimates alone. The MLA is also based on western Amazonia and not on the Guianas which increases the uncertainty. The remaining question is whether we can say something about the lithostratigraphy of the Hepp-3 well. Geochemical results show that the source of sediments from 262 to 61 mbsl (Zone I to II) is cratonic, and that the shift to Andean source becomes clear between 61 and 15 mbsl depth.

Mangrove forests serve as indicators of transgressive and regressive phases along the Suriname coast. High sea levels typically correspond to the presence of swamp and marsh vegetation, while low sea levels are marked by increased rainforest and montane forest cover. Biostratigraphic evidence from the Hepp-3 well reveals the continuous presence of mangrove vegetation throughout the core, with greater dominance in the lower interval (Zone I). In contrast, rainforest and montane forest elements, initially scarce in Zone I, become increasingly prevalent in the upper interval (Zone II), suggesting a shift towards regressive conditions.

Earlier studies (Wong et al., 2016; Krook, 1979) imply that deposits of the Zanderij Formation are of fluvial origin and occurred during a regression. The R1, an erosive surface dated from the Middle Miocene to Early Pliocene, has been identified in Demerara Rise sediments offshore Suriname, (Fanget et al., 2020). Clay-rich deposits from the same region point to the onset of Andean sediment influx during the Pliocene.

Regionally, a Miocene transgression is well-documented in the Barreiras Formation of northeastern Brazil, where sedimentological evidence supports a transition from lower quartz-feldspar wackes to upper sandstone and conglomerate facies (Dias et al., 2021). These deposits, sourced from eastern Brazil's hinterland, reflect a marine influence during the Miocene transgression, followed by fluvial conditions in the upper part of the sequence. Palaeomagnetic and palynological data date the Barreiras Formation from the Miocene to the Pliocene (Bezerra et al., 2001). When correlating these findings with regional stratigraphy, this suggests that deposition of the Zanderij Formation likely started during the Middle to Late Miocene, continuing into the Pliocene. During the Pliocene, sand supply from the hinterland was so much that mudbanks did not develop properly. In the subsequent Pleistocene period an increased amount of Amazon sediment is noticed, resulting in the actual coastal development.

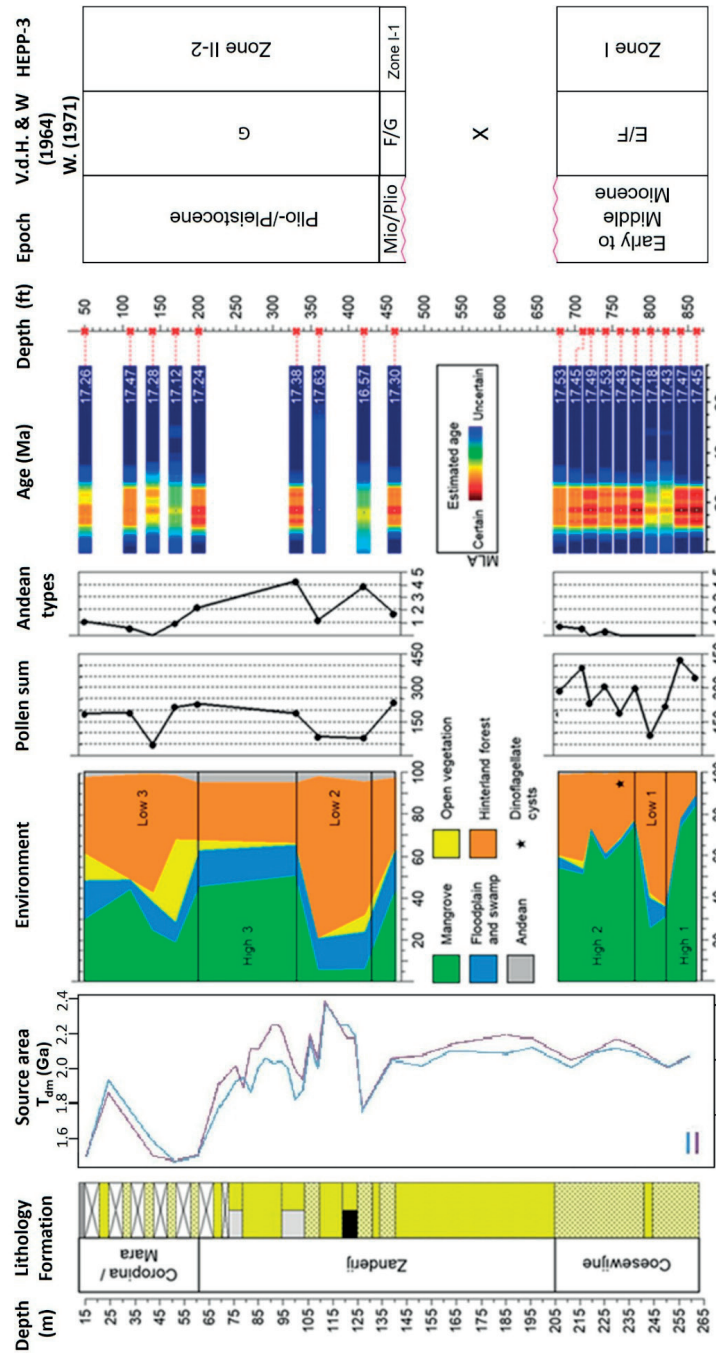


Figure 8: Summary of provenance, palynology, and chronology for the Hepp-3 well. From left to right the diagram shows: ƐNd(0) and TDM as sediment-provenance; relative abundance of most relevant plant groups – mangrove; floodplain (palm swamp, freshwater aquatics, and other pteridophytes); open vegetation (open and savanna); hinterland forests (rainforest, montane forest, and other angiosperms); Andean-affiliated types; counts of total palynomorphs and of Andean types; the presence of dinoflagellate cysts (star symbol); and maximum-likelihood age estimates with their uncertainty intervals. The palynological zonation as explained in the text, and further details can be found in the complete palynological diagram in Figure 7.

6. CONCLUSIONS

This study was set out to determine when and how Amazon influence first reached the Suriname coastline, and how that influence is recorded in vegetation and depositional history. By combining samarium–neodymium provenance data with palynology from the Hepp-3 borehole, it reconstructs both source areas and ecological change across the Miocene to Plio-/Pleistocene.

The isotopic record shows a clear stepwise evolution in sediment sources. The lower part of the section is dominated by sediment derived from the Maroni–Itacaiúnas Province. In the upper section the signal shifts toward the Rio Negro–Juruena Province, and in the uppermost interval a juvenile component appears that requires an Andean contribution. This trajectory is consistent with Neogene drainage reorganization across northern South America and indicates that significant Andean detritus only became part of the Suriname coastal load after the late Miocene.

The palynological record adds earlier and finer detail. Mangroves, palm-swamp and freshwater floodplain communities, and inland rainforest alternate through the section, tracking shifts between brackish and fluvial conditions. Crucially, Andean-affiliated pollen becomes persistent above the mid-section sand body, before the isotopic evidence for Andean detritus appears. This diachrony implies that microfossils were transported over long distances in low concentrations and trapped on the coastal plain while bulk siliciclastic delivery still reflected local cratonic sources. Using both proxies together therefore resolves processes and timings that either proxy alone would miss.

Together, the lines of evidence refine the timeline of Amazon influence at the Guianas' coastal margin. Offshore stratigraphy records growth of the Amazon Fan from the late Miocene onward. The Hepp-3 shows that the Suriname coast first sensed this connection as a biological signal in the Middle Miocene, followed later by a detrital shift in the Late Miocene to Pliocene. The record therefore captures an onset and a reinforcement phase, and it reveals how coastal wetlands and floodplains acted as sensitive archives of regional sediment routing and sea-level change.

The findings have broader significance. They demonstrate that integrating palynology with Sm-Nd provenance links onshore vegetation archives to continental source-to-sink pathways and offshore fan development. They also highlight the role of mangroves and floodplain wetlands as dynamic systems that respond to changes in sediment supply, accommodation, and salinity. The short savanna episode in Zone II shows that brief environmental oscillations can reorganize Neotropical coastal vegetation.

Several steps would strengthen and extend these conclusions. Independent age control, for example magnetostratigraphy or radiometric ties, would narrow the temporal window of key turnovers. Denser sampling and higher palynomorph counts across the 140–131 mbsl interval would test persistence thresholds for the first Amazon signal. A transect of additional onshore boreholes along the Guianas' coastal margin would separate local from regional effects. Finally, continuous deep-sea drilling on the adjacent margin would provide an uninterrupted archive without subaerial weathering or hiatus, allowing direct coupling of coastal records with slope and fan stratigraphy.

In sum, the Suriname coastal plain records both the timing and the character of Amazon influence. The Hepp-3 captures both a Plio-Pleistocene palynological onset and detrital reinforcement, and subsequent modulation by sea-level and coastal dynamics. These results clarify how Andean uplift, drainage integration, and oceanic transport combined to shape one of the world's largest muddy coasts.

ACKNOWLEDGEMENTS

We thank the Suriname Conservation Foundation (SCF) for sponsoring this research, and are deeply grateful to the Suriname Water Company (SWM N.V.) for making the sediment samples available. Also a special thanks to the Geochronology and Isotope Geochemistry Laboratory (University of Brasília). For the dinoflagellate work we like to thank Nico Janssen for preparing, analyzing, and discussing the residues. The maximum-likelihood age estimates benefited greatly from the expertise of Diana Ochoa, who advised on the approach and provided R code used in this study.

Finally, we thank all other individuals that contributed to make this research possible.

REFERENCES

Anthony, E. J., Gardel, A., Gratiot, N., Proisy, C., Allison, M. A., Dolique, F., & Fromard, F. (2010). The Amazon-influenced muddy coast of South America: A review of mud-bank–shoreline interactions. *Earth-Science Reviews*, *103*(3), 99-121. https://doi.org/10.1016/j.earscirev.2010.09.008

Augustinus, P. G. E. F. (2004). The influence of the trade winds on the coastal development of the Guianas at various scale levels: A synthesis. *Marine Geology*, *208*(2), 145-151. https://doi.org/10.1016/j.margeo.2004.04.007

Bezerra, F.H.R. Amaro, V.E., Vita-Finzi, C., Saadi, A. (2001). Pliocene-Quaternary fault control of sedimentation and coastal plain morphology in NE Brazil. Journal of South American Earth Sciences, 14 (1), 61–75.

Bolli, H. M. (1966). Zonation of cretaceous to pliocene marine sediments based on planktonic foraminifera; zonacion de sedimentos marinos del cretaceo hasta el plioceno basada en foraminiferos planctonicos.Boschman, L. M. (2021). Andean mountain building since the Late Cretaceous: A paleoelevation reconstruction. *Earth-Science Reviews*, *220*, 103640. https://doi.org/10.1016/j.earscirev.2021.103640

Brinkman, R., Pons, L.J. (1968). A pedo-geomorphological classification and map of the Holocene sediments in the coastal plain of the three Guianas. Soil Survey Papers 4. Soil Survey Insitute Wageningen, 40 pp.

D'Apolito, C., Jaramillo, C., & Herrington, G. (2021). Miocene Palynology of the Solimões Formation (Well 1-AS-105-AM), Western Brazilian Amazonia. *Smithsonian Contributions to Paleobiology*, iv-134. https://doi.org/10.5479/si.16803493

Dengler, M., Schott, F. A., Eden, C., Brandt, P., Fischer, J., & Zantopp, R. J. (2004). Break-up of the Atlantic deep western boundary current into eddies at 8° S. *Nature*, *432*(7020), 1018-1020. https://doi.org/10.1038/nature03134

Dias, A.N.C., Guadagnin, F., Rangel, C.V.G.T., Chemale Jr., F., Oliveira, T.R.P., Moura, C.A., Pereira, V.Q., Alves, J.S.E. (2021). Provenance of Neogene deposits of Barreiras Formation in the southeastern Brazilian continental margin, International Journal of Earth Sciences, 110, 233–249.

Dixon, V.R. (1972). Public water suppliesand sewerage, Suriname draft, III: Hydrogeological and hydrological investigation UNDP/SF. PAHO/WHO/UN project, Paramaribo, 128 pp.

Eisma, D., & van der Marel, H. W. (1971) "Marine muds along the Guyana coast and their origin from the Amazon basin," Contrib. Mineral. Petrol. 31, 321–334.

Eisma, D., Augustinus, P. G. E. F., & Alexander, C. (1991). Recent and subrecent changes in the dispersal of Amazon mud. *Netherlands Journal of Sea Research*, *28*(3), 181-192. https://doi.org/10.1016/0077-7579(91)90016-T

Fanget, A., Loncke, L., Pattier, F., Marsset. T, Roest, W.R., Tallobre, C., Durrieu de Madron, X., F. Hernández-Molina, J. (2020). A synthesis of the sedimentary evolution of the Demerara Plateau (Central Atlantic Ocean) from the late Albian to the Holocene. Marine and Petroleum Geology, 114 (104195). https://doi.org/10.1016/j.marpetgeo.2019.104195

Figueiredo, J., Hoorn, C., van der Ven, P., & Soares, E. (2009). Late Miocene onset of the Amazon River and the Amazon deep-sea fan: Evidence from the Foz do Amazonas Basin. *Geology*, *37*(7), 619-622. https://doi.org/10.1130/G25567A.1

Fraga, L. M., Cordani, U., Maria Dreher, A., Sato, K., Joaquim Reis, N., Nadeau, S., De Roever, E., Kroonenberg, S., & Camara Maurer, V. (2024). Early Orosirian belts of the central Guiana Shield, northern Amazonian Craton: U-Pb geochronology and tectonic implications. *Precambrian Research*, *407*, 107362. https://doi.org/10.1016/j.precamres.2024.107362

Germeraad, J. H., Hopping, C. A., & Muller, J. (1968). Palynology of tertiary sediments from tropical areas. *Review of Palaeobotany and Palynology*, *6*(3), 189-348. https://doi.org/10.1016/0034-6667(68)90051-1

Green, W. A., Jaramillo, C., & de la Parra, F. (2012). stratigraph: Toolkit for the plotting and analysis of stratigraphic and palaeontological data. See http://cran. r-project. 0rg/web/package5/stratigraph/index. html.

Gomes, B. T., Aguilera, O., da Silva-Caminha, S. A. F., D'Apolito, C., Cárdenas, D., Hocking, E. P., & Lemes, K. K. B. (2023). Biostratigraphy and Paleoenvironments of the Pirabas Formation (Neogene, Pará State-Brazil). *Marine Micropaleontology*, *180*, 102218. https://doi.org/10.1016/j.marmicro.2023.102218

Hoorn, C., Bogotá-A, G. R., Romero-Baez, M., Lammertsma, E. I., Flantua, S. G. A., Dantas, E. L., Dino, R., do Carmo, D. A., & Chemale, F. (2017). The Amazon at sea: Onset and stages of the Amazon River from a marine record, with special reference to Neogene plant turnover in the drainage basin. *Global and Planetary Change*, *153*, 51-65. https://doi.org/10.1016/j.gloplacha.2017.02.005

Hoorn, C., Lohmann, L. G., Boschman, L. M., & Condamine, F. L. (2023). Neogene History of the Amazonian Flora: A Perspective Based on Geological, Palynological, and Molecular Phylogenetic Data. *Annual Review of Earth and Planetary Sciences*, *51*(Volume 51, 2023), 419-446. https://doi.org/10.1146/annurev-earth-081522-090454

Hoorn, C., Wesselingh, F. P., ter Steege, H., Bermudez, M. A., Mora, A., Sevink, J., Sanmartín, I., Sanchez-Meseguer, A., Anderson, C. L., Figueiredo, J. P., Jaramillo, C., Riff, D., Negri, F. R., Hooghiemstra, H., Lundberg, J., Stadler, T., Särkinen, T., & Antonelli, A. (2010). Amazonia Through Time: Andean Uplift, Climate Change, Landscape Evolution, and Biodiversity. *Science*, *330*(6006), 927-931. https://doi.org/10.1126/science.1194585

Jaramillo, C. A., Rueda, M., & Torres, V. (2011). A palynological zonation for the Cenozoic of the Llanos and Llanos Foothills of Colombia. *Palynology*, *35*(1), 46-84. https://doi.org/10.1080/01916122.2010.515069

Jaramillo, C. and Rueda, M. (2024) A Morphological Electronic Database of Cretaceous-Cenozoic Fossil Pollen and Spores from Northern South America and Extant Pollen and Spores V.24. http://biogeodb.stri.si.edu/jaramillosdb/web/morphological/

Krook, L. (1979). Sediment petrographical studies in northern Surinam. Thesis, Free University Amsterdam, 154 pp.

Krook, L. (1984). Geologische Mijnbouwkundige Dienst Suriname, Mededeling 28, pp. 103, 106–107.

Kroonenberg, S. (2025). Introduction. In S. Kroonenberg (Red.), *The Changing Framework of the Guiana Shield* (pp. 1-7). Springer Nature Switzerland. https://doi.org/10.1007/978-3-031-86334-9_1

Lindeman, J.C. (1953). The vegetation of the coastal region of Surinam. Thesis Utrecht. Kemink en Zonen, Utrecht, 1953.

Lorente MA. 1986.. Palynology and palynofacies of the Upper Tertiary in Venezuela. . PhD Thesis, Univ. Amsterdam

Lyell, C. (1832) Principles of Geology. (Quoted via Reyne, 1961).

Mabberley, D. J. (1987). *The Plant-Book: A portable dictionary of the higher plants* (First). Cambridge University Press.

Marchant, R., Almeida, L., Behling, H., Carlos Berrio, J., Bush, M., Cleef, A., Duivenvoorden, J., Kappelle, M., De Oliveira, P., Teixeira De Oliveira-Filho, A., Lozano-Garc ¤ia, S., Hooghiemstra, H., Ledru, M.-P., Ludlow-Wiechers, B., Markgraf, V., Mancini, V., Paez, M., Prieto, A., Rangel, O., & Salgado-Labouriau, M. L. (2002). Distribution and ecology of parent taxa of pollen lodged within the Latin American Pollen Database. In *Review of Palaeobotany and Palynology* (Vol. 121). https://doi.org/https://doi.org/1016/S0034-6667(02)00082-9

McDaniel, D. K., McLennan, S. M., & Hanson, G. N. (1997). Provenance of Amazon Fan Muds: Constraints from Nd and Pb Isotopes. In *Proceedings of the Ocean Drilling Program, Scientific Results*.

Mente, A., 1989: Mission report of a groundwater source in coastal northwest suriname (Nickerie area)

Molleri, G. S. F., Novo, E. M. L. de M., & Kampel, M. (2010). Space-time variability of the Amazon River plume based on satellite ocean color. *Continental Shelf Research*, *30*(3), 342-352. https://doi.org/10.1016/j.csr.2009.11.015

Muller, J. (1959). Palynology of Recent Orinoco delta and shelf sediments; reports of the Orinoco shelf expedition, volume 5. *Micropaleontology*, *5*(1), 1-32.

Muller, J., Di Giacomo, E., & Van Erve, A. (1987). A palynologic zonation for the Cretaceous, Tertiary and Quaternary of northern South America. In *American Association of Stratigraphic Palynologists Contribution Series 19* (pp. 7–76).

Nittrouer, C. A., & DeMaster, D. J. (1996). The Amazon shelf setting: Tropical, energetic, and influenced by a large river. *Continental Shelf Research*, *16*(5), 553-573. https://doi.org/10.1016/0278-4343(95)00069-0

Punyasena, S. W., Jaramillo, C., De La Parra, F., & Du, Y. (2012). Probabilistic correlation of single stratigraphic samples: A generalized approach for biostratigraphic data. *AAPG Bulletin*, *96*(2), 235-244. https://doi.org/10.1306/06201111026

R Development Core Team, 2009. R: A Language and Environment for Statistical Computing. Version 2.10.1, ISBN 3-900051-07-0. http://www.R-project.org.

Regali, M., Uesugui, N., & Santos, A. (1974). Palinologia dos sedimentos Meso-Cenozoico do Brasil. *Boletin Tecnico Da Petrobras 17*, 177–191.

Reyne, A. (1961) "On the contribution of the Amazon River to accretion of the coast of the Guianas," Geologie en Mijnbouw 40(6): 219–236. (See pp. 221–226 for observations; p. 232 for Lyell citation).

Roddaz et al., (submitted). Neogene paleo-drainage divide in Western Amazonia (Madre de Dios Basin, Peru): provenance evidences and implications.

Roeleveld, W. (1969). Pollenanalysis of two sections in the Young Coastal Plain of Surinam. Geologie en Mijnbouw 48: 215–224.

Smith, W. O., & Demaster, D. J. (1996). Phytoplankton biomass and productivity in the Amazon River plume: Correlation with seasonal river discharge. *Continental Shelf Research*, *16*(3), 291-319. https://doi.org/10.1016/0278-4343(95)00007-N

Tassinari, C., & Macambira, M. (1999). Geochronological provinces of the Amazonian Craton. *Episodes*, *22*, 174-182. https://doi.org/10.18814/epiiugs/1999/v22i3/004

Val, P., Figueiredo, J., de Melo, G., Flantua, S. G. A., Quesada, C. A., Fan, Y., Albert, J. S., Guayasamin, J. M., & Hoorn, C. (2021). Chapter 1: Geology and geodiversity of the Amazon: Three billion years of history. In *ResearchGate*. https://doi.org/10.55161/POFE6241

Van der Hammen, T., & Wymstra, T. A. (1964). A palynological study on the Tertiary and Upper Cretaceous of British Guiana. *Leidse Geologische Mededelingen*, *30*(1), 183-241.

Vernal, A. de, Henry, M., Matthiessen, J., Mudie, P. J., Rochon, A., Boessenkool, K. P., Eynaud, F., GrØsfjeld, K., Guiot, J., Hamel, D., Harland, R., Head, M. J., Kunz-Pirrung, M., Levac, E., Loucheur, V., Peyron, O., Pospelova, V., Radi, T., Turon, J.-L., & Voronina, E. (2001). Dinoflagellate cyst assemblages as tracers of sea-surface conditions in the northern North Atlantic, Arctic and sub-Arctic seas: The new 'n = 677' data base and its application for quantitative palaeoceanographic reconstruction. *Journal of Quaternary Science*, *16*(7), 681-698. https://doi.org/10.1002/jqs.659

Wong, T. E. (1986). *Outline of the stratigraphy and the geological history of the Suriname coastal plain*.

Wong, T.E. (1987). Revision of the stratigraphy of Suriname. *Natuurwetenschappelijke Studiekring Voor Suriname En de Nederlandse Antillen (Publications of the Foundation for Scientific Research in Surinam and the Netherlands Antilles*, *125*, 1–64.

Wong, Th. E., de Kramer, R., de Boer, P. L., Langereis, C., & Sew-A-Tjon, J. (2009). The influence of sea-level changes on tropical coastal lowlands; the Pleistocene Coropina Formation, Suriname. *Sedimentary Geology*, *216*(3), 125-137. https://doi.org/10.1016/j.sedgeo.2009.02.003

Wong, T. E., Kroonenberg, S. B., & Augustinus, P. G. E. F. (2017). Geologie en landschap van Suriname. LM publishers.

Wijmstra, T. A. (1971). *The palynology of the Guiana Coastal Basin*. Thesis Universiteit van Amsterdam, Drukkerij de Kempenaer, 71 pp.

Appendix A: Detailed lithology of the Hepp-3 well (Nickerie)

Formation	Source area	Zone	Depth (ft)	Depth (m)	Lithology	Quartz Sand																						Clay			Lignite									Pyrite	Oil
						Color										Shape	Grain size						Sorting	Color			Color														
						White	Grey	Minor-white	Creme	Pink	Yellow	Orange	Brown	Black (or blue)		Subangular to Subrounded	Very-fine	Fine	Medium	Coarse	Very-Coarse	Granulated		Grey	White (sacc)	Yellow	Black	Brown	Flat	Blocky	Oval	Round	Elongate	Subetrogate	Aggregate	Shell fragments Marcasite Limonate matrix		
			50	15	Cly																			94% firm-sft		2% sft										Shl-frag	No fl.
Corsoina/ Mara?	Andean		80	24	Sd	wh	gy	miwh							sbang-sbrnd		x	x	x	o		Moderate	1% sft		3% sft	1% sft	blk	brn	flat					agg	Fe-ox	No fl.
			110	34	CySd	wh	gy	miwh							sbang-sbrnd	x	x	o				well	3% sft		45% sft	2% sft	blk	brn	flat					agg	Fe-ox, shl-frag	No fl.
			140	43	CySd	wh	gy	miwh							sbang-sbrnd	x	x	o				well	40% sft		3% sft	3% sft	blk	brn	flat					agg	Fe-ox	No fl.
			170	52	CySd	wh	gy	miwh							sbang-sbrnd	x	x					well	40% sft		2% sft	2% sft	blk	brn	flat					agg	Fe-ox	No fl.
			200	61	CySd	wh	gy	miwh			yel	orng			sbang-sbrnd		x	x	o			well	40% sft		3% sft	4% sft	blk	brn	flat					agg	Shl-frag	No fl.
			230	70	Sd	wh	gy	miwh		pk	yel	orng			sbang-sbrnd		x	x	x	o		Moderate	3% sft			2% sft	blk	brn	flat					agg	Fe-ox	No fl.
			250	76	Kaosd	wh	gy	miwh				orng			sbang-sbrnd		x	x	x			Moderate	1% sft		30% sft	4% sft	blk	brn	flat					agg	Fe-ox	No fl.
			260	79	Kaosd	wh	gy	miwh				orng			sbang-sbrnd		x	x	x			Moderate	1% sft		30% sft	5% sft	blk	brn	flat	blky		elg	slelg	agg	tr.	No fl.
			270	82	Sd	wh	gy	miwh			yel		brn	bl	sbang-sbrnd		x	x	x	o		Moderate	1% sft		2% sft	1% sft	blk	brn	flat					agg	2%	No fl.
			280	85	Sd	wh	gy	miwh			yel			bl	sbang-sbrnd		x	x	x	x		poor	1% sft		3% sft	1% sft	blk	brn	flat					agg	1% marc, lim-mat	No fl.
			290	88	Sd	wh	gy	miwh			yel		brn		sbang-sbrnd		x	x	x	o		Moderate	1% sft		1% sft	1% sft	blk	brn	flat					agg	tr.	No fl.
			300	91	Sd	wh	gy	miwh			yel		brn		sbang-sbrnd			x	x	x		Moderate	1% sft		1% sft	tr. sft	blk							agg	1%	No fl.
			310	94	Sd	wh	gy	miwh			yel	orng	brn	bl	sbang-sbrnd		x	x	x	x		poor	1% sft		1% sft	1% sft	blk		flat					agg	tr.	No fl.
			320	98	Kaosd	wh	gy	miwh				orng		bl	sbang-sbrnd		x	x	x	x		poor	4% sft		26% sft	tr. sft	blk							agg	tr.	No fl.
			330	101	Kaosd	wh	gy	miwh				orng		bl	sbang-sbrnd		x	x	x	x		poor	8% sft		24% sft	2% sft	blk		flat					agg	1% marc	No fl.
			340	104	Kaosd	wh	gy	miwh				orng		bl	sbang-sbrnd		x	x	x			Moderate	7% sft		23% sft	2% sft	blk		flat	blky				agg	1% marc	No fl.
			350	107	CySd	wh	gy	miwh				orng		bl	sbang-sbrnd		x	x	x	x	o	poor	6% sft		4% sft	1% sft	blk		flat					agg	1% sid	No fl.
			360	110	CySd	wh	gy	miwh				orng		bl	sbang-sbrnd		x	x	x	x		poor	5% sft		4% sft	1% sft	blk		flat					agg	1% sid, chl-mat	No fl.
			370	113	Sd	wh	gy	miwh				orng		bl	sbang-sbrnd		x	x	x			well	1% sft		1% sft	tr. sft	blk							agg	tr. Fe-ox	No fl.
			380	116	Sd	wh	gy	miwh				orng		bl	sbang-sbrnd			x	x	o		well	3% sft		1% sft	2% sft	blk		flat					agg	1% fe-ox	No fl.
			390	119	Sd	wh	gy	miwh				orng		bl	sbang-sbrnd			x	x	x		Moderate	2% sft		1% sft	tr. sft	blk							agg	1%	No fl.
			400	122	LigSd	wh	gy	miwh				orng		bl	sbang-sbrnd				x	x	x	Moderate	3% sft		1% sft	12% sft	blk		flat	blky	oval	rod		agg	1%	No fl.
			410	125	LigSd	wh	gy	miwh				orng		bl	sbang-sbrnd				x	x	x	Moderate	3% sft		1% sft	7% sft	blk		flat	blky	oval	rod		agg	1%	No fl.
			420	128	CySd	wh	gy	miwh				orng		bl	sbang-sbrnd		x	x	x	x		poor	29% sft		3% sft	3% sft	blk		flat	blky	oval	rod		agg	1%	No fl.
			430	131	CySd	wh	gy	miwh				orng		bl	sbang-sbrnd		x	x	x	x	o	poor	28% sft		3% sft	5% sft	blk		flat	blky	oval	rod		agg	1% shl-frag	No fl.
Zanderij	Maroni-Itacaiunas Province		440	134	Sd	wh	gy	miwh				orng		bl	sbang-sbrnd				x	x	x	Moderate	3% sft		1% sft	4% sft	blk		flat	blky	oval	rod		agg	1%	No fl.
			450	137	CySd	wh	gy	miwh				orng		bl	sbang-sbrnd		x		x	x	x	o	Moderate	8% sft		3% sft	4% sft	blk		flat	blky	oval			agg	2% shl-mat	No fl.
			460	140	CySd	wh	gy	miwh				orng		bl	sbang-sbrnd				x	x	x	o	Moderate	6% sft		3% sft	5% sft	blk		flat	blky	oval			agg	2%	No fl.
			470	143	Sd	wh	gy	miwh				orng		bl	sbang-sbrnd				x	x	x	x	poor	3% sft		1% sft	3% sft	blk		flat	blky	oval			agg	2%	No fl.
			480	146	Sd	wh	gy	miwh				orng		bl	sbang-sbrnd				x	x	x		Moderate	1% sft		1% sft	2% sft	blk		flat	blky	oval			agg	1%	No fl.
			490	149	Sd	wh	gy	miwh				orng		bl	sbang-sbrnd				x	x	x	x	poor	3% sft		1% sft	3% sft	blk		flat	blky				agg	2% chl-mat	No fl.
			500	152	Sd	wh	gy	miwh				orng		bl	sbang-sbrnd				x	x	x	x	poor	3% sft		1% sft	2% sft	blk		flat	blky				agg	1%	No fl.
			510	155	Sd	wh	gy	miwh				orng		bl	sbang-sbrnd				x	x	x	x	poor	2% sft		1% sft	1% sft	blk	brn	flat					agg	1%	No fl.
			520	158	Sd	wh	gy	miwh				orng		bl	sbang-sbrnd				x	x	x	o	Moderate	1% sft		1% sft	1% sft	blk		flat					agg	1%	No fl.
			530	162	Sd	wh	gy	miwh	crm			orng		bl	sbang-sbrnd					x	x	x	Moderate	2% sft		1% sft	tr. sft	blk	brn						agg	1%	No fl.
			540	165	Sd	wh	gy	miwh	crm	pk		orng			sbang-sbrnd				x	x	x		Moderate	2% sft		1% sft	tr. sft	blk	brn		blky				agg	1%	No fl.
			550	168	Sd	wh	gy	miwh			yel	orng			sbang-sbrnd				x	x	x		Moderate	2% sft		1% sft	tr. sft	blk	brn						agg	1%	No fl.
			560	171	Sd	wh	gy	miwh			yel	orng			sbang-sbrnd				x	x	x	o	Moderate	2% sft		1% sft	tr. sft	blk	brn						agg	1%	No fl.
			570	174	Sd	wh	gy	miwh			yel	orng			sbang-sbrnd				x	x	x	o	Moderate	2% sft		1% sft	tr. sft	blk	brn						agg	1%	No fl.
			580	177	Sd	wh	gy	miwh			yel	orng			sbang-sbrnd				x	x	x	o	Moderate	1% sft		2% sft	2% sft	blk	brn	flat					agg	1%	No fl.
			590	180	Sd	wh	gy	miwh			yel	orng			sbang-sbrnd				x	x	x	o	Moderate	1% sft		2% sft	2% sft	blk	brn	flat					agg	1%	No fl.
			600	183	Sd	wh	gy	miwh			yel	orng			sbang-sbrnd				x	x	x	o	Moderate	1% sft		1% sft	1% sft	blk	brn						agg	1%	No fl.
			610	186	Sd	wh	gy	miwh			yel	orng			sbang-sbrnd				x	x	x		Moderate	1% sft		1% sft	1% sft	blk	brn						agg	1%	No fl.
			620	189	Sd	wh	gy	miwh			yel	orng			sbang-sbrnd				x	x	x		Moderate	1% sft		1% sft	2% sft	blk	brn						agg	1%	No fl.
			630	192	Sd	wh	gy	miwh			yel	orng			sbang-sbrnd				x	x	x	o	Moderate	1% sft		1% sft	2% sft	blk	brn						agg	1%	No fl.
			640	195	Sd	wh	gy	miwh			yel	orng			sbang-sbrnd				x	x	x	o	Moderate	1% sft		2% sft	1% sft	blk	brn	flat					agg	1%	No fl.
			650	198	Sd	wh	gy	miwh			yel	orng			sbang-sbrnd				x	x	x		Moderate	1% sft		2% sft	1% sft	blk	brn						agg	1%	No fl.
			660	201	Sd	wh	gy	miwh			yel	orng			sbang-sbrnd				x	x	x		Moderate	1% sft		2% sft	1% sft	blk	brn						agg	1% fe-ox	No fl.
			670	204	Sd	wh	gy	miwh			yel	orng			sbang-sbrnd				x	x	x		Moderate	1% sft		2% sft	tr. sft	blk	brn						agg	1%	No fl.
			680	207	CySd	wh	gy	miwh				orng			sbang-sbrnd				x	x	x	o	Moderate	30% sft		2% sft	1% sft	blk	brn	flat					agg	tr. fe-ox	No fl.
			690	210	CySd	wh	gy	miwh				orng			sbang-sbrnd				x	x	x	o	Moderate	30% sft		2% sft	1% sft	blk	brn						agg	tr. fe-ox	No fl.
			700	213	CySd	wh	gy	miwh				orng		bl	sbang-sbrnd				x	x	x	x	poor	40% sft		1% sft	1% sft	blk	brn						agg	tr.	No fl.
			710	216	CySd	wh	gy	miwh				orng		bl	sbang-sbrnd	x	x	x	x	x	o	poor	37% sft		2% sft	4% sft	blk	brn	flat	blky				agg	2%	No fl.
			720	219	CySd	wh	gy	miwh				orng		bl	sbang-sbrnd	x	x	x	x	x	x	poor	38% sft		4% sft	tr. sft	blk	brn	flat	blky				agg	2%	No fl.
			730	223	CySd	wh	gy	miwh				orng		bl	sbang-sbrnd				x	x	x	x	poor	17% sft		2% sft	4% sft	blk	brn	flat	blky				agg	1%	No fl.
			740	226	CySd	wh	gy	miwh				orng		bl	sbang-sbrnd				x	x	x	x	poor	34% sft		3% sft	3% sft	blk	brn	flat	blky				agg	1%	No fl.
			750	229	CySd	wh	gy	miwh				orng		bl	sbang-sbrnd				x	x	x	o	Moderate	43% sft		2% sft	3% sft	blk		flat					agg	1%	No fl.
			760	232	CySd	wh	gy	miwh				orng		bl	sbang-sbrnd	x	x	x	x	x	o	poor	36% sft-firm		2% sft	4% sft	blk		flat	blky				agg	1%	No fl.
			770	235	CySd	wh	gy	miwh				orng		bl	sbang-sbrnd				x	x	x	o	poor	20% sft-firm		2% sft	2% sft	blk	brn	flat	blky				agg	1%	No fl.
			780	238	CySd	wh	gy	miwh				orng		bl	sbang-sbrnd				x	x	x	o	poor	25% sft-firm		4% sft	2% sft	blk	brn	flat	blky				agg	1%	No fl.
			790	241	CySd	wh	gy	miwh				orng		bl	sbang-sbrnd	x	x	x	x	x	o		Moderate	5% sft		2% sft	3% sft	blk	brn	flat	blky				agg	1%	No fl.
			800	244	Sd	wh	gy	miwh				orng		bl	sbang-sbrnd	x	x	x	x	x	x		poor	3% sft		1% sft	3% sft	blk	brn	flat	blky				agg	1% shl-frag, lim-mat	No fl.
			810	247	CySd	wh	gy	miwh				orng		bl	sbang-sbrnd	x	x	x	x	x	o	poor	9% sft		2% sft	3% sft	blk	brn	flat	blky				agg	1%	No fl.
			820	250	CySd	wh	gy	miwh				orng		bl	sbang-sbrnd	x	x	x	x	x	x		poor	9% sft		1% sft	2% sft	blk	brn	flat	blky				agg	1%	No fl.
			830	253	CySd	wh	gy	miwh				orng		bl	sbang-sbrnd	x	x	x	x	x	x		poor	17% sft-firm		2% sft	2% sft	blk		flat	blky				agg	1%	No fl.
			840	256	CySd	wh	gy	miwh				orng		bl	sbang-sbrnd				x	x	x	x	poor	15% sft-firm		1% sft	2% sft	blk		flat	blky				agg	1% fe-ox	No fl.
			850	259	CySd	wh	gy	miwh				orng		bl	sbang-sbrnd				x	x	x	x	poor	9% sft-firm		1% sft	2% sft	blk		flat	blky				agg	1% lim-mat, shl-frag	No fl.
			860	262	CySd	wh	gy	miwh				orng		bl	sbang-sbrnd				x	x	x	x	poor	12% sft-firm		2% sft	2% sft	blk		flat					agg	2% fe-ox	No fl.

Appendix B: Maximum Likelihood Age - estimates dataset

Depth (m)	15.24	33.528	42.672	51.816	60.96	100.584	109.728	128.016	140.208	207.264	216.408	219.456	225.552	231.648	237.744	243.84	249.936	256.032	262.128
Bombacacidites baculatus									1										
Bombacacidites baumfalki																		1	
Clavainaperturites microclavatus	1			1	4	1		2											
Clavatricolpites densiclavatus	1				1														
Echinatisporis muelleri	3				1									1			2		
Echiperiporites akanthos					1		1			1						1			
Echitricolporites spinosus	4		1	1	8			2	1										
Fenestrites spinosus																1			
Grimsdalea magnaclavata															1				
Jandufouria seamrogiformis										1					1		1		
Lanagiopollis crassa							1						1	4	2				1
Magnastriatites grandiosus			1																
Mauritiidites franciscoi franciscoi	1					8		1	25	2			3	1	1	1			
Mauritiidites franciscoi minutus						1			2	2					1	1		6	10
M. franciscoi pachyexinatus																		2	
Monoporopollenites annulatus	4			14	3	2		4		2				1	1	1	1		
Perfotricolpites digitatus										1									
Perisyncolporites pokornyi		1					1	2		4						1	3	1	
Polypodiisporites usmensis		1	1	7	1	1		2	6		2	2	2	1	2	3	5	3	1
Proteacidites triangulatus								1											
Proxapertites tertiaria							1										1	1	
Psilabrevitricolporites devriesi	1					1								2					
Psilabrevitricolporites triangularis			4	1			1					1				1	1		
Ranunculacidites operculatus		1	1	1	2			1			1				2		4	5	
Retibrevitricolporites yavarensis	1				3														
Retitrescolpites? irregularis		1											2					1	1
Retitricolpites maturus															2				
Retitricolpites simplex	2														1	1	1		
Retitriporites dubiosus										1									
Rhoipites guianensis									2			1			1		1		
Rhoipites hispidus		1															1		
Spirosyncolpites spiralis																		1	
Striatopollis catatumbus										2		1						2	
Syncolporites poricostatus		2	1	2			5			1		4		1	4	3	4	3	
Tetracolporopollenites transversalis		1								1									
Verrucatotriletes etayoi									1										
Verrutricolporites rotundiporus		3			1	2			2	9	10	11	20	5	7	1	4	16	6
Zonocostites ramonae	47	79	10	35	98	94	2	5	100	113	190	140	136	100	180	17	49	270	255
Others	122	101	30	155	107	79	73	58	95	146	188	74	142	74	94	58	141	113	73

Appendix C: Pollen count sheet

Depth (ft)	50	110	140	170	200	330	360	420	460	680	710	720	740	760	780	800	820	840	860	Pollen
Depth (m)	**15**	**34**	**43**	**52**	**61**	**101**	**110**	**128**	**140**	**207**	**216**	**219**	**226**	**232**	**238**	**244**	**250**	**256**	**262**	**count**
Pollen and spore types																				
Zonocostites spp. (aff. Rhizophora)	49	79	10	36	98	94	4	5	100	128	190	155	139	115	207	22	55	295	278	2355
Verrutricolporites rotundiporus		3			1	2			2	9	10	11	20	5	7	1	4	16	6	104
Psilastephanocolporites schneideri		3	2							18		2	19	1	10		8	2	9	74
Retitricolpites sp. (aff. *Avicennia*)	5			5	6															16
Lanagiopollis crassa							1						1	4	2				1	10
aff. Adianthaceae, *Acrostichum*	3																			3
TROPICAL LOWLAND PALM SWAMP AND FOREST																				
Arecipites	12	2	2	3	7	11	5		7	5	6	2	4		3	7	7	2	3	94
aff. Arecaceae (*Mauritiinae*)	1					12	4	1	35	7			3	1	3	2		8	10	90
Echimonocolpites spp.				3												1				4
Retimonocolpites maximus?															2					2
Gemmamonocolpites sp. (aff. *Iriartea*?)		1																		1
OPEN VEGETATION																				
aff. Poaceae	16			14	3	2		4		2	13			1	1	1	1			66
aff. Asteraceae	5		1	2	8			2	1							1				20
Psilaperiporites spp. (aff. *Chenopodium*)	3																			3
FRESHWATER AQUATIC ENVIRONMENT																				
Cyperacidites spp.	2			1	19	1			2		4									30

Appendix C: Pollen count sheet (*continued*)

Depth (ft)	50	110	140	170	200	330	360	420	460	680	710	720	740	760	780	800	820	840	860	Pollen
Echiperiporites akanthos					1		1			1						1				7
Corsinipollenites oculusnoctis																		1		1
aff. *Myriophyllum*		1																		1
Monoporopollenites 'microreticulatus'	1																			1
Magnastriatites grandiosus			1																	1
TROPICAL LOWLAND RAINFOREST TO MONTANE FOREST																				
Heterocolpites spp.	1	2	1	13	1	5	4	1	9	1	9	3	4	4	5	3	1	4	3	75
aff. Myrtaceae	3	2	1	3	5	2	6	5	1	1	4	4		1	4	4	4	3		56
aff. Euphorbiaceae	6	11	1		3		1		1	9	1	3	3	2	4		3		2	50
Polypodiisporites usmensis		1	1	7	1	1		2	6		2	2	2	1	2	3	5	3	1	40
aff. Fabaceae, Faboideae	4				4	4			8	1	5									37
Ilexpollenites spp.	3		1		3	6	1	2	5	1					2	1	2	1	1	29
aff. Apocynaceae	4		4	1			2	2		1	1	2				1	1			28
aff. Sapotaceae-Burseraceae		3			2	3	1		4	5	2			1	1		2	1	1	27
aff. Alchornea		1	1	1	5	1		1	4		1				2		4	5		26
aff. Fabaceae					2	3			1		13					1			1	22
aff. Moraceae & Urticaceae	4	1		1			1				2					1	1	5		18
aff. Malpighiaceae		1					1	2		4						1	4	3		16
aff. Rubiaceae					1	3			7								1			12
aff. Vochysiaceae				1	5				3	3										12
Clavainaperturites clavatus					4	4			3											12
Rhoipites caputoi	5								4	2		1								12

Appendix C: Pollen count sheet (*continued*)

Depth (ft)	50	110	140	170	200	330	360	420	460	680	710	720	740	760	780	800	820	840	860	Pollen
aff. Humiriaceae	1			1		1								2						11
Malvacipollis spinulosa																1	7	1	1	10
Retitricolpites spp. (aff. Bignoniaceae)	3				1	2			1		2									9
aff. Euphorbiaceae, *Sapium*	2					1									1	1	1	1		8
aff. Tiliaceae							1						2				3			6
Bombacacidites aff. Bombacoideae				1					1	1								2		5
Retitrescolpites irregularis		1											2					1	1	5
Rhoipites guianensis									2			1			1		1			5
Striatopollis catatumbus										2		1						2		5
aff. Araliaceae					4															5
Retitriporites aff. *crassireticulatus*							1			2							1			4
aff. Fabaceae, Caesalpinoideae, *Chamaecrista*									1	2										3
aff. Myristicaceae, *Virola*	3																			3
Jandufouria seamrogiformis										1					1		1			3
Proxapertites tertiaria							1										1	1		3
Proteacidites aff. *pseudodehaanni*										1			1							2
Psilatriporites corstanjei										1							1			2
Retitricolporites sp. (aff. Hypericaceae, *Vismia*)									2											2
aff. Nyctiganaceae?																	1			1
Perfotricolpites digitatus										1										1
Proteacidites triangulatus								1												1
Spirosyncolpites spiralis																		1		1

Appendix C: Pollen count sheet (*continued*)

Depth (ft)	50	110	140	170	200	330	360	420	460	680	710	720	740	760	780	800	820	840	860	Pollen
SAVANNA																				
aff. *Borreria*				70																70
Polyadopollenites mariae			1																	1
ANDEAN VEGETATION/ANGIOSPERMS																				
Clavainaperturites microclavatus	1			1	4	1		2												9
aff. Scrophulariaceae, *Castilleja*						2														9
Byttneripollis rugulatus?						4														4
Psilastephanocolporites sp.		1								1			1							4
aff. Canabaceae, *Trema*											2									2
Podocarpidites				1	1															2
Rhoipites pseudopilatus						1			1											2
aff. Brassicaceae	1																			1
aff. Cunoniaceae, *Weinmannia*?									1											1
aff. *Hypericum*?									1											1
aff. *Quercus*								1												1
Rhoipites sp. (aff. Malvaceae, *Heliocarpus*)									1											1
aff. Rubiaceae, *Arcythophyllum*?							1													1
aff. Saxifragaceae										1										1
ANDEAN VEGETATION/PTERIDOPHYTES																				
aff. Cyatheaceae, *Cyathea* and/or *Trichipteris*	1				4				1											6

Appendix C: Pollen count sheet (*continued*)

Depth (ft)	50	110	140	170	200	330	360	420	460	680	710	720	740	760	780	800	820	840	860	Pollen
Punctatosporites latrubessei					1															1
UNKNOWN AFFINITY & WIDE DISTRIBUTION/ANGIOSPERMS																				
Retitricolporites latus		27	3	6			4	4		15		5	37	9	4	1	9	1	2	127
Psilatricolporites cf. *varius*		2					1			3		4	2	4	6	2	9	3	1	37
Ladakhipollenites? *garzonii*						5	1		2	1	5			2			2			24
Retitricolpites ovalis												3			2		8	2	2	17
Psilatricolpites minutus		2					2	1					3	1	1	1	4			15
Retitricolporites ticuneorum										4		1	6				3		1	15
Retibrevitricolporites yavarensis	1				3															10
Psilatricolpites acerbus							3			1			2			2		1		9
aff. Solanaceae											8									8
Psilatricolporites crassoexinatus								2		2			1				3			8
Psilatricolporites exiguus												4								6
aff. Solanaceae, *Cestrum*					1															5
aff. *Phyllanthus acuminatus*						1														4
Verrutricolporites desmodiensis				1				1							1		1			4
Psilatricolporites heysti								1				1		1						3
Psilatricolporites sp. (aff. Elaeocarpaceae, Slonaea)																				3
Retibrevitricolpites pseudoretibolus	1								1								1			3
Rhoipites crassicostatus	2								1											3
aff. Malvaceae, *Hibiscus*?								2												2
Clavatricolpites densiclavatus	1				1															2

Appendix C: Pollen count sheet (*continued*)

Depth (ft)	50	110	140	170	200	330	360	420	460	680	710	720	740	760	780	800	820	840	860	Pollen
Gemmatricolpites sp.																	1		1	2
Retitricolpites maturus															2					2
Rhoipites spp.		1																		2
Rhoipites hispidus		1															1			2
aff. Cucurbitaceae, *Cucurbita*										1										1
Crototricolpites sp.			1																	1
Psilastephanocolpites equatorialis?														1						1
Retibrevitricolpites sp.														1						1
Retistephanocolporites sp.					1															1
Retitricolpites colpiconstrictus																	1			1
Retitricolporites milnei														1						1
Striatricolporites spp.									1											1
Others	25	40	14	30	17	13	35	23	12	46	110	25	52	28	26	29	51	53	17	655
UNKNOWN AFFINITY & WIDE DISTRIBUTION/PTERIDOPHYTES																				
Laevigatosporites spp.	6	3		6		2	3	6		2		3	2	3		1		5	5	47
Trilete spores	1	2	4	9	3	1		7			1	1				1	2	2		34
Echinatisporis cf. *muelleri*	3				1									1			2			9
aff. Polypodiaceae, *Adianthum*	4				2															6
Polypodiisporites aff. *minutiverrucatus*					3				1											4
Monolete spores	1								1											2
Polypodiisporites densus					2															2
Polypodiisporites sp.					2															2

Appendix C: Pollen count sheet (*continued*)

Depth (ft)	50	110	140	170	200	330	360	420	460	680	710	720	740	760	780	800	820	840	860	Pollen
Echimonoletes spp.																	1			1
Laevigatosporites aff. *tibuensis*						1														1
Perinomonoletes aff. *Asplenium*	1																			1
Polypodiisporites aff. *planus*									1											1
Polypodiisporites aff. *verruplanatus*	1																			1
Polypodiisporites fossulatus	1																			1
BRYOPHYTES																				
Bryophytes													2				2			4
Total	**187**	**191**	**49**	**217**	**230**	**189**	**85**	**78**	**235**	**286**	**391**	**234**	**308**	**190**	**300**	**90**	**221**	**425**	**347**	



Chapter 4

The interplay between tectonics, climate and sea-level change in the Holocene floodplain and Pleistocene terraces of the Suriname River, tropical South America

Kathleen S. Gersie[a*], Salomon B. Kroonenberg[a,d] & Ronald T. van Balen[b,c]

** Corresponding author*
Afilliations:
[a.] Geosciences Department, Faculty of Technological Sciences, Anton de Kom University of Suriname,
Leysweg 86, Paramaribo, Suriname; kathleen.gersie@uvs.edu;
[b.] Department of Earth Sciences, Vrije Universiteit Amsterdam, De Boelelaan 1085, 1081 HV Amsterdam, The Netherlands; R.t.van.balen@vu.nl
[c.] TNO—Geological Survey of the Netherlands, Princetonlaan 6, 3584 CB Utrecht, The Netherlands
[d.] Civil Engineering and Geosciences, Delft University of Technology, Stevinweg 1, 2628 CN Delft, The Netherlands. S.B.Kroonenberg@tudelft.nl

https://doi.org/10.3390/quat4020011

ABSTRACT

Suriname is part of the Guiana Shield, a cratonic area in northern South America. It is drained by several major rivers that are characterized by river terraces. The formation of terraces along the Suriname river is closely related to climatic changes during the Quaternary, due to the effects of climate on vegetation and precipitation changes. The terraces along the Suriname River valley show levels of 5, 15, and 20 m above the current mean water level. The reason behind the scarce terrace differentiation is the limited amount of long-term vertical incision. Therefore, each level along the Suriname River valley encompasses multiple climate cycles, which cannot be separated on morphological grounds. The limited incision reflects tectonic stability, which is typical for cratonic areas. Fieldwork along the river combined with topographic maps were used to determine and correlate the various terrace levels. While in the upper part of the river. climatically induced changes in vegetation cover and sediment delivery is dominant. In the lowermost reach, sea level change is especially important.

Keywords: fluvial terraces; tropical South America; craton; Northern Suriname

1. INTRODUCTION

Fluvial landscapes are an important part of the general geomorphological system. Among these, rivers in stable cratonic areas covered by rainforest are among the least studied ones. While they may show a large range of mean annual discharges and drainage basin areas, they are distinguished by unusually low sediment yields and sediment yield per square kilometer (Latrubesse et al., 2005). However, contrary to what these authors state, these rivers are not dominated by bedload but instead by a predominance of suspended load. This is due to the fact that the deeply weathered land surfaces hardly provide bedrock gravel but only their weathering products, e.g., sand, silt, and clay. This results in a lack of erosive power of the rivers, even at high discharges, so that when during incision hard bedrock is encountered, they are incapable of eroding them away due to the lack of bedload, and instead the channel splits itself up in several branches in order to avoid the obstacles. In this way, a very specific channel form develops, i.e., multibranch cataracts called raudales in Spanish South America such as in the Orinoco River, and well described by Garner (1967) for the Caroni River

in Venezuela, cachoeiras in Brazil, and sulas in Suriname (Zonneveld, 1972). These channel forms resemble to some extent braided river channels but differ from them in the fact that they consist of rocky islands with fixed positions, instead of sand bars which change position during each flooding event. Even those outcrops in the river do not lead to the formation of bedload gravel as exfoliation sheets falling from them into the river, for instance, which usually disintegrate by weathering before being able to form solid clasts.

Yet, like rivers from other environments, these rivers flowing in cratonic areas may exhibit river terraces with rounded gravel, suggesting different hydrological regimes and climatic environments in the past (Bakker, 1968; De Boer, 1972). We present here a case study on the terraces of the Suriname River in the Guiana Shield in tropical South America, with a drainage basin wholly covered by tropical rainforest. It is known from palynological studies that the Guiana Shield has suffered periods of greater drought and lesser vegetation cover (Van der Hammen, 1963; D'Apolito et al., 2013). The study of terraces in this environment, however, is hampered by several factors, including low uplift rates, deep sediment weathering, and a scarcity of datable material. Terraces are being recognized as an important source of evidence for Quaternary paleoenvironments (Bridgland, 2000) and, therefore, represent paleo-fluvial floodplains. Terrace formation in the lower reaches of rivers is driven by fluctuating sea level (Zeuner, 1945), whereas in areas remote from the marine influence, climate change produces a contrasting effect, with aggradation during glacial and incision during interglacial. However, the upstream influence of sea level fluctuation is likely to be limited because many rivers today flow in valleys that formerly extended over wide areas of continental shelf, but have been truncated by the Holocene marine transgression, which inundated and submerged their lower reaches (Schumm, 1993).

Where the shelf is narrow, sea level fluctuation has given rise to terraces that can be traced for considerable distances inland, which is the case for example for the Susquehanna in North America (Pazzaglia & Gardner, 1994) and other neighboring rivers in northern California (Merrits et al., 1994). The formation of terrace staircases is in most cases a response to regional uplift, which forces long-term incision (Stange et al., 2013; Bridgland, 2000; Boll et al, 1988; Maddy, 1997). The rivers in tropical Suriname have a maximum of about 20 m high, which is much less compared to what is commonly observed in high latitudes. Suriname is underlain by cratonic crust. In general, such crust is tectonically very stable and lacks a weak lower crustal layer, which would otherwise enable vertical motions by isostatic responses to loading (Westaway et al., 2003). Therefore, if this 20-m long term incision is caused by uplift, then this is in agreement with Suriname's cratonic crust.

According to De Boer (1972), the formation of terraces along rivers in Suriname is closely related to climatic changes during the Quaternary due to the effects of climate on vegetation and precipitation changes. In his model, glacial alluvial sediments are deposited in the river valleys and valleys are widened during glacials. During interglacials, the rivers incise, leaving the former floodplain behind as a terrace in the landscape. However, the number of terraces in Suriname (~3) is much smaller than the number of climate cycles during the Pliocene and Quaternary. In addition, close to the coast, climate driven eustatic sea level fluctuations also should have an important control on river terrace formation. For example, when low stand base levels were lowered by up to ~120 m and were submerged, 160 km Suriname shelf was exposed and incised by fluvial systems.

This study gives an overview of the Pleistocene terraces and the Holocene floodplain along the Suriname River valley, located in the central part of Suriname. Economically, this is Suriname's most important river, and it flows along the capital, Paramaribo. River terraces and floodplains are preferred sites for human settlement (villages) in the hinterland of Suriname. A detailed study would give more insight in the key controls (e.g., uplift, sea level fluctuation, climate changes) that are responsible for river terrace development along the Upper and Lower River valley parts. Literature studies, fieldwork, and laboratory analysis were used to determine the various characteristics of the terraces (e.g., height relative to mean water level, lithology). Our results are based on previous field work carried out in the 70s and 80s in the upstream parts and new mapping based on interpretations using historic land use maps in the midstream part, and a combination of Digital Elevation Model DEM and topographic maps analyses and field work in the downstream part. We provide, for the first time, full detailed maps of the distribution of terrace remnants of the whole river, and we show the terrace remnants in a longitudinal profile. Using these results, we discuss the formation mechanism and the relation to climate change.

2. REGIONAL SETTINGS

2.1. General

Suriname is drained by seven rivers that are subdivided in three main groups based on the extent and shape of the drainage area (Fig. 1). The first group consists of the border rivers Marowijne (East) and Courantyne (West), which have their sources in the border mountains with Brazil and drain almost 58% of the country. The second group has their origin in the high uplands in the middle of the country, and is represented by the Suriname and Coppename Rivers, which drain almost 24% of the country and debouch directly into the sea. The third group consists of the Commewijne, the Saramacca, and the Nickerie Rivers, that together drain approximately 16% of the country. The rivers of the last group bend westwards close to the coast to drain into the sea through the mouths of the second group, due to the westward migration of important mud banks along the coast (Amatali, 1993; Augustinus, 1978).

The rivers run through two geologically different parts of the country, first through the hills and mountains of the cratonic Guiana Shield, while the estuary part runs through the Coastal Plain (Amatali, 1993; Gersie et al., 2016).

2.2. GEOLOGICAL AND GEOMORPHOLOGICAL OVERVIEW OF THE STUDY AREA

Suriname can be divided into a southern rainforest-covered interior, which represents almost 80% of the country's surface, and a northern coastal plain that makes up the rest of the country's surface area. The rainforest-covered interior, which forms part of the Guiana Shield, is underlain essentially by Precambrian igneous and metamorphic rocks, also called the basement (Fig. 1 shows that the Guiana Shield roughly corresponds to the areas > 100 m). Thick dolerite dykes with a 1782 Ma age (Avanavero Dolerite) and narrow ones of Jurassic age (Apatoe Dolerite) intersect the basement of Suriname (Kroonenberg et al., 2016).

The morphology of the major part of the rain-forest covered basement consists of an endless mosaic of low hills with flat tops and steeply cut creek valleys. A distinction can be made into mountain tops up to 1280 m high, inselbergs at more than 700 m elevation, duricrust planation levels at more than 500 m, and river terraces at levels of approximately 20 m, 15 m, and 5 m above the mean water level. The terraces along the rivers are the only morphological units that are aligned with the present drainage pattern (Kroonenberg & Melitz, 1983). Structures in the bedrock (e.g., faults and fractures) control the drainage directions, as shown by the rectangular patterns of the larger rivers (Fig. 1).

The coastal plain consists of the Savannah Belt, the Old Coastal Plain, and the Young Coastal Plain. The Savannah Belt is a gently sloping north-facing hilly landscape between 10 to 50 m above sea level. The Savannah Belt is underlain by the Pliocene Zanderij Formation, which consists of horizontally layered deposits of coarse sands with small amounts of loams and fine sands. The Zanderij deposits can reach a thickness of up to 20 m. Gravel deposits, up to 2 m thick, are locally found at the base of this formation. The Zanderij Formation was deposited during dry climate conditions (Wong et al., 2009).

The Old Coastal Plain is situated 4 to 11m above sea level and is a dissected Pleistocene marine terrace, consisting of numerous small plateaus, the so-called "schollenlandschap". This landscape has a variable width of 20 km in the east to 70 km in the west. Remarkable features are the Old Ridge Landscape, and the Old Clay Landscape that originated due to the westward transport of sediments along the coast under the influence of the Guiana Current. The Old Coastal Plain consists of sands and clays of the Coropina Formation, which can be subdivided into the lower clayey Para member and the upper sandy Lelydorp member. The Para member has been deposited around circa 700 ka, while the Lelydorp member is of Eemian age, which is approximately 120 ka (Wong et al., 2009).

The Holocene Young Coastal Plain deposits are subdivided into the Mara Formation, which formed between 10–6 ka, and the Coronie Formation formed between around 6 ka to the present. This younger part of the coastal plain is a flat clay-prone surface that is locally interrupted by east–west oriented sandy cheniers. These cheniers mark former coastlines and appear as single units or bundles (Augustinus, 1978).

The Suriname River valley has a total length of 480 km and has its sources in the highlands (Fig. 1). Its catchment size is approximately 16,500 km^2, and 84.8% of the total catchment area is located in the rainforest-covered interior of the Guiana Shield, 4.5% in the Savanna Belt, and a 10.7% is in the Old and Young Coastal Plain (Amatali, 1993; Duba, 1972). The Afobaka Dam (1964) and Prof. Dr. W.J. van Blommestein Lake (also known as the Brokopondo or Afobaka Storage Lake) lie in the midstream part of the Suriname River valley. Downstream of the Afobaka Dam (194 km) the average annual discharge of the river is 324 m^3/s. At the river mouth, the average annual discharge is estimated to be about 440 m^3/s, while the estimated sediment discharge is 0.25 million tons per year (Gersie et al., 2016).

The river can only incise in saprolite or regolith because of the lack of abrading bedload (Bakker & Müller, 1957). A specific characteristic of all rivers in the basement area, including the Suriname River valley, is the presence of cataracts (sulas, in Surinamese). These are hard rock sills. At such locations the river's channel pattern resembles that of a braided river.

However, in contrast to the gravel or sand banks in real braided rivers, the islands between the branches consist of hard rock (Zonneveld, 1972; 1952). The most downstream sulas in the

Suriname river valley are the Brokopondo and Balling Sulas, just downstream of the Afobaka dam. They are situated at the northern edge of the basement, the Guiana Shield. They form semipermanent knickpoints in the river that they are supposed to be stable but are subject to slow erosion and have an important impact on river dynamics during climate-driven baselevel change and upstream changes in vegetation and sediment output (see Discussion).

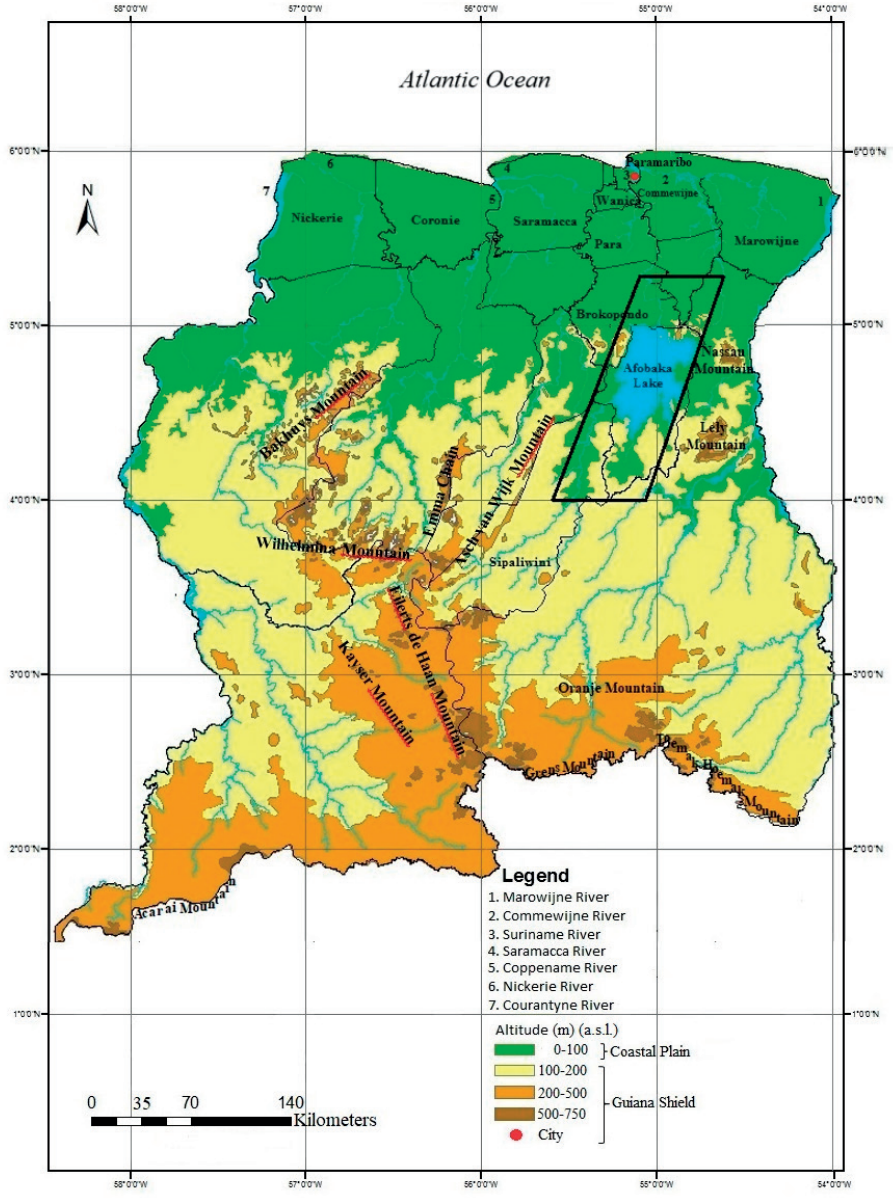


Figure 5: Simplified topographic map and hydrographic network of Suriname with its seven main rivers (Marowijne, Commewijne, Suriname, Saramacca, Coppename, Nickerie, and Courantyne Rivers) in the north. The frame indicates the location of the study area.

2.3. CLIMATE AND ENVIRONMENTAL CONDITIONS FROM THE PLIOCENE TO HOLOCENE IN NORTHERN SOUTH AMERICA

2.3.1. Pliocene and Pleistocene

The Miocene and Pliocene tectonics affected the Eastern Andes, fundamentally changing the regional climate and the drainage patterns, which leads to the formation of the present-day Amazon and Orinoco river systems (Hoorn et al., 1995). The Suriname River valley might have originated during the same time span. Climate conditions during the Pliocene seem to have been generally cooler than during the Miocene. Especially the final part of the Pliocene (between about 3 and 2.5 Ma BP) experienced a strong cooling (Dowsett & Poore, 1991).

Climatically, the Pliocene can be subdivided into a warm early Pliocene, a relatively warm Mid-Pliocene, and a relatively cool Late Pliocene (Haywood et al., 2009). Yet the average climate during the Pliocene appears to have been warmer than present day (Jansen et al., 2007). The pattern of temperature and precipitation change during the Pliocene was similar to weather and climate patterns observed during a modern El Niño event (Molnar & Cane, 2002).

In general, very little is known about the Pleistocene climate in tropical South America before 0.5 Ma (Baker & Fritz, 2015). The best data available refer only to the Last Glacial and the Holocene. We therefore restrict the discussion to that period, taking it as an analogue for previous Pleistocene climate cycles. During the Middle Pleniglacial (ca. 60–26 ka), most or all of warm and cold tropical South America had a considerably cooler climate and relatively high precipitation values. It became markedly drier between ca. 21 and 14 ka during the Late Pleniglacial (last glacial maximum) (D'Apolito et al., 2013). During the relatively cold and dry part of the Late Pleniglacial, savannah vegetation extended in Suriname, replacing the rain forest in the interior. During (and part of) the LGM savannah vegetation replaced wet forest at the entire present coastal area of Suriname (Van der Hammen, 1963; Wijmstra, 1971). It was estimated by Van der Hammen and Absy (1994) and Van der Hammen (1974) that precipitation in Suriname during the LGM was about 500 to 1000 mm/yr., which was needed in order to sustain a natural grass savannah and 1000 to 1500 mm/yr. for a mixed grass/woodland savannah. The rainfall regime was also more seasonal with a prolonged dry season. This is in accordance with predictions of 750 to 1500 mm/yr. for the LGM by global climate models (Kutzbach et al., 1998).

During the Late Glacial (13–11.3 ka), the climate of northern South America became wetter, the rivers carried an increasing quantity of water and a new cycle of sediment deposition began and continued into the Holocene. The increase in water level in the rivers seems to have been considerable, locally leading to temporal permanent inundation of the (upper to) middle river valleys (Vélez et al., 2006; Van der Hammen et al., 1992; Urrego, 1991).

2.3.2. Holocene

Records from the savannas of eastern Colombia, indicate that there was a shift from dry early Holocene to wetter environments after ~6 ka (Vélez et al., 2006). This can be explained by changes in the position of the Inter Tropical Convergence Zone. During the early Holocene, the ITCZ apparently had a more northerly position than today (Haug et al., 2001; Martin et al., 1997), causing dry conditions in the savanna. The ITCZ shifted southwards during the mid- and late Holocene, leading to more precipitation in the savannas.

During the early Holocene (12 to 6 ka BP), sea level rose from a depth of more than 100 m to the present level (Fairbanks, 1989). Sea level rise slowed down between 6 and 7 ka BP (Fig. 2) (Groen, 2002). Precipitation increased during the early Holocene. Rainfall still was concentrated in the the early Holocene. The average yearly temperature was about 5 to 6 °C lower than today during the LGM (Van der Hammen & Absy, 1994; Kutzbach et al., 1998). The yearly actual evapotranspiration was 15% lower than today, which was approximately 1300 mm/yr. in Suriname (Kutzbach et al., 1998).

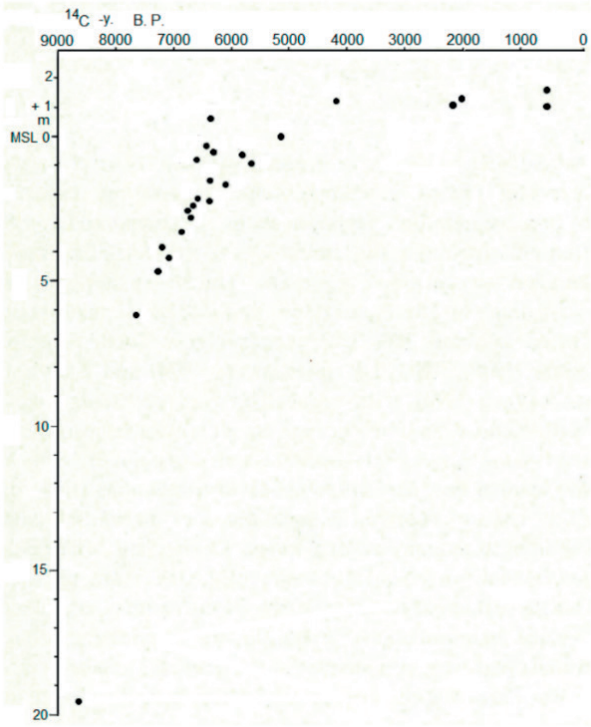


Figure 2: Sea level rise along the Suriname coast (modified after Roelevel & van Loon, 1979)

3. MATERIALS AND METHODS

In the practically inaccessible hinterland of Suriname, aerial map analysis is a very important research method. This is based on the existence of a relationship between soil and landscape. The geology of the study area is also involved in the analysis. However, height and slope differences are at least as important as soil data in the evaluation of the landscape. The research methods of this study consisted of desktop, fieldwork, and laboratory parts.

A preliminary map analysis was made of the study area. This map analysis was aimed at distinguishing geomorphological units (e.g., terraces) that differ markedly from each other in terms of height. Subsequently, a limited number of observations were made to check the preliminary map data to obtain detailed information about the morphometry of the different landscapes (height and slope differences, etc.) and the soil characteristics.

Fieldwork was done from the river inland. On selected locations boreholes were made using an auger and a gouge to determine terrace sedimentary successions and to collect samples. The locations of the boreholes were chosen in parts of the various terraces that were representative of the landscape. This means that data obtained from the drilling survey was considered to be representative of the remaining area.

Samples from five boreholes were selected for analyzing the sediment texture in the laboratory. A Sympatec HELOS laser diffraction machine was used for the particle size analyses, ranging from 0.1 μm to 3500 μm.

Before collecting the field data, terraces were mapped in the upper, middle, and lower Suriname River valley stretches with the aid of a Space Shuttle Digital Eevation Model (SRTM DEM) and topographic maps. Historical topographic maps revealed that inland residents used the terraces for laying out their agricultural lands. This information was used to infer terraces in the midstream part of the Suriname River valley, because this part is nowadays submerged due to the construction of the Afobaka dam.

The resulting terrace maps were largely based on a map of the upper Suriname and Saramacca River areas produced by Balsem and Rhebergen (Balsem & Rhebergen, 1979) in the framework of a geomorphological-soil science cooperation project between the Soil Survey Institute of Suriname (DBK) and the Vrije Universiteit Amsterdam (VU), as well as on a detailed study of the upper Suriname River valley, which was also part of the Soil Mapping Service (Dutch: Dienst Bodem Kartering)/Vrije Universiteit DBK/VU project by Kips and Snel (1979).

4. RESULTS

4.1. GENERAL CHARACTERISTICS OF THE TERRACES

For practical purposes, we divided the Suriname River valley into an upper (Fig. 3), middle (Fig. 4), and lower valley part (Fig. 5), corresponding, respectively, with the part upstream from the Afobaka storage lake, the Afobaka storage lake itself, and the part from the Afobaka dam to Cassipora. The terrace remnants were plotted at a longitudinal profile (Figure 6). Apart from potential correlations, the profile also showed that the current river profile has three important knickpoints.`

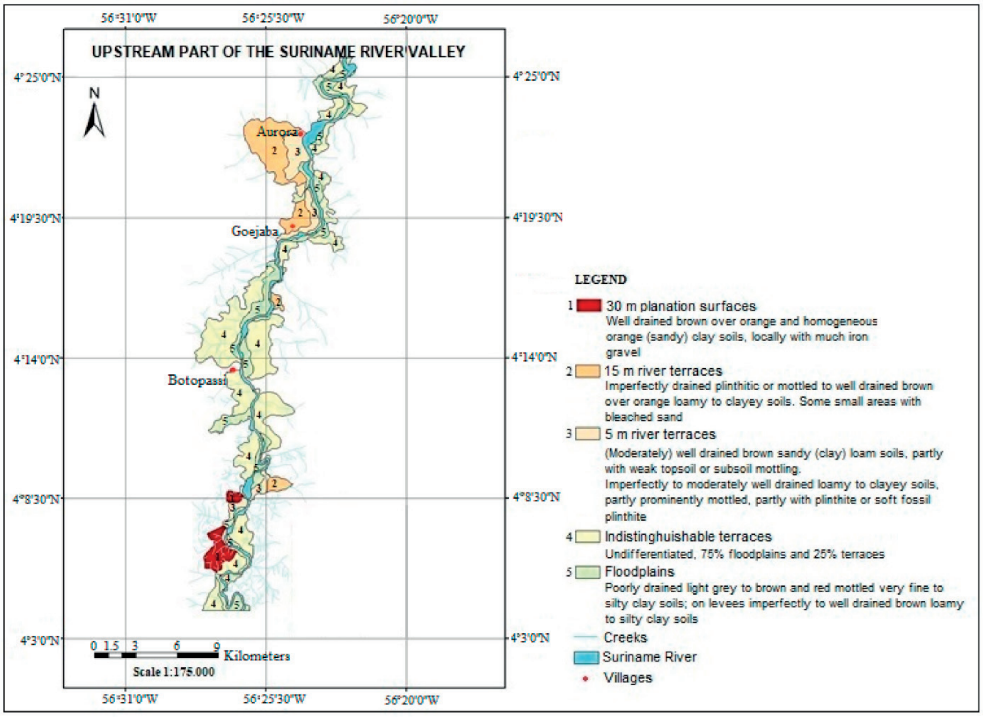


Figure 3: Map of terraces along the upstream river valley part of the Suriname River

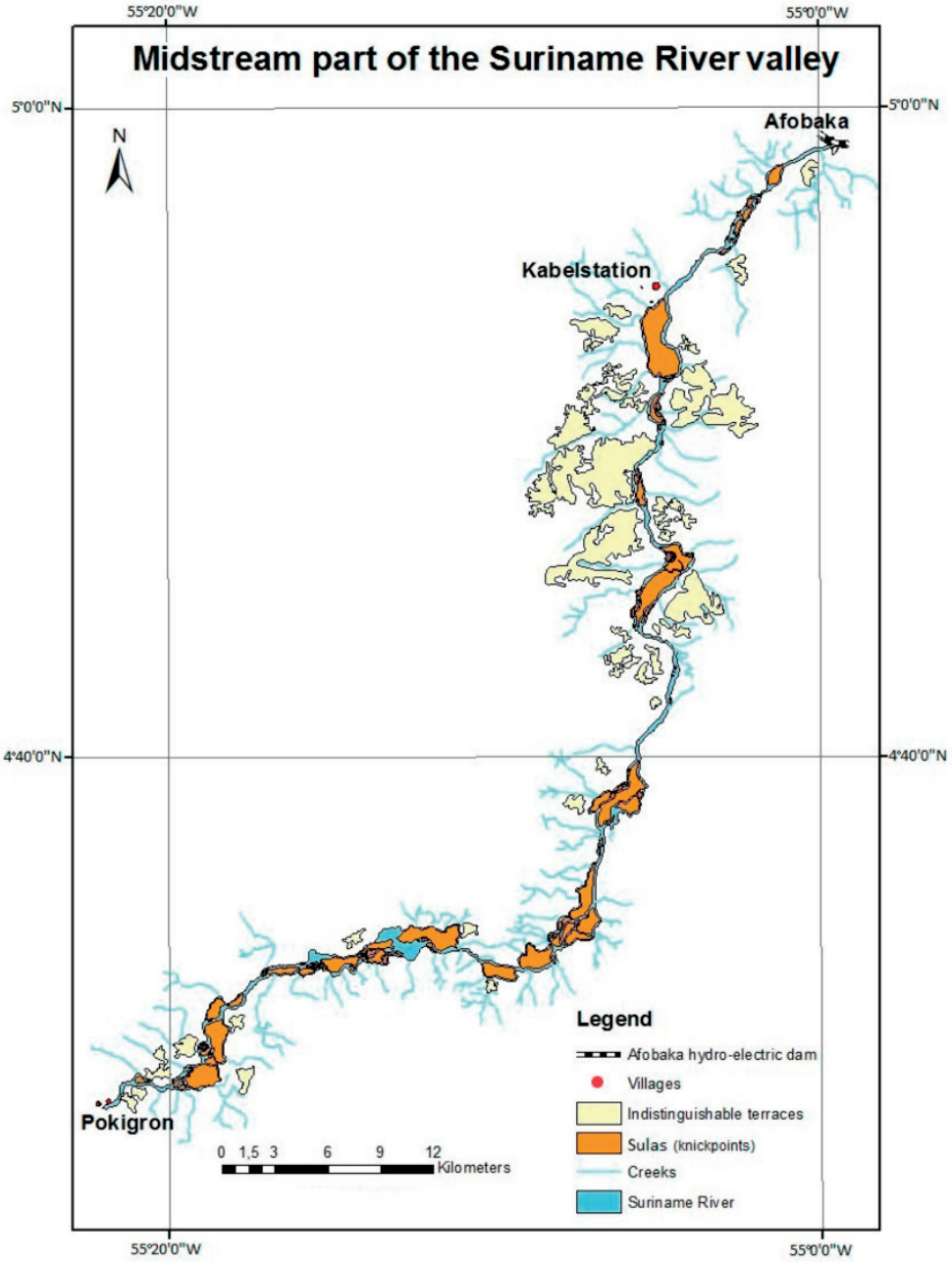


Figure 4: Inferred terraces along the mid-stream valley part of the Suriname River, now submerged in the Afobaka Lake.

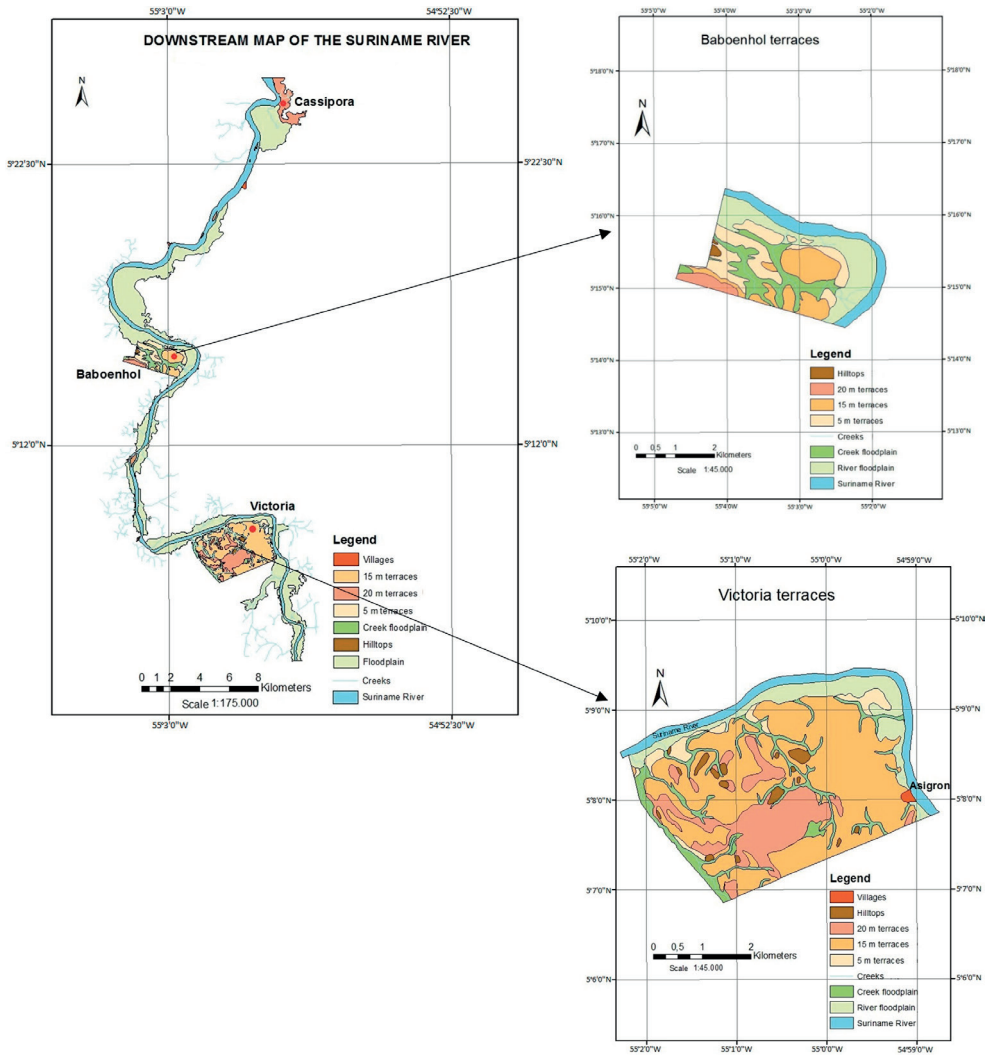


Figure 5 The downstream valley part of the Suriname River

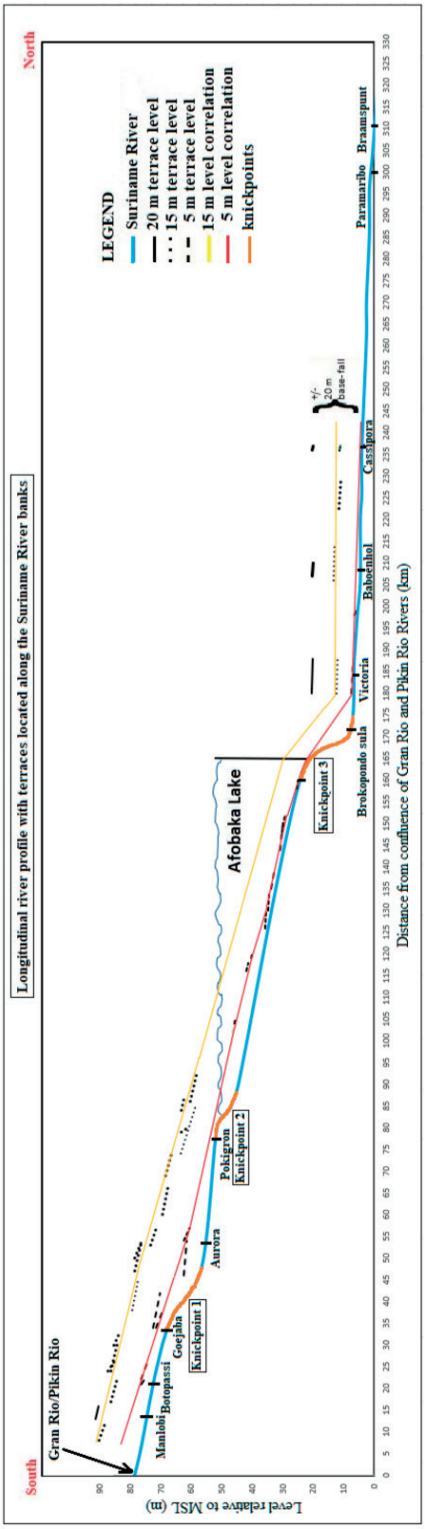


Figure 6: Longitudinal profile of terrace remnants and their correlation along the Suriname valley; knickpoints coincide with larger sulas (cataracts).

4.2. UPPER RIVER VALLEY PART

The terrace map of the upper river valley (Fig. 3) is based on maps of the upper Suriname and Saramacca River areas by Balsem and Rhebergen (Balsem & Rhebergen, 1979). They distinguished a 20 m, 15 m, and a 5 m high terrace level. The 20-m terrace level has a relief up to 25 m and slopes up to 18%, and consists of regolith of mainly felsic rocks, and local river sediments. The 15 m terrace level has an undulating morphology with a relief up to 15 m and slopes up to 8%, consisting of Pleistocene river deposits (50%) (fluviatile sediments) and regolith of mainly felsic rocks (50%). The terrace deposits have a thickness of 0.5 to 4 m. The 5 m terrace level remnants are almost flat plains with depressions, relief up to 5 m, and slopes up to 4%. They consist of relatively thin fluviatile loam deposits.

Kips and Snel (1979) also distinguished a 30-m high level (Fig. 3) with a sediment sequence of 3.5 to 5 m in thickness. The deposits contain fine, rounded gravel and show a fining upwards sequence of loamy sand at the bottom, passing into (sandy heavy) loam at the top of the sequence.

The sediments in the present floodplain differ considerably from the three levels, and according to a few deep auger drillings, consists mainly of silty to heavy clay without any fining upwards sequence. At some locations the floodplain and the 5 m terrace level are absent, and the 15- m and 20- m terrace levels directly border the river channel. According to the Geological Mining Services of Suriname (GMD) the river terraces in the upper reaches have developed entirely on granitoid and gneissic rocks of the Precambrian basement.

The terrace remnants mapped by Balsem and Rhebergen (1979) and Kips and Snel (1979) are plotted in the longitudinal profile of Figure 6. Based on the correlation of the remnants, we conclude that three levels are present, at 5, 15, and 20 m above the present-day river level.

4.3. MIDDLE RIVER VALLEY PART

Up to now, little is known of terraces along this part of the river, especially regarding their height levels. The geological map of sheet Kabel (31) by D'Audretsch (1957), made before the construction of the Afobaka dam, shows a continuous strip of terraces, all developed on tonalitic granitoid rocks. D'Audretsch (1957) gives a terrace height of 10 m above low water level, on which the Maroon villages were built. Martin (1888) measured the height of 7 Maroon villages on a terrace situated between 5 and 9 m relative to the river level. Whether higher terrace levels are also present is unknown, as most earlier researchers mainly surveyed from the river. In the present research, additional lower terrace fragments (Fig. 6) were derived based on the locations of former farmlands depicted on historical maps.

According to D'Audretsch (1957), the present floodplain is up to 6 km wide. Locally, low levees occur in the outer bends. Where the river incises in its own deposits a gravel layer resting on weathered basement rock is exposed. The fill of midstream part of the river valley consists of cream-colored to yellowish clay.

4.4. THE LOWER RIVER VALLEY PART

According to our analyses, the main terrace levels along the downstream reach are situated at heights of 20 m, 15 m, and 5 m above the mean water level of the river. They are particularly well developed at three locations, which we studied in detail, i.e., from south to north the remnants of the Victoria terraces, the Baboenhol terraces, and the Cassipora terraces (for location see Fig. 5). According to the geological map, the Victoria and Baboenhol terrace remnants are developed on basement rocks, whereas the Cassipora terrace remnant sits on Zanderij Formation sands (Fig. 7).

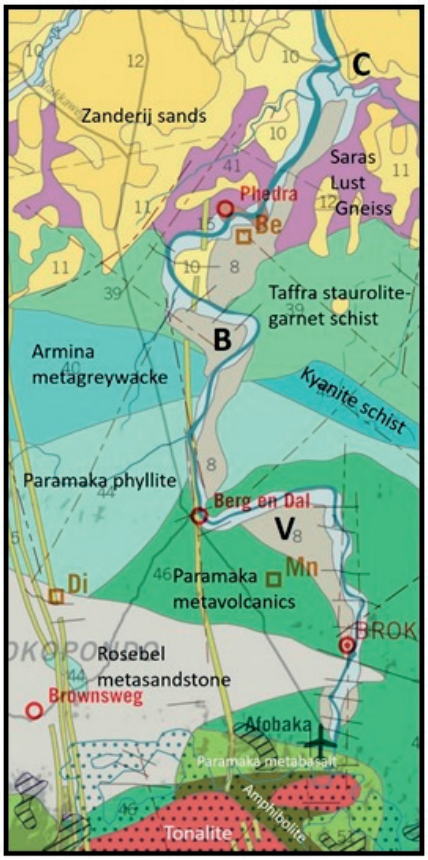


Figure 7: Geological map with Zanderij Formation indicated in yellow. Other colors represent basement rocks (V = Victoria; B = Baboenhol; C = Cassipora).

4.4.1. The 20-m Terrace Level (T20m) at Victoria

The 20-m terrace level situated at Victoria consists of fluvial deposits and is developed on hard rock, while at Cassipora it is developed on the Zanderij Formation of Pliocene age. The lithology at the base at Baboenhol is unknown, but is likely also hard rock. At Baboenhol and Victoria, the topography of the upper surface of this level is irregular as a result of numerous incised local creeks (Fig. 5). The height of the terrace level increases with increasing distance from the river. At Victoria, transitions from the 15 m terrace level to the 20-m terrace level occur gradually. Compared to Cassipora, the sands of the 20-m terrace level at Victoria are loamier (Fig. 7).

The 20-m terrace level located at Victoria, on the left bank, extends to approximately 1.5–2 km inland from the river. The topography is fragmented by small, incised creeks, and shows a gradual increase in height. Its subsurface consists, from top to bottom, of sandy loams with gravel, loamy sands, and loamy sands with gravel (Fig. 8). The sands resemble those of the Zanderij Formation, suggesting they could be related.

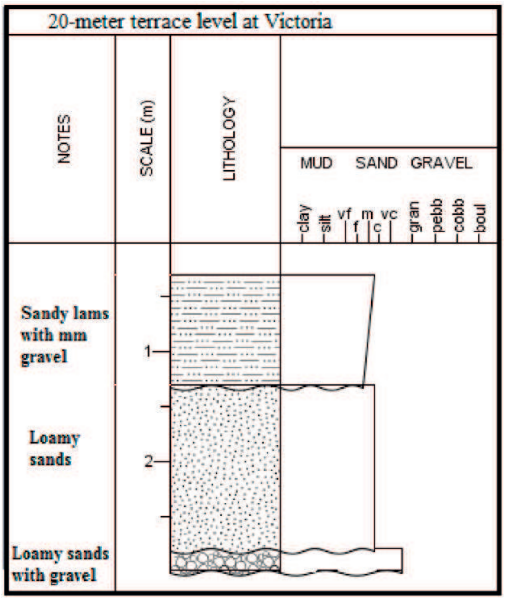


Figure 8: Sediment log of drilling core at the 20 m terrace level at Victoria

The 20-m terrace level at Baboenhol, located at the left bank of the river (Fig. 5), is also fragmented by incising tributary creeks. However, it also shows very different morphological characteristics compared to the 20-m level at Victoria. Starting from the river, the land surface rapidly increases in height from 5 to 15 m. There is a sharp transition from the 15-m to the 20-m terrace levels.

The width of the 20-m terrace levels is about 0.5 km. A sharp transition from the floodplain (at 1 m) and 20-m terrace levels over a distance of circa 50 m occurs at Cassipora (right bank). Both locations had sharp transitions. Baboenhol and Cassipora (right bank) are situated in the outer river bends, while Victoria, with gradual transitions, lies in an inner bend.

The shallow subsurface of the 20-m terrace level at Cassipora consists of fluvial fine and angular quartz gravels, overlain by a clay deposit. The gravels show a fining upward trend (Fig. 9). The gravel clasts have a diameter of up to 2 cm. They are interpreted as part of the Pliocene Zanderij Formation. The overlying clay deposits has orange (oxidized) and green colored (reduced) spots, which are related to soil formation.

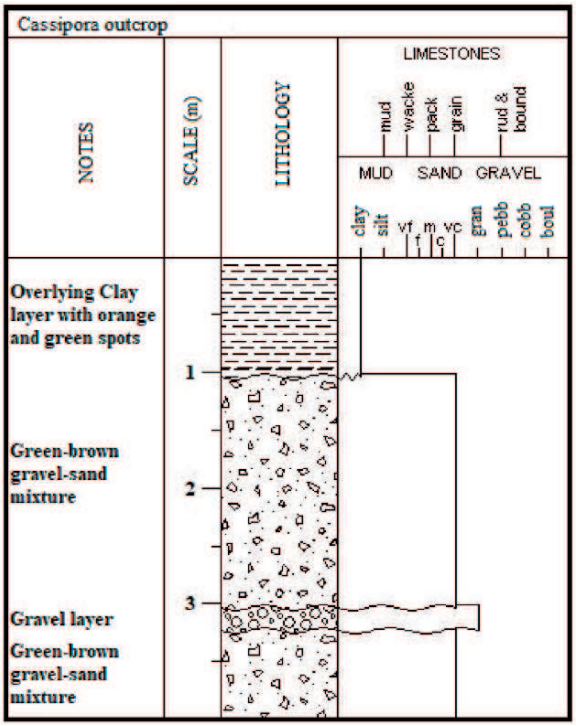


Figure 9: Sediment log of the outcrop at Cassipora

4.4.2. The 15-m Terrace Level (T15m)

The width of the 15-m terrace level ranges from about 0.25 to 0.5 km. The upper surface of the 15-m terrace level ranges between 10 and 20 m above the river, but is mostly at about 15 m, which corresponds with the findings of Kips and Snel (1979) in the Upper Suriname River valley. The terrace landscape is undulating and locally incised by some large creeks in shallow fairly flat valleys.

4.4.3. The 5-m Terrace Level (T5m)

Along the downstream part of the Suriname River valley, the 5 m terrace group is present at Victoria and Baboenhol. At Cassipora the floodplain is absent and the present outcrop of the Zanderij Formation directly borders the river. The average width of the 5-m terrace level goes up to 50 m, but where it is narrow the 5-m passes gradually into the 15-m terrace level. The upper part of the terrace deposits consists of clays locally with rusty or purple spots (soil formation) (Fig. 10).

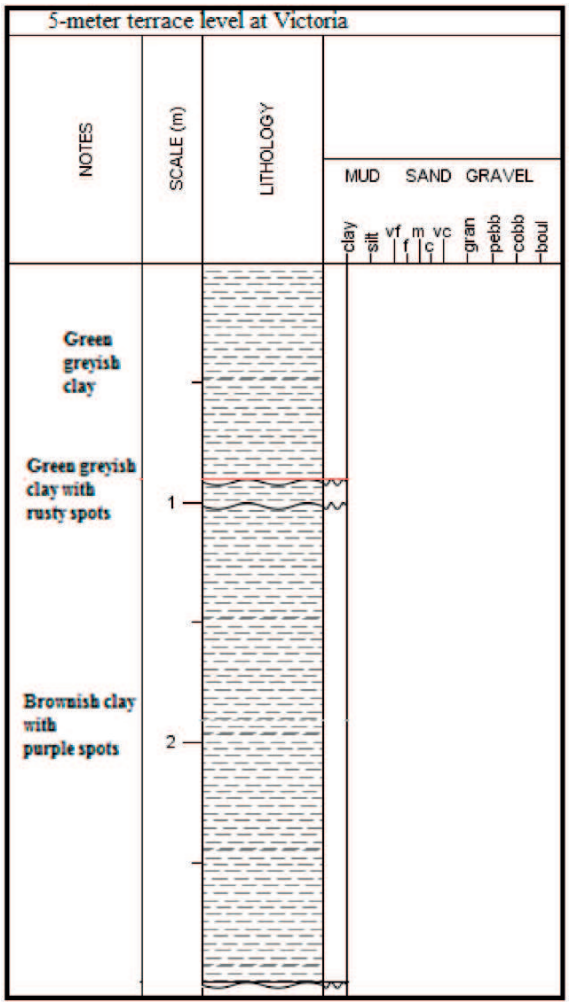


Figure 10: Sediment log of drilling core in the 5 m terrace level at Victoria

At Brokopondo Sula, further upstream between Victoria and the Afobaka Dam, a 5- m terrace level is present on an island in the middle of the river. A profile across the island was obtained for the purpose of exploring a possible dam site (Bleys, 1953). The profile shows an

irregular bedrock surface at 7 to 12 m depth, covered by a fluvial fining upward sequence, with coarse sand at the bottom and loamy sand at the top (Fig. 11) (Bleys, 1953).

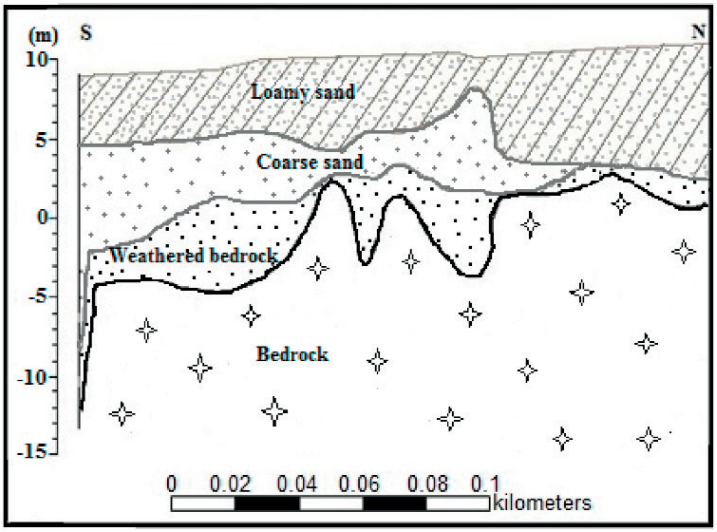


Figure 11: Cross-section through the island at the Brokopondo sula (modified after Bleys (1953))

5. DISCUSSION

The studied section of the Suriname River valley shows generally three terrace levels above the present mean water level. In the most upstream and downstream parts, the highest level is at 20 m above river level. Information about higher terrace levels in the now submerged intermediate part (Afobaka Lake) is lacking, so it is not clear whether these levels are the same. In view of the fact that water levels in the Suriname River valley may vary up to 7 m between high and low discharges (D'Audretsch, 1957), estimations of the height of the terraces above river level may have a large error margin.

We correlated the 20-m level in the upstream part to the level at the same height in the

downstream part for two reasons: (1) this correlation follows the shape of the present-day longitudinal profile, including the sulas; and (2) the number of terrace levels is the same in the upstream and downstream parts. The first argument assumes that the sulas are a permanent feature of the fluvial longitudinal profile, for which we provide arguments below.

The consistently presence of terraces at the 20, 15, and 5 m levels at both the up- and downstream parts of the Suriname River valley (Fig. 12), can be explained by lowering of long-term eustatic sea level and/or low amount of uplift. There is more evidence of recent tectonic movement than originally thought, primarily as a result of rift shoulder develop-

ment due to the separation of South America and Africa, and the development of the Takutu failed arm along the border between Suriname and Guyana. Data from northeastern Brazil suggest a possible uplift of 20 m in the Quaternary (Peulvast et al., 2008). Cenozoic uplift of the Bakhuis Horst in western Suriname along reactivated Precambrian faults parallel to the Takutu rift is even recorded in seismic sections in the coastal plain (Girjasing et al., 2019).

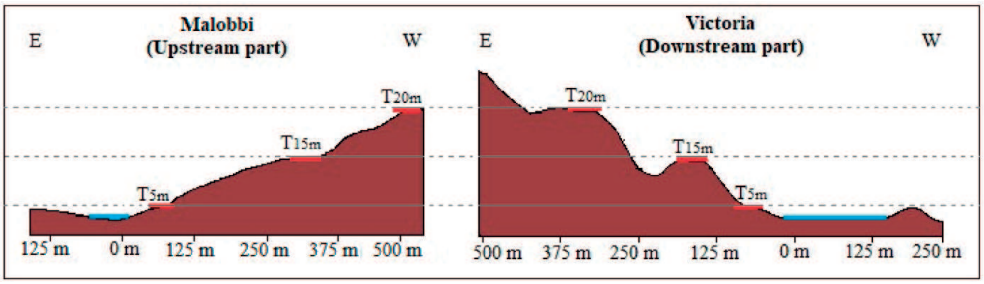


Figure 12: Cross-sectional topographic profiles of Malobbi (Upstream part) and Victoria (Downstream part) with correlated terrace levels.

5.1. A MODEL FOR TERRACE EVOLUTION IN THE UPSTREAM AND MIDDLE PARTS

Terrace development in the humid tropics is largely attributed to the effects of climate change. During glacials, the climate is relatively dry, because less water-vapor is available in the atmosphere, causing reduced precipitation. In contrast, interglacial climates are relatively wet. Reduction of precipitation during a transition from an interglacial to a glacial period leads to the conversion of the dense tropical forest into savannah vegetation. At the same time, because the surface is less covered with vegetation during glacials, more erosion occurs, leading to more sediments available for fluvial transport. Thus, fluvial sediment load increases, whereas transport capacity decreases. This results in sediment storage (aggradation) in the river valleys and raising of the river valley floor. During interglacials rivers incise, because the climate is relatively wet, resulting in increased precipitation and vegetation cover (Vandenberghe, 2015; Bauer & Bull, 1993).

During the Quaternary many glacial/interglacial cycles have occurred, and some rivers, such as the Meuse in the Netherlands, show a terrace for each climate cycle, up to 30 for the whole Quaternary (Veldkamp et al., 1993).

In general, the preservation of terraces in a terrace staircase requires a long-term incision. In case of the Suriname River valley, the 20-m of incision during the Pliocene and Quaternary is insufficient to produce a visible staircase of about 30 terraces, whereby each would represent a climate cycle.

The long-term 20-m incision since the Pliocene requires an explanation. It may have been caused by the long-term eustatic sea level fall since the Pliocene (Haq et al., 1987) and/or by uplift. A slow and relatively low amount of uplift may have resulted from the rifting processes that led to the formation of the Atlantic Ocean (passive margin uplift). According to studies in north-east Brazil (Peulvast et al., 2008) rift shoulder uplift and denudation along the Atlantic coast due to rifting since the Cretaceous amounted to 10 m/Ma, that is 20 m for the whole Quaternary. Alternatively, the differential uplift can be explained as a result of erosional isostasy of the hinterland (Van Balen et al., 1995). The small amount of uplift and the consequent limited vertical separation of the terraces can be explained by absence of lower crustal flow in of this cratonic crust (Westaway et al., 2003).

Knickpoints in the upstream part of the river valley are present in the present-day longitudinal profile, particularly at Goejaba and Pokigron (Fig. 6). The knickpoint at Goejaba is likely caused by a northeast–southwest oriented dolerite dyke that cuts across the river and acts as a sula, whereas the knickpoint at Pokigron is controlled by the Kwai-Kwai sula as a result of differential weathering. Sulas are very stable and nonmigrating on geological timescales. In non-tropical conditions, knickpoints can be abraded by fluvial gravel and sand. However, under tropical conditions such as in Suriname, chemical weathering in the basement is very intense and produces only sand and clay. Any local gravel will also be rapidly transformed into sand and clay before reaching the sulas. Sand and clay are largely transported in suspension, and they are too fine to be able to significantly abrade the sula knickpoints (Bakker & Müller, 1957).

The situation at the knickpoints may have been different in glacial times with semiarid

climatic conditions. The fining upwards sequences in the terraces often show rounded gravel at their base, suggesting less intense weathering in the drainage basins and more bedload transport in the channels. Under such conditions rocky knickpoints can therefore be lowered by the erosive power of the bedload. This is suggested by the northernmost knickpoint, the Brokopondo sula, just downstream of the Afobaka Lake (Fig. 6). The island in the middle of this sula consists of a buried irregular rock outcrop covered by sediments belonging to the 5-m terrace level. This suggests that the buried rock surface has been a sula in its own right in glacial times, which probably first suffered erosion by the increased bed load and then became covered by the fluvial fining upwards sequence.

This possibly encompasses a smoother length profile of the river in glacial times than in the present interglacial times. Unfortunately, the absence of datable material in the terrace sediments so far precludes confirming this scenario.

5.2. A MODEL FOR FLUVIAL DEVELOPMENT IN THE DOWNSTREAM PART

The upstream influence of sea level fluctuation is likely to be limited (Schumm, 1993). Many rivers today, such as those around NW Europe, flow in valleys that formerly extended over a wide continental shelf, but their lower reaches were inundated and submerged by the Holocene marine transgression (Bridgland, 2000).

While the river valleys fill-up in the upstream part of the river during a glacial, in the downstream part they are incising due to sea level fall, and vice-versa, during an interglacial (e.g., Viveen et al., 2013)). The location of the transition between incision and aggradation during a certain climatic situation, the terrace-intersection likely is located at those points in the river valley where the most downstream bedrock-controlled cataracts (sulas or rapids) occur. These sulas limit the upstream migration of sea level induced knick-points. In the case of the Suriname River valley, they are situated at the transition from Guiana Shield bedrock to the coastal plain deposits, at the Brokopondo Sula (Fig. 12).

For example, eustatic sea level dropped to about 120 m during the LGM. During this period the Suriname coastline was situated at 130 to 150 km north of the present coastline (Balsem & Rhebergen, 1979), leading to exposure of the Suriname Continental Shelf and, as a consequence, the extension of the downstream part of the Suriname River valley. From the river mouth, incision migrated landward, incising into the shelf and into the previous river floodplain of the present lower Suriname River valley.

From the LGM to the early Holocene, rivers and creeks close to the sea were very deeply incised (10–30 m). Erosion also took place in the Old Coastal Plain and on the shelf of Suriname (Wong, 1986; Roeleveld & van Loon, 1979; Veen, 1970; Brinkman & Pons, 1968). Moreover, the large Suriname River must have eroded into the sediments of the coastal plain and continental shelf. Core drillings by Groen (2002) show that near Paramaribo the base of the paleochannel of the Suriname River valley was about 35 m (below msl). After the steep sea level rise at the beginning of the Holocene (12 ka BP), the coastline shifted circa 20 km landward of its present position. Sea level reached its current level at 6.5 ka BP (Fairbanks, 1989; Roeleveld & van Loon, 1979). Since then, the coastline shifted seawards 10s of kilometers due to coastal aggradation.

In contrast, for the middle and the upper part of the river valley it is very unlikely that eustatic sea level changes have led to the formation of terraces (i.e., deposition during highstands and incision during lowstands), as the Brokopondo Sula forms a rock sill that cannot be cleared away by headward river erosion.

The 5 m terrace level fragments at Victoria and Baboenhol, i.e., downstream of the Brokopondo sill, theoretically could represent a terrace formed as a result of the 7-m Eemian highstand that also formed the Old Coastal Plain. These terrace deposits do not show the common fining upwards sequence of the upstream 5-m terrace levels but consists primarily of clay (although the depth of the augering was only 3 m). In a similar situation near the mouth of the Marowijne River valley, marine clay was found in a 5 m terrace level profile in the Coropina Formation (Eemian) (De Boer, 1972; Brinkman, 1959).

However, the Victoria 5-m terrace level is located at about 130 km from the mouth of the Suriname River valley, measured along the river channel (100 km as the crow flies), and the nearest Coropina (Eemian) marine deposits of the Old Coastal Plain are 40 km north from Victoria. Moreover, the Old Coastal Plain marine deposits do not reach higher elevations than 7 m above present sea level, whereas the Victoria 5-m terrace level is at 12 m above present sea level. Therefore, we conclude that that the 5-m terrace level at Victoria is a fluvial deposit.

As discussed above, the third knickpoint in the Suriname River valley at the Brokopondo sula shows a fining upwards fluvial sequence on top of an irregular bedrock profile (Bleys, 1953). This sula was buried by fluvial sediments of the 5 m level during the last glacial semiarid period and dissected during the present humid interglacial. Fluvial deposition during the last glacial apparently went downstream beyond the last knickpoint and is probably also responsible for the 5-m terrace levels at Victoria and Baboenhol. Therefore, it is unlikely that any of the studied terraces in the study area has formed as a result of Eemian highstand deposition and Last Glacial dissection.

6. CONCLUSIONS

Like other rivers in cratonic drainage basins covered with exclusively tropical rainforest, the Suriname River at present is characterized by the virtual absence of bedload transport, because the deeply weathered basement does not provide coarse-grained sediment to the rivers. Cataracts (sulas) are formed in the river channel where interglacial incision touches subsurface rock weathering fronts. The absence of bedload forces the Suriname river to avoid the rocky obstacles instead of eroding them away, leading to multichannel cataracts, which only in plain view resemble braided river patterns. However, they are stable rocky features instead of moving gravel and sand bars. The cataracts represent important knickpoints in the length profiles of the rivers.

In the Suriname River in the Guiana Shield, the presence of several gravel-bearing terrace levels above the present flood plain suggests that in glacial times, in this region, were characterized by semi-arid climatic conditions with savannah-type vegetation, fluvial dynamics dif-

fered considerably from the present ones. Three terrace levels at 20, 15 and 5 m above present mean water level were studied in three sectors of the river: an upstream part, a middle part (now submerged below a storage lake), and a lower part. The consistent height difference between these levels and their length profiles being roughly parallel to the present one suggests that they represent major stages in the development of the river basin. The consistent presence of terraces at the 20, 15, and 5 m levels at both the up- and downstream parts of the Suriname River valley can be explained by lowering of long-term eustatic sea level and/or low amount of uplift. As dissection is argued to have started already in the late Pliocene or early Pleistocene, the terrace staircase may represent many more than three climatic cycles. However, because of the absence of datable material individual cycles cannot be resolved as of yet.

The presence of gravel in the fluvial terraces could imply that the role of the knickpoints was less prominent than at present. An island in the northernmost knickpoint, the Brokopondo sula, shows a buried rocky surface under a fining upwards sequence belonging to the 5 m terrace level, suggesting that many cataracts may have suffered bedload erosion indeed during glacial times, becoming covered with so much sediment that their knickpoint function became less effective. As a result, glacial length profiles could be smoother than the present one.

While in the upper part of the river valley the role of upstream controls, notably climatically induced changes in vegetation cover and sediment delivery are obvious, in the lowermost sector of the river the role of downstream controls, especially sea level change must also be discussed. Theoretically, the terraces in this sector could also represent fluvial deposition during sea level highstands and dissection by headward erosion during lowstands. However, even the 5 m terrace levels here are situated at 12 m above present sea level, whereas the oldest marine terrace in the Old Coastal Plain does not reach above 7 m above sea level. Moreover, the distance to the coast of the northernmost terraces is over 100 km, far beyond any evidence of past sea levels. The presence of fluvial deposits on the most downstream knickpoint suggests that the terrace intersection must be situated further north than the present study area.

ACKNOWLEDGEMENTS

We would like to thank Riad Nurmohamed and the Suriname Conservation Foundation. Moreover, a big thanks to mr. Johan Abelintie, villager of Victoria, and the following bachelor students from the Anton de Kom University who helped during field visits: Noel Sardjoe, Arantxa Lieveld, Sharan Bhajan, Kishan Ramdas, Sunaina Pirthipal, Shanice Pique, Saerah Sastrokarijo, Cherishma Beni, Zeinab Abdoelbasir, and Ralph Gogli. Also, a special thanks to Christina Ngai and Roetoe Lugard of the Geological Mining Service Suriname (GMD),

Donovan Bogor from the National Institute for Environmental Development and Research in Suriname (Nimos), and Dana Artist from Gissat for making the various topographical maps available. Last but not least, a very special thanks to Melvin Pigot MSc. Your experience and knowledge of the study area was invaluable.

REFERENCES

Amatali, M. A. (1993). Climate and surface water hydrology. In Freshwater Ecosystems of Suriname; Ouboter, P., Ed.; Kluwer Academic Publishers: Amsterdam, The Netherlands, 29–51.

Augustinus, P. G. E. F. (1978). The Changing Shoreline of Surinam. Ph.D. Thesis, Rijksuniversiteit Utrecht, Utrecht, The Netherlands, p 232.

Baker, P. A., Fritz, S. C. (2015). Nature and causes of Quaternary climate variation of tropical South American Quatarenary Science Reviews 124, 31–47. https://doi.org/10.1016/j.quascirev.2015.06.011.

Bakker, J.P. (1968). Die Flussterrassen Suriname als Hinweise auf etwas trocenere Klimate während der Quartären Eiszeiten. Acta Geog. Debrecina Landscape Environ. 7, 9–17.

Bakker, J. P., Müller, H. J. (1957). Zweiphasige Flussablagerungen und Zweiphasenverwitterung in den Tropen unter besonderer Berücksichtigung von Surinam. Lautensach Festschr. Stuttg. Geogr. Stud., B. 69, 365–397.

Balsem, T., Rhebergen, G. J. (1979). Bodemgesteldheid en geomorfologie langs de Midden-Suriname en de Midden-Saramacca Rivier; Report Dienst Bodemkartering; Unpublished Report; Dienst Bodemkartering: Paramaribo, Suriname.

Bauer, B. O. (1993). [Review of Geomorphic Responses to Climatic Change, by W. B. Bull]. Geographical Review, 83(1), 114–116. https://doi.org/10.2307/215397.

Bleys, C. (1953). Over steenbanken bij het Brokopondoeiland (Suriname). Geol. Mijnb./Netherlands Journal of Geoscience, 15, 194–202.

Boll, J., Thewessen, T. J. M., Meijer, E. L., Kroonenberg, S. B. A. (1988). Simulation of the development of river terraces. Z. Fur Geomorphology, 32, 31–45.

Bridgland, D. (2000). River terrace systems in north-west Europe: An archive of environmental change, uplift and early human occupation. Quaternary Science Reviews, 19, 1293–1303. https://doi.org/10.1016/S0277-3791(99)00095-5

Brinkman, R. (1959). Bodemkartering Albina Zuid; Unpublished Report; Dienst Bodemkartering: Marowijne, Suriname.

Brinkman, R., Pons, L., Brinkman, R., Pons, L. (1968). A pedo-geomorphological classification and map of the holocene sediments in the coastal plain of the three guianas. In Soil Survey Papers; Soil Survey Institute: Wageningen, The Netherlands, 4, pp 40.

D'Apolito, C., Absy, M. L., Latrubesse, E. M. (2013). The Hill of Six Lakes revisited: New data and re-evaluation of a key Pleistocene Amazon site. Quaternary Science Reviews, 76, 140–155. https://doi.org/10.1016/j.quascirev.2013.07.013.

D'Audretsch, F. C. (1957). Geological Map 1:100.000 D7, Sheet Kabel; Geological Mining Services Suriname, 1 Map: Paramaribo, Suriname, 58.

De Boer, M. W. H. (1972). Landform and Soils in Eastern Surinam (South America); Pudoc: Wageningen, The Netherlands, p. 169.

Dowsett, H., Poore, R. (1991). Pliocene sea surface temperatures of the north atlantic ocean at 3.0 Ma. Quaternary Science Reviews, 10, 189–204. https://doi.org/10.1016/0277-3791(91)90018-P.

Duba, D. (1972). Report on Water Balance Studies, Public Water Supplies and Sewage, net-4, Suriname-2200; World Health Organization: Geneva, Switzerland, p. 100.

Fairbanks, R. G. (1989). A 17,000-year glacio-eustatic sea level record: Influence of glacial melting rates on the Younger Dryas event and deep-ocean circulation. Nature, 342, 637–642. https://doi.org/10.1038/342637a0

Garner, H. F. (1967). Rivers in the making. Scientiic American, 216, 84–94. http://www.jstor.org/stable/24931471

Gersie, K.; Augustinus, P.; Van Balen, R. (2016). Marine and anthropogenic controls on the estuary of the Suriname River over the past 50 years. Netherlands Journal of Geosciences, 95, 419–428. https://doi.org/10.1017/njg.2016.18.

Girjasing, R.; Kroonenberg, S. B.; Ramdajal, R.; Wong, T. (2019). Timing of the origin and uplift of the Bakhuis-Tambaredjo Horst, 27. Dowsett, H.; Poore, R. Pliocene sea surface temperatures of the north atlantic ocean at 3.0 Ma. Quaternary Science Reviews, 10, 189–204.

Groen, K. (2002). The Effects of Transgressions and Regressions on Coastal and Offshore Groundwaters. A Case Study of Suriname and Generic Studies into Groundwater Flow Systems, Salinity Patterns, and Paleo Groundwater. Ph.D. Thesis, Vrije Universiteit, Amsterdam, The Netherlands, p. 192.

Haq, B. U., Hardenbol, J., Vail, P. R. (1987). Chronology of fluctuating sea levels since the triassic. Science, 235, 1156–1167. DOI: 10.1126/science.235.4793.1156.

Haug, G. H., Hughen, K. A., Sigman, D. M., Peterson, L. C., Röhl, U. (2001). Southward migration of the intertropical convergence zone through the holocene. Science, 293, 1304–1308. DOI: 10.1126/science.1059725.

Haywood, A. M., Dowsett, H. J., Valdes, P. J., Lunt, D. J., Francis, J. E., Sellwood, B. W. (2009). Introduction. Pliocene climate, processes and problems. Philosophical Transactions A Math. Phys. Eng. Sci., 367 (1886), 3–17. https://doi.org/10.1098/rsta.2008.0205.

Hooghiemstra, H., Cleef, A. M. (1995). Pleistocene climatic change and environmental and generic dynamics in the North Andean montane forest and Paramo. In Biodiversity and Conservation of Neotropical Montane Forests; Churchill, S. P., Balslev, H., Forero, E., Luyeyn, J. L., Eds.; New York Botanical Garden: Bronx, NY, USA, 35-49.

Hoorn, C., Guerrero, J., Sarmiento, G. A., Lorente, M. A. (1995). Andean tectonics as a cause for for changing drainage patterns in Miocene northern South America. Geology, 23, 237–240. https://doi.org/10.1130/0091-7613(1995)023<0237:ATAACF>2.3.CO;2.

Jansen, E., Overpeck, J., Briffa, K. R., Duplessy, J. C., Joos, F., Masson-Delmotte, V., Zhang, D. (2007). Palaeoclimate. Contribution of working group I to the fourth assessment report of the Intergovernmental Panel on Climate Change, 2007. In Climate Change 2007: The Physical Science Basis; Cambridge University Press: Cambridge, UK.

Kips, P. H. A., Snel, A. R. (1979). Landschap, bodemgesteldheid en landgeschiktheid langs de Midden-Suriname Rivier (Goejaba–Botopassi); Unpublished Report; Dienst Bodemkartering: Paramaribo, Suriname, p. 229.

Kroonenberg, S., De Roever, E., Fraga, L., Reis, N., Faraco, T., Lafon, J.-M., Cordani, U., Wong, T. (2016). Paleoproterozoic evolution of the Guiana Shield in Suriname: A revised model. Netherlands Journal of Geosciences, 95, 491–522. https://doi.org/10.1017/njg.2016.10.

Kroonenberg, S. B., Melitz, P. J. (1983). Summit levels, bedrock control and the etchplain concept in the basement of Surinam. Geologie en Mijnbouw, 62, 389–399.

Kutzbach, J., Gallimore, R., Harrison, S., Behling, P., Selin, R., Laarif, F. (1998). Climate and biome simulations for the past 21,000 years. Quaternary Science Reviews, 17, 473–506. https://doi.org/10.1016/S0277-3791(98)00009-2.

Latrubesse, E., Stevaux, J., Sinha, R. (2005). Tropical rivers. Geomorphology, 70, 187–206. https://doi.org/10.1016/j.geomorph.2005.02.005.

Maddy, D. (1997). Uplift-driven valley incision and river terrace formation in southern England. Journal of Quaternary Science, 12, 539–545. https://doi.org/10.1002/(SICI)1099-1417(199711/12)12:6<539::AID-JQS350>3.0.CO;2-T

Martin, K. (1888). Aantekeningen bij een geognostische overzichtskaart van Suriname. Tijdschrift Koninklijke Nedederlands Aardrijkskundig Genootschap, 5, 444–453.

Martin, L., Bertaux, J., Corrège, T., Ledru, M.-P., Mourguiart, P., Sifeddine, A., Soubiès, F., Wirrmann, D., Suguio, K., Turcq, B. (1997). Astronomical forcing of contrasting rainfall changes in tropical South America between 12,400 and 8800 cal yr B.P. Quaternary Research., 47, 117–122. https://doi.org/10.1006/qres.1996.1866.

Meritts, D. J., Vincent, K. R., Wohl, E. E. (1994). Long river profiles, tectonism, and eustasy: A guide to interpreting fluvial terraces. Journal of Geophysical Research Space Phys., 99, 14031–14050.

Molnar, P., Cane, M. A. (2002). El Niño's tropical climate and teleconnections as a blueprint for pre-Ice Age climates. Paleoceanography, 17 (2), 11-1–11-11. https://doi.org/10.1029/2001PA000663.

Pazzaglia, F. J., Gardner, T. W. (1994). Late Cenozoic flexural deformation of the middle U.S. Atlantic passive margin. Journal of Geophysical Research Space Physics., 99, 12143–12157. https://doi.org/10.1029/93JB03130.

Peulvast, J. P.; Sales, V. C.; Bétard, F.; Gunnell, Y. (2008). Low post-Cenomanian denudation depths across the Brazilian Northeast: Implications for long-term landscape evolution at a transform continental margin. Global and Planetary Change, 62 (1-2), 39–60. https://doi.org/10.1016/j.gloplacha.2007.11.005.

Raymo, M. E., Lisiecki, L. E., Nisancioglu, K. H. (2006). Plio-pleistocene ice volume, antarctic climate, and the global σ^{18}o record. Science, 313 (5786), 492–495. DOI: 10.1126/science.1123296.

Roeleveld, W., Van Loon, A. J. (1979). The Holocene development of the young coastal plain of Suriname. Geologie en Mijnbouw/Netherlands Journal of Geoscience, 58 (1), 21–28.

Schumm, S. A. (1993). River response to baselevel change: Implications for sequence stratigraphy. Journal of Geology, 101 (2), 279–294.

Stange, K. M.; Van Balen, R.; Vandenberghe, J.; Peña, J. L.; Sancho, C. (2013). External controls on quaternary fluvial incision and terrace formation at the Segre River, Southern Pyrenees. Tectonophysics, 602, 316–331. https://doi.org/10.1016/j.tecto.2012.10.033.

Urrego, L. E. (1991). Sucesion Holocenica de un bosque de Mauritia flexuosa L.f. en el valle del Rio Caqueta (Amazonia colombiana). Colombia Amazónica., 5 (2), 99–118.

Van Balen, R., Van Der Beek, P., Cloetingh, S. (1995). The effect of rift shoulder erosion on stratal patterns at passive margins: Implications for sequence stratigraphy. Earth Planetary Science Letters, 134 (3-4), 527–544. https://doi.org/10.1016/0012-821X(95)98955-L.

Vandenberghe, J. (2015). River terraces as a response to climatic forcing: Formation processes, sedimentary characteristics and sites for human occupation. Quaternary International, 370, 3–11. https://doi.org/10.1016/j.quaint.2014.05.046.

Van der Hammen, T. A. (1963). Palynological Study on the Quaternary of British Guiana; Leidse Geologische Mededelingen: Leiden, The Netherlands, 29 (1), 125–180.

Van Der Hammen, T. (1974). The pleistocene changes of vegetation and climate in tropical South American Journal of Biogeography, 1, 3–26.

Van der Hammen, T., Absy, M. L. (1994). Amazonia during the last glacial. Palaeogeography, Palaeoclimatology, Palaeoecology, 109 (2-4), 247–261. https://doi.org/10.1016/0031-0182(94)90178-3

Van Der Hammen, T., Hooghiemstra, H. (2000). Neogene and Quaternary history of vegetation, climate, and plant diversity in Amazonia. Quaternary Science Reviews 19 (8), 725–742. https://doi.org/10.1016/S0277-3791(99)00024-4.

Van Der Hammen, T.; Urrego, L. E.; Espejo, N.; Duivenvoorden, J. F.; Lips, J. M. (1992). Late-glacial and Holocene sedimentation and fluctuations of river water level in the Caquetá River area (Colombian Amazonia). Journal of Quaternary Science, 7 (1), 57–67. https://doi.org/10.1002/jqs.3390070106.

Van Der Hammen, T., Duivenvoorden, J. F., Lips, J. M., Urrego, L. E., Espejo, N. (1992). Late quaternary of the middle Caquetá River area (Colombian Amazonia). Journal of Quaternary Science, 7 (1), 45–55. https://doi.org/10.1002/jqs.3390070105.

Veldkamp, A., Vandenberg, M., Veldkamp, T. (1993). Three-dimensional modelling of Quaternary fluvial dynamics in a climo-tectonic dependent system. A case study of the Maas record (Maastricht, The Netherlands). Global and Planetary Change, 8 (4), 203–218. https://doi.org/10.1016/0921-8181(93)90009-D.

Veen, A. W. L. (1986). On Geogenesis and Pedogenesis in the Old Coastal Plain of Suriname (South America); Dienst Bodemkartering Suriname: Amsterdam, The Netherlands, 1970; p. 176.

Vélez, M., Hooghiemstra, H., Metcalfe, S., Wille, M., Berrío, J. (2006). Late Glacial and Holocene environmental and climatic changes from a limnological transect through Colombia, Northern South America. Palaeogeography, Palaeoclimatology, Palaeoecology, 234 (1), 81–96. https://doi.org/10.1016/j.palaeo.2005.10.020.

Viveen, W., Schoorl, J., Veldkamp, A., Van Balen, R., Desprat, S., Vidal-Romani, J. (2013). Reconstructing the interacting effects of base level, climate, and tectonic uplift in the lower Mino River terrace record: A gradient modelling evaluation. Geomorphology, 186, 96–118. https://doi.org/10.1016/j.geomorph.2012.12.026.

Westaway, R., Bridgland, D., Mishra, S. (2003). Rheological differences between Archaean and younger crust can determine rates of Quaternary vertical motions revealed by fluvial geomorphology. Terra Nova, 15 (5), 287–298. https://doi.org/10.1046/j.1365-3121.2003.00497.x

Wijmstra, T. A. (1971). The Palynology of the Guiana Coastal Basin. Ph.D. Thesis, University of Amsterdam, Amsterdam, The Netherlands, p. 71.

Wong, T. (1986). Outline of the stratigraphy and the geological history of the Suriname coastal plain. Geologie en Mijnbouw/ Netherlands Journal of Geoscience, 65, 223–241.

Wong, T., De Kramer, R., De Boer, P., Langereis, C., Sew-A-Tjon, J. (2009). The influence of sea-level changes on tropical coastal lowlands; the Pleistocene Coropina Formation, Suriname. Sedimentary Geology, 216 (3-4), 125–137. https://doi.org/10.1016/j.sedgeo.2009.02.003.

Zeuner, F. E. (1945). The Pleistocene Period, Its Climate. Chronology and Faunal Successions. Nature 156, 730-731. https://doi.org/10.1038/156730a0.

Zonneveld, J. I. S. (1972). Sulas and sula complexes. Gottinger Geogr., 93–105.

Zonneveld, J. I. S. (1952). Waarnemingen langs de kust van Suriname. Tijdschrift Koninklijke Nederlands Aardrijkskundig Genootschap, 71, 18–31.



Chapter 5

Understanding westward deflection due to river-coast interactions in the Holocene coastal Plain of Suriname

Kathleen Gersie[2,3], David Klink[1], Pieter Augustinus[1], Jaap Nienhuis[1], Nisha Bharos[1], Iris de Vos[3], Steven de Jong[1]

Affiliations:
[1,] Department of Geosciences, Earth Surface and Water, Utrecht University, Utrecht, The Netherlands. d.t.klink@students.uu.nl; P.G.E.F.Augustinus@kpnmail.nl; j.h.nienhuis@uu.nl; S.M.deJong@uu.nl
[2,] Department of Geosciences, Anton de Kom University of Suriname, Leysweg 86, Paramaribo, Suriname. Kathleen.gersie@uvs.edu; nisha.bharos@uvs.edu.
[3,] Institute of Biodiversity and Ecosystem Dynamics, University of Amsterdam, Amsterdam, The Netherlands. k.gersie@uva.nl

ABSTRACT

The coastline of Suriname is part of the world's longest, continuous, muddy coast. This coastline is shaped by interactions with rivers, through river discharges, migrating mudbanks and mangrove forests. Suspended Amazon mud from the Amazon River Basin is crucial for the coastal development of the coast of the Guianas, and various factors have been suggested to influence the behaviour of river mouths along this coastline. The westward deflection of small river mouths is influenced by the interaction between fluvial and marine forces, and probably has started 6500 and 2500 yr BP during the development of the Young Coastal Plain. This coincides with the Wanica Phase in Suriname, which started after mid-Holocene sea-level stabilization, indicating a potential tipping point in the coastal system. In contrast with watershed size, both cheniers and, unexpectedly, seasonality displayed minimal influence on river behaviour. Here we investigate the key driving factors of westward deflection of rivers exhibited on the Suriname coast, how these factors interacted to influence river behaviour, and the development of the Young Coastal Plain during the Holocene. First, we identified which rivers across the Suriname Coastal plain currently exhibit westward deflection patterns, and which maintain a more direct course towards the Atlantic Ocean. We quantified river deflection, and explored the relationship with watershed size (as a proxy for river discharge). By estimating the age of river deflection points, we explored if these geomorphological features indicate a tipping point in the evolution of the Suriname coastal plain.

This research improves understanding of the Suriname coastal system by examining the interplay between coastal processes and fluvial forces. The findings contribute to understanding of the coastal evolution and providing useful information for coastline management.

Keywords: river, mudbank, deflection, watershed, progradation

1. INTRODUCTION

The coastline of the Guianas is part of the world's longest continuous muddy coast. This coastline is shaped by interactions with rivers, through river discharges, migrating mudbanks and mangrove forests, which are important for coastal progradation and to prevent coastal erosion. Alongshore migrating mudbanks act as natural protection barriers for the coastline as they absorb the energy of incoming waves (Toorman et al., 2018). Together with the present mangrove forests these mudbanks play a crucial role in both coastal progradation and erosion control.

Spatial variations in sediment deposition are evident along the Guianas coast. This coastline displays uneven development with notable differences in sediment deposition across the region. A bend in the Guiana Shield near western Suriname has enabled substantial coastal accretion. Alongshore migrating sediment has favoured settling in this bend in the Guiana Shield, because it is a favourable concave section of the coastline. As a result, in western Suriname there is considerably more coastal accretion compared to eastern Suriname (Augustinus, 1978).

In Suriname, sedimentation phases alternated with short periods of coastal erosion (Augustinus, 2004). Most coastal sediment deposits are formed by cheniers and most cheniers are concentrated in eastern and central Suriname (Fig. 1) because of the sand supply from the Marowijne and Mana Rivers or due to the winnowing from the mud originating from the Amazon river (Berrenstein, 2010). These sediments are characterized by wave-reworked shell and sand deposits, and are transported along the coast (swash/backwash and littoral drift processes). In western Suriname cheniers are scarce because the winnowing process takes a lot of time and due to the lack of local sand supply. The cheniers mark old coastlines, and are important geomorphological markers that offer insight into the historical evolution of the coastal plain (Augustinus et al., 1989).

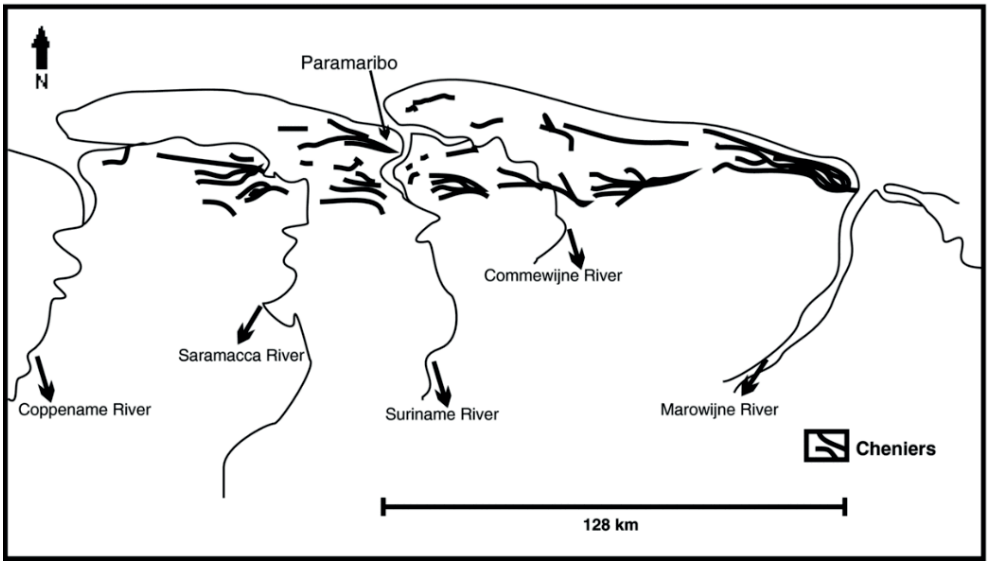


Figure 1: Schematic map of central and eastern Suriname with simplified cheniers in the coastal plain (Zonneveld, 1968; Gersie, 2016)

Satellite imagery clearly reveals a pattern of selective westward deflection among rivers in the Suriname coastal plain (Fig. 2). This phenomenon represents a complex dynamic of geomorphological processes with implications for the local population and environment. The contrast between deflecting rivers (e.g. Saramacca, Commewijne, and Cottica Rivers) and those maintaining direct courses (e.g. Corantijn and Marowijne Rivers) as they approach the Atlantic Ocean suggesting complex underlying mechanisms.

The Young Coastal Plain consists of heavy clays alternated with sand and shell cheniers. There are mainly levees tied to the historical or present course of local rivers which also consist of heavy clays. Rivers flowing from south to north often had to adapt to the development of the coastal plain, and have in some cases deflected in more or less western direction. Zonneveld (1955) described the development of the eastern part of the Suriname coast during the Wanica phase, where ridge formation prevented the Cottica River drainage system discharging into the Atlantic Ocean, and ultimately join the Commewijne River (Fig. 3).

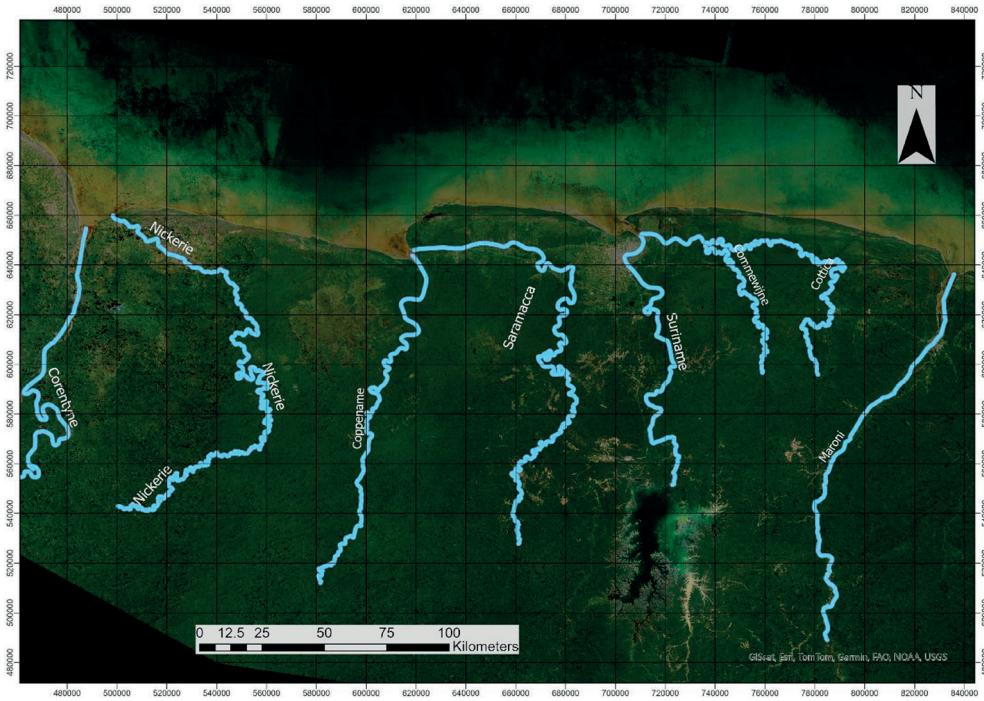


Figure 2: Major rivers in Suriname showing varied behaviour in the coastal plain. The Saramacca, Commewijne, and Cottica Rivers display pronounced westward deflection, while the Nickerie River shows deflection without a clear point of change in orientation. The Coppename and Suriname Rivers exhibit deflection only near their mouths. In contrast, the Corantijn and Marowijne Rivers maintain direct courses to the Atlantic Ocean without substantial deflection (Source: OpenStreetMap, 2024).

This coastal plain has substantially developed since the Pleistocene with the deposition of the Old Coastal Plain. In the first millennia of the Holocene (10.000 C^{-14} years ago to present), global sea level rose due to melting of ice caps in the northern hemisphere. However, about 6000 years ago the ice in Northern America and Scandinavia had run out, ending the glacio-eustatic component of sea level rise, and which has thus caused sea levels to rise more slowly since then (Wong et al., 2016). The Young Coastal Plain of Suriname consists of the Mara Formation and the Coronie Formation (Brinkman & Pons, 1968). While the Mara Formation was deposited in the Early Holocene during a rapid sea level rise, the Coronie Formation started approximately 6000 years BP when sea level rise started to cease (Van der Hammen, 1963). The latter consists of three phases of sediment deposition, dated by Brinkman and Pons in 1968, i.e. the Wanica phase (6000-3000 years BP), Moleson phase (2500-1300 years BP), and Comowine phase (1000 years BP – Present).

Phases of erosion occurred in between these three depositional phases, due to variations in sediment supply from the Amazon River, possible shifts in sea levels (Nedeco, 1968) and wind directions. These two phases of erosion or non-deposition coincide with radiocarbon dating of Delaney (1966) in the central part of the Young Coastal Plain showing two distinct

sets of cheniers (Augustinus, 1989). The alternation in accretion and erosion phases is very important, as it indicates that the development of the coast appears to be substantially impacted by sediment supply from the Amazon River in combination with coastal geomorphological processes. It is unknown how the river's courses did keep up with the development of the Young Coastal Plain up during the Holocene and how this has impacted the deflection of small rivers.

Mudbanks, wind direction, and ocean currents

The coastal development of Suriname is substantially influenced by sediment supply from the Amazon River basin of which 20% is transported westward along the coast towards the Guianas (Eisma et al., 1991). According to Wells and Coleman (1978), approximately 150 million tons migrate west in suspension, while 100 million tons are stored in mudbanks. Mudbanks, defined by Wells & Coleman (1981b), are mostly muddy subtidal features, obliquely attached to the coast through its subaerial intertidal extension (Fig. 3). This suspended Amazon mud is crucial for the coastal development of the Guianas. The South Equatorial Current (SEC) flows from Sub-Saharan Africa towards Brazil, and splits up in the Brazilian Current (BC) and the North Brazilian Current (NBC) near the coast of Brazil. The resulting Guiana Current along the coast of the Guianasis then is created, as the NBC encounters the North Equatorial Current (NEC). Driven by the Trade winds, waves, and the Guiana Current (Allison and Lee, 2004; Augustinus, 2004), the Amazonian mud continues in northwestern direction, while the coast deflects to the west. This creates a kind of blind spot off the coast of Suriname and Guyana, in which a weak residual current causes the water to flow westward.

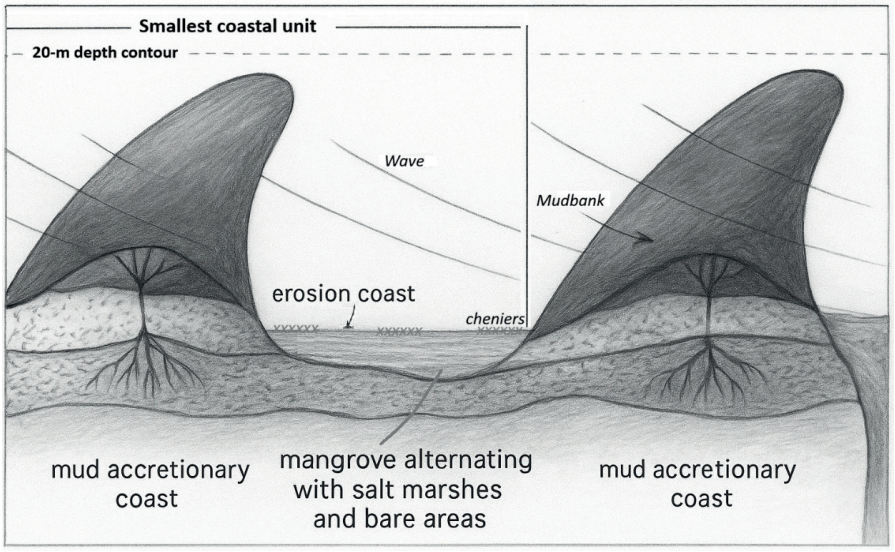


Figure 3: Simplified non-scale sketched map of the smallest coastal unit of Suriname (modified after Augustinus, 2004)

Augustinus (2004) explained the driving force of wind direction in correlation with westward mudbank propagation. As a result of high suspended matter concentration, fluid mud is formed in the western (front) part of a mudbank. The northeastern Trade Winds with average wind speeds of 3 to 9 m/s (De Vries et al., 2022) generate waves that migrate towards the coast of Suriname. These generated waves transform into solitary waves as they move over the mudbanks, pushing fluid mud towards the shore, and enhancing the deposition on the western (front) flank of the mudbank (Wells & Coleman, 1981). As the mud bank migrates westward, compaction increases due to physical maturation and water extraction by the mangroves, and the originally soft mud turns into a young clay. This can be eroded due to the lack of wave-attenuating properties. In between mudbanks, the interbank area (Fig. 3), waves can propagate directly toward the shore until they break. The average alongshore width of mudbanks along the Guianas coast is 30 km (Chevalier et al., 2008), while the average alongshore width of mudbank and interbank area combined is 45 km (Augustinus, 2004). Westward migration speeds of mudbanks range from 500 meters per year to a maximum of 5 km per year, with an average of 1.5 km per year. This indicates an approximately 30-year cycle (Augustinus, 2004).

Wind direction is crucial in the shape and migration of mudbanks. As northeastern trade winds gain a stronger northern component and thus a weaker eastern component, waves will propagate from a northern dominant direction. This tends to increase the cross-shore wave energy component, resulting in stronger erosion. In the case of a more eastern dominant component in northeast trade winds, the longshore wave energy component is enhanced. Promoting the long-shore transport of sediment, resulting in longer mudbanks (Augustinus, 2004).

Littoral steering and river deflection

The behaviour of river mouths is greatly impacted by the interaction between fluvial and marine forces. The river mouths are shaped by the balance between river discharge, wave energy, and alongshore sediment transport (Anthony, 2015; Nienhuis et al., 2016a; Nienhuis et al., 2016b). A key process in this system is littoral steering, where wave-driven currents and sediment transport influence river mouths along the coast. Waves breaking at an angle to the coastline drive alongshore sediment transportation (Komar, 1971). This connects to the northern and eastern components of the northeastern Trade Winds discussed by Augustinus (2004), and highlighting the importance of wind direction on erosion and sediment transport. Furthermore, Ashton and Murray (2006a; 2006b) concluded that sediment transport is optimal at an approach angle of approximately 45 degrees. Coincidentally, waves approaching Suriname mainly are driven by northeastern Trade winds, resulting in an optimal approach angle for alongshore sediment transport. Alongshore sediment transport is interrupted by river discharge near at the river mouth, which can act as a 'hydraulic groin' and partly or entirely block the alongshore sediment transport (Zenkovich, 1967). As summarized by Nienhuis et al., (2016a), studies of Dominguez (1996) and Zenkovich (1967) indicate that

this blockage results in sediment build-up updrift from river mouths with strong river discharge, and limits alongshore sediment bypassing, which drive the formation of mud capes updrift from river mouths and initiates migration of river mouths.

In essence, the key factors of driving downdrift river mouth migration are (1) Alongshore sediment flux, (2) Wave energy and direction, (3) Sediment bypassing at the river mouth (Nienhuis et al., 2016a). Sufficient alongshore sediment supply is necessary to migrate the river mouth downdrift, otherwise no downdrift migration occurs. Furthermore, consistent waves with an approach angle of around 45 degrees aids in pushing the sediment along the coastline. Lastly, river discharge and fluvial sediment influence sediment bypassing along the river mouth. These fluvial influences can act as a barrier, limiting sediment bypassing and promoting updrift sediment accumulation which forces a river mouth to shift downdrift.

Accretion, Erosion and Rivers

Throughout history the Suriname coast has displayed a net accretion on large timescales of 1000 years and more (sediment cycles of the Holocene). However, erosion has also occurred on the scale of the 30-year mudbank cycle which is part of the migrating mudbank system (Augustinus, 1978). An example of an area currently subject to severe erosion is the Weg Naar Zee area north of the city of Paramaribo. High-energy waves from the ocean continuously cause a cycle of coastal accretion and erosion as a result of natural and anthropogenic activities. This part of the coastline is receding partly thanks to the removal of natural protective barriers such as mangroves. In contrast, areas such as Braamspunt mud cape, updrift of the Suriname River, and Coppename mud cape illustrate zones of coastal progradation. As the mudbanks migrate westwards along the coast of the Guianas, they eventually encounter river mouths. At these junctures, the sediment at a certain point must traverse the river mouth. This process involves a combination of forces driving westward migration of mudbanks, while at simultaneously river discharge interrupts this alongshore movement. Consequently, sediment effectively "jumps" across the river mouth to continue its migration along the coast.

Some rivers are effective in flushing out the sediment at their river mouth, even when a mudbank is passing in front, while others are struggling to do so. This difference likely contributes to the varying westward river behaviour in the coastal plain of the Guianas. Rivers with relatively low discharge, such as the Cottica/Commewijne, Nickerie, Saramacca Rivers, Mana, and Counamama Rivers, tend to exhibit pronounced westward bends near the coastline, with some even discharging into larger rivers. Rivers with higher discharges, such as the Suriname and Coppename rivers, display a smaller westward bend, while the Marowijne River and Corantijn River, which have even greater discharges, show no signs of westward bending and both flow directly into the ocean. While various factors have been suggested to influence the westward deflection of rivers in the Guianas, a comprehensive understanding of how these factors interact over time remains minimally explored.

In this study we investigate the Holocene course of the main rivers during the development of the Young Coastal Plain, the phenomenon of westward deflecting rivers in the Suriname Coastal plain, and the role of mudbanks and cheniers influencing this river behaviour. The aim is to determine how the main local rivers have kept pace with the development of the Young Coastal Plain and provide a comprehensive overview of the key factors, such as mudbanks and cheniers, driving westward river deflection. Therefore, it is important to understand the correlation between river discharge and the westward deflection of river mouths. To do so the following research question is formulated: What are the key drivers behind the westward deflection of small rivers in the Holocene Young Coastal Plain of Suriname? The sub-questions are as follows: 1) how did the Young Coastal Plain develop during the Holocene? 2) How did the Braamspunt and Coppenamepunt mudcapes change in surface area in the last decades? 3) What is the orientation of the main river courses in the coastal plain?, and 4) Can we quantify and date river deflection quantification?

2. METHODS

2.1 SITE DESCRIPTION

The coastal plain of Suriname (4°-6° NB; 54°-56° WL) mainly comprises sedimentary deposits consisting of marine clay, silt and sand overlying the old bedrock formations. In comparison, the coastal region substrate is more prone to changes due to the highly dynamic coastal environment compared to the less dynamic environment of the inland area. This contrast between the inland and coastal regions results in distinct geomorphological processes. The inland area provides a relatively stable geomorphological setting, due to the resistant rocks of the Guiana Shield (Fig. 4). This limits river incision and river movement. In contrast, the coastal plain is comprised of sedimentary deposits, which are more susceptible to geomorphological changes.



Figure 4: Map of the Guiana Shield (compiled after Esri, 2025). The natural curve in the Guiana Shield at the border area between Guyana and Suriname has been gradually filled with sediment throughout the Tertiary and Quaternary Periods, resulting in the region's widest coastal plain

2.2 DATA COLLECTION

2.2.1 Satellite imagery and timeseries creation

A timeseries of Landsat (5 and 8) satellite imagery was used to observe and analyse changes in the coastal morphology, river pathways and to get a detailed overview of the area throughout the last decades. A 5-year interval was selected, to capture long term changes and patterns, starting in 2024 until 1989. Through Google Earth Engine (GEE) the pre-processed imagery was gathered, further processed and compiled into a near cloudless mosaic. Images were collected based on range up to a year wide with a focus on the dry season, as the research area is prone to clouds above the land mass, to filter out the clouds and take the median pixel. Subsequently, the mosaic was combined into one GeoTIFF file. The Landsat imagery used in this study contains a spatial resolution of 30 meters per pixel. The main spectral bands used in this study are the visible and near-infrared bands, chosen to observe changes in the landscape and differentiate water from land using the Normalized Different Water Index (NDWI) index. Furthermore, all imagery and maps in this study were projected to UTM Zone 21N Zanderij 1972.

2.2.2 Historical maps

We used both analogue and digital historic topographical maps compiled from former department of Central Department of Aerial Mapping (CBL) and online sources. As usable satellite imagery for the study area ends in the 1980s due to a decrease in quality, historic maps are a decent alternative to explore the landscape of the past. The gathered historical maps range from the 1970s to the 18th century and beyond. The scale of used maps ranged from 1:40.000 to 1.200.000. It is worth noting that older maps are less accurate. Maps dating from colonial times often focused on plantations and were less focused on the accuracy of the landscape. The map scans contain drawn maps, maps based on 20th century areal pictures and thematic maps (geological, geomorphological, soil). These Geo TIFF files were loaded into ArcGIS Pro and georeferenced. Georeferencing was performed by matching landmarks on the map, that were possible to locate on the 2024 Landsat 8 mosaic satellite image. This allowed for exploratory research and ultimately provided a continuation to the satellite imagery, which aided in the possibility to detect changes in river orientation in the coastal plain and coastline changes.

2.3 DATA ANALYSIS

First, to analyse progradation rates, we reconstructed the development of the three different phases of the Young Coastal Plain (Zonneveld, 1955) using cheniers as a reference for former coastlines (Augustinus, 1978). Secondly, to determine the orientation of the coastline, we created manual river mouth points at the middle of each river's outlet. Furthermore, channel width was measured in the coastal region for each river. Subsequently, a buffer zone around the river mouth, ten times the width of the river, was created to clip the coastline around the river mouth. This established a local coastline in ratio with the size of the river. The Simplify Line tool was used to determine an average coastline of which the orientation was measured.

Mudcape analyses were conducted on Braamspunt (near the Suriname River) and Coppenamepunt (near the Coppename River), in order to track changes in the surface area throughout the last decades. Satellite time series were used as the basis for this analysis. An arbitrary part near the spit of both mudcapes was clipped, subsequently NDWI was used to make both a water and a land polygon, such that the land polygon could be tracked. This resulted in observable changes as a slideshow, while also graphs of the area increase or decrease for each 5-year interval. The year 1987 marks the start of the satellite time series. Therefore, analyses of the Braamspunt mudcape near the Suriname Rivier mouth, was conducted between 1987 and 2024.

2.3.1 River Deflection Quantification

We used two methods to quantify river deflection behaviour in the Young Coastal Plain, which means a clearly observably change in river orientation in the coastal region. The first method (A), determined the orientation of a straight line drawn from the last bend across the middle of the river towards the river mouth, with the coastline rotated to a horizontal line (Fig. 5). The second method (B), determined the deflection angle based on a clearly observable change in river orientation in the coastal zone. If there is a clearly observable change, two lines were drawn. One for the average orientation before the change, while the other is for the part of the river after the change. Between these two lines, the river deflection angle was determined on the left-hand side of the river lines. If no clear change was observed of river orientation in the coastal region, only one line was drawn, meaning no river deflection (Appendix A.1-2). Since both methods are comparable, and only 3 data points were used on method B, we only focused on method A.

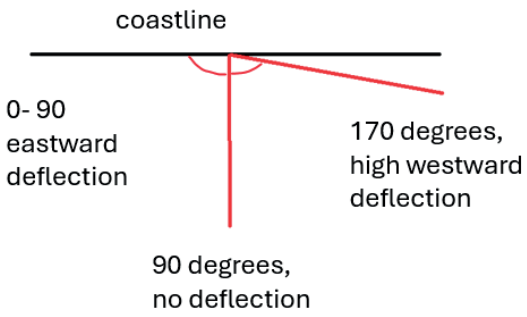


Figure 5: Method A for river deflection. Local coastline is rotated to horizontal axis

2.3.2 Dating of river deflection points:

Rivers in the Young Coastal Plain such as the Cottica, Commewijne, Saramacca, Nickerie show a clear change in river orientation. First, their points of river deflection was identified followed by the measurement of the distance to the coastline. To estimate the age of the deflection points, progradation rates were calculated for the coast near each river by measuring the distance from the start of the Young Coastal Plain deposits till the coastline and dividing this by 6000 years, the onset of the evolution of the Young Coastal Plain. The age of the river deflection points was then calculated by dividing the measured distance between deflection point and the current coastline and dividing it by the progradation rate.

3. RESULTS

3.1 PROGRADATION RATES

To address research question 1, we analysed old topographical maps (scale 1:40.000). The results indicate that the Wanica phase, marked as the start of coastal progradation, was more developed in the east, while the Moleson phase was more developed in the west "filling up" the characterizing bend in the Guiana Shield between Suriname and Guyana. From a 1000 years ago up till now the Comowine phase started to develop (Fig. 6). Since then the coast has prograded over a distance of approximately 20 km in the east and 60 km in the west. The influence of cheniers was and still seems minimal in the coastal development and these cheniers have followed the rivers' course. Before the Wanica phase no westward deflection of rivers is noticed, so during this phase the system must have changed resulting in the deflection of small rivers.

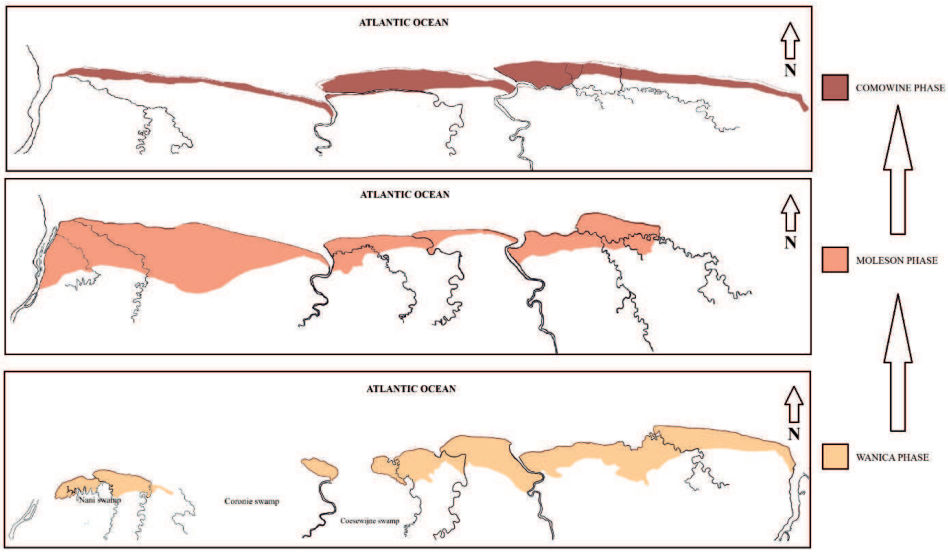


Figure 6: Non-scale schematic representation of the development of the Wanica, Moleson and Comowine phase in the Young Coastal Plain in Suriname

Many rivers in Suriname have been relatively stable over the last centuries, and show minimal changes in the major part of their course. Comparison between historical topographic maps and current satellite imagery show no notable changes (e.g. the Cottica River on map from 1882 and 2019 (Fig. 7), despite the inaccuracy of maps made in the 19th century). However, along the coastline rivers are considerably more dynamic compared to the terrestrial interior.

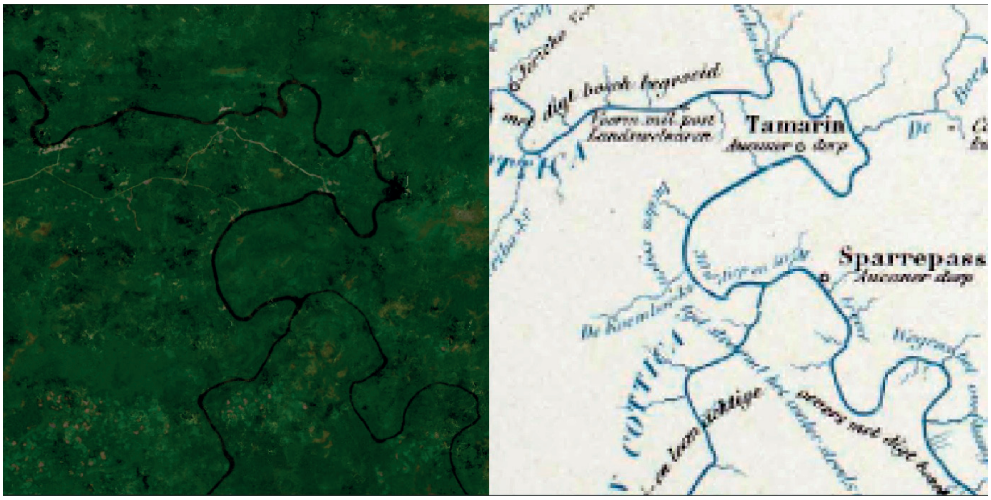


Figure 7: Cottica River, Suriname. A) 2019 Landsat 8 mosaic image. B) Map of northern Suriname 1882

3.2 MUD CAPE ANALYSIS

The Braamspunt mudcape has mainly decreased in size since 1987 (Fig. 8). The largest decrease in surface area occurred between the sandspit and circa 10 km east of the spit. From 1987 to 1999 there was a steady decrease of approximately 400 m^2 per year (Appendix B.1), while from 1999 to 2014 minimal changes of the area size occurred. However, a steady decline of roughly 600 m^2 occurred. Comparison of the change of each interval with the previous one first shows a decrease, then a period of net stability, followed by period of area decrease (Appendix B.2).

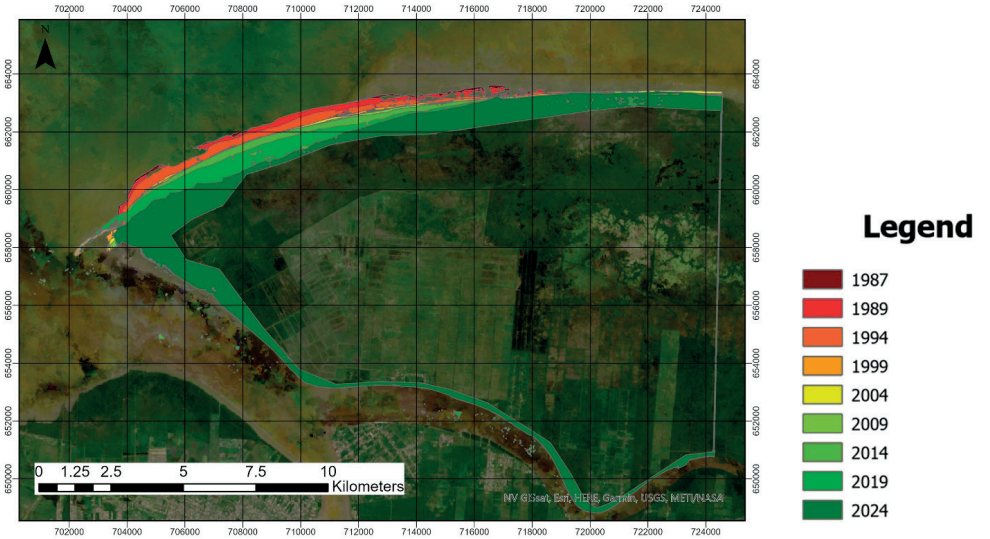


Figure 8: Surface area changes of the Braamspunt mud cape

3.2.1 Coppenamepunt

In contrast with the Braamspunt mudcape, the Coppenamepunt mudcape mainly increased in size. The Coppenamepunt mudcape is characterized with a relatively flat coastline and a square shaped front (Fig. 9). From 1987 until 1994 the size in surface area has increased, with minimal changes between 1994 and 1999 (Appendix C.1). From 1999 to 2014, a notable increase of approximately 5 km^2 per year occurred. From 2014 to 2024 minimal changes in the surface area occurred. Appendix C.2 reflects these changes, indicating cyclicity. The area change of Coppenamepunt cape displays the inverse of Braamspunt cape. While Braamspunt cape decreases, becomes stable, and decreases again, Coppenamepunt cape increases, becomes stable, increases again, and stabilizes again.

In 2024, the cape has substantially prograded, and has its shape changed from convex to concave due to the land mass increase. Simultaneously, the coastline appears more fragmented, with a patchier structure.

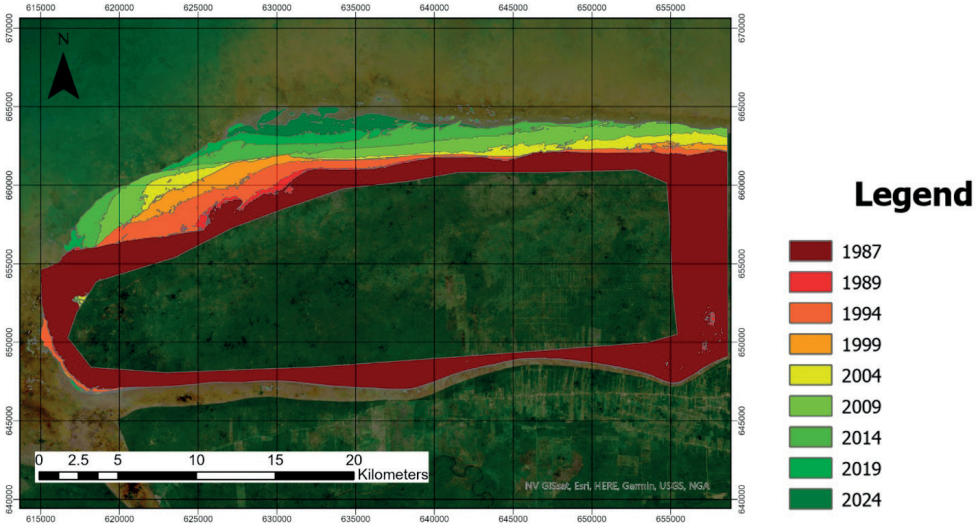


Figure 9: Change in surface area of Coppenamepunt mud cape from 1987 till 2024 (©Landsat 8, 2024 RGB image as base layer).

3.3 RIVER DEFLECTION ANALYSIS

To answer research question 3 we analysed the orientation of river courses and the deflection of their river mouths. Rivers in Suriname flowing from south to north show a minimal deflection or a westward deflection of their river mouth (Fig. 10).

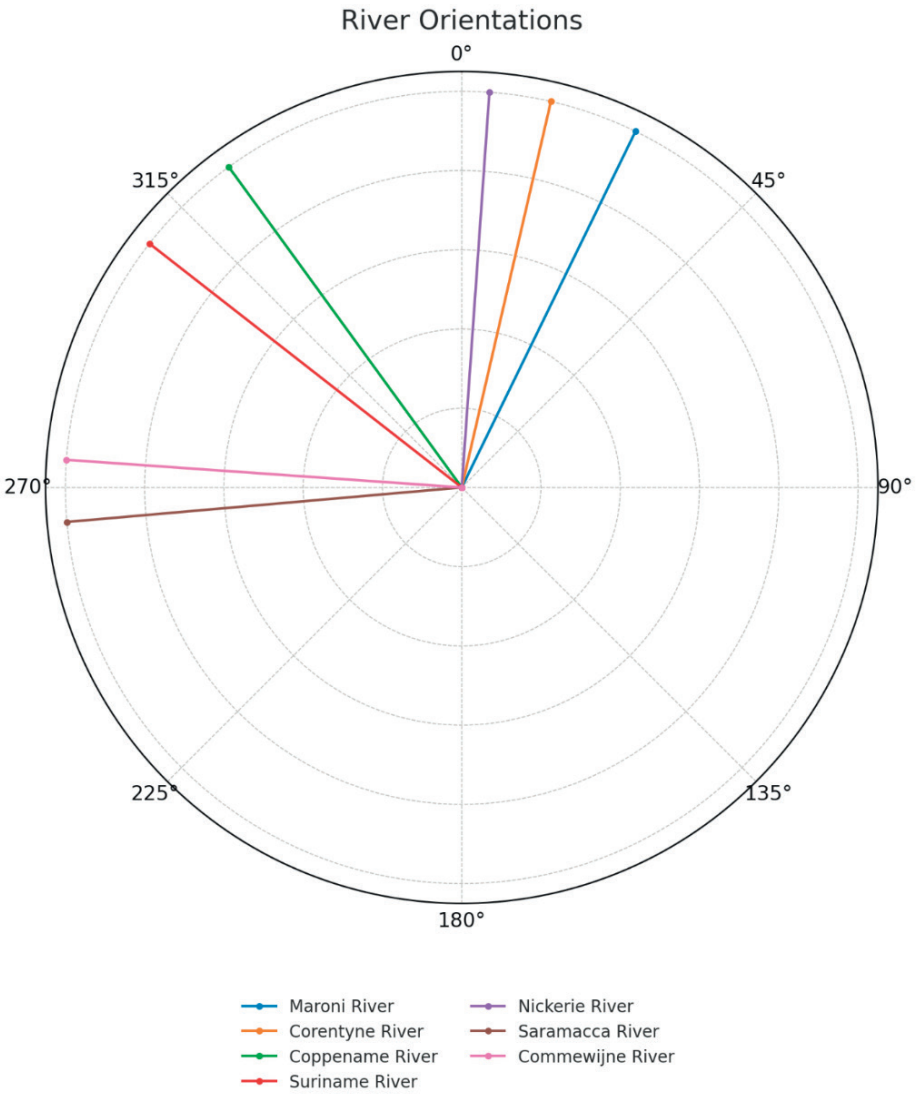


Figure 10: Orientations of the main rivers in Suriname

3.3.1 Watershed area vs. deflection angle (method A)

There is a positive relationship between the angle on which the river approaches its local coastline and the watershed area of the river (Fig. 11 & 12). There is a large spread for rivers with a watershed area smaller than 30.000 km^2. On the contrary, rivers with a relatively large watershed area (larger than 50.000 km^2), have a deflection angle between 86 and 104 degrees. Of such rivers, the Corantijn River angle is above 90 degrees, indicating a minimal westward deflection. While the Marowijne River angle is slightly below 90 degrees. Of the rivers with a watershed area below 30.000 km^2 only the Nickerie Rivers angle is below 90 degrees. This indicates that almost all rivers with a relatively small watershed area have the tendency to

deflect westwards. Considering the data on a country-by-country basis it emphasizes notable differences. Rivers in French-Guiana have relatively high deflection angles between 134 and 175 degrees, but the watershed areas are rather small. Guyana rivers have a more moderate deflection angle compared to rivers in French-Guiana, with deflection angles ranging mostly between 100 and 120 degrees. Suriname has a large spread in both deflection angles and watershed areas and is the least clustered of all three countries.

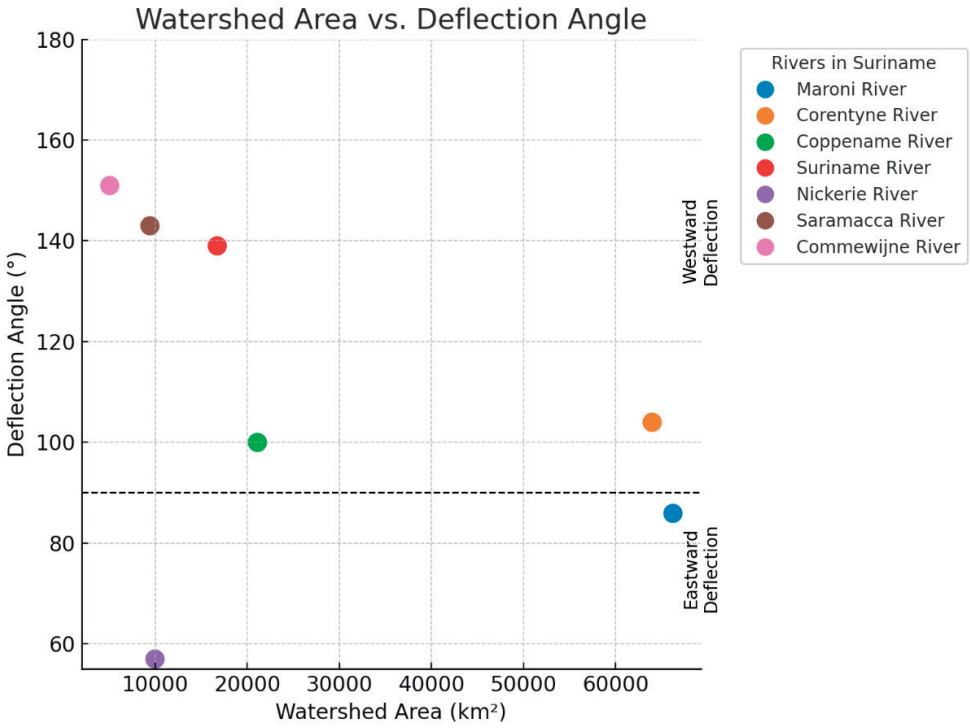


Figure 11: Regression plot between watershed area (proxy for discharge) and deflection angle (method A)

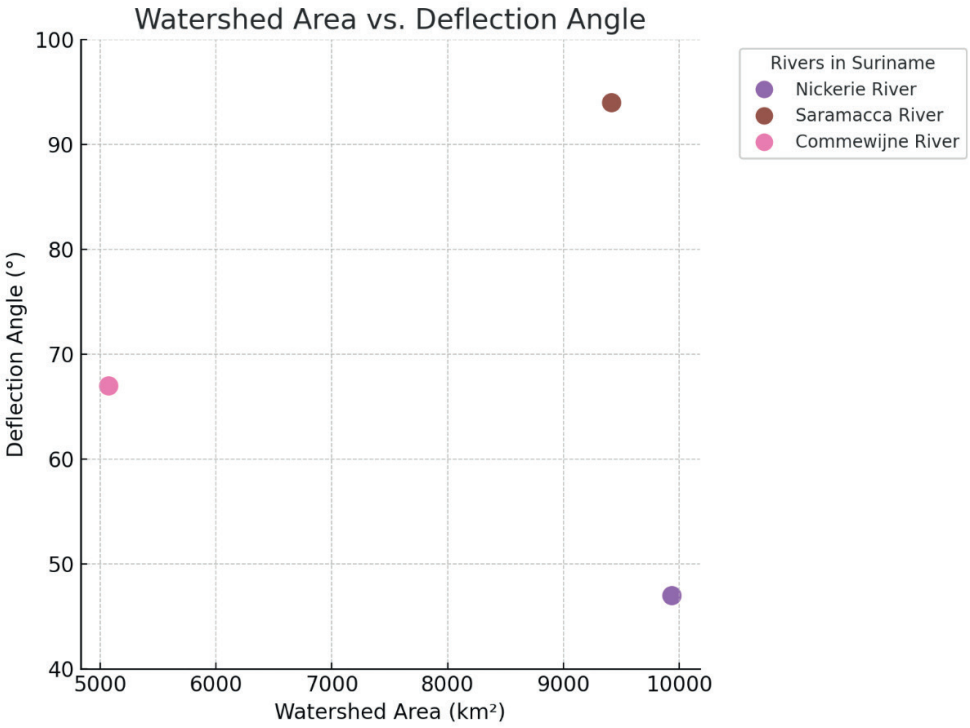


Figure 12: Regression plot between watershed area against deflection angle (method B)

3.3.4 Age of river deflection

Focussing on deflecting rivers in the coastal plain of Suriname, four rivers have been plotted to connect the start of river deflection with the evolution of the coastal plain. The determined points of river deflection for the Cottica, Commewijne, and Saramacca Rivers range from 16 to 20 km from the current coastline, while the deflection point of the Nickerie is a distinct outlier with roughly 42 km inland from the coastline. A clear progression of increasing distance to the coastline from east to west is illustrated in Figure 13. Dating of the point of river deflection determined by rough estimates of progradation rates for the coastal section of each river does not exhibit a west to east progression. Instead, estimated ages range from 2600 yr BP to 6500 yr BP. In contrast to the distance to coastline, now the Commewijne River is the outlier with a point of deflection dated substantially closer to the present. Excluding the Commewijne River results in a range of 4700 yr BP – 6500 yr BP as suggested in earlier studies (Fig. 13) .

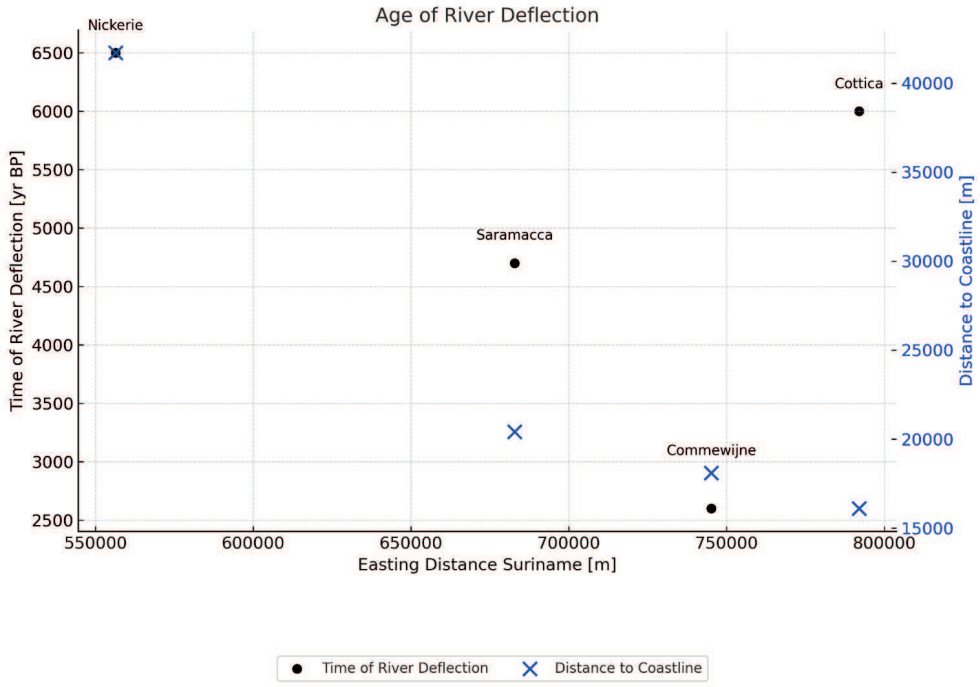


Figure 13: Distance of point of river deflection to coastline and estimated age of point of river deflection for four rivers in Suriname

5. DISCUSSION

5.1 MAIN FINDINGS

The results indicate that the influence of westward migrating mudbanks on river deflection of rivers along the Suriname coast is especially evident in the pronounced westward bend. This is observed in the terminal sections of low-discharge rivers as they approach the coastline, where coastal processes such as wave action, alongshore sediment transport and ocean currents are most active. The observed river mouth changes and the alternated progradation and retrogradation of mud capes seem to correlate with ocean current, wave action, and wind direction being the key drivers of westward mudbank migration (Allison and Lee, 2004; Augustinus, 2004). These processes directly and indirectly impact the morphological behaviour of rivers. While a correlation between river discharge and the degree of deflection was identified using different methods, this relationship was less than initially anticipated, with smaller rivers such as the Commewijne and Saramacca Rivers exhibiting a large range of deflection angles. Analysis of the chenier formations in Suriname indicated negligible influence on overall river patterns. Furthermore, discharge seasonality illustrated limited impact on river deflection, despite an apparent logical correlation (discussed later). These findings highlight

the complexity of the main influencing factors and their interactions driving westward river deflection in the Guianas. And highlight the need for full understanding of this complex coastal system, which could aid in deciphering its coastal evolution.

5.1.1 River deflection

The dominant role of alongshore sediment transport in driving the westward river deflection is supported by the observed coastal changes that appear when a mudbank migrates in front of the river mouth of a low-discharge river, like the Sinnamary River, French-Guiana. This results in progradation of the coastline. Mudbanks protect the coastline from erosion by high-energy wave impact, creating favorable conditions for mangrove colonization of the low energy mudbank area. Simultaneously, this alongshore sediment transport is the driving force behind the downdrift migration of the river mouth as the lack of suspended sediment concentration and low discharge result in a limited 'hydraulic groin' effect. Consequently, the alongshore sediment transport (or bypassing) is uninterrupted, which according to the proposed framework by Nienhuis et al. (2016a) facilitates downdrift migration of the river mouth, since sediment is more easily distributed along the coast. This explains why some rivers like the Pomeroon, Waini and Sinnamary Rivers have long river channels parallel to the coastline, while lacking large mud capes. On the contrary, rivers like the Suriname and Coppename Rivers in Suriname and Berbice Rivers in Guyana do have pronounced mud capes, while having limited westward migration of the river mouth. This implies an increased effect of fluvial forces, acting as 'hydraulic groin', which interferes with alongshore sediment transport, resulting in reduced sediment bypassing at the river mouth leading to sediment accumulation updrift from the river mouth (Zenkovitch, 1967). In turn, this sediment accumulation leads to pronounced mud capes like Braamspunt and Coppenamepunt updrift from the Suriname and Coppename Rivers. Although the watershed sizes of the Suriname and Pomeroon Rivers suggest similar overall discharge, marked differences exist in river mouth migration and mud cape dimensions. A critical factor distinguishing these rivers is that the Suriname, Coppename and Berbice Rivers receive additional discharge from smaller rivers becoming tributaries near their mouths: for example, the Commewijne and Cottica Rivers discharge into the Suriname River; the Saramacca River into the Coppename River; the Canje River into the Berbice River. This confluence results in a higher combined discharge, which enhances fluvial force (hydraulic groin effect), thereby reducing downdrift migration of the river mouth and facilitating pronounced mud cape formation. It should be noted that using watershed area as a proxy for river discharge in this research does not account for this influence. The Essequibo River in Guyana, and the Marowijne and Corantijn Rivers in Suriname do not fit the proposed framework by Nienhuis et al., (2016a). These rivers display minimal river deflection and no mud cape formation, despite the relatively high discharge in comparison to other rivers along the Guianas coast. A study about sediment accommodation in the Marowijne River estuary may help explain the absence of mud capes and river deflection. It highlights the strong discharge and tidal influence in the Marowijne River estuary, indicating high-energy conditions. Furthermore, Amazon-derived mud enters the estuary

during the dry season, however this mud is pushed offshore during the rainy season during which the discharge can increase from the average 1700 m^3/s to 3500 m^3/s (Gardel et al., 2021). This emphasizes the hydraulic groin effect driven by high-discharge conditions, while underscoring the role of seasonality.

The impact of river discharge on westward river deflection can be conceptualized as a dynamic equilibrium between marine-driven alongshore sediment flux and fluvial forces that disrupt this process. A gradual relationship between river discharge and river deflection would seem logical, as low discharge favors river deflection, while increasing discharge eventually results in complete disruption of the river deflection driving forces. However, the relationship between deflection angle and river discharge is weaker than expected. The high range in river deflection angles among low-discharge rivers and clear limited deflection for the few rivers with high discharge are clearly illustrated in Figures 11 and 12. This outcome may be influenced by that the confluence of rivers is not accounted for in the watershed as a proxy for discharge method, instead converging rivers like the Saramacca and Coppename Rivers are separated. Second, determining river deflection is complex which may contribute to the high spread among low-discharge rivers.

5.1.2 Holocene coastal development

The westward deflection of small rivers probably must have started 6500 and 2500 yr BP, during the development of the Young Coastal Plain, because major changes in river orientation mainly occur near the coastline. For the Cottica, Commewijne, and Saramacca Rivers a clear point of deflection could be determined, however for the Nickerie River the point of deflection is uncertain. A distinct bend in the river is situated relatively far inland compared to the other rivers and coincides with the relatively fast progradation rate of western Suriname. However, it is unclear whether this deflection is the result of local morphology or river-coast interactions.

Estimating the age of river deflection points introduces uncertainty, as this approach relies on the extent of the Young Coastal Plain deposits to derive progradation rates near each river. These progradation rates roughly align with suggested progradation rates in previous studies. The progradation rates used for these rivers are between 2.7 and 6.8 m/yr, while suggested average progradation rates for Suriname range between 2 and 8 m/yr (Augustinus, 1978; Pearson et al., 1986). The outlier of the age estimations of the river deflection points is the Commewijne River with a substantially younger deflection age of 2500 yr BP (Comowine Phase) (figure 7), while the other deflection ages are between 4500 and 6500 yr BP. Deposits of the Young Coastal Plain from the Wanica Phase are situated substantially farther inland near the Commewijne River in comparison to the Saramacca and Cottica River. All estimated river deflection ages correspond with the Wanica Phase. This suggests that the onset of the Wanica Phase, coinciding with mid-Holocene sea-level stabilization, triggered a shift in the regional coastal dynamics, resulting in the westward river deflection patterns observed today.

5.1.3 River seasonality

The DSI analysis implies minimal correlation between seasonal discharge fluctuations and long-term river deflection. While discharge variability, such as droughts or storm-driven discharge, affects seasonal river-coast interactions as highlighted for the Marowijne River estuary (Gardel et al., 2021), these variations do not seem to impact long-term river deflection. This lack of correlation becomes evident in Figure 12, which indicates no significant relationship between discharge seasonality and magnitude of river deflection. However, some sort of correlation would have been expected. For instance, droughts substantially reduce discharge, thus fluvial energy, and favor marine-driven sediment bypassing. While increased discharge events can promote sediment blocking, increasing sediment trapping updrift of the river mouth. However, the absence of a seasonal influence on the degree of river deflection suggests that the long-term river-coast interaction overrides seasonal effects. Important to note is that the Suriname River has upstream dams, significantly reducing the influence of discharge seasonality for these rivers.

5.1.4 Chenier impact

Historical data indicates that rivers simply incise through cheniers as they meander through the coastal plain, despite a change from mud-dominated to sand-dominated substrates, and suggesting that rivers are capable of incising through these sandy coastal deposits without any substantial deviation from their overall course. Thus, while chenier formations are important coastal evolutionary markers, they do not appear to play a major role in influencing river behaviour.

5.1.5 Consistency between methods

Quantifying river deflection is inherently difficult due to the complex nature of a fluvial system. There are 3 categories: rivers that flow south-north to the sea, rivers that flow south-north up to a certain point and then more or less deflect abruptly, and rivers that flow south-north and at a certain point gradually deflect to the northwest, such as the Nickerie River. The Mana River in French-Guiana also displays this behaviour until it suddenly deflects to the west near the shore. The difference between the second and third category is probably caused by a difference in river discharge, which is not certain due to a lack of data.

The two different methodological approaches used in this research illustrated similar results. Although the river deflection was measured in two distinctively different ways, the observed relationships between river discharge and deflection remained consistent. Despite the influence of subjectivity, the consistent outcome between different methods strengthens the overall findings and emphasizes the reliability of the conclusions of this research about the river-coast interactions.

5.2 EVALUATION OF METHODOLOGY

The methods applied in this research, which include a comparison between different approaches to quantifying river deflection, offer insight into the dominant factors influencing river behaviour along the Guianas coast. Despite the straightforward approach, each method has limitations and strengths.

A key strength of the applied methodology is the comprehensive approach. Providing an overview of river-coast interactions in the study area and eventually narrowing the scope once important drivers of the system are identified. By illustrating different examples of river-coast interactions, a comprehensive overview of the geomorphological processes at play ensures a clear understanding of the Guianas coastal system. As quantifying river deflection is inherently complex, especially identifying a point of deflection, using two different methods of measuring river deflection provides cross-validation. Furthermore, the use of different methods provides multiple perspectives on river deflection dynamics.

Despite the highlighted strengths of the methodology used, this study deals with several limitations influencing the interpretation of the findings. A major limitation is the reliance on proxy data. Western countries provide plenty of high-quality open-source data, however countries such as Suriname, Guyana and French-Guiana lack resources to produce and publish extensive high-quality datasets. While global datasets exist, they can lack detail. Global data aggregators like Global Runoff Data Center (GRDC), lack extensive coverage for remote locations. Hence, this research relied on proxy data, specifically the use of watershed and channel width as proxies for discharge. Despite the necessity of using proxy data, it introduces uncertainties which could affect interpretation of the results. While watershed size and channel width generally show good correlation with river discharge, it does not capture temporal variations or in-depth hydrological processes. For comparison, rivers in French-Guiana have relatively high deflection angles between 134 and 175 degrees, but the watershed areas are rather small. Guyana rivers have a more moderate deflection angle compared to rivers in French-Guiana, with deflection angles ranging mostly between 100 and 120 degrees. The Essequibo River in Guyana is the only outlier of the large watershed rivers as this river exhibits an eastward deflection near its mouth. Observing the overview map of the Guiana rivers reveals that in some parts rivers show minimal or no deflection, like in eastern Guyana with rivers such as the Berbice, Demerara, Corentyne, and Essequibo Rivers. While other clusters such as western Guyana, central and eastern Suriname and eastern French-Guiana rivers exhibit substantial westward deflection.

Hence, the reliance on proxy data should be considered when interpreting the results. Another point of consideration is the subjectivity in deflection measurement. Defining exact river orientation and point of deflection introduces subjectivity into the analysis, which may

contribute to observed variability. This highlights the importance of using different methods for cross-validation.

6. CONCLUSIONS

Although previous studies identified coastal processes and identified individual factors, like northeastern trade winds, ocean currents, waves and mudbanks, they did not focus on how these factors interact to drive river deflection. The littoral steering framework of Nienhuis et al. (2016a), provided an important foundation for linking observed river deflection to river-coast interactions along the Guianas coast. Although this relationship was validated and further expanded, it did not exhibit mud cape formation or river deflection. The complexity of the relationship between river discharge and river deflection was indicated by the high spread among low-discharge rivers. While cheniers are valuable markers of former coastlines, no clear influence of cheniers on river deflection was found. The use of proxy data and the subjectivity in quantifying river deflection introduces uncertainty, but the overall findings provide valuable insights into river-coast dynamics. Future research should focus on identifying the energy threshold that separates rivers with a strong hydraulic groin effect limiting sediment bypassing. Below this threshold, mud cape formation occurs updrift of the river mouth introducing a westward bend near the river mouth. Above this threshold, the high energy conditions nullify the coastal processes driving westward river deflection

In conclusion, behaviour of rivers along the Guianas coast reflects a dynamic equilibrium between alongshore sediment supply, Amazon originating mudbanks, wind driven and marine forces and river discharge. The Amazon originating mudbanks are subject to a large-scale behaviour in which they increase sharply in size (particularly in length) over a period of 160-200 years and then decrease again. Especially if the banks are long, the influence on the estuaries will be strong (risk of deflection). The dynamic balance between driving and interrupting forces of westward river deflection highlights the ever-changing nature of these river-coast systems and underscoring the role of studying present-day processes to better understand the past.

While this study increases the understanding of river deflection dynamics along the Guianas coast, some questions remain and require further research.

The findings of this research largely agree with existing literature. The littoral steering dynamics framework of Nienhuis et al. (2016a) explains most variances in river behaviour along the Guianas coast. However, it does not account for the high-discharge rivers like the Essequibo, Corantijn, and Marowijne Rivers. The high energy conditions at river mouths, driven by high discharge and strong tidal influence, implies the existence of an energy threshold that inhibits mudcape formation and suppresses river deflection. However, the exact magnitude of this

threshold remains unquantified. Future research could model the energy balance controlling these river mouths, highlighting how increased river discharge and tidal influence change river deflection dynamics.

Although the dating of river deflection seems to align with earlier research of the coastal development during the Wanica Phase by Zonneveld (1955), suggesting a rough correlation with mid-Holocene sea-level stabilization, temporal resolution remains coarse. Therefore, interpretations of these findings should be considered with caution. Further research could aim at improving the temporal resolution of these river deflection estimations, allowing for improved understanding of how changing coastal dynamics relate to coastal evolution during the Holocene.

7. REFERENCES

Allison, M. A., & Lee, M. T., 2004. Sediment exchange between Amazon mudbanks and shore-fringing mangroves in French Guiana. Marine Geology, 208(2-4): 169-190.

Anthony, E. J. (2015). Wave influence in the construction, shaping and destruction of river deltas: A review. Marine Geology, 361, 53-78. DOI: 10.1016/j.margeo.2014.12.004.

Anthony, E. J., Gardel, A., Gratiot, N., Proisy, C., Allison, M. A., Dolique, F., & Fromard, F., 2010. The Amazon-influenced muddy coast of South America: A review of mud-bank–shoreline interactions. Earth-Science Reviews, 103(3-4): 99-121. DOI: 10.1016/j.earscirev.2010.09.008.

Ashton, A.D., Murray, A.B., 2006a. High-angle wave instability and emergent shoreline shapes: 1. Modeling of sand waves, flying spits, and capes. Journal of Geophysical Research, 111, F04011. http://dx.doi.org/10.1029/2005JF000422.

Ashton, A.D., Murray, A.B., 2006b. High-angle wave instability and emergent shoreline shapes: 2. Wave climate analysis and comparisons to nature. Journal of Geophysical Research, 111, F04012. http://dx.doi.org/10.1029/2005JF000423.

Augustinus, P. G. E. F., 1978. The changing shoreline of Surinam (South America). Doct. Thesis, Univ. Utrecht. (Publ. Sci. Res. Surinam and Neth. Antilles 95, 232 pp.).

Augustinus, P. G. E. F., Hazelhoff, L., & Kroon, A., 1989. The chenier coast of Suriname: modern and geological development. Marine Geology, 90 (4): 269-281. DOI: 10.1016/0025-3227(89)90129-1.

Augustinus, P. G., 2004. The influence of the trade winds on the coastal development of the Guianas at various scale levels: a synthesis. Marine Geology, 208(2-4): 145-151. DOI: 10.1016/j.margeo.2004.04.007.

Berrenstein, H. J., 2010. Coastal changes along the Suriname coast with emphasis on the changing coastline of Coronie from 1914 to 2007 and its influence on Avicennia germinans L.(Avicenniaceae). Academic Journal of Suriname, 1(1): 86-95.

Brinkman, R., & Pons, L. J., 1968. A pedo-geomorphological classification and map of the Holocene sediments in the coastal plain of the three Guianas. Soil Survey Institute, Wageningen, Soil Survey Papers 4, 40 pp.

Chevalier C., Froidefond, J.-M. & Devenon, J.-L. (2008) Numerical analysisof the combined action of littoral current, tide and waves on thesuspended mud transport and on turbid plumes around FrenchGuiana mudbanks. Continental Shelf Research, 28 (4–5), 545–560. https://doi.org/10.1016/j.csr.2007.09.011.

Dominguez, J.M.L., 1996. The São Francisco strandplain: a paradigm for wave-dominated deltas? Geol. Soc. (Lond.) Spec. Publ. 117, 217–231. DOI: 10.1144/GSL.SP.1996.117.01.13.

Eisma, D., Augustinus, P. G. E. F., & Alexander, C., 1991. Recent and subrecent changes in the dispersal of Amazon mud. Netherlands Journal of Sea Research, 28(3): 181-192.

Gardel, A., Anthony, E. J., Dos Santos, V. F., Huybrechts, N., Lesourd, S., Sottolichio, A., Maury, T., Jolivet, M. (2021). Fluvial sand, Amazon mud, and sediment accommodation in the tropical Maroni River estuary: Controls on the transition from estuary to delta and chenier plain. Regional Studies in Marine Science, 41, 101548. DOI: 10.1016/j.rsma.2020.101548.

Gersie, K., Augustinus, P. G. E. F., & Van Balen, R. T., 2016. Marine and anthropogenic controls on the estuary of the Suriname River over the past 50 years. Netherlands Journal of Geosciences, 95(4): 419-428. DOI: 10.1017/njg.2016.18.

Komar, P.D., 1971. Mechanics of sand transport on beaches. J. Geophys. Res. 76, 713–721. http://dx.doi.org/10.1029/Jc076i003p00713.

Kroonenberg, S.B., 2016. Paleoproterozoic evolution of the Guiana Shield in Suriname. A revised model. Geologie en Mijnbouw 95 (4): 491-522. DOI: 10.1017/njg.2016.10.

Kroonenberg, S.B., & Noordam, D., 2017. Geology, landforms and soils. Natural History and Ecology of Suriname. LM Publishers, Volendam: 22-39.

Nedeco, 1968. Surinam transportation study. Report on hydraulic investigations. Nedeco, The Hague, 293 pp.

Nienhuis, J. H., Ashton, A. D., & Giosan, L. (2016a). Littoral steering of deltaic channels. Earth and Planetary Science Letters, 453, 204-214. DOI: 10.1016/j.epsl.2016.08.018.

Nienhuis, J. H., Ashton, A. D., Nardin, W., Fagherazzi, S., & Giosan, L. (2016b). Alongshore sediment bypassing as a control on river mouth morphodynamics. Journal of Geophysical Research: Earth Surface, 121(4), 664-683. DOI: 10.1002/2015JF003780.

Pearson, G. W., Pilcher, J. R., Baille, M. G. L., Corbett, D. M., & Qua, F. (1986). High-precision C14 measurements of Irish oaks to show the natural C14 variations from AD 1840 to 5210 BC. Radiocarbon, 28, 911-934.

Toorman, E.A., Anthony, E., Augustinus, P.G.E.F., Gardel, A., Gratiot, N., Homenauth, O., Huybrechts, N., Monbaliu, J., Moseley, K., Naipal, S., 2018. Interaction of Mangroves, Coastal Hydrodynamics, and Morphodynamics Along the Coastal Fringes of the Guianas. Threats to mangrove forests, Coastal Research Library 25, pp. 429-473, Springer. DOI: 10.1007/978-3-319-73016-5_20.

Van der Hammen, T., 1963. A palynological study on the Quaternary of British Guiana. Leidse Geol. Meded., 29: 125-180.

De Vries, J., van Maanen, B., Ruessink, G., Verweij, P. A., & de Jong, S. M., 2022. Multi-decadal coastline dynamics in Suriname controlled by migrating subtidal mudbanks. Earth Surface Processes and Landforms, 47(10): 2500-2517. DOI: 10.1002/esp.5390.

Wells, J. T., & Coleman, J. M., 1981. Physical processes and fine-grained sediment dynamics, coast of Surinam, South America. Journal of Sedimentary Research, 51(4): 1053-1068. DOI: 10.1306/212F7E1E-2B24-11D7-8648000102C1865D.

Wong, T. E., 1986. Outline of the stratigraphy and the geological history of the Suriname coastal plain. Geologie en Mijnbouw, 65(2): 223-241.

Wong, T. E., Kroonenberg S.B., Augustinus, P.G.E.F., 2017 . Geologie en landschap van Suriname, 183 pp.

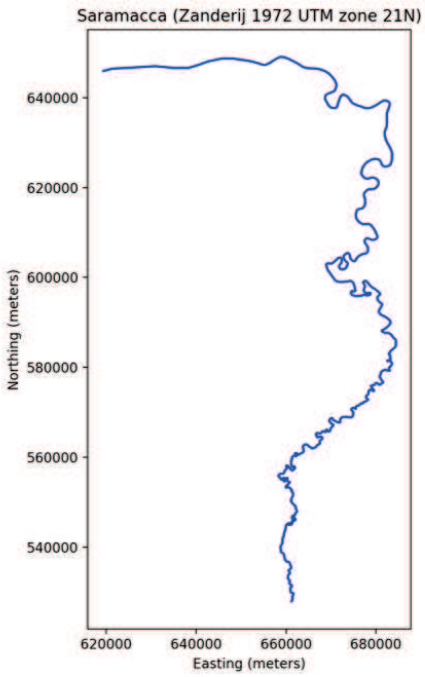
Zenkovich, V. P. (1967), Processes of Coastal Development, 1st ed., edited by J. A. Steers, Oliver & Boyd, Edinburgh.

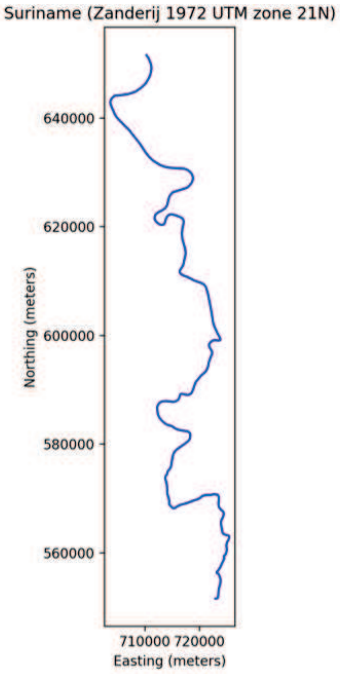
Zonneveld, J.I.S., 1955. Over de geologische en palaeogeografische ontwikkeling van de Surinaamse kustvlakte. Leidse Geologische Mededlingen, 20(1), 214-224.

Zonneveld, J.I.S., 1968.The evolution of the coastal area of Surinam (South America). In: Morrison, R.B., & Wright, H.E. (eds): Means of correlation of Quaternary successions. 17th Congress of the International Association for Quaternary Research. Conference proceedings 8. University of Utah Press (Salt Lake City): 577-589.

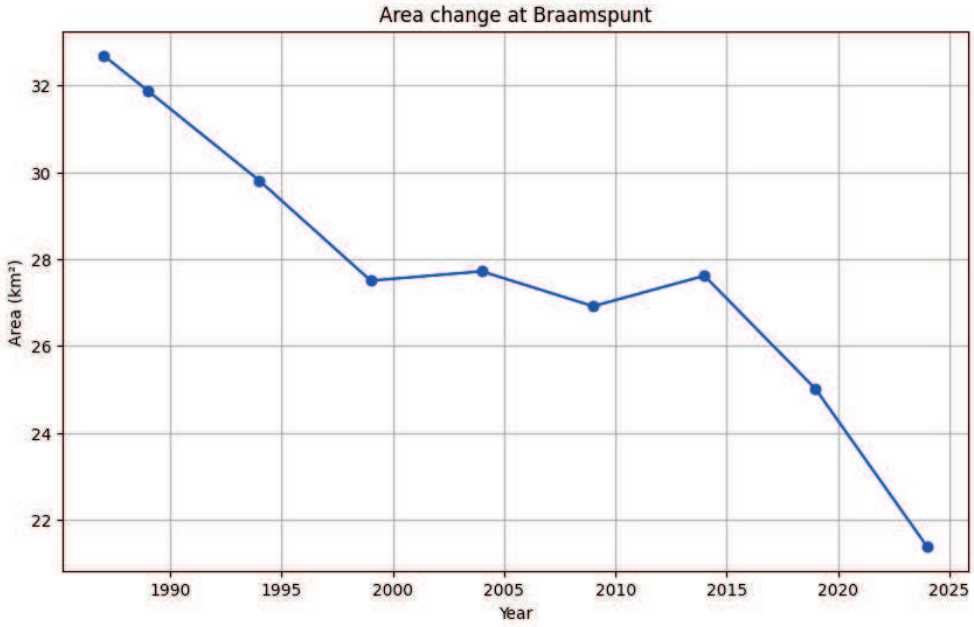
APPENDICES

Appendix A: Examples of river. I) Clear change in main river orientation. II) No clear change in main river orientation

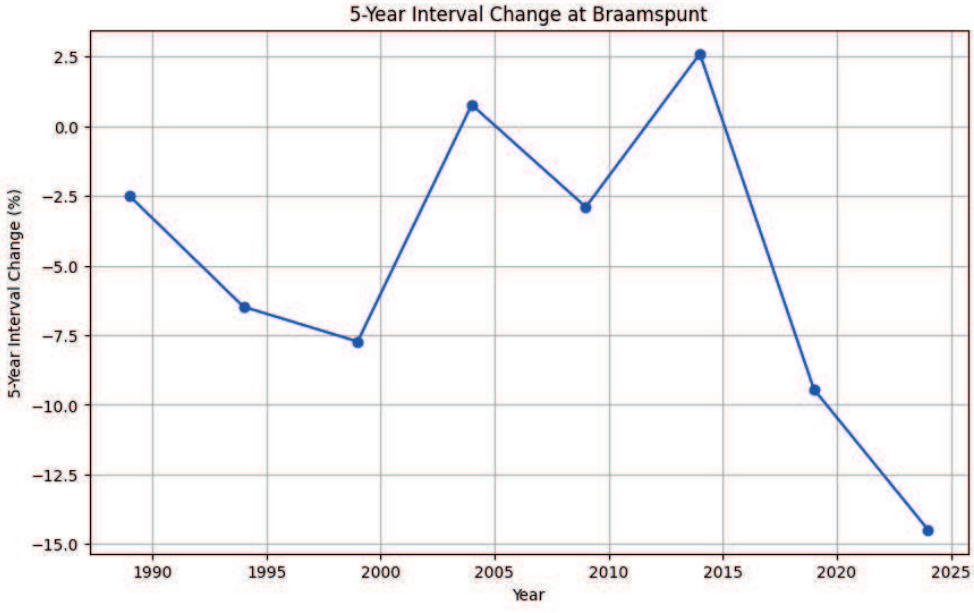




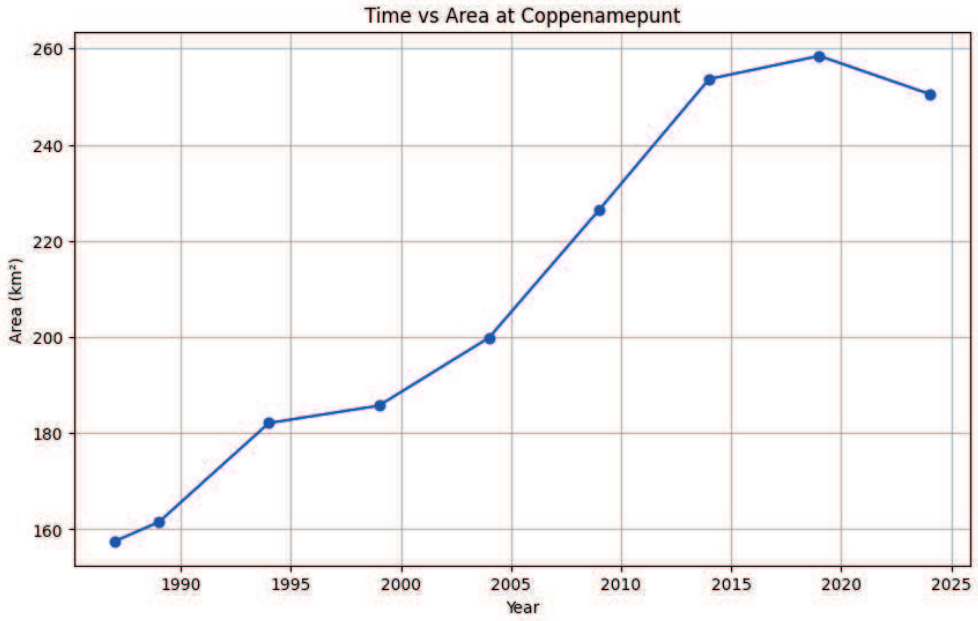
Appendix B.1: Area change over time of Braamspunt mud cape



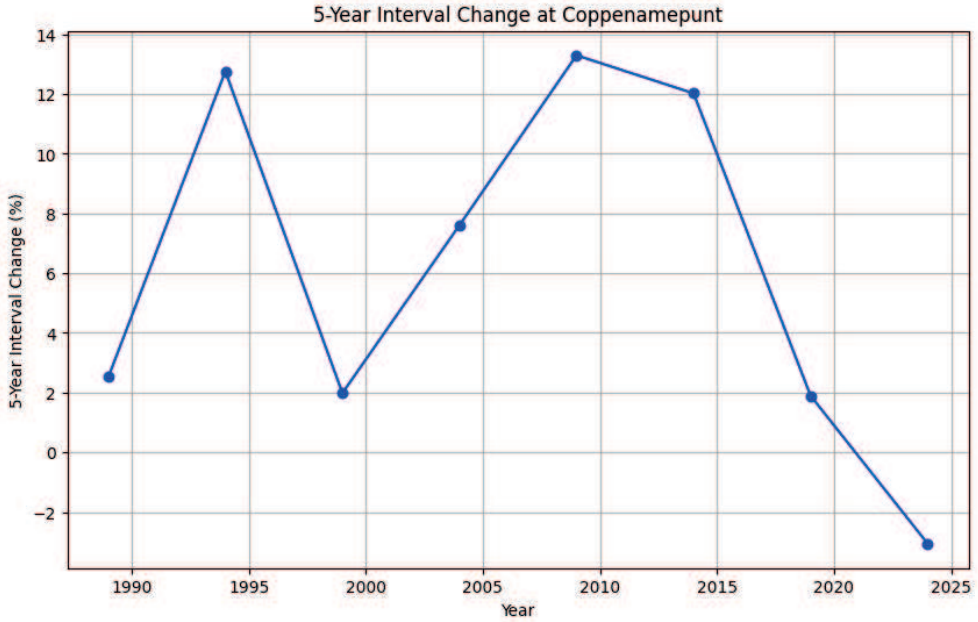
Appendix B.2: 5-Year interval change at Braamspunt mud cape



Appendix C.1: Area change over time of Coppenamepunt mud cape



Appendix C.2: 5-Year interval change at Coppenamepunt mud cape





Chapter 6

Marine and anthropogenic controls on the estuary of the Suriname River over the past 50 years

K. Gersie[1], P.G.E.F. Augustinus[2], R.T. Van Balen[3]

Affiliations
1. Department of Geosciences, Anton de Kom University of Suriname, Leysweg 86, Paramaribo, Suriname. Kathleen.gersie@uvs.edu
2. Department of Geosciences, Earth Surface and Water, Utrecht University, Heidelberglaan 8, 3584CS Utrecht, The Netherlands. P.G.E.F.Augustinus@kpnmail.nl
3. Department of Earth Sciences, VU University of Amsterdam, De Boelelaan 1100, 1081HZ, Amsterdam, The Netherlands. r.t.van.balen@vu.nl

Doi:10.1017/njg.2016.18

ABSTRACT

Humans have played an important role in fluvial systems because of the impact of their land-use activities, frequently leading to degradation of environmental conditions. Rivers, which are the primary agents in sediment transport, have thus been subject to changes in sediment fluxes. The Suriname River has been affected by anthropogenic activities since colonial times, and has experienced strong discharge and sediment-load changes since the construction of the Afobaka Dam in 1964. The river's estuary sediments largely consist of fine-grained sediments, originating, ultimately, from the Amazon River and transported by the strong tidal current. The influence of this tidal current is diminished at the head of the estuary, allowing the river flow to become dominant. Also remarkable is the interaction of the Suriname River and the westward-migrating mudbanks which is evident in the changing magnitude and volume of Braamspunt, a mudcape located at the mouth of the estuary. The regulated discharge of the river results in a change of the river's morphology, resulting, among other things, in the growth of river bars.

1. INTRODUCTION

Land-use activities, like converting natural landscapes for human use, have transformed a large proportion of the Earth's land surface. Although land-use activities vary greatly across the world, the ultimate outcome is generally the same: obtaining natural resources for human needs or purposes frequently causes degradation of environmental conditions (Foley et al., 2005). Fluvial systems play a key role in human impacts on the global system because rivers are the primary agents of transport of sediments from the land to the coasts and oceans. Changes in fluxes of sediments have been inferred in almost every catchment that has been converted for land use. For example, numerous studies have shown that fluxes to oceans have been reduced in catchments where reservoirs have been constructed (Wasson, 1996). However, while considerable research has been done on northern mid-latitude fluvial systems, much less attention has been paid to the human impact on tropical river systems. The objective of this study is to analyse the hydrologic and geomorphic evolution of the lower Suriname River, especially its estuary, in response to marine and anthropogenic controls during the last 50 years.

Suriname is located in the tropics of northern South America and has two rainy and two dry seasons each year. The country is drained by four large rivers, the Marowijne, Suriname, Coppename and Courentyne (Fig. 1). These rivers have a south to north orientation, and flow from the crystalline Precambrian Guyana Highlands via the unconsolidated sedimentary deposits of the coastal plain to the Atlantic Ocean. The two largest rivers in Suriname, the Marowijne and the Courantyne, run straight into the ocean without deflection (Rine, 1980). The mouths of the Suriname and Coppename rivers have westward orientations, which is common for the Guiana coast. The westward deflection is the result of lateral growth of the eastern, outerbank of the rivers. The Marowijne and Courentyne are not deflected because of the large discharge, especially in the rainy seasons. In such periods the river mouth is flushed.

The smaller main rivers, the Cottica, Commewijne, Saramacca and Nickerie fluvial systems, do not flow straight into the ocean. They deflect westward in their lower, coastal reaches, where they confluence with one of the large rivers. Augustinus (1978) attributes this westward deflection to the coincidence of relatively small river discharges and the westward migration of coastal mudbanks, when these cross the related river mouths (see previous chapter).
This study focuses on the Suriname River, from an economic point of view the most important river in Suriname. It has been controlled by anthropogenic activities since colonial times (after 1900) when plantations were cultivated and fortresses were founded. Because of the river's importance and the resulting need to understand its behaviour, many measurement data have been collected in the past in its lower course and in the estuarine part.

This study is based on field observations and measurements described in the literature, supplemented with interpretations of aerial photographs and satellite imagery. Internal reports

of the Maritime Authority Suriname (MAS) are also used, including depth measurements along channel cross-sections.

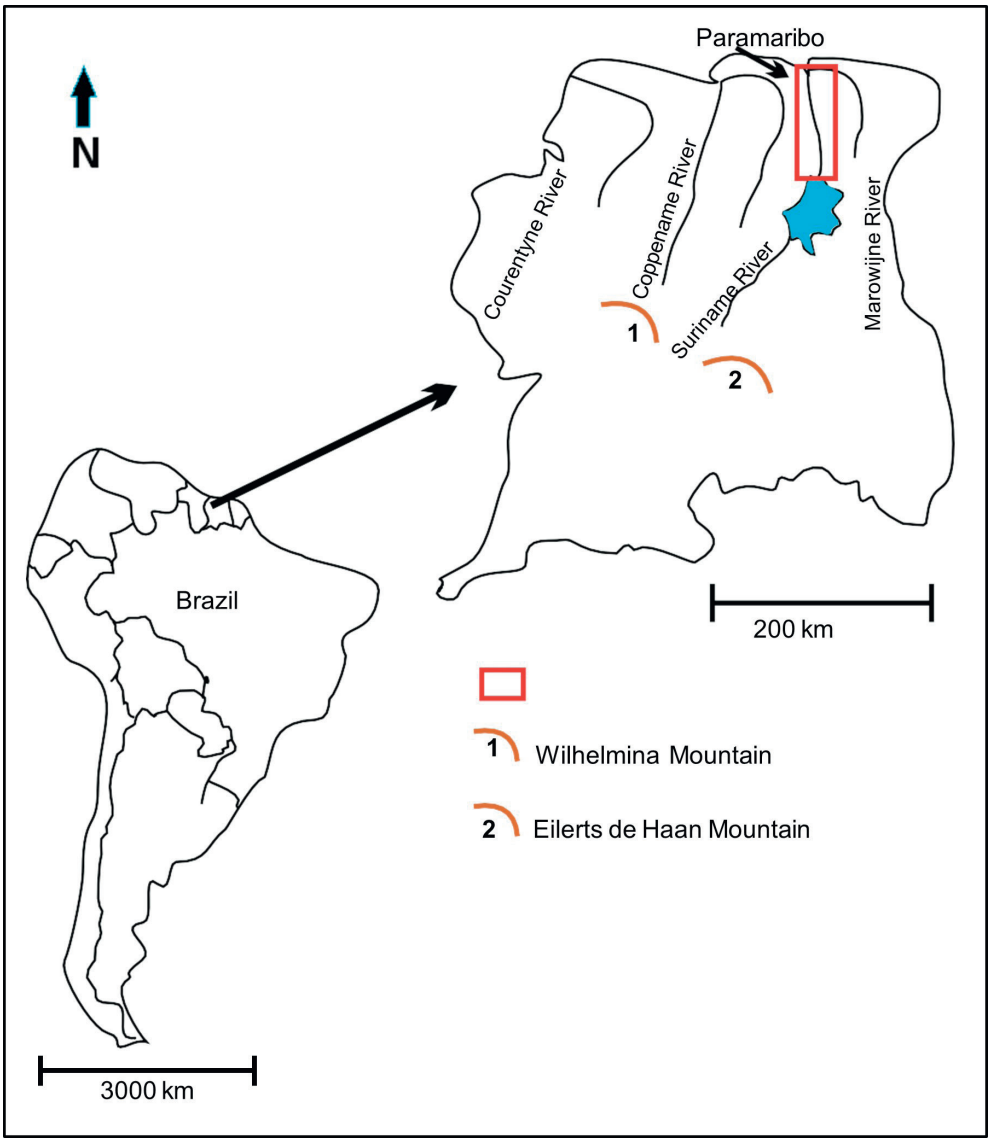


Figure. 1. South America with Suriname, its four main rivers and the study area (red rectangle: Suriname River estuary).

2. SETTING

The Suriname River is 480 km long, and has its sources between the Wilhelmina Mountain and the Eilerts de Haan Mountain. The capital of Suriname, Paramaribo, is located on the left

bank of the Suriname River estuary (Fig. 2). In 2009, to stop erosion processes, the government began constructing a dyke along the east bank of the estuary, dyke over c. 2 km, from Jachtlust to Nieuw Amsterdam.

The Suriname River has an estimated average annual discharge of 440 $m^3 s^{-1}$ and an average annual sediment load of 0.25 × 10^6 t a^{-1} (Nedeco, 1968). Discharge and sediment load are strongly affected by the Afobaka Dam, located in the northern part of the shield region of the Suriname River basin (Fig. 2). This dam was constructed between 1961 and 1964, and started to operate in 1965 to provide electricity for the processing of bauxite and for domestic use in Paramaribo. Construction of the dam has diminished and regulated the downstream discharge. In addition, the artificial lake is a trap for coarser sediments (sand) supplied from upstream, and, as a result, the downstream riverbed is probably eroded. Sand currently dredged from the river bottom near Paranam, a small town downstream of the dam (Fig. 2), must have been deposited before the hydroelectric plant came into operation (Nedeco, 1968).

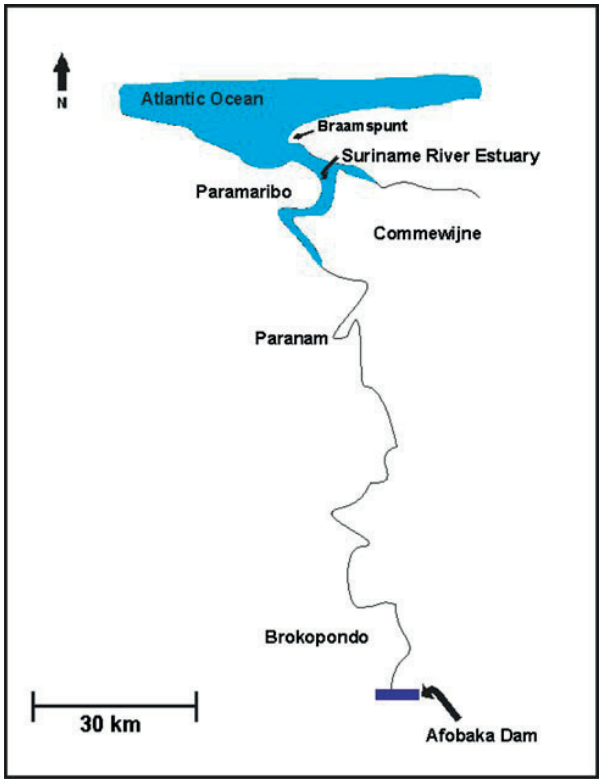


Figure 2. The Suriname River estuary with the Braamspunt mudcape at the river mouth.

Downstream of Paranam, the clay content of the riverbed sediments increases in the seaward direction. The (slightly) sandy clays in the estuary (Fig. 2) contain only a small percentage of

sand which, according to the mineralogical composition, originates from the nearby beach sand. It contains, however, a relatively high percentage of zircon, which points to an influence of the upstream Suriname River (Krook, 1979), before the construction of the Afobaka Dam. The beach sand both east and west of the Suriname River mouth originates from the Marowijne and Mana rivers (Augustinus, 1978), and its heavy mineral association differs from that of the Suriname River (Krook, 1979). However, the fine-grained sediments in the estuary ultimately originate from the Amazon River. They are transported by tidal currents into the estuary. The estimated amount is c. 250,000 t a^{-1}, based on an average sediment concentration of 20 g m^{-3} (Nedeco, 1968; SRK Consultants, 2008).

On both sides of the river, former coastlines can be recognised. They are marked by cheniers, which consist of sand and shells (or shell fragments). As previously mentioned, the sand originates from the Marowijne River, and is characterised by a heavy mineral association dominated by staurolite (Kiel, 1955; Augustinus, 1978; Krook, 1979). Shells are of (deep) marine origin and are, due to their form and low density, more easily transported than quartz sand (Augustinus, 1978). Sand and shells of the current spit at Braamspunt (Fig. 2) are from the same sources.

3. INTERACTION OF THE COASTAL ZONE AND ESTUARY

The coastal waters in front of the 364 km long coast of Suriname are mainly characterized by the Guiana current, which is a continuation of the South Equatorial Current. However, due to its low velocity, the Guiana current is not very important for the Suriname River estuary. Current velocities in the shallow coastal waters along the coast of Suriname are just high enough to enable the transport of silt and (very) fine sand (Nedeco, 1968; Augustinus, 1978).

In the near-coastal area, natural waves are very important for coastal development. In the estuary, however, they quickly lose energy due to refraction in response to shoaling towards the banks. Ship-induced waves, however, can play an important role in riverbank erosion (Van Heuvel, 1983).

3.1 THE TIDAL SYSTEM IN THE ESTUARY AND ITS RELATED MORPHOLOGY

The tide along the coast of Suriname is semi-diurnal. The average tidal range is 1.80 m. It can be classified as mesotidal since the mean wave height at spring tide is 2.80 m; at neap tide it is 1.00 m (Nedeco, 1968).

The tidal wave approaches the Suriname coast from an almost perpendicular (NNW–N) direction. The sea water flows with rising tide via a shallow flood channel into and along the east side of the estuary (Fig. 3). Under these conditions, flow velocities of c. 1 m s^{-1} were observed by Van Heuvel (1983). In the westerly-situated fairway, the maximum flow velocity was 0.85 m s–1.

The incoming floodwater tends to flow as straight as possible. Near Resolutie, upstream, flow velocities of over 1 m s–1 were measured. Further upstream the flood channel ceases to exist. In the narrow flow profile between Leonsberg and Voorburg, only one channel is visible (Fig. 3). Flow velocities in this channel are up to 1.5 m s–1 (Van Heuvel,1983; Sunecon Consultants, 2004).

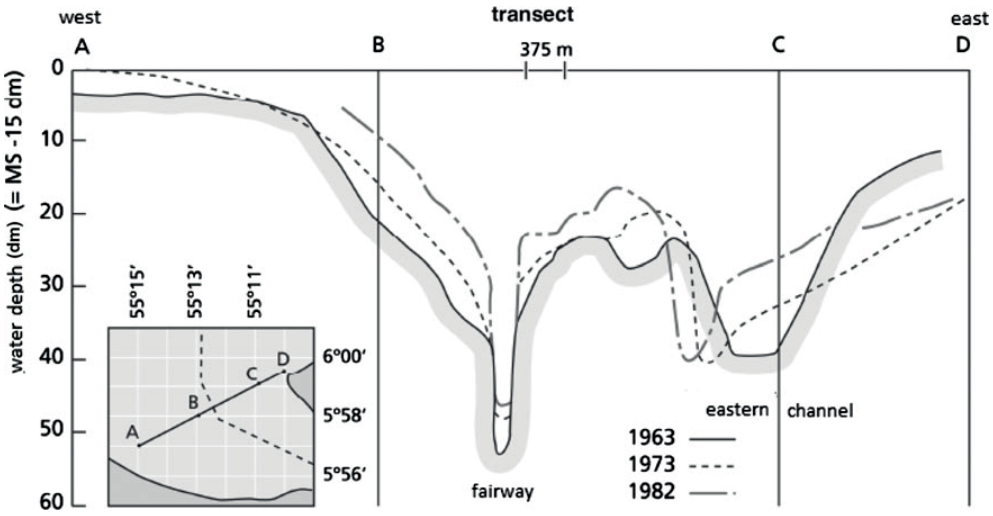


Figure 3. Cross-section through the Suriname River estuary, showing the position of the fairway and, further east, a flood channel, over the years 1963, 1973 and 1982 (after Van Heuvel, 1983).

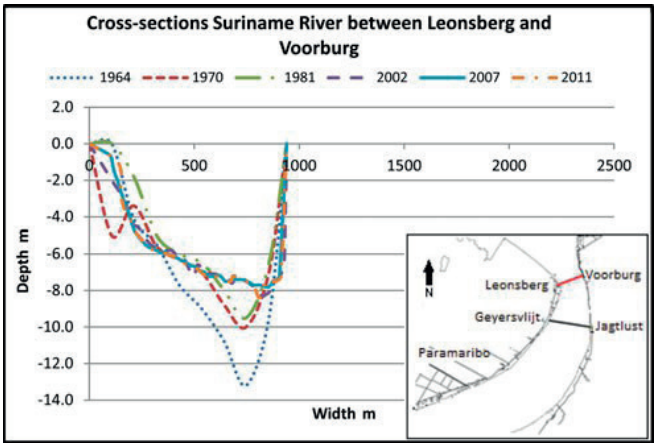
During ebb tide the deep westerly channel, the fairway, now functions as an ebb channel with flow velocities of c. 1 m s–1 (Van Heuvel, 1983; Sunecon Consultants, 2004).

There is a lack of flow velocity and discharge data for the tributary, the Commewijne River. Nevertheless, from the colour difference of the outflowing water near the confluence it can be inferred that during ebb tide the discharge of the Suriname River is much larger than that of the Commewijne River, despite the effects of the Afobaka Dam (Van Heuvel, 1983).

In the narrow passage between Leonsberg and Voorburg (Fig. 4) the outflowing fresh river water and in- and outflowing salty tidal water concentrate in the outer bend.

Cross-sections of the Suriname River, between Geyersvlijt and Jagtlust, show depressions with depths up to 4 m (Fig. 5) near the east bank of the river (Commewijne), reaching a maximum in 1981. They probably function as flood channels.

Silt bars (Resolutie, Jagtlust, Dijkveld) are almost aligned with the current flow (Fig. 6), and in front of the river mouth a mouth bar, known as the Outer bar, is present. Therefore, according to the morphological classification of Dalrymple et al. (1992), the mesotidal Suriname River estuary can be classified as tide-dominated, although tide-dominated estuaries are more likely to occur in macrotidal areas. This is due to the strong flood tidal currents compared to the relatively small effects of the incoming waves. The tidal influence is diminished at the head of the estuary, allowing the river flow to become dominant (Dyer, 1997).



Figuer 4. Cross-section of the Suriname River estuary between Leonsberg and Voorburg.

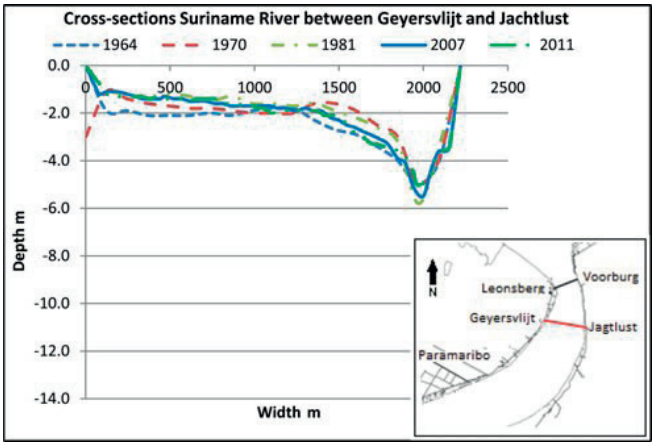


Figure 5. Cross-section of the Suriname River estuary between Geyersvlijt and Jagtlust.

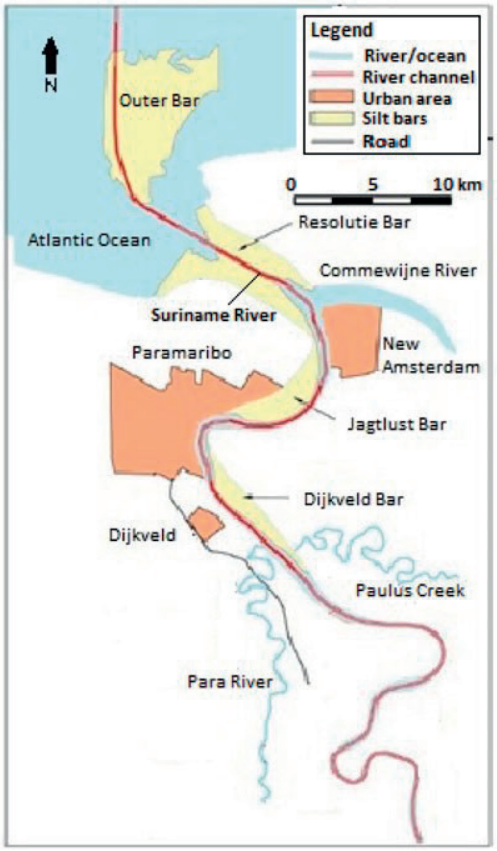


Figure 6. Bars in the Suriname River (modified after SRK Consultants, 2008).

The bars are the result of the influx of silt from the Atlantic Ocean into the estuary and are especially prevalent along the riverbanks because the fairway is fixed with the aid of beacons. The silt ultimately originates from the Amazon River. The contribution from the upstream interior is estimated to be in the order of 2% (Nedeco, 1968). The Old and Young Coastal Plain consist for the most part of marine-deposited clays. Land-based runoff from that area will contribute silt that is also of Amazon origin.

3.2 COASTAL MUDBANKS

Coastal development in Suriname is determined by the continuously westward-migrating system of mudbanks and interbank areas (see previous chapter). Mudbanks vary in length between 30 and 60 km (Wells & Coleman, 1978). They extend offshore to about the 20 m isobaths (Nedeco, 1968). The migration of the mudbanks is the result of deposition at their west side and erosion at their eastside. Deposition at the west (down-drift) side of the mudbanks mainly takes the form of fluid muds (sediment concentrations of 10–330 g l–1). The high silt

content of the sea water, together with resuspended particles from the east (up-drift) side of the mudbanks, can cause over-concentration at the down-drift side, giving rise to fluid mud formation. A property of fluid mud is that waves propagating over it are attenuated and even damped completely (Delft Hydraulics Laboratory, 1962; Diephuis, 1966). This calm environment favours further sedimentation; coastal accretion can be very fast (up to 200 m a–1; Boye´, 1962). With ongoing migration of the mudbanks, in the course of time the original fluid mud consolidates and becomes overgrown with mangroves, furthering dehydration of the young soil. As a result, at the east side of the mudbank, the soil has matured to a young clay, which can be eroded by wave action. Migration due to erosion of the east side and sedimentation at the west side mainly takes place during the short dry season (February–April) when the trade winds are strongest (Augustinus, 1978).

In the interbank areas there is no fluid mud. Here the coast is subject to wave attack and rapid erosion of the mangrove fringe (Augustinus, 1978; Plaziat et al., 1994). If sand or shell material is available in this erosive environment, small beach ridges, cheniers, are formed on the clayey subsoil, due to wave action (Russell & Howe, 1935; Price, 1955). Cheniers run parallel with or at small angles to the common shoreline and characteristically cluster at one or both sides of a major river (Fig. 7). Along the eastern part of the Suriname coast, the chenier sand mainly originates from the Marowijne/Mana river system. Shells and shell fragments are the remains of molluscs and gastropods living in the coastal waters (Price, 1955).

In specific cases a chenier can grow seaward and form an extensive beach or spit. This occurs if a retreating coast cuts into an older chenier, which thenceforth acts as a local source of coarse sediment (Augustinus, 1978).

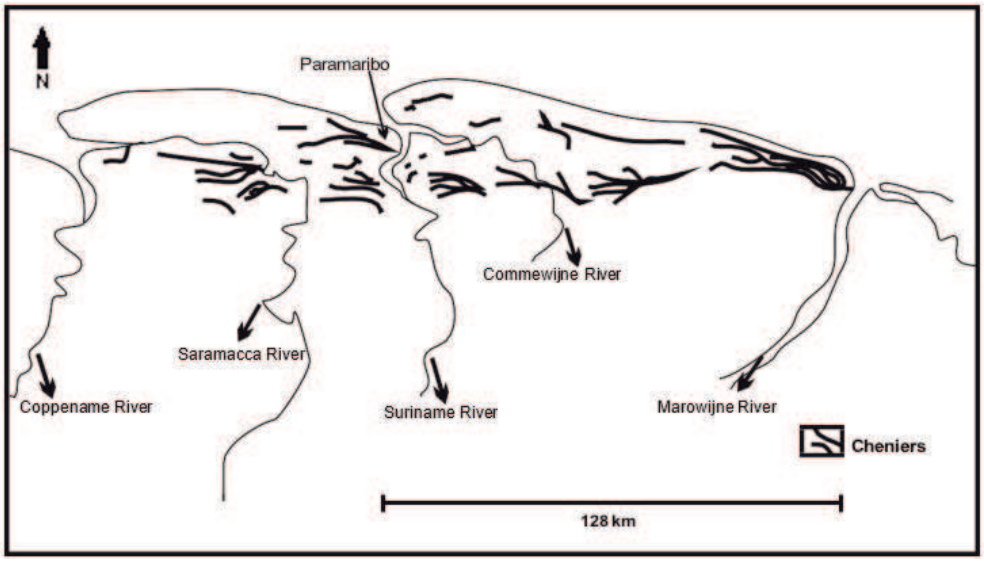


Figure 7. Part of the coastal area of Suriname with east–west-oriented cheniers (black) (Zonneveld, 1968).

The migrating mudbanks are the driving force behind the development of the smallest coastal unit. Between the mudbanks interbank areas exist. Together the mudbanks and adjacent interbank areas form the smallest coastal unit (Augustinus, 2004).

Their migration velocity varies roughly between 0.5 and 1.5 km a−1. The period of one cycle of coastal accretion (mudbank) and coastal erosion (interbank area) is 30–35 years.

The variation in the length of the mudbanks and in their migration velocity appears to be related to coastal development at a higher temporal (150–200 years) and spatial (100–150 km) scale. This large-scale coastal behaviour appears to be governed by a change in frequency of wind directions and wind force (Eisma et al., 1991; Augustinus, 1993, 2004). Analysis of wind data from Kourou (French Guiana) has demonstrated a steady change in wind directions from northeast to east, together with an increase in wind force over the period 1957–1986. Waves generated by these winds will approach the more or less east–west-running coast under a smaller angle as compared to waves generated by northeasterly winds. This means that the alongshore component of the wave energy flux becomes stronger, favoring alongshore transport, and the cross-shore component becomes weaker, leading to a reduction in coastal erosion. As a result, mudbanks should grow longer, which indeed appears to be the case over the period 1947–2001 (Augustinus, 2004). In 2001, the length of the mudbank east of the Suriname estuary was in the order of 70 km.

After mudbanks are colonized by vegetation, they develop into brackish and salty Avicennia marshes (Fig. 8). Due to chenier formation, these are cut off from regularly flooding with sea water. If they subsequently become desalinized, they change into clay marshes with fresh forests or grass swamps. On top of the tidal clay flats, eustatic peat sometimes forms in swamps (Teunissen, 1978).



Figure 8. Avicennia germinans marsh.

Mudbanks migrating westward in front of an estuary are situated at a certain distance from the coast. This feature was described by Delft Hydraulics Laboratory (1962) and attributed to the influence of the river discharge. This fits very well the new mudbank hypothesis of Allison and Lee (2004), that the mudbanks consist of two parts: a free migrating mudwave consisting of fluid mud (high-density suspended mud), and a second part consisting of deposited mud (formed out of suspended and of fluid mud). The second part is located at the landward side of the mudbank, in the lee of currents and waves, and is connected to the coast. In front of an estuary this connecting part will not come into being, due to the turbulence of the in- and outflowing water.

The Braamspunt mudcape

The effect of alongshore-migrating mudbanks on the estuary is also expressed by the magnitude and volume of the Braamspunt mudcape on the east bank of the river mouth (Fig. 2). The cape exists due to east–west alongshore processes (e.g. mud supply and wind orientation), and extends when a mudbank is passing and the river discharge is too small to stop this development. The cape retreats in response to an interbank environment.

The influence of a westward-migrating mudbank on a down-drift estuary was studied by Allison et al. (2000) for the Cassipore mudcape in Brazil. This mudcape is subject to periodical mud supply due to seasonal and decadal cycles in trade wind energies. resulting in alternating periods of formation and starvation in the coastal zone.

The behaviour of Braamspunt in relation to coastal development can be inferred from historical maps, aerial photographs and satellite images (Figs 9 and 10). In the period 1947–1970 a mudbank migrated beyond Braamspunt, and the cape generally showed accretion. In the following years, coastal erosion dominated, resulting in coastal retreat. Episodically, Braamspunt is characterised by a sand spit. Evidently, this can only occur in an interbank environment. Zonneveld (1953) described the evolution of a sand spit at Braamspunt, based on recent surveying and topographic maps. From 1914 to 1930 a sand spit existed.

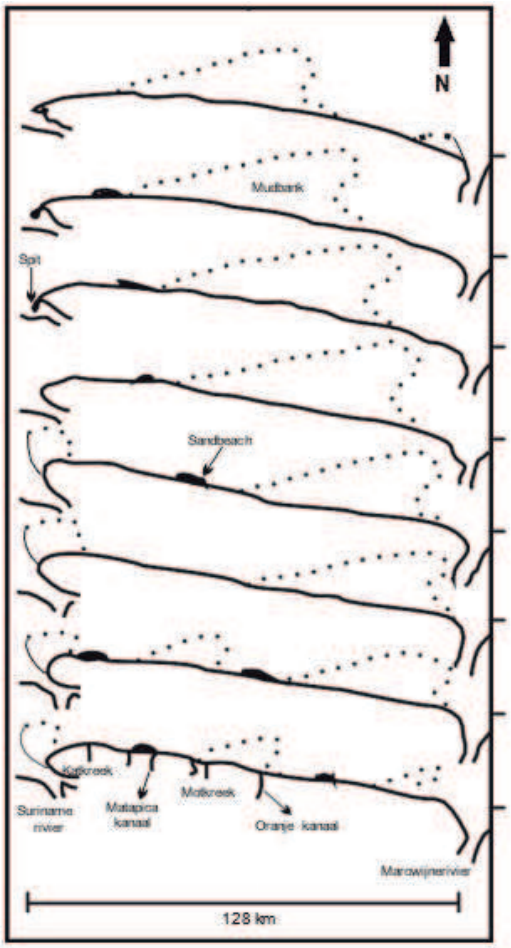


Figure 9. Mudbank migration from 1947 to 2007 (modified after Zonneveld, 1953).

By 1938 it was no longer present (Fig. 10); part of the sand was transported across the estuary to form a new chenier north-west of Paramaribo, while another part was transported into the estuary to form a small sandy riverbank, south of the former spit (Fig. 10). Some 50–55 years later, during the 1980s, a new sand spit started to develop at Braamspunt; it is still present, so it appears that spit formation is not related to the 30 year cycle of coastal development in Suriname.

The formation of a spit requires a certain volume of sand. During normal longshore transport conditions, selection of the sediment takes place. Coarser and heavier grains are likely to stay behind, so the amount of sand in a chenier decreases and its mean grain size becomes finer in the westward direction (Augustinus, 1978). As a result, the relatively fine sand that finally reaches Braamspunt is too small in quantity for the formation of a sand spit.

If, however, due to severe coastal erosion, a chenier of a former coastline is eroded, a new sand source is tapped; in such cases large sandy beaches can develop. Augustinus (1978) indicates this situation as a 'sand accretionary coast'. At the mouth of creeks and rivers, and along protruding parts of the coast, accretionary cheniers develop as spits.

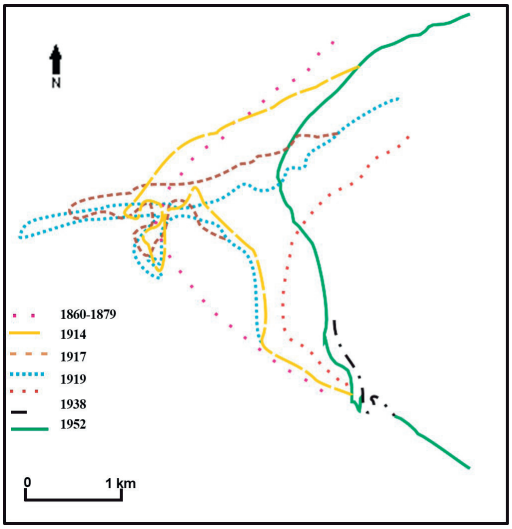


Figure 10. Coastlines at Braamspunt from different years (1860–1968) (modified after Zonneveld, 1953).

These accretionary cheniers and spits always develop in interbank areas, as can be deduced from Fig. 9. In 1947, two accretionary beaches were present. Until 1957, both migrated westward, in phase with the east and west adjoining mudbanks. In 1966, however, the more westerly of the two appears to be

overtaken by the eastward adjoining mudbank. Not until the mid-1980s did this sand became available again to form a new spit at Braamspunt. This, at least partly, explains why spit formation at Braamspunt is an episodic feature (Fig. 11).

Actually, the spit at Braamspunt is in its final phase, which is accelerated by the extraction of sand at its east side for the purpose of construction in Paramaribo (Fig. 11). These sand extractions seem to decrease the volumes of sand at Braamspunt. From the east a new accretionary sand beach and an adjacent mudbank are approaching (Fig. 9). The question is which of these two, the spit or the mudbank, will arrive first at Braamspunt. In the latter case, the spit will be fixated for the coming decades before it will reach Braamspunt.

Looking at Fig. 9, it is striking that no new accretionary cheniers and spits formed after 1947. Apparently, ever since that time, erosion of the coast of East Suriname has not been severe enough to erode an older chenier along a former coastline. This is in tune with the increasing

length of the mudbanks (Eisma et al., 1991; Augustinus, 2004), indicating the increase in coastal mud accretion. The phenomenon appears to be related to the (expected) phase of large-scale coastal behaviour in which (net) coastal retreat is predominant.

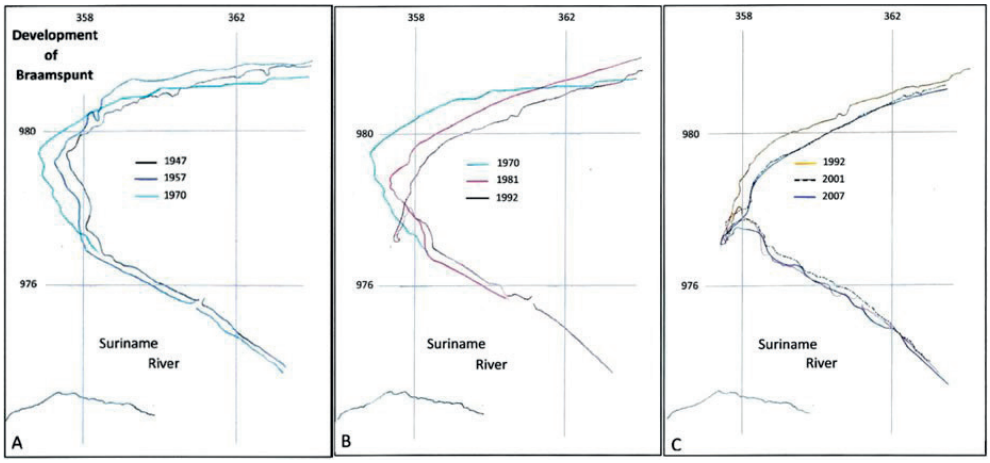


Figure 11. The coastline of Braamspunt: (A) coastal accretion from 1947 to 1970; (B) coastal erosion and starting spit formation from 1970 to 1992; (C) coastal erosion and spit development from 1992 to 2007. Note: black arrows refer to sand extraction activities.

4. RESPONSE TO DAM CONSTRUCTION

Channel cross-section evolution

The channel cross-section between Leonsberg and Voorburg (Fig. 4) shows that the fairway has silted up and has become shallower since 1964, corresponding to the construction of the Afobaka Dam. A few years after the construction, this process was demonstrated by Bles & De Hartog (1968). The depth decreased from 13.2 m in 1964 to 10 m in 1970, 9.5 m in 1981, and 7.4 m in 2011. Thus, approximately 4.8 m was silted up in 48 years. In the beginning, silting up was faster, about 3m in 6 years, and lateral migration of the channel towards the outside bend stopped completely. After 1981, silting-up slowed to about 2m in 31 years. From 1992 onwards, the channel shows a distinct migration towards the outside curve, as is the normal process in outside river bends. Sometime between 1981 and 1992 the response time appears to be over. As the fairway (channel) comes closer to the riverbank, the latter will be strongly undermined, resulting in steeper bank slopes. Losing stability, the bank finally collapses. Along the riverbank between Nieuw-Amsterdam and Jagtlust, several examples of this process were noticeable. Therefore, a dyke has recently been constructed to defend this area (Fig. 12).

As shown by the cross-section in Fig. 5, the channel between Geyersvlijt and Jagtlust silted up between 1964 (construction of the Afobaka Dam) and 1970. This can be ascribed to the

response of the river to changes caused by the construction of the Afobaka hydroelectric dam. Thus, adaptation of the Suriname River channel to changes due to construction of the Afobaka Dam took at least 17 years. Although the channel depth decreased significantly between 1964 and 1970, by 1981 the channel became deeper, reaching a depth of 5.8 m (Fig. 5). This can be explained by the increase in number of

deeply loaded ore ships passing the channel between 1960 and 1973, combined with their increase in size (till 1979). An indication of the development of the number and size of ships for the periods 1957–1981 and 1983–2015 is presented in Figs 13 and 14. Finally, in 2007 a depth of 5.5 m was measured, and in 2011 a depth of c. 5.0 m.



Figure 12. Dyke construction along the right bank of the Suriname River.

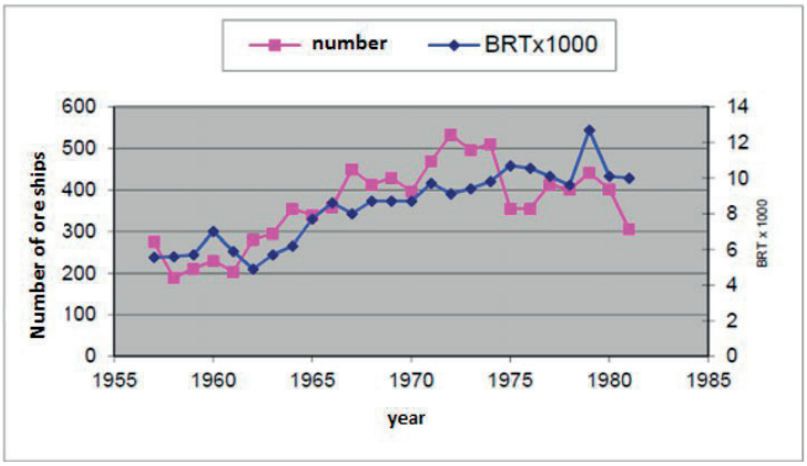


Figure 13. Changes in the number and size of ore ships passing through the Suriname River (after Van Heuvel, 1983).

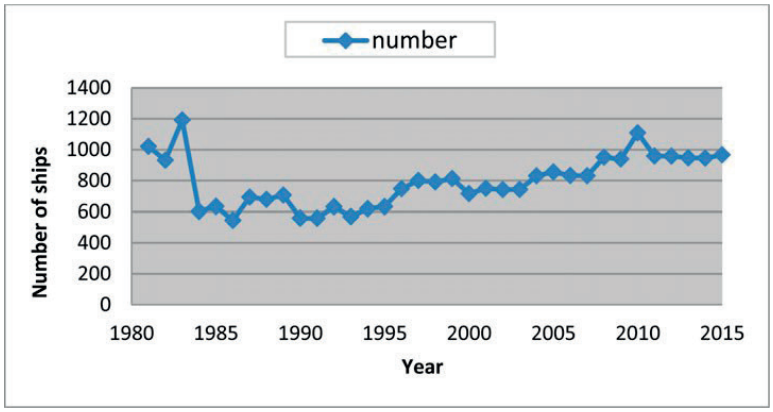


Figure 14. Changes in the number of ships passing through the Suriname River (MAS, 2016).

5. CONCLUSIONS

Both coastal factors and dam construction appear to have led to significant changes in the estuary system. Significant impacts are the consequences of the construction of the Afobaka Dam: the reduced and regulated discharge of the Suriname River and the trapping of mainly coarse sediment behind the dam. The regulated discharge leads to major import of sediments from the coast, changing the rivers' morphology over the years and resulting in the growth of river bars (e.g. the Jagtlust Bar). Another result was that the estuary became more tidal-dominated. From the cross-sections in Figs 4 and 5 it is apparent that the bedding of the Suriname River has silted up since the construction of the Afobaka Dam. The river channel adaptation to the change in discharge took at least 17 years; however, erosion processes in the outer bends never stopped. The influence of the westward-migrating system of mudbanks and interbank areas is expressed by changes in the magnitude and volume of Braamspunt (Fig. 11). The episodic development of a sand spit at Braamspunt is related to the development of accretionary cheniers in periods of severe coastal erosion (within the cycle of large-scale coastal behaviour). When an accretionary chenier during its migration is overtaken by a mudbank that migrates with a higher velocity, it will be fixated for some 15–20 years, making the feature even more

episodic. The erosion and finally disappearance of the sand spit at Braamspunt is caused by a shortage of sand supply. This is usually due to an approaching mudbank which hampers sand transport. Erosion is accelerated by the local extraction of sand. It is recommended that monitoring activities be executed by local authorities in the future.

ACKNOWLEDGEMENTS

Professor Dr Hans Renssen is thanked for his support and views, Professor Theo Wong for his support, Mrs Bernice Mahabier, Ms. Nancy Yang and Mr Lloyd Gemerts from the Maritime Authorities Suriname (MAS) for their help and making data available.

REFERENCES

Allison, M.A. & Lee, M.T., (2004). Sediment exchange between Amazon mudbanks and shore-fringing mangroves in French Guiana. Marine Geology, 208 (2-4), 169–190. https://doi.org/10.1016/j.margeo.2004.04.026.

Allison, M.A., Lee, M.T., Ogston, A.S. & Aller, R.C., (2000). Origin of Amazon mudbanks along the northeastern coast of South America. Marine Geology 163 (1-4), 241–256. https://doi.org/10.1016/S0025-3227(99)00120-6.

Augustinus, P.G.E.F., (1978). The changing shoreline of Surinam (South-America). PhD Thesis. Utrecht University: 232 pp. Also published as: Publications of the Foundation for Scientific Research in Surinam and the Netherlands Antilles, Utrecht, no. 95: 232 pp.

Augustinus, P.G.E.F., (1993). Coastal development in Suriname at different temporal and spatial scales. In: List, J.H. (ed.): Large scale coastal behavior '93. US Geological Survey Open File Report 93, 1–4.

Augustinus, P.G.E.F., (2004). The influence of the trade winds on the coastal development of the Guianas at various scale levels: a synthesis. Marine Geology 208 (2-4), 145–151. https://doi.org/10.1016/j.margeo.2004.04.007

Bles, A.M. & De Hartog, A.H., (1968). Nota betreffende de verondieping van de benedenloop van de Suriname Rivier. Waterloopkundige Afdeling Paramaribo, 68-3.

Boye´, M., (1962). Les pale´tuviers du littoral de la Guyane franc¸aise: ressources et problemes d'exploitation. Les Cahiers d'Outre-Mer 15: 271–290.

Dalrymple, R.W., Zaitlin, B.A. & Boyd, R., (1992). Estuarine facies models; conceptual basis and stratigraphic implications. Journal of Sedimentary Research 62 (6), 1130–1146. https://doi.org/10.1306/D4267A69-2B26-11D7-8648000102C1865D.

Delft Hydraulics Laboratory, (1962). Demerara Coastal Investigation. Report on siltation of Demerara bar channel and coastal erosion in British Guiana. Delft Hydraulics Laboratory (Delft): 240 pp.

Diephuis, J.G.H.R., (1966). The Guiana coast. Tijdschrift van het Koninklijk Nederlands Aardrijkskundig Genootschap 83: 145–152.

Dyer, K., (1997). Estuaries, a physical introduction, 2nd edn. John Wiley and Sons (Chichester): 195 pp.

Eisma, D., Augustinus, P.G.E.F. & Alexander, C.A., 1991. Recent and sub recent changes in the dispersal of Amazon mud. Netherlands Journal of Sea Research 28: 181–192.

Foley, J.A., DeFries, R., Asner, G.P., Barford, C., Bonan, G., Carpenter, S.R., Chapin, F.S., Coe, M.T., Daily, G.C., Gibbs, H.K., Helkowski, J.H., Holloway, T., Howard, E.A., Kucharik, C.J., Monfreda, C., Patz, J.A., Prentice, I.C., Ramankutty, N. & Snyder, P.K., (2005). Global consequences of land use, Science 309 (5734), 570–574. DOI: 10.1126/science.1111772.

Kiel, H., (1955). Heavy mineral investigations of samples of Suriname. Geology and Mining 17: 93–103.

Krook, L., (1979). Sediment petrographical studies in northern Suriname. PhD Thesis. Vrije Universiteit Amsterdam (Amsterdam): pp 154.

Maritime Authority Suriname (MAS), (2016). Statistics concerning vessels navigating through the Suriname River. MAS (Paramaribo).

Nedeco, (1968). Surinam Transportation Study: a report on hydraulic investigation. Nedeco (The Hague): pp 293.

Plaziat, J.C., Prost, T., Baltzer, F. & Rudant, J.P., (1994). Specificities of exposed shoreline mangals in French Guiana. Abstracts of the 14th International Sedimentological Congress. Recife, Brazil: 69–70.

Price, W.A., (1955). Environment and formation of the chenier plain. Quaternaria 2: 75–86.

Rine, J.M., (1980). Depositional environments and Holocene reconstruction of an argillaceous mud belt – Suriname, South America. PhD Thesis. University of Miami (Tallahassee): 222 pp.

Russell, R.J. and Howe, H.V., (1935). Cheniers of southwestern Louisiana. Geographical Review 25 (3), 449–461. https://doi.org/10.2307/209313.

SRK, Consultants, (2008). Sediments and geomorphology baseline study for Suriname River Dredging Project (SRDP). Maritime Authority Suriname (Paramaribo): 207 pp.

Sunecon, Consultants, (2004). Morfologische aspecten en natuurlijke oeverbescherming. Ministerie van Openbare Werken (Paramaribo): 45 pp.

Teunissen, P.A., (1978). Reconnaissance Map Surinam Lowland Ecosystems (Coastal Region and Savanna Belt), scale 1:200.000. Ed. STINASU/LBB (Paramaribo): pp 50.

Van Heuvel, T., (1983). Studie naar het gedrag van slib in en rond het estuarium van de Suriname rivier, in verband met de bevaarbaarheid van de toegangsgeul vanuit zee naar Paramaribo. Afstudeerwerk Technische Hogeschool Delft, Nederland, vakgroep Kustwaterbouwkunde, Eindstudie: 123 pp. + Bijlagen.

Wasson, R.J., (1996). Land-use and climate impacts on fluvial systems during the period of agriculture. PAGES Workshop Report, Series 96-2: 51 pp.

Wells, J.T., Coleman, J.M., (1978). Longshore transport of mud by waves: northeastern coast of South-America. Geologie en Mijnbouw 57: 353–359.

Zonneveld, J.I.S., (1953). Kustveranderingen aan de mond van de Surinamerivier. Geologie en Mijnbouw 15: 251–254.

Zonneveld, J.I.S., (1968). The evolution of the coastal area of Surinam (South America). In: Morrison, R.B. & Wright, H.E. (eds): Means of correlation of Quaternary successions. 17th Congress of the International Association for Quaternary Research. Conference proceedings 8. University of Utah Press (Salt Lake City): 577–589.



Chapter 7

General discussion



SYNTHESIS

The low-lying coastal zone of Suriname, which serves as the country's economic center and accommodates the majority of its population, is increasingly threatened by climate change effects, particularly sea-level rise. Its coastline is naturally protected by a unique ecosystem which evolved through the effects of mangroves, hydrodynamic processes, and sediment deposition. In addition, mud discharge variability by the Amazon River plays a large role in shaping the Suriname coastline through the longshore mudbank cycle (Anthony et al., 2019; Augustinus et al., 1989).

The aim of this thesis was to increase the understanding of the contribution of mud from the Amazon River and the Suriname River, but also smaller rivers, to the geological and morphological development of the Suriname Coastal plain from the Paleogene-Neogene transition to the present. This has been achieved by answering the proposed research questions from the general introduction:

1) When was the onset of the deposition of mud originating from the Amazon River on the Suriname Coastal Plain start, and how is the coastal vegetation related to the sediment composition?
2) When was the transition of Amazon craton to Andean sediments in the western coastal plain of Suriname, and how did it affect the sediment-lithological composition?
3) What are the key controls behind terrace development along the Upper and Lower River valleys?
4) What are the driving processes behind the westward deflection of the small main rivers in the Holocene Young Coastal Plain of Suriname?
5) How is the behaviour of the Suriname River controlled by natural processes and anthropogenic activities?

The research questions were studied from multiple perspectives, performing palynological analyses, using light microscopy, sediment geochemistry, satellite imagery observations and analyses of, both analog and digital, historical, geomorphological and topographic maps.

In the first part of my thesis (chapter 2) I showed the changes in sediment composition and coastal vegetation in Suriname from the Paleogene to the Neogene. I demonstrated that the Paleocene/Eocene Thermal Maximum is represented in the Paleogene section and that there was a major turnover in mangrove composition between the Paleogene and Neogene. However, this transition was not caused by the Amazon River influence. In the second part (chapter 3) I focused on the vegetation evolution during the Neogene and the shift in sediment supply to the Suriname coast shifted from locally derived by Guiana Shield rivers to the addition of Andean-derived contributions; the latter transition occurred during the Pliocene to Pleistocene. In the third part (chapters 4 to 6) I showed that fluvial terraces along the

upstream and middle parts of the Suriname River are the result of a combination of (slight) tectonic uplift and climate-driven changes in discharge and sediment supply, whereas the downstream terraces are controlled by sea level fluctuations. fluctuations. I argue that the local rivers have kept pace with the coastal progradation, and that anthropogenic factors such as the Afobaka hydro-electric dam have influenced the hydrodynamics in and morphology of the river channel.

In this chapter, I will highlight how my research has contributed to the understanding of the development of the Suriname coastal area. I will discuss my results in the context of paleo- and neo-geology and -geomorphology. Finally, I will give suggestions for future research and summarize the general conclusions of this PhD thesis.

2. THESIS TOPICS

2.1 EVOLUTION OF THE SURINAME COASTAL ENVIRONMENT BASED ON A CENOZOIC SEDIMENTARY RECORD (POWISI-01)

Extensive mudflats cover the coastline of Suriname, which is part of the extensive Guiana coastline which lies between the Amazon and Orinoco Rivers. These mudflats are a result of sediment discharge from the Amazon River (Anthony et al., 2013; Augustinus, 2004). In **Chapter 2**, we reconstructed the vegetation composition changes of the nearshore coastal area and determined the changes in sediment provenance, the Andean versus the Craton sources. Sediments derived from the Andes had a major impact on the evolution of the northeastern coast of South America, including Suriname, by means of the Amazon River and longshore current transport. Additionally, we revised the existing age model for the Paleogene and Neogene deposits (Wong, 1986 & pers. comm, 2024) and compared the updated age model to other regional sporomorph zonations.

We generated pollen, spores and dinoflagellate data from processed cuttings samples from the Powisi-01 well using light microscopy (400X and 10000X magnification). Based on their botanical affinities, the pollen grains and spores were categorized according to their ecological groups. First and Last Occurrence Dates of both, pollen and spores, and dinoflagellate cysts were linked to other biostratigraphical regional zonations. I gained data from 9981 sporomorphs obtained from 30 cuttings samples representing seven ecological groups across 43 taxonomic affinities. I performed Coniss cluster analyses and obtained two main palynological zones, zone I and zone II, separated by a barren interval, and divided into six subzones. An age assessment was conducted based on biostratigraphic markers to construct an age model that was compared to regional biostratigraphic schemes for the sedimentary

basins along the Guianas coastline and Brazilian Equatorial Margin, and northern South America. I obtained data of dinoflagellate cyst assemblages from fifteen cuttings samples and distinguished two main associations characterized by the species diversity and dominance of common species. All these factors were further evaluated to reconstruct the paleoenvironment and determine the onset of the influence of the Amazon River on the coastal Plain of Suriname. This chapter answered the following questions:

2.1.1 Evidence for the Paleocene–Eocene Thermal Maximum (PETM) in the Suriname coastal record

In **Chapter 2** I assessed the occurrence of dinoflagellate cysts and their biostratigraphic meaning. Compared with Wong's (1986) age model—which integrates seismic, wireline log, and biostratigraphic data—the Powisi-01 age model shows notable differences. Most importantly, the Late Paleocene–Early Eocene boundary occurs at a greater depth in the present study, with palynological evidence placing the start of the Eocene at approximately 610–600 mbsl. In my study, the findings of both analyses (i.e. dinoflagellate cysts and biostratigraphy) implied the presence of the Paleocene-Eocene Thermal Maximum (PETM, a rapid global warming event ~56 Ma years ago (Koch et al., 1992) within the sample interval 610-600 mbsl, and a barren interval (600-500 mbsl) with no preservation of dinoflagellate cysts and palynomorphs. The co-occurrence of an *Apectodinium* acme, *Eocladopyxis* and *Homotryblium* (dinoflagellate cysts), and the occurrence of *Bombacacidites annae* (pollen grain), respectively associated with the PETM and restricted to Paleocene to PETM, supports the presence of deposits formed during this period of global warming. The link between the *Eocladopyxis* and *Homotryblium* and the PETM is supported by studies on the New Jersey Shelf by Sluijs & Brinkhuis (2009).

2.1.2 Cenozoic evolution of the coastal vegetation composition on the Suriname coastal plain?

Palynological data from the Powisi-01 well indicate that the section can be subdivided into two intervals. The Paleogene (lower interval) is dominated by high percentages of the *Proxapertites* and *Longapertites* group, a fossil type of mangroves, and an abundance of Palmae. A distorted representation of palynological diversity in this interval is caused by the occurrence of caved taxa (e.g., *Alnipollenites verus* and *M. maristellae*), due to downhole contamination from Miocene intervals. Hereafter, in the Miocene the coastal vegetation is dominated by the *Verrutricolporites rotundiporus* and *Zonocostites* group. Lastly, in the Plio-Pleistocene upper interval there is a turnover to Andean and vegetation types from the hinterland. A major part of the presented sporomorphs are of unknown affinity. The results further imply that ecological zones not necessarily coincide with sediment-lithological changes, and that the development of the modern mangrove belt is independent of Amazon River mud deposition along the Suriname coast. The Shannon Index, Pielou's evenness, and species richness analyses revealed that the sporomorph diversity is high, but is only visible with the deliberate omission of the dominating *Zonocostites* group.

2.1.3 Is the onset of the Amazon River and plume recorded in the Suriname Cenozoic coastal record?

To determine the onset of the Amazon River, geochemical analyses were conducted by colleagues from the Universidade de Brasilia and Université de Toulouse, including determining the samarium (Sm) en neodymium (Nd) concentrations, in order to calculate the T_{DM} for each sediment sample. The findings revealed different concentrations of ƐNd(0) and T_{DM} over the Powisi-01 well sample range between 700mbsl and 140 mbsl. The ƐNd(0) values reflect the sediment source, which is > 10–20 ppm for crustal rocks, and <10 ppm for basalt and mafic rocks. In the Powisi-01 well but only for the interval starting from 200 mbsl and shallower, ƐNd(0) values are greater than -13.5. The resulting T_{DM} values were between 1.40 and 2.28 Ga. In short, our geochemistry data suggest that between 200 and 175 mbsl (Plio-Pleistocene) there is sediment input from the Andean origin, wich is much later than proposed in previous studies by Krook (1979) and Wong (1986) who considered the arrival of the Andean sediments on the Suriname coastal area during the Miocene. Additionally, Orinoco- and Amazon-sourced sediments occur intercalated within cratonic sediments.

2.2 TRACING AMAZON INFLUENCE ON THE SURINAME COASTLINE: RESULTS FROM A STUDY ON A NEOGENE COASTAL SEDIMENTARY RECORD

Coastal development of Suriname has been governed by Andean sediment supplied through the Amazon River system. The onset of its influence on the Surinamese coastal plain has been estimated as Late Miocene. In **Chapter 3**, in collaboration with Eva Visser (MSc student, University of Amsterdam) we reconstructed the Neogene development of Suriname's coastline using palynological and geochemical data from the Hepp-3 borehole (Nickerie district). We generated pollen, spores and dinoflagellate data from processed cuttings samples from the Hepp-3 well using light microscopy (400X and 1000X magnification). The botanical affinity of pollen grains and spores enabled us to assemble the sporomorph data in ecological groups. Both pollen and spores were correlated with regional zonations using their First and Last Occurrence Dates. Preservation of dinoflagellate cysts was generally poor, and nearly all residues were barren. Therefore, a finer paleoenvironmental interpretation was not possible. Data was gained from 4253 sporomorphs obtained from 18 cuttings samples representing seven ecological groups across 45 taxonomic affinities. We performed Coniss analyses and obtained two main palynological zones (zone I and zone II) separated by a barren interval, of which zone II is divided into two subzones. An age assessment was conducted based on biostratigraphic markers to construct an age model that was compared to stratigraphic diagrams of sedimentary basins along the Guianas coastline and Brazilian Equatorial Margin, and northern South America. We also did a Maximum Likelihood Age (MLA) assessment with 19 samples to provide an age certainty across the section. All factors were further evaluated to reconstruct the change in vegetation in the coastal area of Suriname in the Neogene and

determine the influence of onset of the Amazon River. This chapter answered the following questions:

2.2.1 When did the onset of the Amazon influence on the Suriname coastline started?

Geochemical findings (Sm-Nd isotope data) from the Hepp-03 well reveal a clear shift in sediment provenance with decreasing depth. The lower interval contains more negative εNd values and older T_{DM} ages, indicating sediments sourced mainly from ancient cratonic areas of the Guiana Shield (Maroni-Itacaiúnas Province and Rio Negro-Juruena Province). In the upper interval, εNd values become progressively less negative and T_{DM} ages younger, pointing to a contribution from more juvenile Andean sources. Two major provenance transitions occur at ~131 mbsl and ~61 mbsl. Overall, the isotopic pattern records a shift from predominantly local cratonic river input to mixed or Andean-influenced sediment supply, which took place during the Plio-Pleistocene; this is later than indicated by regional models of late Neogene Amazon drainage reorganization.

2.2.2 How does stratigraphic age determination in the Hepp-3 contribute to our understanding of vegetation development of the coastal area in the Neogene?

Results from **Chapter 3** show that throughout the core mangroves persist with their strongest presence in the lower section (Zone I) pointing to high sea level conditions. Rainforest and montane forest species, initially limited in Zone I, become more common in the upper section (Zone II) corresponding to regressive conditions. Based on the occurrence or absence of biostratigraphic markers the lower part of the well corresponds to palynological zone E/F from Guyana (Van der Hammen & Wijmstra, 1964) and Suriname (Wijmstra, 1971) of Early to Middle Miocene age, while the upper part corresponds to pollen zone G from Guyana (Van der Hammen & Wijmstra, 1964) of Plio-/Pleistocene age. The lithology points to the Coesewijne Formation for the lower part, and the Zanderij Formation for the upper part. Maximum Likelihood estimations agree with biostratigraphic results for the lower interval, but conflict with those of the upper interval. For the upper part we rely on existing age models for the regional lithostratigraphy.

2.2.3 What were the ecological conditions along the Suriname coastline?

The lower interval shows two mangrove-dominant phases separated by a period of decreased coastal influence, alongside repeated expansions of floodplain and hinterland forests, and the first arrival of Andean-derived pollen. A barren, sand-rich interval from 204–140 mbsl separating the lower and upper intervals, marks a substantial progradation of the coastline driven by a regression, and replacing stable coastal wetlands with dynamic environments. The upper interval, including the Zanderij and Coropina/Mara formations, features reduced but variable mangrove presence, continuous input from rainforest and montane forests, persistent freshwater palm swamps, and a short-lived savanna expansion.

2.3 THE INTERPLAY BETWEEN TECTONIC ACTIVITY, CLIMATE AND SEA-LEVEL CHANGE IN THE SURINAME RIVER VALLEY, TROPICAL SOUTH AMERICA

In **Chapter 4** an overview of the Pleistocene terraces and Holocene floodplains along the Suriname River valley is presented. This study provides the key controls behind the development of the river terraces along the upper and lower river valley parts. Maps and fieldwork from the 70s and 80s in the upstream part (Kips et al., 2025; Kips et al., 1979) combined with Digital Elevation Models and topographic maps of the downstream part were used to analyze and interpret the remnants of these river terraces.

In general, rivers flowing in cratonic areas often display terraces that consist of rounded gravel which points to historical differences in hydrological regimens and climatic environments (Bakker, 1968; De Boer, 1972). The mechanisms of formation of river terraces depends on their location along the rivers. Terraces along the lower reaches of rivers are driven by fluctuating sea levels (Bridgland, 2012; Maddy et al., 2001; Zeuner, 1945), while those along upstream river parts are more the result of climate change and tectonic uplift.

This chapter answered the following research questions:

2.3.1 What are the key controls behind the development of river terraces along the Upper and Lower Suriname river valley?

To address this research question I divided the Suriname River valley into two parts, the combined upstream and middle river parts, and the downstream river part. Terrace remnants that occur along the upper River valley part were mapped based on previous research by Balsem and Rhebergen (1979) and Kips and Snel (1979); they were categorized into a 20 m, 15 m, and 5 m level. The results show that each terrace level has a different gradient and composition. The 20-m terrace level has a gradient of up to 18% and is composed of regolith derived from felsic rocks and local river sediments. In contrast, the 15-m terrace level has a gentler gradient, up to 8 %, and consists of Pleistocene fluviatile sediments and regolith of primarily felsic rocks. The lowest terrace remnants are found on 5 m level have gradients of around 4 % and consist of thin fluviatile loam deposits. The current floodplain consists of silty to heavy clays. The 5-m terrace and floodplain are not continuously present along the river profile. Where they are present the 20-m and 15- m terraces directly border the river channel.

Due to the construction of the Afobaka Dam and the storage lake, the presence of higher terrace levels remains unknown in that area. In the Lower River valley part, well-developed terrace levels are found on 20-m, 15-m, and 5-m above mean water level at Victoria, Baboenhol, and Cassipora. Each terrace level differs in composition and morphology, and the

transition from one level to another varies from gradual to abrupt depending on their location along the river. Gradual transitions occur in the inner river bends, while abrupt ones occur in outer bends. The composition of the 20-m terrace levels ranges from sandy loams with gravel, loamy sands, and loamy sands with gravel at Victoria to quartz gravels and gravel clasts at Cassipora. The 15-m terrace level has an undulating landscape and its composition is currently unknown. The 5-m terrace level, which is only present at Victoria and Baboenhol, and consists of clays with signs of local soil development. Correlation between the upstream and downstream terraces suggests a lowering of eustatic sea levels and/or slight tectonic movement during formation of the terrace staircae.

2.3.2 How was the terrace evolution in the upstream and middle river valley parts?

The 20-meter of total incision that has occurred since the Pliocene in the Suriname River valley was too limited to create a river terraces for each climatic cycle (>= 30) like elsewhere. It is suggested that this 20-m total incision may have been the result of a long-term drop in eustatic sea level or minor tectonic uplift. Distinct knickpoints in the river's profile—particularly at Goejaba and Pokigron—are the result of differential weathering processes. In tropical environments like Suriname, fine sediment resulting from intense chemical weathering are unable to significantly erode these knickpoints (Gersie et al., 2021; Kroonenberg et al., 1983). During glacial periods with dry climate conditions, however, more gravel was present in river channels due to limited chemical weathering. Gravel transport potentially caused larger vertical erosion (by abrasion) and thus lowering of the knickpoints. This is evidenced at the Brokopondo Sula, that is now part of the 5-m terrace level, which may have been actively eroded by increased gravel bedload during glacial times. This points to possible smoother river profiles during glacial periods compared to interglacial times. Due to a lack of data, it is difficult to validate this hypothesis.

2.3.3 How was the fluvial development in the downstream river part?

I assesed the difference in behaviour between the upstream and downstream parts of the Suriname River valley parts during glacial periods. Upstream of the river tends to aggradate, while the downstream it incises due to sea level fall. The transition between these river parts occurs at the Brokopondo Sula, situated on the boundary between the Guiana Shield and the coastal plain. A 120-meter lowering of the sea level during the Last Glacial Maximum caused the Suriname River to cut deeply into its floodplain and shelf, with incisions up to 120 meters. However, sea level rise likely did not affect the formation of terraces upstream of the Brokopondo Sula because it prevents the incisional knickpoint from moving further upstream. As a result of the distance between the river mouth and located terraces, I suggest that 5-m terrace level remnants at Victoria and Baboenhol are fluvial deposits from the last glacial period as they sit higher than known marine deposits and consist mainly of clay without typical marine characteristics. To summarize, the fluvial development in the downstream Suriname river part occurred due to sea level changes.

2.4 UNDERSTANDING WESTWARD DEFLECTION DUE TO RIVER-COAST INTERACTIONS IN THE HOLOCENE COASTAL PLAIN OF SURINAME

The uneven development displayed by the coastline along the Guianas (French-Guiana, Suriname, and Guyana) is attributed to a difference in sediment deposition along the coast caused by migrating mudbanks (Augustinus, 2004). In addition, the East-west migrating mudbanks and mangrove forests ensure natural protection of the coastline (Toorman et al., 2018). The mudbank migration is cyclic causes alternating periods of erosion and deposition, which in turn cause significant changes in the size of morphological units, such as the Braamspunt and Coppenamepunt mudcapes along Suriname's coast. The westward deflection of small rivers in the coastal zone is attributed to the interaction between fluvial and mudbank migration (Augustinus, 1989).

In **Chapter 5**, I determined how the main local rivers have kept pace with the progradation rate of the Holocene Young Coastal Plain and I studied the driving force(s) behind the westward deflection of the small rivers. I captured and compiled long-term changes by using 5-year interval digital satellite photo images from 1989 to 2024, together with analogue and digital historic topographical maps from the 1970s to the 18th century and earlier. The coastal progradation rate was reconstructed using old cheniers that represent former coastlines (Augustinus, 1978). In addition, I tracked the changes in surface area of the Braamspunt and Coppenamepunt mudcapes from 1987 to 2024. I further assessed the deflecting behaviour of rivers in the Young Coastal Plain through determination of their deflection angle with respect to the orientation of the coastline. The identified deflection points were used to calculate the coastal progradation rates using the onset of the Young Coastal Plain as the starting point. This chapter answered the following questions:

2.4.1 How did the Young Coastal Plain develop during the Holocene?

Results from **Chapter 5** show that the Wanica phase exhibits a larger progradation in the eastern part of the country than the west, unlike the Moleson phase, which shows a larger progradation in the west. This is attributed to the bend in the Guiana Shield along the Guianas' coastline, which in turn is a result of the separation of Africa and South America during the Gondwana break-up (Will and Frimmel, 2018).

2.4.2 How did the Braamspunt and Coppenamepunt mudcapes changed in surface area in the last decades?

Results from the analyses of surface areas of the mudcapes showed that the Braamspunt mudcape has been a subjected to a steady decline in surface area of 400 m^2 p/yr between 1987 and 1999, followed by another period of steady decrease of 600 m^2/yr. Each period of erosion is followed by a period of net stability. The Coppename mudcape with a relatively flat coastline has also reflected a cyclicity of increase and stability of the surface area. Starting

in 1987 with a surface area of more than 5 km^2, and since then this concave shaped part of the coastline has changed significantly in size from about 157 to 250 km^2. According to Augustinus (2004) this substantial progradation is related to the natural straightening of the coastline. Due to the characteristic shape of the Guiana Shield a so-called blindspot is created in the coastline which is easily filled with longshore-transported sediments.

2.4.3 What is the orientation of the main river courses in the coastal plain?

The analyses of river courses and their westward deflecting river mouths was carried out for the seven main rivers flowing from south to north. The results display deflections angles between 86 and 104 degrees, and indicate minimal deflection for rivers with large watersheds, such as the Marowijne and Corantijn Rivers. In contrary, rivers with smaller watersheds, such as the Commewijne and Saramacca Rivers, indicate a westward deflection angle between 250 and 290 degrees. The Nickerie River is an exception and shows a deflection angle close to 90 degrees. Compared to rivers in French-Guiana and Guyana, where deflection angles vary between 134 and 175 degrees, and between 100 and 120 degrees respectively, the Suriname rivers display a large distribution in the deflection angles. The main drivers behind the deflections are the northeasterly trade winds causing waves to drive longshore sediment transport, east-west migrating mudbanks, and the fluvial discharge. The variation in deflections can be explained by the difference in river discharge, coastal orientation with respect to incoming winds waves, and the size of migrating mudbanks. This study is the first to analyse the deflection angle along the Guianas, in particular the Suriname coast, and has given insight into the importance of the interaction between fluvial and marine processes.

2.4.4 Can we quantify and date river deflection quantification?

I addressed this research question by plotting the relationship between the start of deflection of four rivers and the development of the coastline in northward direction. The distance of this deflection point to the present coastline lies between 16 to 20 km for the Cottica, Commewijne, and Saramacca Rivers, except for the Nickerie River which deflection point starts at approximately 42 km from the current coastline. These distances were used to estimate the age of the river deflection points and ultimately the progradation rates of the coastal plain. The estimated progradation rates in this study ranged from 2.7 to 6.8 m/yr which coincides with average progradation rates between 2 and 8 m/yr suggested by Augustinus (1978) and Pearson et al. (1986). The estimated age of the deflection point of the Commewijne River is 2500 yrs BP, coinciding with the Comowine Phase, while that of the Cottica and Saramacca ranges between 4500 and 6500 yrs BP which corresponds to the Wanica Phase. The onset of the Wanica Phase points to the mid-Holocene sea-level stabilization (Pons, 1966) that resulted in a change of coastal dynamics and ultimately the westward deflection of river courses. The Wanica phase is also found in the middle of French Guiana (Pons, 1966) between the Sinnamay and Kourou rivers (Wong, 1989).

2.5 MARINE AND ANTHROPOGENIC CONTROLS ON THE ESTUARY OF THE SURINAME RIVER OVER THE PAST 50 YEARS

In general, since the start of the Holocene, human activity has had an increasing impact on fluvial systems and changed natural sediment fluxes, which has resulted in the change of river's morphology (Maaß et al., 2021). More recently, river regulation for hydro-electric power purposes has clearly altered discharges and sediment loads of fluvial hydrosystems (Petts, 1984; Bravard and Petts, 1996). Today, large amounts of sediments carried by tropical rivers get trapped in lake reservoirs. The reduced sediment load can also result in the change of tropical coastal dynamics (Ezcurra et al., 2019), like in Suriname.

In **Chapter 6** I focused on the behaviour of the Suriname river that has been influenced by anthropogenic activities since colonial times. I analyzed the hydrologic and geomorphic evolution of the lower part and estuary of the Suriname River over the past 50 years. This was achieved by field observations and level measurements supplemented by studying aerial photographs and satellite imagery. Additionally, depth measurements along bathymetric cross-sections were studied, together with internal reports of studies done in the Suriname River regarding channel depth and rivier morphology of the Maritime Authority of Suriname.

This chapter answered the following questions:

2.5.1 What is the interaction of processes in the coastal zone and the Suriname estuary?

Currents and waves in the near-coastal area are very essential for coastal development and the estuary (Gersie et al., 2016). In general, across the Guianas, estuaries are influenced by the interaction between fluvial and marine processes such as waves, longshore sediment transport, and river discharge. Suriname, the tidal current flows with different velocities into the easterly flood- and westerly ebb channel of the estuary, depending on whether it is rising or falling tide. The flow velocity increases up to 1.5 m/s in the flood channel, while flow velocities of approximately 1 m/s flow were measured in the ebb channel. As waves enter the estuary their impact on river banks diminishes rapidly, while the impact of the tidal wave increases on the morphology of the river. Cross-sections of the fairway display the occurrence of depressions and silt bars in respectively the outer and inner bends. Influence of the tidal wave decreases towards the head of the estuary, where in contrary the rivers' discharge impact increases.

2.5.2 What has been the rivers' response to dam construction?

This paragraph describes the impact of the Afobaka Dam constructed in 1964 on the fairway of the Suriname River. Various cross-sections along the River estuary display the silting up of the river channel of approximately 4.8 m in 48 years, and the alternated migration of this

channel towards the eastern and western river banks. Initially, the relaxation response was fast, but slowed down after 1981. The response time of the river to the imposed change halted between 1981 and 1992.

3. GENERAL DISCUSSION

Part 1: Why study the development of the Suriname coastal plain?

The Amazon started to deliver Andean sediments to the Amazon fan at ~ 10 Ma (Figueiredo et al., 2009). A major part of the Amazon borne sediments was transported by the North Brazil Current (Nittrouer and DeMaster, 1996; Hoorn et al., 2017) towards the northeastern coast of South America, and is the source of clayey and silty sediments transported to the Suriname coast by the Guiana current. Krook (1979), Wijmstra (1971), and Wong (1986) indicated that the influence of the Amazon River on the Suriname coast started during the Late Miocene (roughly 11.6 to 5.3 Ma) during a transgression. It resulted in the deposition of large amounts of clay (Wong, 1986) and a change in coastal vegetation. Sediments originated from the Amazon naturally carry a specific geochemical signature (Hoorn et al., 2017). Therefore, the Amazon Fan formed by Amazon River deposits, is used as a basis to study the evolution of the Amazon River (Hoorn et al., 2017), and in this thesis, the northeastern coast of South America.

I studied the development of the Suriname coastal plain because of its dynamic characteristics which have influenced and shaped the hydrodynamics and morphology of not only the coastline, but also the south-north running rivers. Furthermore, it has been at least 50 years since the last palynological studies in the coastal plain were conducted. However, these studies were brief and therefore, a more extended and detailed updated research was needed.

In the results we were able to detect the global PETM (Srivastava and Prasad, 2019) pointing to the Late Paleocene/Early Eocene period. Furthermore, the lithostratigraphy of the nearshore Suriname coastal area represents an age interval that ranges from the Late Paleocene to the Holocene. Biostratigraphic analyses have not shown this clearly, but the geochemical signature in the sediments suggest a delayed arrival at the Suriname coast which is estimated (also based on regional data) as Late Miocene.

Mangrove forests occur in a salty to brackish environment, and can therefore be used to detect sea level changes (Amstelveen, 1969) or processes related to coastal dynamics. The first occurrence of *Rhizophora* mangroves was reported by Wijmstra (1971). In my results mangroves show an alternating appearance from the Paleocene to the Plio/Pleistocene indicating several climate alternations with temperature- and sea levels changes and dynamic processes on the coastal plain.

Both studied wells (Powisi-01 and HEPP-3) provided a good insight into the changes in vegetation along the Suriname coast. First, in the Paleogene, we see the *Proxapertites* and *Longapertites*, fossil mangrove types that represent a whole other mangrove system than the present, together with a variation of palms. Also remarkable in the Powisi-01 well was the clear presence of the PETM. Subsequently, in the Early Miocene (Neogene) *Zonocostites* and *Verrrutricolporites* represent the arrival of 'modern' mangroves in the section. Then, in the Upper Miocene to Plio-/Pleistocene the Andean signal is displayed with Andean pollen types and vegetation from the hinterland (Guiana Shield), representing the coast as it is developing into the situation of the present day.

Part 2: Reappraised age model for coastal Suriname

The latest age model for the Suriname coast was constructed by Wijmstra (1971) and van der Hammen and Wijmstra (1964), and later revised by Wong (1986). Therefore, a reappraised model for the coastal area of Suriname was needed.

The age and depositional history of the coastal area of Suriname in the Neogene is constrained by biostratigraphic and geochemical evidence. The lower section is dated as by Late Paleocene and Eocene sediments by means of biostratigraphic markers. Instead, the age of the upper section assessed based on the absence of important age markers (e.g. Oligocene marker *Cicatricosisporites dorogensis*) combined with Maximum Likelihood Age estimates (17.53–17.18 Ma), which point to an Early to Middle Miocene age. Compared to Wong (1986), the boundary between the Late Paleocene and Early Eocene (~610–600 mbsl) is situated deeper in our age model. The transition from Oligocene to the Early Miocene is also situated deeper than Wong's age model.

Geochemical signatures show a shift from a cratonic sediment source to Andean input from Upper Miocene to Plio-/Pleistocene, vegetation trends show a shift from mangrove-dominated assemblages to rainforest and montane forests, reflecting a transition from transgressive to regressive conditions. Correlations with the R1 unconformity in the Demerara Rise offshore Suriname, and clay-rich deposits from the same region, support an onset of Andean sediment influx in the Late Miocene. Regional correlations with the Barreiras Formation in northeastern Brazil suggest that deposition of the Zanderij Formation began in the Late Miocene and continued into the Pliocene, prior to increased Amazonian influence in the Pleistocene.

Part 3: Development of the Suriname coastal plain through time

Suspended Amazon river sediments were transported by the Guiana Current and deposited along the Suriname coast as shore-attached mudbanks (Augustinus, 1980). These westward moving mudbanks reflect a coastal system with an alternation of accretion and erosion (Augustinus, 2004), and have a major impact on the geomorphology of the Suriname coast (Anthony et al., 2013). The large-scale coastal development of Suriname seems to be influ-

enced not only by transported Amazon sediments and shifting mudbanks, but also by the contributions of both small and large rivers draining the Guiana Shield (Anthony et al., 2013). In my results the westward deflection of the low-discharge rivers is clearly noticed in the terminal section as the river approaches the coastline, which is the result of dominance of marine processes over river discharge. It is not the cheniers that play a major role in this river behaviour, but it is the magnitude of the river discharge. Gravel deposits and coarse sands from the Pliocene that occur along the Suriname, Marowijne, and Saramacca rivers, resulted from river incision (Wong et al., 2016), consistent with my observations of 20, 15, and 5 m river terraces at Victoria, Baboenhol, and Cassipora in the lower Suriname River. As global sea level dropped 120 m during the Last Ice Age (about 20.000 yrs ago) and as a result, the coastline moved 150 km northward further which resulted in expansion of the coastal plain (Wong et al., 2016). My results indicate that intense weathering and erosion processes resulted in further flattening of the terraces. Amazon mud was not transported immediately along the Suriname coast, but was deposited in the Guiana Basin. Changes in sediment transport due to human interventions have also been observed in many tropical rivers, where increased siltation in river channels downstream of dams has contributed to higher flood risks (Latrubesse, 2009). Anthropogenic activities in the coastal plain, in particular along the Suriname River, go back to the colonial time when plantations were established close to the river for irrigation and transport purposes. The construction of the Afobaka hydro-electric dam and Afobaka Lake in 1964 resulted in the regulation of the rivier discharge and prevention of sediment discharge from the hinterland. This has impacted the river and coastal morphology west from the Suriname River mouth. As the flow and amount of sediment carried to the Atlantic ocean has decreased, marine processes start to dominate the estuary. The westward debouching of the river mouth and the varying change in size and shape of the sandspit at Braamspunt are an example of this. On the other hand, my results show that since the construction the import of Amazon-derived sediments into the Suriname Estuary has increased which in turn has resulted in the river channel becoming shallower.

4. GENERAL CONCLUSIONS

The following conclusions can be drawn from this thesis:

(i) The concentration of sporomorphs was high and diverse, reflecting the high terrigenous input from a highly biodiverse mangrove and hinterland forest along the Suriname coast, with sediment input from the Amazon craton and the Andes. Biostratigraphic markers and the updated age model highlights the correlation of vegetation shifts with major climatic and sea level events. This includes the PETM and subsequent regressions and transgressions throughout the Paleogene and Neogene. Findings revealed that Andean-derived sediments from the Amazon River deposited in the Suriname coastal area occurred from the uppermost Miocene to Plio-/Pleistocene revealing a significant time lag

between the formation of the Amazon Fan and the arrival of its sediments in the Guyanas coastal region. Nevertheless, deep sea marine records are needed to provide the complete history, as there are many hiatuses in the nearshore record. **(Chapter 2)**.

(ii) Sm-Nd isotopes reveal an early dominance of cratonic material from the Maroni–Itacaiúnas Province, followed by increased input from the Rio Negro–Juruena Province, and finally a juvenile component indicating Andean sediment arrival from the latest Miocene onwards. However, palynological records show environmental changes and alternating mangrove, swamp, and rainforest communities, evidencing earlier Amazon influence than the detrital signal. The inconsistency of Andean pollen appearing earlier than Andean clastic sediment input implies long-range microfossil transport prior to changes in bulk sediment routing. The results demonstrate how coastal wetlands archive regional changes in sediment routing, sea level, and drainage evolution **(Chapter 3)**.

(ii) The input of insufficient coarse sediment from the weathered basement rock causes the Suriname River to transport minimal bedload transport. The stable multichannel cataracts are formed where the river channels are forced to navigate around bedrock exposures rather than erode them. The presence of various gravel-bearing terrace levels above the present flood plain implies semi-arid climatic conditions where fluvial dynamics were different from present day. The consistency in terrace levels represent major developing stages of the river drainage basin and are either the result of long-term global sea level drop or limited tectonic uplift **(Chapter 4)**.

(iii) River behaviour along the Suriname coast is governed by a dynamic equilibrium between alongshore sediment transport, Amazon-sourced mudbanks, marine and wind-driven wave forces, and river discharge. Long-term fluctuations in mudbank size (over 160–200 years) strongly influence estuarine dynamics and river deflection. These insights highlight the importance of present-day processes for reconstructing past coastal development **(Chapter 5)**.

(iv)Natural and human factors such as dam construction have significantly altered the flow of the Suriname River, and led to increased import of sediments into its estuary. As a result, the river morphology has changed, which has led to growth of bars and a shift to a more tidal-dominated system. Adaptation of the river channel to imposed changes took nearly 17 years. At the same time moving mudbanks have affected the sandspit at Braamspunt, whose growth is linked to sediment supply from the east **(Chapter 6)**.

5. OUTLOOK

Sediments from the Amazon River will continue to play an important role in the development of the coastline of Suriname and the entire Guianas. Climate change will have a major impact on sediment transport from the Amazon to the Suriname River, and on Suriname's coastal vegetation in the near future. Rising temperatures and decreasing rainfall in the Amazon River Basin could result in less sediment being deposited along the Surinamese coast, with significant consequences for the shape of the coastline. For example, a landward shift of the coastline could cause the low-lying coastal plain to inundate, resulting in floodings of nearby areas. East-west migrating mudbanks will become smaller and offer less protection to the coast. Together with decreasing fluvial discharges these changing coastal dynamics will also impact the deflection rate of the rivers, in particular the Suriname River.

Urbanization of floodplains since the colonial period (>1492 CE) will remain a problem, because the proximity of water is important for village residents in the hinterland. A rise or drop in water level of the river due to human interventions or natural factors can increase the flood risk in the future or affect sediment discharge. Therefore, future research should aim to improve the understanding of the interplay between changing coastal dynamics and evolution of the current coastal plain. To conserve coastal ecosystems and prevent floodings of coastal areas and riverbanks, governmental and NGO's should integrate to ensure that the coastal area is managed in a sustainable manner. Monitoring and measuring of sediment budget, erosion and deposition rates, and human activities by local authorities should be executed on a regular basis to mitigate degradation and negative impacts on coastal areas.

REFERENCES

Amstelveen, A. L. E. (1969). A palynological on three water wells in the coastal area of Surinam (Saramacca and Suriname Districts). *Geologische Mijnbouwkundige Dienst Mededeling*, *20*, 165–172.

Augustinus, P. G. E. F., (1978). The changing shoreline of Surinam (South America). PhD Thesis Utrecht University, 232 pp. Uitgaven "Natuurwetenschappelijke studiekring voor Suriname en de Nederlandse Antillen, Utrecht, 95, 232 pp.

Augustinus, P. G. E. F. (1980). Actual development of the chenier coast of suriname (South America). Sedimentary Geology, 26 (1-3), 91-113. https://doi.org/10.1016/0037-0738(80)90007-X.

Augustinus, P. G. E. F., Hazelhoff, L., & Kroon, A., 1989. The chenier coast of Suriname: modern and geological development. Marine Geology, 90(4): 269-281. DOI: 10.1016/0025-3227(89)90129-1.

Augustinus, P. G. E. F. (2004). The influence of the trade winds on the coastal development of the Guianas at various scale levels: a synthesis. Marine Geology, 208 (2-4), 145-151. https://doi.org/10.1016/j.margeo.2004.04.007.

Anthony, E.J. (2013). Storms, shoreface morphodynamics, sand supply, and the accretion and erosion of coastal dune barriers in the southern North Sea. Geomorphology, 199, 8-21. https://doi.org/10.1016/j.geomorph.2012.06.007.

Anthony, E. J., Brunier, G., Gardel, A., Hiwat, M. (2019). Chenier Morphodynamics on the Amazon-Influenced Coast of Suriname, South America: Implications for Beach Ecosystem Services. Frontiers in Earth Science, 7: 1-20. https://doi.org/10.3389/feart.2019.00035.

Bakker, J.P. Die Flussterrassen Suriname als Hinweise auf etwas trocenere Klimate während der Quartären Eiszeiten. Acta Geog. Debrecina Landscape Environ. 1968, 7, 9–17.

Balsem, T.; Rhebergen, G.J. Bodemgesteldheid en geomorfologie langs de Midden-Suriname en de Midden-Saramacca Rivier; Report Dienst Bodemkartering; Unpublished Report; Dienst Bodemkartering: Paramaribo, Suriname, 1979.

Bridgland, D. R. (2012). *Quaternary of the Thames*. Springer Science & Business Media.

De Boer, M.W.H. Landform and Soils in Eastern Surinam (South America); Pudoc: Wageningen, The Netherlands, 1972; p. 169.

Ezcurra E., Barrios, E., Ezcurra, P., Ezcurra, A., Vanderplank, S., Vidal, O., Villanueva-Almanza, L. , Aburto-Oropeza, O. (2019). A natural experiment reveals the impact of hydroelectric dams on the estuaries of tropical rivers. Science Advances, 5 (3), 1–9 DOI: 10.1126/sciadv.aau9875.

Figueiredo, J.; Hoorn, C.; Van der Ven, P.; Soares, E. (2009). Late Miocene onset of the Amazon River and the Amazon deep-sea fan: Evidence from the Foz do Amazonas Basin. Geology, 37 (7): 619–622. https://doi.org/10.1130/G25567A.1.

Gersie, K. S., Van Balen, R. T., & Kroonenberg, S. B. (2021). The Interplay between Tectonic Activity, Climate and Sea-Level Change in the Suriname River Valley, Tropical South America. *Quaternary*, *4*(2), 11. https://doi.org/10.3390/quat4020011.

Hoorn, C., Bogotá-A, G. R., Romero-Baez, M., Lammertsma, E. I., Flantua, S. G. A., Dantas. E. L., Dino, R., Do Carmo, D. A., Chemale Jr, F. (2017). The Amazon at sea: Onset and stages of the Amazon River from a marine record, with special reference to Neogene plant turnover in the drainage basin. Global and Planetary Change, 153, 51-65. https://doi.org/10.1016/j.gloplacha.2017.02.005.

Kips, P.H.A.; Snel, A.R. Landschap, bodemgesteldheid en landgeschiktheid langs de Midden-Suriname Rivier (Goejaba–Botopassi); Unpublished Report; Dienst Bodemkartering: Paramaribo, Suriname, 1979; p. 229.

Kips, F. , Snel, A., Schuurman, A. E., Gersie, K., Kroonenberg, S. (2025). Tracing the legacy of past semiarid morphodynamics in multiconvex tropical rainforest morphology in the Guiana Shield of Suriname. Catena, 258, 109286. https://doi.org/10.1016/j.catena.2025.109286.

Koch, P. L., Zachos, J. C., Gingerich, P. D. (1992). Correlation between isotope records in marine and continental carbon reservoirs near the Palaeocene/Eocene boundary. Nature, 358, 319-322. https://doi.org/10.1038/358319a0.

Krook, L. (1979). Sediment petrographical studies in Northern Suriname. PhD Thesis, VU University Amsterdam. 154 pp.

Kroonenberg, S. B., Melitz, P. J. (1983). Summit levels, bedrock control and the etchplain concept in the basement of Suriname. Geologie en Mijnbouw, 0016-7746/83/62Ü3-Ü389, 389–399.

Latrubesse, E.; Stevaux, J.; Sinha, R. Tropical rivers. Geomorphology 2005, 70, 187–206.

Maaß, A. L., Schüttrumpf, H., Lehmkuhl, F. Frank Lehmkuhl (2021). Human impact on fluvial systems in Europe with special regard to today's river restorations. Environmental Sciences Europe, 33 (119), 1-13. https://doi.org/10.1186/s12302-021-00561-4.

Maddy, D., Bridgland, D., & Westaway, R. (2001). Uplift-driven valley incision and climate-controlled river terrace development in the Thames Valley, UK. *Quaternary International*, *79*(1), 23-36. https://doi.org/10.1016/S1040-6182(00)00120-8.

Nittrouer, C. A., DeMaster, D. J. (1996). The Amazon shelf setting: tropical, energetic, and influenced by a large river. Continental Shelf research, 16 (5-6), 553-573. https://doi.org/10.1016/0278-4343(95)00069-0.

Pearson, G. W., Pilcher, J. R., Baille, M. G. L., Corbett, D. M., & Qua, F. (1986). High-precision C14 measurements of Irish oaks to show the natural C14 variations from AD 1840 to 5210 BC. Radiocarbon, 28, 911-934.

Petts, G. E. (1984). Sedimentation within a regulated river. Earth surface processes and landforms, 9 (2), 125-134. https://doi.org/10.1002/esp.3290090204.

Petts, G.E., Bravard, JR. (1996). A drainage basin perspective. In: Petts, G.E., Amoros, C. (eds) The Fluvial Hydrosystems. Springer, Dordrecht. https://doi.org/10.1007/978-94-009-1491-9_2.

Pons, L. J. (1966). Geogenese en pedogenese in de jong-Holocene kustvlakte van de drie Guianas. Tijdschrift Koninkelijk Nederlands Aardrijkskundig Genootschap, 83, 153–172.

Sluijs, A., & Brinkhuis, H. (2009). A dynamic climate and ecosystem state during the Paleocene-Eocene Thermal Maximum: inferences from dinoflagellate cyst assemblages on the New Jersey Shelf. *Biogeosciences*, *6*(8), 1755–1781.

Srivastava, J., & Prasad, V. (2019). Evolution and paleobiogeography of mangroves. In *Marine Ecology* (Vol. 40, Issue 6, pp. 1–12). Blackwell Publishing Ltd. https://doi.org/10.1111/maec.12571.

Toorman, E.A., Anthony, E., Augustinus, P.G.E.F., Gardel, A., Gratiot, N., Homenauth, O., Huybrechts, N., Monbaliu, J., Moseley, K., Naipal, S., 2018. Interaction of mangroves, coastal hydrodynamics, and morphodynamics along the coastal fringes of the Guianas. Threats to mangrove forests, Coastal Research Library 25, pp. 429-473, Springer. DOI: 10.1007/978-3-319-73016-5_20.

Van der Hammen, Th., & Wijmstra, T. A. (1964). *A palynological study on the Tertiary and Upper Cretaceous of British Guyana. Leidse Geologische Mededelingen, 30*. 183–241.

Will, T. M., Frimmel, H. E. (2018). Where does a continent prefer to break up? Some lessons from the South Atlantic margins. Gondwana, 53, 9-19. https://doi.org/10.1016/j.gr.2017.04.014.

Wong, Th. E. Kroonenberg, S.B., Augustinus, P. G. E. F. (2016). Geologie en landschap van Suriname. LM Publishers, Edam, 182 pp.

Wong, Th. E. (1986). Outline of the stratigraphy and the geological history of the Suriname coastal plain. Geologie en Mijnbouw, 65, 223-241.

Wong, Th. E. (1989). Revision of the stratigraphy of the coastal plain of Suriname. Natuurwetenschappelijke Studiekring Voor Suriname En de Nederlandse Antillen (Publications of the Foundation for Scientific Research in Surinam and the Netherlands Antilles, 125, 1–64.

Wijmstra, T. A. (1971). The palynology of the Guiana Coastal Basin. PhD Thesis, Vrije Universiteit Amsterdam, 71 pp.

Zeuner, F.E. The Pleistocene Period, Its Climate. Chronology and Faunal Successions; Ray Society: London, UK, 1945.

CO-AUTHORSHIP STATEMENT

Chapter 2
Provenance and paleoenvironmental evolution of the Suriname–Guyana Basin based on a Cenozoic nearshore sedimentary record (Powisi-01)

Kathleen Gersie, Roel Verreusel, Elton Luiz Dantas, Roberto Ventura Santos, Martin Roddaz, Raul Giovanni Bogota-Angel, Henry Hooghiemstra, Angelo Plata Torres, Hanna van den Hil, Ronald van Balen, Carina Hoorn

Submitted and being reviewed in *Palaeogeography, Palaeoclimatology, Palaeoecology*

K.G., R.V. and C.H. conceptualized the research. K.G. collected and analyzed the data with contribution of C.H., R.V., E.L. Dantas, R.V.S., M.R., R.G.B., H.H., A.P.T., H.v.d.H. K.G. wrote the first draft of the manuscript with contribution of C.H. and R.v.B. E.L.D., R.V.S. and M.R. conducted the geochemical analyses. R.V. conducted the dinoflagellate analyses. H.v.d.H. conducted the diversity analyses and designed the diagrams. All authors revised and approved the submitted manuscript.

Chapter 3
Tracing Amazon influence on the Suriname coastline: Results from a study on a Neogene coastal sedimentary record

Eva Visser, Kathleen Gersie, Roel Verreusel, Elton Luiz Dantas, Roverto Ventura Santos, Martin Roddaz, Raul Giovanni Bogota-Angel, Henry Hooghiemstra, Hanna van den Hil, Carina Hoorn

(Prepared for submission)

K.G., R.V. and C.H. conceptualized the research. K.G. collected the data, E.V. C.H., and R.V. analyzed the data with contributions from E.L. Dantas, R.V.S., M.R., R.G.B., H.H., A.P.T., H.v.d.H. E.V. wrote the first draft of the manuscript with contribution of K.G. and C.H. K.G. and C.H. contributed substantially to the revisions. E.L.D., R.V.S. and M.R. conducted the geochemical analyses and diagrams. R.V. conducted the dinoflagellate analyses. H.v.d.H. contributed to the design of diagrams. All authors revised and approved the prepared manuscript.

Chapter 4
The Interplay between Tectonic Activity, Climate and Sea-Level Change in the Suriname River Valley, Tropical South America

Kathleen Gersie, Ronald T. van Balen, Salomon B. Kroonenberg

Quaternary (2021): 4 (2), 11.
DOI: 10.3390/quat4020011

K.G. and R.v.B. conceptualized the research. K.G. and R.v.B. collected and analyzed the data. K.G. wrote the first draft with contributions of R.v.B. and S.K. K.G. designed all diagrams and figures. R.v.B. and S.K. contributed substantially to the revisions. All authors revised and approved the submitted manuscript.

Chapter 5
Understanding westward deflection due to river-coast interactions in the Holocene coastal Plain of Suriname

Kathleen Gersie, David Klink, Pieter Augustinus, Jaap Nienhuis, , Nisha Bharos, Iris de Vos, Steven de Jong

In preparation for submission

K.G., S.d.J., and P.A. conceptualized the research. D.K. conducted the study, analyzed the data, and wrote the first draft with contributions from K.G., S.d.J., P.A., and J.N. All authors revised and approved the chapter.

Chapter 6
Marine and anthropogenic controls on the estuary of the Suriname River over the past 50 years

Kathleen S. Gersie, Ronald T. van Balen, Pieter G.E.F. Augustinus

Netherlands Journal of Geosciences - Geologie en Mijnbouw. 2016; 95(4).
DOI: 10.1017/njg.2016.18

K.G., R.v.B., and P.A. conceptualized the research. K.G. collected and analyzed the data. K.G. wrote the first draft with contributions of R.v.B. and P.A. K.G. designed all diagrams and figures. R.v.B. and P.A. contributed substantially to the revisions. All authors revised and approved the submitted manuscript.

ACKNOWLEDGEMENTS

This PhD journey in the coastal development of Suriname was incredible and made possible by my supervisors, collaborators, and financial sponsors (Treub Fund and Suriname Conservation Foundation). I received the unconditonal support of my family, friends, and colleagues.

I am greatful for Ronald van Balen and Carina Hoorn for their immense patience and supervision. Ronald van Balen gave me the opportunity to conduct the first part of this research. He led and taught me in the world of Quaternary Science, and was always willing to advise and answer questions, relevant or not. Despite the physical distance, his door was always open to help to navigate into the academic world. Through the years, as funding became a challenge, he did not give up, but encouraged to keep going no matter what. Ronald, thank you for setting the bar high and being supportive in all circumstances.

Carina Hoorn, an incredible female scientist and like a mother and friend to her PhD-students. Always positive, but persistent as a supervisor. Your perfectionism has taught me a lot and given me different view in the world of academics. Whenever, wherever, you always had a listening ear and advise for me. Your support to collaborate with other scientists and students from other institutes all over the world was proof that you can achieve more together. Thank you for being always there for me.

Pieter and Carmen Augustinus, my bonus parents and Pieter being the one who led me into the world of coastal science. Thank you for the useful insights, guidance, discussions and being there for me and my family whenever I needed it.

Nina Witteveen, our paths crossed in 2023 during a barbecue event at Science Park. Our shared love for my home country Suriname has created a strong friendship. Thank you for the academic advice, revisions, and personal conversations. I hope we can have more of these laughs and amazing experiences together in the future.

Salomon Kroonenberg, as a co-author and colleague, you have been an inspiration to finish this journey. Thank you for never getting tired of questions and sending literature. You never forgot or hesitated to include me in studies regarding my research topic.

I would like to thank everyone who collaborated during this research. Roel Verreusel, thank you for the advice and relevant literature. Despite your busy scheme you always took the time for response.

Elton Luis Dantas, Roberto Ventura Santos, and Martin Roddaz, the collaboration with you was very interesting and helpful. Thank you for introducing me into another discipline, and also understanding it.

Angelo Plata-Torres, we crossed paths at a congress in Prague in 2024. There was an instant click between us, as we sat during the breaks trying to identify as much pollen as possible. Your knowledge on, especially pollen from the Caribbean areas has contributed significantly to my research. Thank you for everything.

Raul Giovanni Bogota-Angel, though we have never met and your busy agenda, you still contributed to my research. Thank you for your time and advice.

Henry Hooghiemstra, our paths already crossed in 2012 during a short visit at the University of Amsterdam. I am very grateful for your time, when you sat down with me to discuss the manuscripts. Your encouragement helped me to keep going. Thank you very much for that.

Hanna, your incredible contributions to the research with all the diagrams was very helpful. Thank you very much for your tireless efforts.

Annemarie Philip, thank you for preparing the pollen slides, asking how I am doing and your support.

I am grateful for Docia Agyapong, Johannes de Groeve and Stacey Shinneman for helping me with creating the maps in ArcGIS. Thank you very much!

A special thanks to David Klink, Iris de Vos, Eva Visser, and Nisha Bharos for conducting parts of this research. Your contribution has been more than valuable.

Grateful and thankful for, especially the last conversations with the late Prof. dr. Theo Wong, his insights, knowledge of the Guiana Basin and advice during his sickbed. I will always remember you as a great supporter during my PhD journey.

I would like to thank everyone from the Anton de Kom University of Suriname for the support and their full cooperation in shifting schedules to enable me to conduct my research. Dewany Monsels, Lynette Afindoe, Ramon Finkie, Gordon Babel, Kenneth Goenopawiro, Oclaya Verwey, Renoesha Naipal, Fydji Sastrohardjo, Ginny Bijnaar, Nicole Kioe-A-Sen, Glenn Gemerts, Gwendolyn Landburg, Ewald Poetisi, Nico Mwakipesile, and Rene Artist thank you for all you did!

I also like to extend my appreciation to everyone from IBED and ELD for welcoming and treating me as one of yours. Thank you for the support, asking how it is going, and the advice

Will Gosling, Crystal McMichael, Johan Mols, Kenneth Rijsdijk, Caixia Wei, Sandeep Sen, Helanlin Xiang, and Eileen Enderle.

This would not have been possible without the support of the State Oil Company Suriname (Staatsolie Maatschappij Suriname N.V.) and the Suriname Water Company (Surinaamse Waterleiding Maatschappij Suriname). Thank you for making drill samples available to conduct my research. Also, I am thankful for the help of Soraya Tirbeni, Faizel Idoe, Patrick Brunings, Eshita Narain, Shaiza Simons from Staatsolie N.V. for speeding up company procedures, and Mitch Jie-A-Looi, Rachel Ramdin and Vandana Gangaram Panday from Suriname Hydrocarbon Institute N.V. for providing data. Also Patrick Wandi from Schlumberger, thank you for providing important information about the wells.

Ramona Biswane and Ashwinie Hemai from the Suriname Water Company, thank you for providing samples to conduct parts of this study.

I am grateful for the Board and employees of the Suriname Conservation Foundation (SCF). A special thanks to the former project manager Nathalie Emanuels, the current manager Iseah Reigman, Stan Malone, Jacyntha Asinga, Theo Sno, Henna Uiterloo and all other SCF employees. There are not enough words to describe how much you contributed to make this research possible.

Thankful for my Corpall family who supported me during this journey. Thank you for regularly informing about the status of my study Cor Pigot, Melvin Pigot, Juan Pigot, Gwendolyn Landburg, Muriel Held, Yolanda Babb and Truus Warsodikromo. Melvin your knowledge about the hinterland of Suriname, your efforts in helping with fieldwork through wind, sun and rain were incredible.

I am more than grateful for my friends who gradually became famliy and unconditionally supported me. Thank you Nicole Jonathas, Rosanne Doornkamp, Cindy Smuller, Natalie Ceuppens, Natasha Winter, Chiquita Venloo, Carolyn Verwey, Mercedes Nijhove, Mireya Rodriquez, Danielle Kranenburg, Rodney Griffith, Joseph Seffie Held, Judith Simson, Irene Simson-Rotsburg, Maureen Benschop-Abel, Wendell Gonesh, Crystal Kensen, Nikita Drielsma, Aishel Bradley, Ortwin Sedoc, Saidha Esajas, Romeo Abaisa, Molly Pinas, Sharine Fiquera, Jaleesa Joval, Tessora Kertodikromo, Mireille Tjin Kon Kiem, Jean-Paul Gooswit, Frank Raijmann, Priscilla Crisis, Cerilde and Stephan Heyns, and my former Etos colleagues Suzanne Kruger, Sandra Wierink, Chantal Krieger, and Gloria Edusei.

My family and in-laws have been very supportive and involved through my PhD journey. Elisabeth, Muriel and Steven Gersie, thank you for being there for me. Even so for Tanisha Robinson, Jerrol Verwey, Damiën Verwey and Anverney Verwey, Kimberley Gersie and Charissa Gersie, Mildred Woerdings, Reinier Pinas, Harvey Pinas, Santusia Pinas, Eric Schalkwi-

jk, Zunzuella Abena, Jurgen and Merlyn Codfried, Rodney Codfried, Sarita Martina, Mireille and Wout† Meyer-Benjamin, my mother-in-law Ina Lemmer, who never stopped praying for me, my brother-in-law Rogilio Lemmer and his wife Evie Aarden, Yently and Latisha Lemmer, Urely Sedoc, and Eugenie Hoffman.

Also thankful for my late father Michel Gersie and late stepfather Rene Etnel for supporting whenever and wherever they could.

My best friend Eartha Baarn, you deserve a special thanks for your unconditional support. You always have my back, no matter how, no matter what. Grateful to have someone like you in my life!

To my late mother Junita Woerdings. Though you are no longer among us, I can say that I am grateful for the unconditional love you showed me. You supported me in everything I did or planned to do. You taught me standards and values and gave everything to make sure that I got educated well. I therefore dedicate this thesis to you, knowing you would be very proud of me!

Finally, I would like to thank my partner Dwight, daughters Nyanne and Ziane Lemmer, and my foster son Djamiro Vismale for their support, patience, and advices. I know that you are proud of and happy for me. Without your understanding this journey would have been very difficult. You stood with me during the highs, but also the lows, and you never left. Let us celebrate this new milestone, and prepare together for the next. I love you!

BIOGRAPHY



Kathleen was born on the 14th of January 1976 in Paramaribo, Suriname. The youngest in the family and as a child constantly telling her mother that one day she would go to the big school. She has always been ambitious to take the next step and to reach higher. From childhood she wanted to be the best and became a motivation and role model for other family members.

At first she wanted to become a medical doctor, but was not selected for the study. She decided to study Earth Sciences at the Anton de Kom University of Suriname, Paramaribo, Suriname which she finished in 2004. In 2006 she was selected for a scholarship to study Physical Geography at the Utrecht University, Utrecht, The Netherlands. She obtained her Master's degree in March 2009 in Coastal and River Morphology.

From April 2009 to present day she lectures at the Geoscience Department of the Anton de Kom University of Suriname. She has also been a member of the examination and training committee. In 2011 she started her PhD-research at the Vrije Universiteit Amsterdam, The Netherlands, under supervision of Ronald van Balen. Her project focused on the natural and anthropogenic controls of the Suriname River and also the river terraces along the Suriname River. Due to financial issues there has been a significant delay in her research. In 2023 she obtained funding from the Suriname Conservation Foundation to finish her PhD partly at the University of Amsterdam. This part of her study focused on the influence of the Amazon River on the coastal development of Suriname.

She is ready to start the next chapter in her life and to make a positive contribution to Earth sciences, especially in Suriname.

